



The
University
Of
Sheffield.

Graph Theory and Molecular Currents

Martha Borg

May 2019

A thesis submitted in partial fulfilment of the requirements for the degree of
Doctor of Philosophy

Department of Chemistry
Faculty of Science
University of Sheffield

Supervised by:

Prof. P.W. Fowler, FRS

Graph theory and molecular currents

*To
my family,
with exceptional appreciation
to my mother
and to those special persons
who constantly show
unconditional love and support*

Acknowledgements

- I sincerely thank Prof. Patrick W. Fowler for continuous and consistent support in the development of the present thesis, and for the unique opportunity to work in a highly scientific and united team.
- A very special thanks goes to our collaborators Prof. Barry T. Pickup (University of Sheffield) and Prof. Irene Sciriha (University of Malta) for their very valuable scientific ideas and suggestions.
- I would like to express my gratitude to the University of Sheffield for providing me with the chance to carry out this research.
- Lastly, but not in importance, I would also like to thank my wonderful family and friends for the endless love, patience, support and encouragement that they gave me.

Abstract

Ballistic transport of electrons through a two-wire device based on a π -conjugated carbon nanostructure is studied using the tight-binding source-and-sink-potential (SSP) model (Chapter 2). This is equivalent to solving a purely graph-theoretical adjacency eigenvalue problem on an augmented molecular graph under scattering boundary conditions (Chapter 2). From previous work it is known that *transmission* of a two-wire device as a function of energy, $T(E)$, can be expressed in terms of four characteristic polynomials $\{s, t, u, v\}$, which are respectively those of graphs G , $G - \bar{L}$, $G - \bar{R}$, $G - \bar{L} - \bar{R}$, where G is the molecular graph and \bar{L} , \bar{R} are the vertices of G that are in contact with left and right wires. The triple $\{G, \bar{L}, \bar{R}\}$ defines a *device*. Selection rules for Fermi-level ($E = 0$) conduction of two-wire devices are proved (Chapter 3) using the nullity properties of s, t, u, v and their determinantal combination $j^2 = ut - sv$. The Interlacing-Theorem-based partition of graph vertex types as lower, middle and upper, according to the effect $\Delta g_s = -1, 0$ or $+1$ on the nullity g_s of the molecular graph caused by a vertex deletion, is used to give a general classification of conduction types for arbitrary graphs, identifying the possible types of omni-conducting and omni-insulating *distinct* ($\bar{L} \neq \bar{R}$) and *ipso* ($\bar{L} = \bar{R}$) two-wire devices (Chapter 4). In Chapter 5, this is refined for *bipartite* graphs to a three-letter acronym for each nullity class ($g_s(G) = 0, g_s(G) = 1, g_s(G) > 1$); of 81 hypothetically possible combinations with inter, intra and *ipso* sets of contacts, it is proved that exactly 14 can be realised by connected simple bipartite graphs. A final extension (Chapter 6) based on the inter-contact graph-theoretical distance (odd, even or zero) gives a final three-letter acronym for each nullity class applicable to all connected simple graphs, bipartite and non-bipartite. All but four of the 81 hypothetical cases are resolved: 35 are realised by examples, (chemical graphs in at least 28 cases), 42 are provably unrealisable by any connected simple graph, and four have as yet neither an example nor a proof of unrealisability. Chapter 7 describes a shift of viewpoint in which the edge-based conduction in the SSP model (an ‘atomic/orbital’ formulation) is replaced by conduction through eigenspace channels (‘shells of π molecular orbitals’) with applications to conduction of conjugated π systems in which, selection rules based on active and inert channels are operating. Finally (Chapter 8), further applications of the mathematical framework are made to graph-theoretical construction of omni-insulating devices, mathematical results on factorisation of graph structural polynomials are given to be used in the future to allow the treatment of the effects of distortivity, and improvements of the theoretical chemistry treatment to allow for interacting molecular and conduction electrons are outlined. The thesis concludes with an overview of the main results (Chapter 9).

Contents

Acknowledgements	vii
Abstract	ix
List of mathematical terms and abbreviations	xvii
1 Introduction	1
1.1 Graph theory	1
1.2 Molecular conduction	3
1.3 Experiments on MEDs	5
1.4 Theoretical techniques	10
1.5 Hückel molecular orbital theory	12
1.6 A note on programs	20
1.7 Conclusion	21
2 Theoretical chemistry background	23
2.1 The Source–and–Sink Potential (SSP) Model	23
2.2 The SSP model and characteristic polynomials	27
2.2.1 The SSP Hamiltonian and solution of the Schrödinger equation for MEDs	28
2.3 Extreme values of the transmission function	31
2.4 Selection rules for conduction in MEDs	33
2.5 Conclusion	35
3 Interlacing–extremal graphs	37
3.1 The adjacency matrix and cores of singular graphs	38
3.2 Characteristic polynomials	39
3.3 Jacobi’s identity	40
3.4 The three vertex types	42
3.5 Restrictions on the nullity of $G - \bar{L} - \bar{R}$	44
3.5.1 Restrictions arising from interlacing	44

3.5.2	Restrictions arising from Jacobi's identity	45
3.6	Kinds of graphs	47
3.6.1	Graphs of variety 1	47
3.6.2	Graphs of variety 2	48
3.6.3	Graphs of variety 3	49
3.7	Graphs with analogous vertex pairs	49
3.7.1	Uniform-core graphs	50
3.7.2	Non-singular graphs with a complete weighted inverse	52
3.8	Chemical implications	53
3.9	Conclusion	54
4	Omni-conducting and omni-insulating molecules	55
4.1	Introduction	55
4.2	Background	57
4.2.1	The SSP model	57
4.2.2	Characteristic polynomials	58
4.3	Devices and varieties	59
4.4	Implications for omni-conductors and omni-insulators	63
4.4.1	Deductions by device type: distinct connections	63
4.4.1.1	Graphs of nullity $g_s = 0$	63
4.4.1.2	Graphs of nullity $g_s = 1$	65
4.4.1.3	Graphs of nullity $g_s > 1$	66
4.4.2	Deductions by device type: <i>ipso</i> connections	67
4.4.3	Deductions by conduction class	67
4.5	Results	68
4.5.1	Statistics of conduction of molecular graphs	68
4.5.2	Some families of omni-conductors	72
4.5.3	Some families of omni-insulators	73
4.6	Conclusion	76
5	Near omni-conductors and insulators in the SSP model	77
5.1	Introduction	77
5.2	Classification of distinct and <i>ipso</i> devices	79
5.3	A classification scheme for alternant hydrocarbons	81
5.4	Calculations	81
5.5	Elimination of remaining cases	82

5.6	Rare cases	83
5.6.1	Cases XXC, CXI and ICX	83
5.6.2	Case IIC	83
5.6.3	Case XIX	87
5.7	Refining the TLA description	87
5.7.1	Singular bipartite graphs with $g_s = 1$	87
5.7.2	Singular bipartite graphs with $g_s > 1$	87
5.8	Benzenoids	88
5.8.1	Kekulean benzenoids	89
5.8.2	Non-Kekulean benzenoids	91
5.9	Conclusion	91
5.10	Appendix: Theorems for case-by-case proofs	92
5.10.1	Non-singular molecular graphs ($g_s = 0$)	92
5.10.2	Singular molecular graphs with $g_s = 1$	93
5.10.3	Singular molecular graphs with $g_s > 1$	94
6	A complete classification: the d-omni-conductors	95
6.1	Abstract	95
6.2	Introduction	95
6.3	Background	97
6.3.1	The SSP model	97
6.3.2	Selection rules	98
6.3.3	Vertex types	98
6.3.4	Calculations	100
6.4	Classification of conduction behaviour	100
6.4.1	Two-letter codes (all graphs)	100
6.4.2	Three-letter codes (bipartite graphs)	100
6.4.3	Three-letter codes (all graphs)	101
6.5	Method	102
6.6	Results	103
6.6.1	Allowed d -omni codes	103
6.6.2	Expanded d -omni codes	106
6.7	Conclusions	108
6.8	Appendix: Theorems for d -omni codes	110

7	A molecular orbital view of the SSP method	117
7.1	A rederivation of the SSP equations	117
7.1.1	Flux normalisation	119
7.1.2	The SSP equations in the atomic orbital basis	120
7.1.3	The SSP equations in the MO basis	122
7.2	A mathematical toolkit	123
7.2.1	Structural polynomials in the MO basis	124
7.2.2	Expansion of the reduced structural polynomials	125
7.2.3	The expansion of $D(E)$	127
7.3	Solution of the SSP model in the AO basis	128
7.3.1	Transmission	129
7.3.2	Bond currents	129
7.3.3	A physical corollary for <i>ipso</i> devices	130
7.4	General solutions of the SSP equations in the MO basis	131
7.4.1	Solutions away from eigenvalues	131
7.4.2	Active and inert orbitals and shells	132
7.5	Solutions of the SSP equations in the MO basis at molecular eigenvalues	132
7.5.1	Shell partitioning of the SSP equations	132
7.5.2	The shell connection matrix, rank and the echelon representation	134
7.5.3	Shell and bond currents in the echelon representation	135
7.5.4	The eleven canonical molecular conduction cases for a shell with eigenvalue ϵ_K	136
7.5.5	Conduction in <i>ipso</i> devices	137
7.5.6	A difference between conduction of <i>ipso</i> - and <i>non-ipso</i> devices	138
7.6	Conduction in molecules with bipartite graphs	139
7.6.1	The Coulson–Rushbrooke theorem	139
7.6.2	Structural polynomials for bipartite graphs	141
7.6.3	Conduction properties of alternant molecules	141
7.6.4	Conduction at the Fermi level for bipartite graphs	142
7.7	Some illustrative examples	143
7.7.1	Molecular conduction of LOMO and HUMO shells	144
7.7.2	Conduction in chains	144
7.7.3	Conduction in rings	145
7.7.4	An alternant molecule with a space of non–bonding orbitals .	146
7.8	Inertness/activity and core/core–forbidden vertex sets	146

7.9	Conclusions	147
7.10	Appendix: Detailed analysis of the 11 canonical cases	148
7.10.1	Devices with rank–2 connection matrices	149
7.10.2	Devices with rank–1 connection matrices	150
7.10.3	Devices with rank–0 connection matrices	151
8	New developments in applications of graph theory to MEDs	155
8.1	The starification construction	155
8.1.1	The rare cases	156
8.1.2	Trees and their stars	157
8.2	Conduction in distortive and topologically exotic carbon frameworks .	162
8.2.1	Graphs derived from alternating ladders and treadmills	164
8.3	Including the Pauli exclusion principle in the SSP model for MEDs .	166
8.3.1	From the ‘empty–molecule’ to the many–electron picture . . .	166
8.3.2	Some mathematical consequences of the Pauli SSP model . . .	168
8.3.3	What survives under the Pauli Effect	168
8.4	Conclusion	171
9	Overview	173
	Bibliography	175

List of mathematical terms and abbreviations

graph	carbon skeleton
vertices	atoms
order, n	number of vertices of a graph
edges	bonds
size, m	number of edges of a graph
degree	the number of edges ij that contain a given vertex i
eigenvalue	orbital energy
eigenvector	orbital
nullity, g_s	dimension of the eigenspace corresponding to the zero eigenvalue corresponding to the non-bonding orbitals
multiplicity	degeneracy
connected graph	a path from any vertex to any other vertex
π system	a connected graph with degree ≤ 3
bipartite graph	the vertices of a graph can be partitioned into two disjoint sets such that no two vertices within the same set are adjacent
non-bipartite graph	a graph that has odd cycles
tree	an acyclic connected graph
path	“unbranched tree”
cycle	graph with exactly two paths between any two vertices
core vertex, CV	a vertex corresponding to a non-zero entry for some kernel eigenvector
core-forbidden vertex, CFV	a vertex corresponding to a zero entry in every kernel eigenvector
nullspace	the kernel of the adjacency matrix of graph G such that the vectors in the nullspace represent the non-bonding orbitals
kernel eigenvector	a non-zero eigenvector in the nullspace

device	a graph having two connection vertices \bar{L} and \bar{R}
uniform–core graph	a connected graph in the device (G, \bar{L}, \bar{R}) with all pairs of vertices (\bar{L}, \bar{R}) being of variety 1(i), that is, insulating for all distinct connections
SSP	source–and–sink–potential
NBO	non–bonding orbital
MED	molecular electronic device
STM	scanning tunnelling microscope
AFM	atomic force microscope
DFT	density functional theory
TLA	three–letter acronym
MO	molecular orbital
HOMO	highest occupied molecular orbital
LUMO	lowest unoccupied molecular orbital
HUMO	highest unoccupied molecular orbital
LOMO	lowest occupied molecular orbital

Chapter 1

Introduction

Graph theory has long been studied since the 1730s, and has a history of applications in fields such as chemistry and physics [1]. Many researchers with different graph theoretical interests in coding theory, bioinformatics, quantum physics, molecular chemistry, nanotechnology, computer and internet networks and social network analysis have undertaken research in this area. The appeal of graph theory in chemistry is as a surprisingly useful qualitative model for the behaviour of molecular systems.

The present introductory chapter includes a review of the applications of spectral graph theory to carbon nanostructures. The importance of graph theory being linked to theoretical chemistry is introduced in Section 1.1. Section 1.2 discusses briefly the main idea behind the investigations discussed, whereas, Section 1.3 lists the latest improvements of molecular electronic devices. Section 1.4 illustrates some experimental techniques used to describe the transmission of electrons in molecular systems. The Hückel molecular orbital theory is tackled in Section 1.5 and Section 1.6 is a remark about the programs used throughout the thesis.

1.1 Graph theory

A science that has benefited significantly from the combination of graph theory and linear algebra is theoretical chemistry. Since the award of the Nobel Prize to Kroto from the UK, and Smalley and Curl from the USA in 1996 for their sixty-carbon, C_{60} , buckminsterfullerene molecule, this area has exploded and bridged over to nanotechnology. In the initial graph theoretical molecular model of C_{60} , for instance, the eigenvalues [2] of this planar graph yielded significant information on physical and chemical characteristics [3, 4]. The keen interest shown by chemists in the subject is evident from the large number of related papers published not only in purely chemical journals but also in others, specifically dedicated to the interaction between chemistry and mathematics, such as *The Journal of Mathematical Chemistry*, *MATCH*, *Ars Mathematica Contemporanea* and *Journal of Chemical Information and Modelling*.

Graph theory is the mathematical theory of the properties and applications of graphs, whereas spectral graph theory is the study of the properties of a graph in relation to the characteristic polynomial, eigenvalues and eigenvectors of the matrices associated with the graph. Both are used to interpret and predict physical

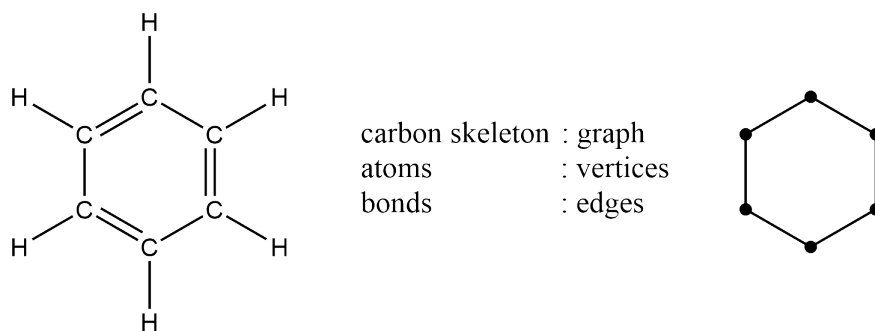


Figure 1.1: Graph-theoretical representation of the benzene molecule.

and structural properties. In Hückel molecular theory for unsaturated hydrocarbons, there is a direct relation between the molecule and a graph. The molecule is stripped of its hydrogen atoms and only its carbon skeleton is used (see Fig. 1.1). In these terms, the vertices of a graph can represent the atoms of a molecule – their number defines the order of a graph. Its edges can represent the bonds that exist between the atoms. The number of edges determines the size of a graph. The adjacency matrix of the graph is an $n \times n$ symmetric matrix, where $A_{ij} = 1$ if vertex i is adjacent to vertex j , that is, i and j are vertices connected by an edge, and, otherwise, $A_{ij} = 0$. The number of edges ij that contain a given vertex i is the degree of i .

The terminology used in graph theory has a natural relation to chemistry and this link has proved useful for the understanding of energy levels of molecules and their electron distributions, in particular, through the spectrum [2] of the graph. The spectrum of a graph is the set of its eigenvalues or as it is chemically known, the set of orbital energies (see Table 1.1). This is based on the Hückel molecular orbital theory which gives an approximation of the π -molecular orbitals of a molecule by expressing them as linear combinations of atomic p_π -orbitals. Bonding, non-bonding and anti-bonding orbitals correspond to positive, zero and negative eigenvalues of A_{ij} , respectively. If the multiplicity of an eigenvalue corresponding to an eigenvector is greater than one, then we have the case of a degenerate orbital. Hence, the three main chemical principles (the Aufbau and Pauli principles and Hund's rule of maximum multiplicity) for determination of the ground-state electronic configuration are:

- (i) by the Aufbau principle the orbitals are filled up in order of decreasing eigenvalue;
- (ii) the Pauli principle demands that each orbital can contain no more than two electrons; and
- (iii) Hund's rule defines the way of filling up the degenerate orbitals, that is, each orbital receives first one electron before any one orbital in the degenerate set is doubly occupied.

The non-bonding orbital (NBO), associated with the zero energy level, lies at what in physics is called the Fermi level, that is at the eigenvalue zero. The number of NBOs and the special properties of molecules at the Fermi level of energy provide

an understanding of some important characteristics of nano-structures, as we shall see in Section 2.4.

Graph theory	Chemistry
Eigenvalue	Orbital energy
Eigenvector	Orbital
Nullity	Number of NBOs

Table 1.1: The equivalence of a graph and the skeleton of a molecule.

An important early application of spectral graph theory was to determine the nullity [2], that is, the dimension of the eigenspace corresponding to the zero eigenvalue of the graph of a particular molecule that corresponds to the non-bonding orbitals (NBOs) of the molecule [5,6]. When NBOs are present, they may point to instability of the molecule through ease of electron transfer to and from the system.

A *connected* graph [7,8] is a graph which is connected in the sense that there is a path from any vertex to any other vertex in the graph, that is, starting from any vertex one can reach any other by walking along edges. A graph that is not connected is said to be *disconnected* and to consist of connected *components*. A *chemical graph* is a graph that can act as a molecular graph for π systems that are connected and have maximum degree ≤ 3 . A *bipartite* graph is a graph whose vertices can be partitioned into two disjoint sets such that no two graph vertices within the same set are adjacent. The eigenvalues of a bipartite graph are paired [5]. A graph is *non-bipartite* if and only if it contains an odd cycle. A *tree* is a graph in which any two vertices are connected by exactly one path. In other words, any connected graph without cycles is a tree. Two special classes of graphs of interest in chemistry are the paths P_n and cycles C_n . The *path* P_n is a sequence of n vertices such that from each there is an edge to the next vertex in the sequence and no vertex is repeated. The vertices at the end of a path are of degree two. Both are *terminal vertices*. Other vertices in the path are internal vertices of degree two. The size of P_n is $m = n - 1$. The *cycle* C_n is similarly defined, but any vertex may serve as the start and end vertex. The cycle has size $m = n$.

1.2 Molecular conduction

The study is motivated by questions that are by no means new and were already posed many decades ago: how do electrons move through molecules [9,10]? Can a molecule mimic the behaviour of an ordinary microelectronics component or maybe provide new electronic functionality? How might one interconnect molecular devices and integrate them into complex architectures [11]? Understanding the movement of electrons to and through a single molecule on the nanoscale is central to the field of molecular electronics. This realisation of molecular conduction as an important possibility for applications came about in the 1950's after the revolution in electronics due to the invention of the transistor and in view of the difficulties to radically miniaturise the existent electronic components. Hence, single molecules might be regarded as the ultimate goal in the miniaturisation of the transistor. As Cuevas and Scheer report in [11], it was Arthur von Hippel, a German physicist

working at MIT, who formulated in 1956 the basis of a bottom-up approach that he called molecular engineering [12], which led to the first notion of molecular electronics [13]. He argued that “instead of taking prefabricated materials and trying to devise engineering applications consistent with their macroscopic properties, one could build materials from their atoms and molecules for the purpose at hand”. However, miniaturisation of silicon-based electronic devices is nearing its practical limit and could soon become prohibitively expensive [14]. If devices are to continue becoming smaller, rather than reducing the size of macro materials one must instead consider the possibility of a bottom-up synthetic approach [15]. Not only does a molecular approach make the position and distance of atoms within devices easier to control, but also brings in quantum effects, which can give exceptional properties [16] to some materials. Molecular electronic devices have the potential to replace traditional solid state devices such as transistors, rectifiers [17] and switches and also have prospective uses in solar energy harvesting and thermoelectronics [18].

The miniaturisation of electronic devices presents a significant experimental and theoretical challenge because it includes dependence on the chemical structure of the molecules, the metal-molecule-metal bonding geometry, the structure of the contact surface and the influence of the surroundings. This understanding can be traced back to the 1970s. Even a hundred years ago the atomistic viewpoint was somewhat controversial and many renowned scientists of the day questioned the utility of postulating entities called atoms that no one could see [19]. However, now that the field of molecular electronics has been around for more than 40 years and some fundamental problems as those listed above have been overcome, researchers are not only describing charge transport but also exploring numerous intrinsic features of molecules.

As stated in a commentary by Ratner [20], the movement of electrons through single molecules can happen either by electron transfer, involving a charge moving from one end of the molecule to the other, or by molecular charge transport, involving current passing through a single molecule that is strung between two electrodes [11, 21]. Although it is quite difficult to solve all the problems that surround molecular electronics, this field has made considerable progress in recent years and a variety of important mechanistic insights have been obtained, which could have implications for the development of devices by taking advantage of the small size of the molecules.

Molecular electronics could offer the following major advantages [22]:

- (i) The small size of molecules in the nanoscale could lead to a higher packing density of devices thus being more cost-effective and efficient and with advantages as regards power dissipation.
- (ii) Small size of molecular devices could reduce the time for an operation to occur.
- (iii) Apart from forming structures by nanoscale self-assembly, molecular recognition could be used to modify electronic behaviour.
- (iv) Special properties of molecules, such as the existence of distinct stable geometric structures or isomers, could lead to new electronic functions that are not possible to implement in conventional solid state devices.

- (v) Transport, binding, optical and structural properties of a molecule can be varied altering the chemical structure of the device or the way in which it is connected to the leads.

The disadvantages that come along with use of molecules as components are instabilities at high temperatures, and difficulties in fabrication. Fabrication of reliable molecular junctions requires the control of matter at the atomic level, which can be not only difficult, but also slow and costly [22]. Another area which benefits from an increase in packing density is the realm of computing. The length of a field-effect transistor was $\sim 10\mu\text{m}$ in 1960 but by the year 2000 it was significantly reduced to $\sim 0.1\mu\text{m}$, allowing circuit designers to pack 10 000 times more transistors into a chip of given surface area. In Ref. [23], Moore noted that the number of transistors in a dense integrated circuit doubles about every year, and suggested that this could in fact continue for another decade. However, in 1975, Moore revised this idea and forecast that the doubling trend could take place every two years [24]. This rate was true for the initial years but in 2015, Moore comments that this law would die in about a decade as it would have reached saturation [25]. Advancements in digital electronics are strongly linked to Moore's law: to name a few, memory capacity, sensors and the number and size of pixels in digital cameras [26]. The miniaturisation of the transistor is also governed by this law. The transistor is currently being manufactured with a characteristic dimension of around 20nm, a factor of over a million smaller than originally [27]. As Datta remarks [19], how much longer this downscaling can continue nobody knows, but, one will in any case have to learn how to model and describe the electronic properties of device structures that are engineered on an atomic scale. The ultimate goal in miniaturisation is the single molecule-device and this leads to the topic of this thesis.

1.3 Experiments on MEDs

Molecular electronics has recently seen a huge improvement, especially in the last two decades, due to the advances made in traditional semiconductor materials [22,28–30]. We would hope that it is possible to find an appropriate molecule for any imaginable application, but for the many reasons listed in Section 1.2, so far only a few classes of molecules have been explored in molecular electronics. Such molecules need to mimic common functional elements in digital electronic circuits. Table 1.2 names a few of the main elements and their requirements together with possible candidates [11].

Different methods have been developed for the fabrication of metallic atomic-sized contacts. One of the most versatile and speedy tools for the fabrication of atomic-size contacts is the scanning tunnelling microscope (STM) [31]. Experimentally, it was the first technological platform capable of contacting single molecules adsorbed on metallic surfaces. A fine metallic tip (of about $200\mu\text{m}$) is held at a distance or 'inserted' into the electrode surface. In the latter way, making use of the exponential distance dependence of the tunnelling current, the tip can be indented into the surface and carefully withdrawn until an atomic size contact or short atomic wire forms. The main drawbacks are its limited stability with respect to the change of external parameters such as the temperature or magnetic fields and the short lifetime of the contacts in general because of the sensitivity of STM to vibrations.

Main element	Requirements	Possible molecular candidates
Conducting wires	Low resistance, high ampacity (the maximum current, in amperes, that a conductor can carry continuously under the conditions of use without exceeding its temperature rating)	Polyenes and alkynes
Insulators	High resistivity, high breakdown voltage	Alkanes
Switches	High on/off resistance ratio, reliable switching, small leak current in off position	cis/trans conformation changes of manifold molecules, the prototype being azobenzene
Storage elements	Long storage time, low loss	All kinds of molecules with at least two states
Diodes	High forward/backward current ratio	Molecules which consist of two different, and electronically decoupled parts
Amplifiers	High gain	All molecules of which the electronic levels can be tuned by a gate electrode
Anchoring groups	Reliable contact between functional molecular unit and electrode	Thiols, amines, nitro-, cyano- or hetero-substituted cyclic molecules with the substituent atoms serving as linkers to the metal electrodes

Table 1.2: Common functional elements in digital electronic circuits, their requirements and the possible molecular candidates [11].

The tight-binding approach has been used to describe a variety of problems related to the electronic transport in atomic-scale junctions and one of the first was the analysis of the operation of the STM, and the interpretation of images taken with this instrument [32–36]. This approach has been very important in elucidating the role of the tip-substrate distance.

Another scanning probe technique which is considered to be a versatile tool in surface sciences in various environments and temperature ranges is the atomic force microscope (AFM). It can work on insulating substrates. Unlike STM, it does not use the tunnel current but the distance dependence of the force between a fine tip and a surface. Its working principle is to measure the force by recording the deflection of a cantilever that carries the tip. The deflection is detected by for example optical means. When in use with the STM which records the current, the AFM measures the force to form or break contacts [37].

There are also many methods that can be used to contact molecules with metal electrodes. Devices including at least one semi-conductor electrode have also been realised. The molecular junction fabrication is two-fold in the sense of what kind of electrodes and deposition method of molecules are used. It should follow a precise contacting scheme based on the way how, the moment when and the conditions under which the molecules are brought into electric contact with the electrodes [11]. The main problem in the fabrication of single molecular electronic devices is that the size of the molecule is smaller than the resolution of the lithographic methods. Thus, there exists no method on its own which allows one to perform systematic measurements of the electronic transport and to characterise the geometry of a given junction with atomic precision. Therefore, various methods, such as the STM and AFM mentioned above, are used and can be divided into two classes. Firstly, there are those that produce rather stable devices for which the geometry cannot be varied, and contamination cannot be excluded. Secondly, there are those methods that enable clean contacts and modification of the junction geometry, but offer only limited stability.

Unimolecular electronics were first discussed as being a potentially promising subject in the late 1950s and gave rise to more work in 1974 when Aviram and Ratner proposed that a single organic molecule can act as a rectifier [29]. A rectifier, or diode, is a two-terminal in which current flow is allowed for a given polarity of the voltage applied across its terminals (forward bias), but blocked when the polarity is inverted (reverse bias). An ideal rectifier is thus a voltage-controlled switch [38]. A donor π system and an acceptor π system are separated by a σ bonded tunnelling bridge. When a field is applied rectifier properties appeared. Current passed to the right and only if the reversed voltage was high enough did current flow through the π system from anode to cathode. At this stage it is important to note that if single organic molecules are to be used in devices then materials and synthesis problems need to be overcome. Note that the original proposal has been subjected to criticism and refinement by authors such as Metzger [39].

Another interesting paper for those working on carbon nanostructures is that presented by Park *et al.* where they discuss the fabrication of single-molecule transistors based on individual C_{60} molecules connected to gold electrodes [40]. They demonstrated that single-electron-tunnelling events can be used to excite and probe the motion of a molecule. The single C_{60} transistor behaved as a high-frequency

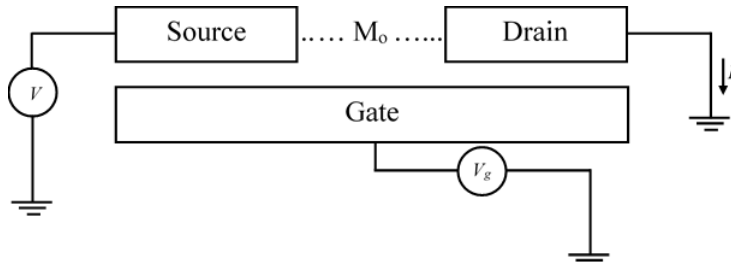


Figure 1.2: Schematic of a gated–device used in the Coulomb blockade and Kondo effect study [41] (based on Figure 1 from that paper). M_o is the $[\text{Co}(\text{tpy}-(\text{CH}_2)_5\text{-SH})_2]^{2+}$. See [41] for further details.

nanomechanical oscillator. It is a quantum ‘mechanical’ system since the oscillations of C_{60} molecule must be treated in a quantised fashion.

Park *et al.* also investigate the Coulomb blockade and Kondo effect (defined below) in single–atom transistors [41] see Fig. 1.2. The transistors used incorporated a transition–metal complex designed such that electron transport occurs through well–defined charge states of a single atom. Here two molecules attached to insulating tethers of different lengths but both containing a Co ion were used to enable the fabrication of devices that exhibit either single–electron phenomena, such as Coulomb blockade, or the Kondo effect. The longer molecule exhibited behaviour as that of a single–electron transistor [42], which is a device containing a small island, in this case the single Co ion, which is attached to gold electrodes by tunnel organic barriers. These are used to control the length, that is, to control the coupling between the ion and electrodes. Also, the charge state of the transistor can be tuned using a gate voltage and at most values, the charge state of the ion is stable at low voltage. The electron does not have enough energy to tunnel onto the Co ion showing Coulomb blockade. This is a powerful tool to unveil fine details of electron transport in nanoscopic systems [38]. On the other hand, the shorter molecule showed the Kondo effect, which is the formation of a bound state between a local spin on an island and the conduction electrons in the electrodes that enhances the conductance at low bias. In fact, significantly larger conductances occurred with the shorter tether length.

Molecular electronics and the study of physics of nanometre–scale systems depend on the ability to design the electronic states of a molecular device and to measure individual molecules. The work of Reed *et al.* [43] investigates the self–assembly of molecules of benzene onto two–fold electrodes in order to observe the charge transport through the molecules. The study is a quantitative measure of the conductance of a junction containing a single molecule. Metal–molecule–metal junctions are also dealt with in the study by Kergueris *et al.* [44]. The electronic transport properties through the molecules used in this study are investigated through the use of mechanically controllable break junctions, such that different types of current–voltage curves can be obtained. To switch between such curves it is enough to vary the distance between the two electrodes. The results obtained can be interpreted in two ways; firstly, as a coherent model which treats the molecule as scattering impurity between the two metallic wires for the low bias range. In this case the current–voltage characteristics at room temperature are not always symmetric with respect to the polarity of the applied bias and show a linear regime. The second interpretation could be that of a sequential tunnelling model, where the molecule is assumed

to be weakly coupled through tunnel junctions to each metallic electrode for the high bias range. Here the current–voltage characteristics are of a highly non–linear regime.

The work of Cui *et al.* [45] developed a reliable method for chemically bonding metal contacts to either end of an isolated molecule and measuring current–voltage characteristics of the resulting circuit. This method avoids the effects of variations in contact force and other problems encountered with non–bonded contacts. In fact non–bonded contacts are highly resistive, have different current–voltage characteristics from those of molecules with bonded contacts, and dominate the electrical properties. In contrast, molecules with bonded contacts are highly reproducible and lead to measurements that are in better agreement with first principles simulations without adjustable parameters.

Another interesting paper about the conductance of single molecules used in field–effect transistors is that by Schön *et al.* [46]. The conductance through the field–effect transistors can be varied by changing the applied gate bias. The conduction modulation happens through a third electrode. These single–molecule transistors are shown to be the basis of inverter circuits with gain. Schön *et al.* remark that the demonstration of field–effect transistor action with a single electroactive molecule is an important step toward molecular electronics, and with molecular heterostructures and molecular wires, it might be possible to combine the insulating and semiconducting properties as well as the contacts within a single molecule or supramolecular architecture.

As we have seen from the various experimental contributions presented so far, there are different techniques that can be used to deposit nanoparticles on a surface. A new technique developed by Bezryadin *et al.* [47] in 1999 uses electrostatic trapping that allows for controlled deposition of a single nanoparticle between two metal electrodes. It is based on the attraction of polarised particles to the point of the strongest electric field in the gap between the electrodes. This technique of electrostatic trapping can be used for various nanoparticles and it opens the way to explore the transport properties of single molecules or clusters.

Currently various groups of researchers are studying molecular electronic *devices*. In Ref. [48], Chen *et al.* report on the observation of large reversible switching behaviour in an electronic device that uses molecules as the active component. The essential feature of the fabrication process here is the use of a nanoscale device area, which gives rise to a small number of self–assembled molecules and also eliminates pinhole and other defect mechanisms that hamper through–monolayer electronic transport measurements. Chen *et al.* obtained good control over the device area, created intrinsic contact stability, and concluded that apart from the obvious size advantages for scaling, the intrinsic device characteristics may be superior to those of solid–state devices. A candidate mechanism for the negative differential resistance is a two–step reduction process that modifies charge transport through the system. As voltage increases, the molecule initially undergoes a one–electron reduction, thereby supplying a charge carrier for electron flow through the system. If voltage increases further, there is a second reduction with subsequent blocking of current.

The work of Collier *et al.* [49] is an example of another study developing an electronically singly configurable junction that consists of a molecular monolayer and a tunnelling barrier sandwiched between lithographically fabricated metal wires. This

junction can be used as a switch but because it is only singly configurable they cannot be used for random access memory. However, they scale down to molecular dimensions without appreciable loss of performance. When the molecular switches are closed, current flows by resonant tunnelling into the molecular electronic states leading to good noise immunity in future logic circuits. These switches are robust with respect to dimension tolerances in manufacturing as they depend on voltage. For the junctions used in this study only two wires are needed: one voltage is used to read the device, and a voltage of opposite polarity is applied to configure it. So, it is easy to design circuits incorporating these switches and it is highly modular. Their fabrication is also inexpensive. If they are scaled-down enough to integrate the molecular switches with molecular-scale wires then they can be used with carbon nanotubes.

Current studies of molecular junctions focus on general methodologies on the one hand and on detailed studies of specific systems on the other. One main area is the study of prototypes of molecular wires, which has become the subject of intense research and development effort [10]. A molecular wire is a structure which can serve as a conduit for electrons, and can function as an elementary building block for nanoscale devices [27]. In fact, in particular, one class of such molecular wires is carbon nanotubes. In 1997, Dekker stated that the long cylindrical fullerenes called carbon nanotubes are the smallest metallic wires [50] and have exceptional electrical properties as they can be semiconductors or metals. This depends on their diameter and chiral angle which determines the angle of the helical strips of hexagons in a chiral nanotube [51]. They are predicted to be prototype one-dimensional quantum wires and this makes them unusual, since, as Peierls [52] showed in 1930, one-dimensional metallic wires are intrinsically unstable and normally turn out to be semiconducting. The exceptional properties of nanotubes make them exploitable in molecular electronics, such as, the self-assembly of functionalised nanotubes into single-molecule devices.

Studying single-molecule electronic devices entails the collaboration of chemists, material scientists, physicists and engineers in order to integrate the organic molecular world with hard electronics, such that molecular electronics from laboratory-based research evolves into industrial applications [53]. For such devices to exist then three aspects that have an important role in their performance and stability are the electrode material, interface and molecular bridge. These can be modified by investigating the fundamental properties of the materials at the molecular or atomic level, for example, by precisely controlling the energy gap between the Fermi level of the electrode and the energy levels of the molecular orbitals [11, 16]. As Xin *et al.* report in [53] this would help in the fabrication of electrical nanocircuits with unexpected functionalities, such as switching, rectification and many others. Theoretical models that fully explain experimental phenomena at quantitative level help in overcoming the challenges in both scientific research and industrial manufacture as a slight variation at atomic level may influence conductance performance.

1.4 Theoretical techniques

The theory of ballistic conduction deals with the transport of electrons in molecules having negligible resistivity caused by scattering, through carbon frameworks on

the nano-scale. This theory analyses the molecular conductivity that many research groups are treating via individual *ab initio* treatments in order to obtain detailed information on molecular conduction in particular systems (e.g., [54–59]). An alternative approach [60–63] is to use qualitative models to focus on generic types of conduction behaviour. This approach is explored in Chapter 4. A starting point for theoretical accounts of this type of conduction is the study of molecular conjugated structures, where electron transmission is known to be a sensitive function of, amongst others, three major factors, namely, electron energy, contact position and underlying molecular structure. As mentioned above, this field has a long history, and methods continue to develop [20]. Carbon frameworks offer the required versatility to realise most of the common functional elements in digital electronic circuits that molecules are supposed to mimic, namely, conducting wires, insulators, switches, storage elements, ... Possible carbon frameworks that qualify for this realisation include graphite, diamond, graphene, molecules like the cage-shaped fullerenes and the quasi one-dimensional nanotubes [11].

This section discusses, but not exhaustively, some standard theoretical techniques that are used to describe the transport in molecular systems. One of these techniques is the scattering or Landauer approach, which provides an appealing framework to describe coherent transport in nanostructures. Rolf Landauer put forward this approach in the late 1950's [64]: if one can ignore inelastic interactions, a transport problem can always be viewed as a scattering problem, that is, in practice, transport properties like the electrical conductance are intimately related to the transmission probability for an electron to cross the system. Experiments in mesophysics [19] (systems in the range of 100nm to 1000nm), in the 1980s, showed that contacts play an important role and should not be considered as minor distractions. Landauer's model gained popularity in these years. In this model, the conductor itself is assumed to be a wire free of all interactions: irreversibility and dissipation arise from the connection to the contacts. This model seems relevant to the modelling of electronic devices as they scale down to atomic dimensions [19]. In spite of being one of the most popular theoretical formalisms to describe the coherent transport in nanodevices, the scattering approach has limitations [11]:

- (i) It gives no hints on how to compute the actual transmission of an atomic contact or a molecular circuit, unless it is combined with simple models, or with more sophisticated techniques such as random matrix theory [65]. Then the scattering approach can predict the transport properties of a great variety of systems such as diffusive wires, chaotic cavities, superconducting nanostructures, resonant tunnelling systems, tunnel junctions, *etc.*
- (ii) It is a one-electron theory which is valid only as long as inelastic scattering processes can be neglected.

The theoretical description of transport where inelastic scattering plays an important role can be achieved through Green's function techniques, as they can calculate the elastic transmission of real systems such as atomic and molecular junctions, and, can generalise the Landauer formula to take into account correlation effects and inelastic mechanisms. The Green's function theory is an elegant, formally complete solution to the non-equilibrium transport problem, and is used widely in theoretical physics [11,66]. It can be formulated to include explicit electron-electron interaction.

Ratner, Reuter, Solomon and others based their work on the Green’s function theory [56,67]. They explored various aspects of multichannel transport by considering the limit of weak coupling between two single channel molecular conductors based on the Green’s function approach applied within a tight–binding model. This tight–binding model is an approach to the calculation of electronic band structure using an approximate set of wavefunctions based upon superposition of wavefunctions for isolated atoms located at each atomic state. The Green’s function theory is not considered any further here but Fowler *et al.* show in [68] that it becomes equivalent to the theory that will be used in the present study when electron interactions are neglected.

The theoretical method that will be exploited in this thesis to describe molecular electronic devices (MEDs) is the graph theoretical source–and–sink potential (SSP) model, which is a simple approach devised by Ernzerhof in [69] for dealing with π systems. The SSP model will be described in detail in Chapter 2, which deals with both Ernzerhof’s original formulation and the graph–theoretical version that has been central to the work of the Sheffield group. It can be used to test for ballistic conduction in single–molecule conductors. It gives information about the influence of molecular structure and contact position during ballistic conduction. In particular, the possibility that some molecular structures may display a much reduced dependence of the predicted transmission on precise positioning of the contacts is investigated in Chapter 4. Given the difficulties of attaching ‘wires’ with atomic resolution, such insensitivity may have some practical advantages, and this motivates the definitions of omni–conductors and omni–insulators and the search for classes of chemical graphs that conform to these definitions. As has been discussed in work by Pickup and Fowler [68,70], a conjugated molecule is a “molecular wire” that connects input and output reservoirs of electrons which are connected by metallic wires, that is, a semi–infinite linear chain of atoms (see Fig. 1.3). The work of Fowler *et al.* [70] classifies molecular devices within Ernzerhof’s [69] SSP model according to the change in the number of NBOs obtained on deleting the connection vertices from the graph of the molecule. In the light of the partition of vertices into the three types according to the change in the number of NBOs on deletion [71], the selection rules given in [70] take on a new interpretation. For instance, the vertex type of the connection vertex (see Table 1.3) determines conductivity properties and identifies structural requirements for conduction or insulation.

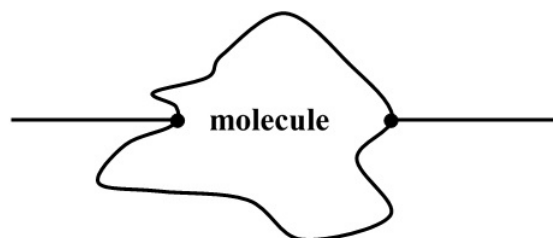


Figure 1.3: Schematic representation of a molecule. The circles represent the selection of two connection vertices to which semi–infinite wires are connected.

1.5 Hückel molecular orbital theory

References [72–74] have been used extensively in order to compile this section.

Vertex type	Graph theory	Chemistry
Core vertex	A vertex corresponding to a non-zero entry for some kernel eigenvector [2]	Non-zero charge density contribution
Core-forbidden vertex	A vertex corresponding to a zero entry in every kernel eigenvector	Zero charge density contribution

Table 1.3: Partitioning of vertices for singular graphs: graphical and chemical interpretation.

In 1931, Erich Hückel developed a very simple form of molecular orbital theory which has proved to be extremely valuable for correlating the properties of unsaturated organic molecules that undergo a wide variety of reactions [73]. We can consider the construction of π molecular orbital energy level diagrams of conjugated molecules by formalising the assumptions used by Hückel. The π orbitals are treated separately from the σ orbitals, where the latter form a rigid framework that determines the general shape of the molecule. All the C atoms are treated identically, so all the Coulomb integrals α for the atomic orbitals that contribute to the π orbitals are set equal. These are negative and represent the energy of the electron. As we shall see the main key points of the Hückel approximation are the following [72]

- (i) The method neglects overlap, such that the negative resonance integral β vanishes. It also neglects interactions between atoms that are not neighbours.
- (ii) It is expressed in a compact manner by introducing matrices.
- (iii) The strength of the π bonding in conjugated systems is expressed by the π -binding energy, the delocalisation energy and the π -bond formation energy.

In quantum chemistry, a useful method for finding approximations to the ground-state wavefunction, when the Schrödinger equation cannot be solved exactly, is the application of the Variation Principle. This principle states that if an arbitrary wavefunction is used to calculate the energy, the value calculated is never less than the true energy. This leads to

$$\tilde{E} = \langle \tilde{\psi} | \hat{H} | \tilde{\psi} \rangle \geq E_0 \quad (1.1)$$

which is a statement that the expectation value of the Hamiltonian for any normalised trial wavefunction $\tilde{\psi}$ must be greater than or equal to the actual ground state energy, E_0 [75]. We are using Dirac bra-ket notation for wavefunctions, so that $\langle \tilde{\psi} | \hat{H} | \tilde{\psi} \rangle$ is shorthand for the integral of the function $\tilde{\psi}^* \hat{H} \tilde{\psi}$, taken over all space. A useful form for the trial wavefunction $\tilde{\psi}$ is often a linear combination of n known basis functions χ_r

$$|\tilde{\psi}\rangle = \sum_{r=1}^n c_r |\chi_r\rangle \quad (1.2)$$

In what follows, it will be assumed for simplicity that c_r are real numbers and that all basis functions are real. The first restriction will need to be lifted when we consider conducting systems. Here r and s are vertex indices. If the basis is orthonormal $\langle \chi_r | \chi_s \rangle = \delta_{rs}$, where δ_{rs} is the Kronecker delta, equal to one if $r = s$ and zero otherwise, then normalisation of the trial wavefunction gives

$$\langle \tilde{\psi} | \tilde{\psi} \rangle = \sum_{r,s=1}^n c_r c_s \langle \chi_r | \chi_s \rangle = \sum_{r=1}^n |c_r|^2 = 1 \quad (1.3)$$

For a basis of non-orthogonal functions

$$\langle \tilde{\psi} | \tilde{\psi} \rangle = \sum_{r,s=1}^n c_r c_s \mathbf{S}_{rs} \quad (1.4)$$

where the overlap matrix element is $\mathbf{S}_{rs} = \langle \chi_r | \chi_s \rangle$, with $\mathbf{S}_{rs} = \mathbf{S}_{sr}$ for real functions.

In a similar way, the expectation value can be written in terms of the Hamiltonian matrix elements, $\langle \chi_r | \hat{H} | \chi_s \rangle = \mathbf{H}_{rs}$, as

$$\langle \chi_r | \hat{H} | \chi_s \rangle = \left\langle \sum_{r=1}^n c_r \chi_r \middle| \hat{H} \middle| \sum_{s=1}^n c_s \chi_s \right\rangle = \sum_{r,s=1}^n c_r c_s \langle \chi_r | \hat{H} | \chi_s \rangle = \sum_{r,s=1}^n c_r c_s \mathbf{H}_{rs} \quad (1.5)$$

Now the utility of the Variation Principle becomes clear. If \tilde{E} is always greater than or equal to the exact energy, then it is possible to define the best approximate wavefunction of a given form by minimising \tilde{E} with respect to all embedded parameters. In the case of a linear combination Eq. (1.2), this amounts to requiring $(\partial \tilde{E} / \partial c_r)$ to vanish for $r = 1, \dots, n$.

The minimisation is carried out using the method of Lagrange multipliers [76] to incorporate the normalisation constant.

$$\mathcal{L} = \sum_{r,s=1}^n c_r c_s \mathbf{H}_{rs} - E \sum_{r,s=1}^n c_r c_s \mathbf{S}_{rs} \quad (1.6)$$

Partial differentiation of the function $\mathcal{L}(c_1 \dots c_n, E)$ with respect to c_r , noting that \tilde{E} is stationary, gives an equality for every $r = 1, 2, \dots, n$

$$\frac{\partial \mathcal{L}}{\partial c_r} = \sum_{s=1}^n c_s \mathbf{H}_{rs} + \sum_{s=1}^n c_s \mathbf{H}_{sr} - 2E \sum_{s=1}^n c_s \mathbf{S}_{sr} = 0 \quad (1.7)$$

and by the Hermitian property of the Hamiltonian, this reduces to

$$\sum_{s=1}^n c_s (\mathbf{H}_{rs} - E \mathbf{S}_{rs}) = 0 \quad (1.8)$$

Thus, we have a square array of “secular equations”, which is suitably expressed as a single matrix equation. By setting up these secular equations and calculating the secular determinant, the coefficients c_s can be found. The secular determinant is solved for the energies which in turn are used in the secular equations to find the coefficients of the atomic orbitals for each molecular orbital. In Hückel theory, the variation method is applied to each molecular orbital. The molecular orbitals will be labelled ψ_i , $i = 1, \dots, n$ and the functions used to approximate them will be labelled χ_r , $r = 1, \dots, n$ where χ_r is a p_π orbital on centre r . The equivalent of Eq. (1.2) is then

$$\psi_i = \sum_{r=1}^n c_r^{(i)} \chi_r \quad (1.9)$$

where the coefficients $c_r^{(i)}$ are specific to orbital i .

In this case \hat{H} now stands for an effective Hamiltonian operator, applicable to each orbital in turn, and the energies that emerge will be orbital energies. Thus, for an n -centre π system, \mathbf{H} is the $n \times n$ matrix of the Hamiltonian in the basis of atomic p_π functions, \mathbf{S} is the overlap matrix in that basis, E is the orbital energy to be found and \mathbf{c} is the vector of the coefficients for that orbital. From the minimisation with respect to each coefficient in each molecular orbital ψ_i , we find n equations

$$\begin{aligned} c_1(\mathbf{H}_{11} - E\mathbf{S}_{11}) + c_2(\mathbf{H}_{12} - E\mathbf{S}_{12}) + \dots + c_n(\mathbf{H}_{1n} - E\mathbf{S}_{1n}) &= 0 \\ c_1(\mathbf{H}_{21} - E\mathbf{S}_{21}) + c_2(\mathbf{H}_{22} - E\mathbf{S}_{22}) + \dots + c_n(\mathbf{H}_{2n} - E\mathbf{S}_{2n}) &= 0 \\ &\vdots \\ c_1(\mathbf{H}_{n1} - E\mathbf{S}_{n1}) + c_2(\mathbf{H}_{n2} - E\mathbf{S}_{n2}) + \dots + c_n(\mathbf{H}_{nn} - E\mathbf{S}_{nn}) &= 0 \end{aligned} \quad (1.10)$$

where the superscript (i) is to be understood for each c_r , and the subscript i for each E .

These equations could now be solved numerically, case by case, given a basis of p_π functions in explicit form and a molecular geometry, but Hückel introduced a set of simplifying assumptions which allow a qualitative solution of the problem in general.

First, it can be noted that the overlap between parallel p_π functions is a rapidly diminishing function of distance between the atomic centres, owing to the exponential form of the wavefunctions. The assumption made by Hückel is that this overlap can be ignored, to a first approximation, and hence

$$\mathbf{S}_{rs} = \delta_{rs} \quad (1.11)$$

so that, the atomic p_π basis is effectively already orthonormal.

Other assumptions are made for the Hamiltonian in the linear equations (1.10). The first is for the matrix elements of the form \mathbf{H}_{rr} , which represent the Coulomb integrals (for example, the energy of a π electron isolated on a carbon atom of the molecule). Integrals of this type are assigned values α_r , and because the carbon atoms in a π system are similar, all diagonal matrix elements of \hat{H} are generally taken to have $\alpha_r = \alpha$ and hence $\mathbf{H}_{rr} = \alpha$. The second assumption is for the integrals

of the form \mathbf{H}_{rs} where r and s are not equal. In Hückel theory it is assumed that if r and s are adjacent the interaction will be non-zero, but otherwise it will be set equal to zero. These resonance integrals are assigned the value β_{rs} .

Using these assumptions, Eq. (1.10) is reduced to

$$\begin{aligned} c_1(\alpha_1 - E) + c_2\beta_{12} + \dots + c_n\beta_{1n} &= 0 \\ c_1\beta_{21} + c_2(\alpha_2 - E) + \dots + c_n\beta_{2n} &= 0 \\ &\vdots \\ c_n\beta_{n1} + c_2\beta_{n2} + \dots + c_n(\alpha_n - E) &= 0 \end{aligned} \tag{1.12}$$

In most cases $\alpha_r = \alpha$ for all r and $\beta_{rs} = \beta$ for all pairs connected by a σ bond. In the case of molecular devices, different β values will generally be used to distinguish the connections within the molecule from those between the molecule and the wire. The solution to Eqs (1.12) is given by requiring

$$\begin{pmatrix} \alpha_1 - E & \beta_{12} & \beta_{13} & \dots & \beta_{1n} \\ \beta_{21} & \alpha_2 - E & \beta_{23} & \dots & \beta_{2n} \\ \vdots & \vdots & \vdots & \vdots & \vdots \\ \beta_{n1} & \beta_{n2} & \beta_{n3} & \dots & \alpha_n - E \end{pmatrix} \begin{pmatrix} c_1 \\ c_2 \\ \vdots \\ c_n \end{pmatrix} = \mathbf{0} \tag{1.13}$$

and hence

$$\begin{vmatrix} \alpha_1 - E & \beta_{12} & \beta_{13} & \dots & \beta_{1n} \\ \beta_{21} & \alpha_2 - E & \beta_{23} & \dots & \beta_{2n} \\ \vdots & \vdots & \vdots & \vdots & \vdots \\ \beta_{n1} & \beta_{n2} & \beta_{n3} & \dots & \alpha_n - E \end{vmatrix} = 0 \tag{1.14}$$

Expanding this determinant leads to a polynomial equation of n^{th} degree, the n roots of which are the orbital energies. Substituting each orbital energy into the secular equations leads to the set of coefficients appropriate to each orbital.

The α (Coulomb) and β (resonance) parameters are of negative sign and have the units of energy. In general, α provides an origin and β provides a unit for the energy scale, and so for many purposes it is not necessary to assign particular numerical values. Hückel theory then becomes a purely graph-theoretical model because it depends only on the patterns of the σ bonds, that is, the positions of the edges in the molecular graph. Hückel theory can be used to give a qualitative characterisation of the forms of the π molecular orbitals, their relative energies, the populations and bond orders in the molecule and to predict trends in stability for different classes of molecules.

The electron density distribution can be analysed in terms of the molecular orbitals. Recall that the probability interpretation of the wavefunction leads to the normalisation condition for each molecular orbital

$$\int \psi_i^2 dV = 1 \tag{1.15}$$



Figure 1.4: The carbon skeleton for butadiene.

Using Eq. (1.2), this becomes

$$\int \left(\sum c_r^{(i)} \chi_r \right)^2 dV = 1 \quad (1.16)$$

in terms of the overlap integrals

$$\sum c_r^{(i)} c_s^{(i)} \mathbf{S}_{rs} = \sum c_r^{(i)} c_s^{(i)} \delta_{rs} = \sum (c_r^{(i)})^2 = 1 \quad (1.17)$$

Let us now set up and solve the matrix equations within the Hückel approximation for the π orbitals of butadiene, which in graph theoretical terms is the path on four vertices, Fig. 1.4. The adjacency matrix for the graph is

$$\mathbf{A} = \begin{pmatrix} 0 & 1 & 0 & 0 \\ 1 & 0 & 1 & 0 \\ 0 & 1 & 0 & 1 \\ 0 & 0 & 1 & 0 \end{pmatrix} \quad (1.18)$$

The secular equations are

$$\begin{aligned} xc_1 + c_2 &= 0 \\ c_1 + xc_2 + c_3 &= 0 \\ c_2 + xc_3 + c_4 &= 0 \\ c_3 + xc_4 &= 0 \end{aligned} \quad (1.19)$$

where $x = (\alpha - E)/\beta$, so that the orbital energy E is $\alpha - x\beta$. Note that the formulation in terms of the variable x , as is traditional in chemical accounts of Hückel theory, is equivalent to the spectral problem in graph theory. The value of x for the i th molecular orbital is equal to $-\lambda_i$, where λ_i is the eigenvalue of the adjacency matrix that corresponds to the eigenvector $(c_1^{(i)} \dots c_n^{(i)})^T$. Orbital energies are then $E_i = \alpha + \lambda_i\beta$. Positive values of x correspond to anti-bonding orbitals, and negative to bonding orbitals. $x = 0$ corresponds to the non-bonding level with energy α . To find the solutions of Eq. (1.19) note that either $\mathbf{c} = 0$ or

$$\begin{vmatrix} x & 1 & 0 & 0 \\ 1 & x & 1 & 0 \\ 0 & 1 & x & 1 \\ 0 & 0 & 1 & x \end{vmatrix} = 0 \quad (1.20)$$

Expanding this gives

$$x^4 - 3x^2 + 1 = 0 \quad (1.21)$$

which has solutions $x = \pm(1 + \sqrt{5})/2 = \pm\phi$ and $x = \pm(\sqrt{5} - 1)/2 = \pm\phi^{-1}$. If we take one of the solutions, say $x = -\phi$, and substitute it back into the secular Eqs (1.19) we have

$$\begin{aligned} c_2 &= \phi c_1 \\ c_3 &= -c_1 + \phi c_2 = \phi c_1 \\ c_4 &= -c_3/x = c_1 \end{aligned} \quad (1.22)$$

Normalisation requires

$$c_1^2 + c_2^2 + c_3^2 + c_4^2 = 1 \quad (1.23)$$

This gives $c_1 = a = \phi^{-1/2}/(\sqrt{2}\sqrt[4]{5}) \approx \pm 0.37$ but since the overall sign of a wavefunction has no physical significance, we can take the positive solution for c_1 . Hence, $c_2 = b = \phi^{1/2}/(\sqrt{2}\sqrt[4]{5}) \approx 0.60$, $c_3 = b$ and $c_4 = a$. Thus, the orbital energy is

$$E = \alpha + \phi\beta \quad (1.24)$$

and the corresponding molecular orbital is

$$\psi_1 = a\chi_1 + b\chi_2 + b\chi_3 + a\chi_4 \quad (1.25)$$

In a similar way, the remaining three orbital energies and molecular orbitals can be obtained to be as follows (see Fig. 1.5):

$$\begin{aligned} E_2 &= \alpha + \phi^{-1}\beta; & \psi_2 &= b\chi_1 + a\chi_2 - a\chi_3 - b\chi_4 \\ E_3 &= \alpha - \phi^{-1}\beta; & \psi_3 &= b\chi_1 - a\chi_2 - a\chi_3 + b\chi_4 \\ E_4 &= \alpha - \phi\beta; & \psi_4 &= a\chi_1 - b\chi_2 + b\chi_3 - a\chi_4 \end{aligned} \quad (1.26)$$

The molecular orbitals are mutually orthogonal and, with overlap neglected, normalised.

There are two important points to be noted about the butadiene orbitals. Firstly, they occur in pairs with energies $\alpha \pm x\beta$, and secondly, the coefficients of the paired orbitals are either the same or simply change sign. These are general properties of so-called alternant hydrocarbons, which are discussed in more detail in Chapter 5.

The sum of orbital energies is not equal to the total electronic energy, since, it does not take into consideration the details of electronic repulsion, but, there is a rough correlation between the two. For this reason the total Hückel energy of a molecule is a useful quantity.

An important point emerges when we calculate the total π -electron binding energy, E_π , the sum of the energies of each π electron, and compare it with that of ethene. In ethene, the total energy is

$$E_\pi = 2(\alpha + \beta) = 2\alpha + 2\beta \quad (1.27)$$

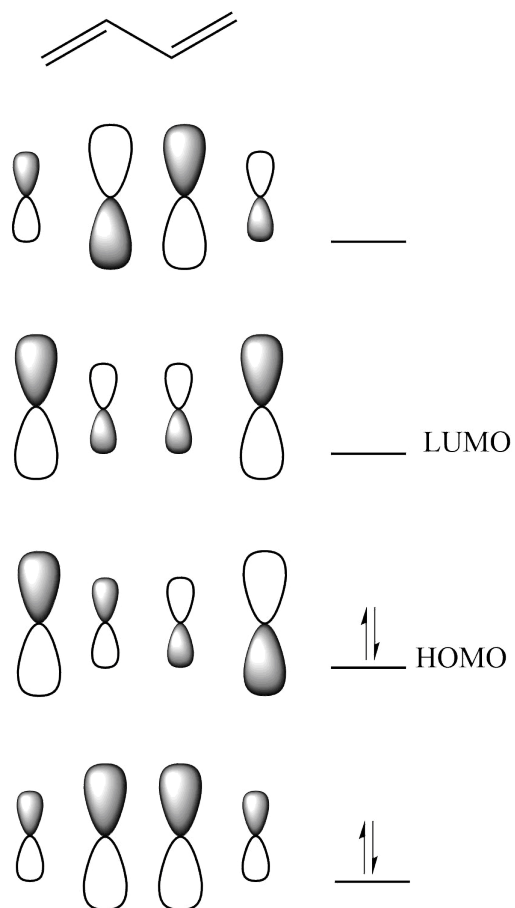


Figure 1.5: The Hückel molecular orbital energy levels of butadiene and the corresponding π orbitals, where the four p electrons (one supplied by each C) occupy the two lowest π orbitals, that are delocalised. The greater the number of internuclear nodes, the higher the energy of the orbital.

In butadiene it is

$$E_{\pi} = 2(\alpha + \phi\beta) + 2(\alpha + \phi^{-1}\beta) = 4\alpha + 2\sqrt{5}\beta \approx 4\alpha + 4.48\beta \quad (1.28)$$

Therefore, the energy of the butadiene molecule lies lower by $\approx 0.48\beta$ than the sum of the two individual π bonds. This extra stabilisation of a conjugated system compared with a set of localised π bonds is called the delocalisation energy of the molecule.

A closely related quantity is the π -bond formation energy, E_{bf} , the energy released when a π -bond is formed. Because the contribution of α is the same in the molecule as in the atoms, we can find the π -bond formation energy from the π -electron binding energy by writing

$$E_{bf} = E_{\pi} - N_C\alpha \quad (1.29)$$

where N_C is the number of C atoms in the molecules. The π -bond formation energy in butadiene is $\approx 4.48\beta$.

Hückel theory provides a method of correlating experimental results for a class of related compounds such that it provides simplified models for understanding chemistry. It is most useful when the class is large, and the parameters involved are few, otherwise to have a detailed understanding modern *ab initio* molecular methods must be used. The assumptions used in the Hückel theory are drastic and its limitations are that it is very approximate; it cannot calculate energies accurately (electron-electron repulsion is not calculated), and it typically overestimates predicted dipole moments. However, despite its utility, it is highly qualitative and can be extended to address other types of atoms in conjugated molecules. In the context of molecular junctions, at the end of the 1980s Sautet and Joachim pioneered the use of the tight-binding approach within the extended Hückel approximation to compute the current and conductance of single-molecule junctions [77, 78]. It can also be used to treat σ orbitals.

In the physics literature, Hückel theory is often referred to (as the simplest form of) the tight-binding approximation (TBA) [79]. In TBA, used for molecules and solids, the molecular or crystal orbitals are represented as linear combinations of well-localised basis functions. These functions may be represented explicitly and all integrals calculated, or they may be treated under the Hückel approximations, with all integrals represented by notional site and hopping parameters (equivalent to the Hückel α and β).

1.6 A note on programs

Programs in Fortran77 for graph construction and manipulations, and determination and classification of conduction behaviour were written by Prof. P.W. Fowler and modified where necessary by M. Borg. These are used throughout the thesis, for example in Chapters 4, 5 and 6. The program set within the Maple suite giving algebraic computations were written by Prof. B.T. Pickup and the results have been used in Chapters 4 and 7.

1.7 Conclusion

In spite of the different treatments of many research groups, there is still the need for a simple theory that captures the crucial global features of molecular conduction processes. This would help us understand whole classes of examples without the need of repeating experiments and/or calculations; consequently, universal explanations would be provided as opposed to calculations only. Nonetheless, the understanding of conduction on the nanoscale is a challenge because it includes, for example, dependence on the chemical structure of the molecules and the metal–molecule–metal bonding geometry. Thus, the nano–scale poses practical “soldering problems” at the connection vertices for a molecule. This means that the electronic transport in single molecules depends crucially on the exact coupling between the molecule and the metal electrodes, that is, on the precise atomic arrangement of the contacts. With the identification of omni–conductors and omni–insulators (see Chapter 4) the problem would be lessened as conduction and insulation, respectively, occurs independently of the connection vertex–pair on the molecule.

Chapter 2

Theoretical chemistry background

This chapter presents the theory of ballistic conduction in the form used in the rest of the thesis. It gives a detailed description of the source-and-sink potential (SSP) approach as developed in the Ernzerhof group [62], which was then applied at the Hückel level in the Sheffield group’s graph-theoretical SSP model [63] (Section 2.2).

The SSP approach was devised to treat the steady-state currents created by injecting ballistic electrons via external contacts into unsaturated π systems. This approach was then linked to graph-theoretical notions of molecular structure, to allow a fully analytical expression to be obtained for transmission as a function of electron energy and the placing of the contacts. The present chapter reviews these developments.

2.1 The Source-and-Sink Potential (SSP) Model

In the work of Ernzerhof *et al.* [62] an account of ballistic current in molecular devices is given and they show that the transport between reservoirs and through a molecule can be modelled by a source and sink potential, which can be implemented in the form of a tight-binding scattering theory. In this way, the development of a molecular orbital (MO) theory of MEDs is facilitated. The authors present a model Hamiltonian for the description of open systems where complex potentials act as source and sink, respectively, of probability current density. The applied voltage across a MED is always time dependent but it can be kept constant long enough such that a stationary current is obtained. The authors of [62] assume that this state is established by the boundary condition [80] of having an incoming travelling wave with a normalised amplitude in the left (electron emitting) contact as well as reflected wave that has been scattered off the molecule, whilst in the right (electron absorbing) contact, there is only an outgoing travelling wave. The left contact is assumed to be at a chemical potential μ_L , above the chemical potential μ_R of the right contact [62]. The model is restricted to non-interacting systems and so correlation effects are excluded. The main interest is to obtain the current (I) versus voltage (V) curve for a molecular conductor, or the differential conductance

$$g = \frac{dI}{dV} \tag{2.1}$$

In SSP, the transmission probability $T(E)$ is obtained from a direct calculation of the reflection coefficient r , which is the amplitude of the travelling wave reflected off the molecular scatterer. The key idea in SSP is that the asymptotic behaviour of the wavefunction in the left and right contacts (leads) are each specified in terms of a single parameter [62]. These parameters are the reflection coefficient r and the transmission coefficient t , respectively.

As mentioned in the previous chapter, Green's function theory is the usual way that is used to describe ballistic current in MEDs. The SSP method has some aspects in common with this theory. Both use a basis set of localised orthonormal functions and the system is partitioned into three parts: the left 'contact' (L), the supermolecule (M) and the right 'contact' (R). The authors of [62] use the term 'contacts' for what we will call 'leads' to avoid confusion with 'contact atoms' at the junctions of molecule and leads.



Figure 2.1: The partitioning of the system into three parts: a semi-infinite lead L on the left, a 'supermolecule' including finite clusters of contact atoms, and a semi-infinite lead R on the right (Figure adapted from [62]).

In SSP, the Hamiltonian matrix \hat{H} of the device can be written as

$$\hat{H} = \begin{pmatrix} \mathbf{H}_L & \mathbf{M}_{L,M} & \mathbf{0} \\ \mathbf{M}_{L,M}^\dagger & \mathbf{H}_M & \mathbf{M}_{M,R} \\ \mathbf{0} & \mathbf{M}_{M,R}^\dagger & \mathbf{H}_R \end{pmatrix} \quad (2.2)$$

where \mathbf{H}_L and \mathbf{H}_R are the Hamiltonian matrices for the contacts L and R , respectively, \mathbf{H}_M is the Hamiltonian matrix for the supermolecule, and $\mathbf{M}_{L,M}$ and $\mathbf{M}_{M,R}$ are the matrices describing the contact between L and M , and R and M , respectively. In this equation the adjoint matrix symbol \dagger denotes the Hermitian conjugate. The leads do not interact directly with each other. The aim is to describe the steady-state current through the device, and this will be done via construction of a device vector, with entries \mathbf{C}_L , \mathbf{C}_M , \mathbf{C}_R giving coefficients of the basis functions in regions L , M and R . These entries will necessarily be complex quantities as if all are real, current is identically zero. Thus, the eigenvalue equation for the required vectors is

$$\begin{pmatrix} \mathbf{H}_L & \mathbf{M}_{L,M} & \mathbf{0} \\ \mathbf{M}_{L,M}^\dagger & \mathbf{H}_M & \mathbf{M}_{M,R} \\ \mathbf{0} & \mathbf{M}_{M,R}^\dagger & \mathbf{H}_R \end{pmatrix} \begin{pmatrix} \mathbf{C}_L \\ \mathbf{C}_M \\ \mathbf{C}_R \end{pmatrix} = E \begin{pmatrix} \mathbf{C}_L \\ \mathbf{C}_M \\ \mathbf{C}_R \end{pmatrix} \quad (2.3)$$

In lead L , the wavefunction \mathbf{C}_L is a combination of forward (\mathbf{C}_L^+) and backward (\mathbf{C}_L^-) travelling waves. The left boundary condition is therefore

$$\mathbf{C}_L = \mathbf{C}_L^+ + r\mathbf{C}_L^- \quad (2.4)$$

where r is a reflection coefficient that is directly related to the transmission probability for electrons of energy E ,

$$T(E) = 1 - |r(E)|^2 \quad (2.5)$$

The right boundary condition is for an outgoing electron wave

$$\mathbf{C}_R = t\mathbf{C}_R^+ \quad (2.6)$$

where t is the transmission amplitude satisfying $T(E) = |t(E)|^2$.

We can consider the subsystem involving simultaneously \mathbf{C}_L , \mathbf{C}_M and \mathbf{C}_R (from Eq. (2.3)), which is described by

$$\mathbf{M}_{L,M}^\dagger \mathbf{C}_L + \mathbf{H}_M \mathbf{C}_M + \mathbf{M}_{M,R} \mathbf{C}_R = E \mathbf{C}_M \quad (2.7)$$

To solve Eq. (2.7) for \mathbf{C}_M , the part of the device wavefunction that determines current inside the molecule, \mathbf{C}_L and \mathbf{C}_R must be eliminated. To do this, artificial source and sink potentials are introduced. Ernzerhof *et al.* write these as

$$\boldsymbol{\Sigma} = \boldsymbol{\Sigma}_L + \boldsymbol{\Sigma}_R \quad (2.8)$$

and define them so that they can replace \mathbf{C}_L and \mathbf{C}_R in Eq. (2.7) with effective terms depending only on \mathbf{C}_M

$$\mathbf{M}_{L,M}^\dagger \mathbf{C}_L = \boldsymbol{\Sigma}_L \mathbf{C}_M \quad (2.9)$$

and

$$\mathbf{M}_{M,R} \mathbf{C}_R = \boldsymbol{\Sigma}_R \mathbf{C}_M \quad (2.10)$$

Here $\boldsymbol{\Sigma}_{L(R)}$ are blocks of a diagonal matrix $\boldsymbol{\Sigma}$ and their entries can be determined individually by inserting the last two equations, as

$$\Sigma_{L_{kk}} = \frac{(\mathbf{M}_{L,M}^\dagger \mathbf{C}_L)_k}{\mathbf{C}_{M_k}} \quad (2.11)$$

and

$$\Sigma_{R_{kk}} = \frac{(\mathbf{M}_{M,R} \mathbf{C}_R)_k}{\mathbf{C}_{M_k}} \quad (2.12)$$

With these substitutions, Eq. (2.7) defines the SSP Hamiltonian through

$$\hat{H}^{SSP}(E, r)\mathbf{C}_M = E\mathbf{C}_M \quad (2.13)$$

where the dependence of \hat{H}^{SSP} on E and r is made explicit. (In essence, this arises because Σ depends on \mathbf{C}_L and \mathbf{C}_R which in turn depend on $r(E)$.)

$$\hat{H}^{SSP}(E, r) = \mathbf{H}_M + \Sigma_L(E, r) + \Sigma_R(E) \quad (2.14)$$

In general, the unknown r in \mathbf{C}_L , and so in $\Sigma_L(E, r)$, can be obtained iteratively [62]. In this way the SSP method has built the boundary conditions into the effective Hamiltonian $\hat{H}^{SSP}(E, r)$. The SSP formalism can be applied to *ab initio* or density functional theory (DFT) calculations, and in fact was used in this way by Ernzerhof and co-workers [55, 81] before they gave the formal description in [62]. However, the main strength of the SSP method is that it can be adapted to the Hückel level, and hence to a pictorial and essentially graph-theoretical account of conduction, with all the advantages for interpretation that follow.

The Hückel approximations enter the SSP model of the MED in three places. They are used in the treatment of the leads, to describe \mathbf{C}_L and \mathbf{C}_R in terms of r and E ; they can be used within the molecule, to simplify \mathbf{H}_M ; they also define the contact terms $\mathbf{M}_{L,M}$ and $\mathbf{M}_{M,R}$.

We imagine the lead $L(R)$ to consist of a chain of atoms where β_L is the nearest-neighbour hopping matrix element (resonance integral) and diagonal Coulomb matrix elements are α_L (α_R). In each lead β_L (β_R), the wavefunctions are combinations of plane waves e^{iqn} and e^{-iqn} , where n indexes the atoms. In [62], the indexing convention is that the rightmost atom of lead L has index n .

The complex potentials in the two leads are therefore defined by their roles in the secular equations for top and bottom blocks of Eq. (2.3).

These blocks are

$$\mathbf{H}_L\mathbf{C}_L + \mathbf{M}_{L,M}\mathbf{C}_M = E\mathbf{C}_L \quad (2.15)$$

and

$$\mathbf{M}_{M,R}^\dagger\mathbf{C}_M + \mathbf{H}_R\mathbf{C}_R = E\mathbf{C}_R \quad (2.16)$$

The final row of the block Eq. (2.15) involves the penultimate atom of lead L , the final atom of lead L and the first atom of the molecule (call it \bar{L}).

From the asymptotic behaviour in the lead we know the ratio of entries on the last two lead atoms and so we can replace the whole effect of lead L by the complex potential Σ_L , with

$$\frac{\Sigma_L}{\beta_L} = \frac{(C_L)_{n-1}}{(C_L)_n} = \frac{e^{iqL(n-1)} + re^{-iqL(n-1)}}{e^{iqLn} + re^{-iqLn}} = \frac{e^{-iqL} + \tilde{r}e^{iqL}}{1 + \tilde{r}} \quad (2.17)$$

where $\tilde{r} = e^{-2iq_L n} r$. As multiplication of r by any complex number of unit modulus can have no effect on the physical current, Ernzerhof then drops the tilde from \tilde{r} in all further working. This slightly clumsy device can be avoided by numbering outwards from the molecule (in both leads) [82].

Likewise, the block Eq. (2.16) gives

$$\frac{\Sigma_R}{\beta_R} = e^{iq_R} \quad (2.18)$$

In these equations, the wavenumbers q_L and q_R are related to E , the energy of the incoming electron by the Hückel dispersion relations

$$\begin{aligned} E &= \alpha_L + 2\beta_L \cos(q_L) \\ &= \alpha_R + 2\beta_R \cos(q_R) \end{aligned} \quad (2.19)$$

The link between molecule and lead L , and molecule and lead R are both described at Hückel level with appropriate hopping matrix elements, and within the molecule itself the usual Hückel Hamiltonian is applied.

In [62], the Hückel version of the SSP Hamiltonian is used to find the reflection coefficient by an iterative method. In fact, a fully analytical solution is possible, as is shown by the work of Pickup and Fowler [63] described in the following section.

2.2 The SSP model and characteristic polynomials

The first article by the Sheffield group on the graph theoretical approach to SSP [63] discusses the derivation of a general formula for a transmission of electrons through a molecule, as a function of the energy, expressed in terms of purely graph theoretical quantities. This follows from the Hückel approximations made in the previous section. Specifically, the authors of [63] consider a molecular π system that has a carbon skeleton with an adjacency matrix \mathbf{A} , where $A_{ij} = 1$ if $i \neq j$, and i bonded to j , and $A_{ij} = 0$ otherwise. The Hückel Hamiltonian for the isolated molecule is then

$$\mathbf{H}^M = \alpha \mathbf{1} + \beta \mathbf{A} \quad (2.20)$$

where α and β are the usual Coulomb and resonance integrals. The model device consists of the molecule with a pair of semi-infinite wires (1-dimensional chains) attached to it. Molecule and wires will be represented by graphs with vertices for atoms and edges for σ bonds. The molecular graph has n vertices, and m internal edges. Left and right wires are then in contact with the molecule through single distinct wire vertices labelled L and R , and the contacting vertices in the molecule are labelled \bar{L} and \bar{R} (Fig. 2.2 (a)). The ballistic electron is represented by a

wave (Fig. 2.2 (b)). Hückel parameters for the leads are (α_L, β_L) and (α_R, β_R) , respectively, leading to band energies from $\alpha_L + 2\beta_L$ to $\alpha_L - 2\beta_L$ and $\alpha_R + 2\beta_R$ to $\alpha_R - 2\beta_R$, respectively (Fig. 2.2 (c)). The molecule–lead links are single edges with parameters $\beta_{L\bar{L}}$ and $\beta_{R\bar{R}}$, respectively (Fig. 2.2 (c)).

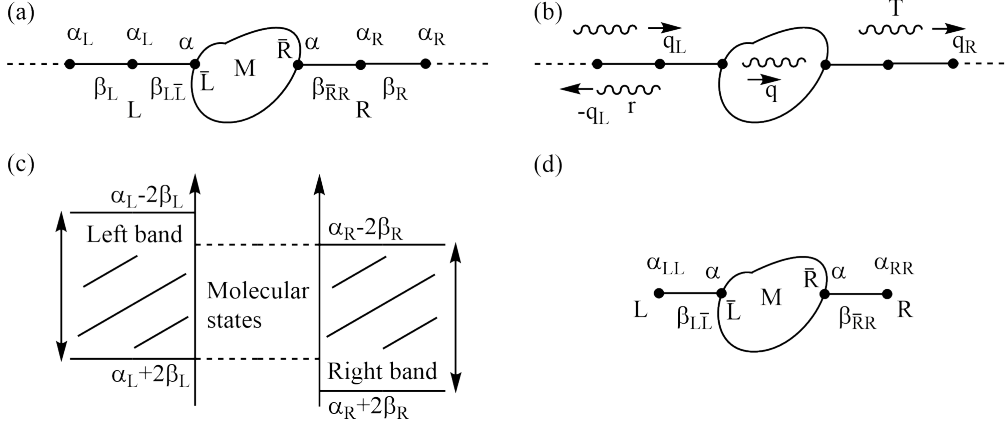


Figure 2.2: A schematic molecular electronic device. (a) Parametrisation of molecule and leads; (b) wavevectors of incoming, reflected and transmitted waves; (c) energy level scheme with range of transmission indicated by dotted lines; (d) the graph used in the SSP method. Adapted from [63].

As noted in the general description given earlier of the SSP model, the leads are replaced by single source and sink atoms bearing effective (complex) potentials, and so in this graph–theoretical formulation the MED is represented by a graph with $n + 2$ vertices and m edges (Fig. 2.2 (d)).

2.2.1 The SSP Hamiltonian and solution of the Schrödinger equation for MEDs

In [63] the SSP Hamiltonian is rewritten in a block form where rows 1 to n refer to the molecule, row $n + 1$ to the source, L , and row $n + 2$ to the sink, R :

$$\mathbf{H}^{SSP} = \begin{pmatrix} \mathbf{A} & \beta_{L\bar{L}}\mathbf{e}_{\bar{L}} & \beta_{R\bar{R}}\mathbf{e}_{\bar{R}} \\ \beta_{L\bar{L}}\mathbf{e}_{\bar{L}}^+ & a_{LL} & 0 \\ \beta_{R\bar{R}}\mathbf{e}_{\bar{R}}^+ & 0 & a_{RR} \end{pmatrix} \quad (2.21)$$

The column vectors in the border are unit vectors given by $(\mathbf{e}_{\bar{L}}) = \delta_{\bar{L}i}$ and $(\mathbf{e}_{\bar{R}}) = \delta_{\bar{R}i}$ which represent the two single–edge connections between the external and internal contact vertices.

The contact matrix elements of \mathbf{H}^{SSP} are [63]

$$a_{RR} = \alpha_R + \beta_R e^{iqR} \quad (2.22)$$

and

$$a_{LL} = \alpha_L + \beta_L \frac{\mathbf{e}^{-iqL} + r\mathbf{e}^{iqL}}{1+r} \quad (2.23)$$

respectively, where r is the reflection coefficient defined in [62].

The SSP Schrödinger equation for the device wavefunction

$$(E\mathbf{1} - \mathbf{H}^{SSP})\mathbf{c} = \mathbf{0} \quad (2.24)$$

contains a fixed energy (E), and the required eigenvector is \mathbf{c} , which depends on E and r as discussed above. The solution is found by equating the determinant $\det(E\mathbf{1} - \mathbf{H}^{SSP})$ to zero.

The equations of the full SSP method are solved analytically in [63] by expanding the secular determinant along the rows and columns of the border. Hence, the determinantal condition is the “quadratic equation”

$$(E - a_{LL})(E - a_{RR})s + \beta_{LL}^2\beta_{RR}^2v - \beta_{LL}^2(E - a_{RR})t - \beta_{RR}^2(E - a_{LL})u = 0 \quad (2.25)$$

where s , t , u and v are minors of the molecular secular determinant

$$\begin{aligned} s(E) &= \det(E\mathbf{1} - \mathbf{A}) \\ t(E) &= \det(E\mathbf{1} - \mathbf{A})^{\bar{L},\bar{L}} \\ u(E) &= \det(E\mathbf{1} - \mathbf{A})^{\bar{R},\bar{R}} \\ v(E) &= \det(E\mathbf{1} - \mathbf{A})^{\bar{L}\bar{R},\bar{L}\bar{R}} \end{aligned} \quad (2.26)$$

in a notation [83] where the superscripts define the removed rows and columns. For example, $\mathbf{M}^{[i_1\dots i_2, j_1\dots j_2]}$ is a matrix \mathbf{M} from which rows $i_1\dots i_2$ and columns $j_1\dots j_2$ have been deleted. The quantities s , t , u , and v , are then the characteristic polynomials of four graphs: those of the molecule (s), the molecule with vertex \bar{L} deleted (t), with vertex \bar{R} deleted (u) and with both \bar{L} , \bar{R} deleted (v). The authors of [63] note that through these four fundamental polynomials, the solutions of Eq. (2.25) depend on both the internal structure of the molecule, and on the way in which it is connected to the contact wires. They also define ‘scaled’ polynomials to simplify the writing of further equations. These are

$$\begin{aligned} \tilde{s} &= s \\ \tilde{t} &= \tilde{\beta}_L t \\ \tilde{u} &= \tilde{\beta}_R u \\ \tilde{v} &= \tilde{\beta}_L \tilde{\beta}_R v \end{aligned} \quad (2.27)$$

with scaling parameters

$$\begin{aligned} \tilde{\beta}_L &= \beta_{LL}^2 / \beta_L \\ \tilde{\beta}_R &= \beta_{RR}^2 / \beta_R \end{aligned} \quad (2.28)$$

expressing the relative strengths of bonds within and between the wire and the molecule (Fig. 2.2 (a)). With the typical parameter choices made in [62], $\tilde{\beta}^2$ is about $\frac{1}{2}$. It is apparent from the structure of a_{LL} that Eq. (2.25) can be converted to an equation linear in r , by multiplying throughout by $1 + r$. The analytical solution presented in [63] is

$$r(E) = -\frac{e^{iq_L}F - G}{e^{-iq_L}F - G} \quad (2.29)$$

where

$$\begin{aligned} F &= e^{-iq_R}\tilde{s} - \tilde{u} \\ G &= e^{-iq_R}\tilde{t} - \tilde{v} \end{aligned} \quad (2.30)$$

It follows that r is fully determined by the energy, through q_L, q_R (where $0 \leq q_L, q_R \leq \pi$) and the four characteristic polynomials s, t, u and v . The transmission factor is [62, 63]

$$T(E) = 1 - |r(E)|^2 \quad (2.31)$$

The expression for T is obtained by substitution of Eq. (2.29) in Eq. (2.31), and after some algebra, the following expression is obtained

$$T(E) = \frac{4 \sin q_L \sin q_R (\tilde{u}\tilde{t} - \tilde{s}\tilde{v})}{|\mathbf{e}^{-i(q_L+q_R)}\tilde{s} - \mathbf{e}^{-iq_R}\tilde{t} - \mathbf{e}^{-iq_L}\tilde{u} + \tilde{v}|^2} \quad (2.32)$$

The degenerate (*ipso*) case $\bar{L} = \bar{R}$, where left and right leads are connected to the same atom $L = R$, follows by setting $v = 0$ and $u = t$.

Eq. (2.32) makes explicit the dependence of transmission on both molecular skeleton and its mode of connection. The term $4 \sin q_L \sin q_R$ in the numerator is non-negative, as the angles satisfy $0 \leq q_L, q_R \leq \pi$, and it acts as what the authors of [63] call a “band-pass” filter, cutting off transmission at the ends of the range defined by the intersection of left and right conduction bands.

In another article [69], Ernzerhof defined the wide-band limit (WBL). In the WBL, the width of the conduction bands in the leads is assumed to be large compared to the spread of molecular energies, so that effectively all wavevectors q can be taken to have the constant value of $\frac{\pi}{2}$ and then Eq.(2.29) becomes

$$r_{WBL}(E) = \frac{(\tilde{s} + \tilde{v}) - i(\tilde{u} - \tilde{t})}{(\tilde{s} - \tilde{v}) - i(\tilde{u} + \tilde{t})} \quad (2.33)$$

and the transmission takes the form [63]

$$T_{WBL}(E) = \frac{4(\tilde{u}\tilde{t} - \tilde{s}\tilde{v})}{(\tilde{s} - \tilde{v})^2 + (\tilde{u} + \tilde{t})^2} \quad (2.34)$$

This expression coincides with the exact Eq. (2.32) for $E = 0$, the Fermi level energy, and is often more convenient to use.

2.3 Extreme values of the transmission function

Having achieved an expression for $T(E)$ in Eq. (2.32) which depends on both the molecular skeleton and its mode of connection, it is now possible to discuss the properties of such a function for $T(E)$ [63]. Considering the factor $(\tilde{u}\tilde{t} - \tilde{s}\tilde{v})$ within the numerator, it can be remarked that it is a concealed square, since by applying the Jacobi/Sylvester determinant identity [83] to the unscaled polynomials (see Appendix 2, [83]),

$$\tilde{u}\tilde{t} - \tilde{s}\tilde{v} = \tilde{\beta}_L\tilde{\beta}_R(ut - sv) = \tilde{\beta}_L\tilde{\beta}_R(\det(E\mathbf{1} - \mathbf{A})^{\bar{L}\bar{R}})^2 \quad (2.35)$$

The right-hand side of Eq. (2.35) is expressed in later work [82, 84] as the square of a polynomial $\tilde{j}^2 = \tilde{\beta}_L\tilde{\beta}_R j^2$ with j^2 called the opacity polynomial, and sometimes denoted Op . The denominator is also non-negative, and $T(E)$ as defined by Eq. (2.32) satisfies $T(E) \geq 0$. Since $|r|^2 \geq 0$, it follows that $T(E) \leq 1$. The transmission factor given by Eq. (2.32) is even in E for bipartite graphs (alternant hydrocarbons) since the vertex-deleted subgraphs of a bipartite graph are bipartite, too. This aspect is discussed in further detail in Chapter 5.

The transmission factor is typically a strongly varying function of E [63] as it is a ratio of high-order polynomials. Perfect opacity is achieved when $T(E) = 0$ and requires the vanishing of the numerator of Eq. (2.32) and the reflection coefficient, r , to have unit modulus. This occurs when $\tilde{u}\tilde{t} - \tilde{s}\tilde{v}$ vanishes, within the allowed energy range. The opacity condition has no dependence on the β resonance parameters that describe the semi-infinite leads. The authors of [63] list six cases for which $T(E) = 0$. These depend on which of the characteristic polynomials s , t , u and v are equal to zero.

For perfect transparency, $r = 0$ such that $T(E) = 1$ and the ballistic electron passes through the molecule π system without any hindrance. In this case, the authors of [63] note that the conditions are given by the vanishing of real and imaginary parts of the numerator and this leads to three possible cases for which $T(E) = 1$.

The authors of [63] also comment on the results of $T(E)$ for linear chains and rings, which both have characteristic polynomials with very simple analytical expressions, which are given explicitly for the case of symmetric connections ($\alpha_L = \alpha_R = 0$, $\beta_L = \beta_R = \beta_C$, and $\beta_{L\bar{L}} = \beta_{R\bar{R}} = \beta$, with $\beta_C = \gamma\beta$ where γ is often taken to be 1.4 [63]). Using the characteristic polynomial of a linear chain, it is possible to find the opacity and transparency points by using the simple form of the combination $ut - sv$. The results in [63] show that the opacity points depend only on the positions of the connection and perfect transparency is determined by both topology of the molecule and its connections, as well as the parameters of the semi-infinite leads (see Fig. 2.3). For the case of rings, opacity depends on the number of vertices, or ring size, and connection topology (see Fig. 2.4).

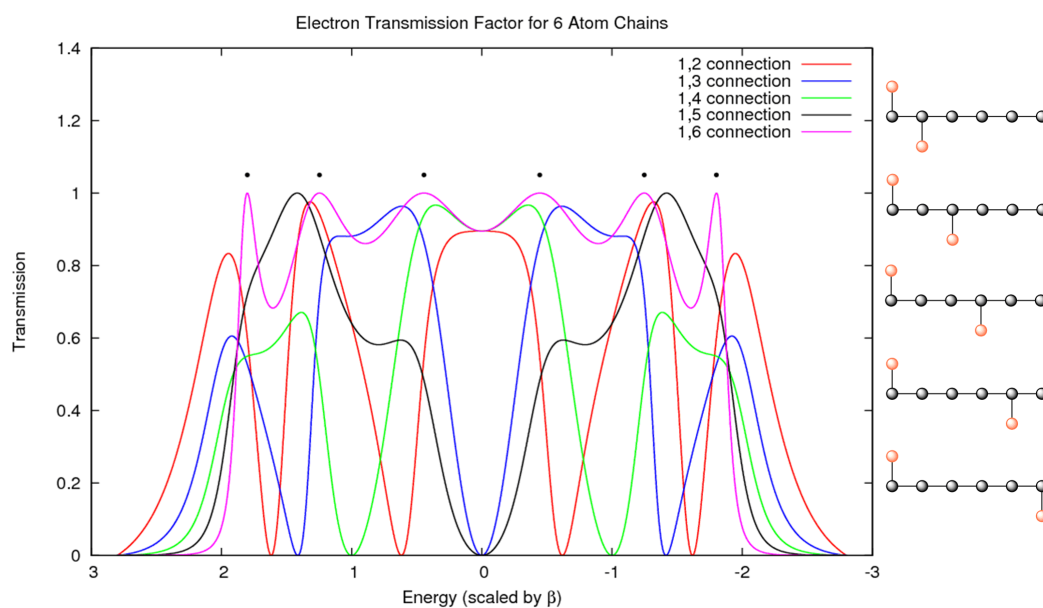


Figure 2.3: Transmission curves for six-membered chains. Curves for each connection pattern are distinguished by colours as given in the key. Molecular eigenvalues are shown as solid circles. (A similar figure for five-membered chains is given in [63].)

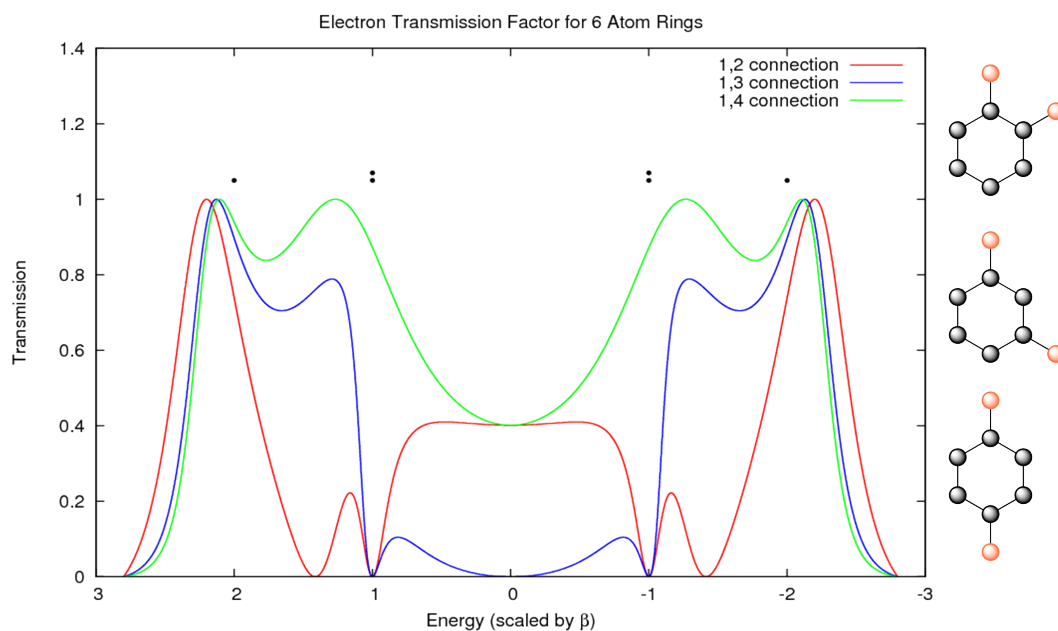


Figure 2.4: Transmission curves for six-membered rings. Curves for each connection pattern are distinguished by colours as given in the key. Molecular eigenvalues are shown as solid circles (Figure adapted from [63]).

2.4 Selection rules for conduction in MEDs

In further work of Fowler and co-workers [70], an account is given of how Eq. (2.32) can be used to find the conditions for transmission of a π -conjugated molecular conductor in terms of numbers of zero adjacency eigenvalues of four graphs: the molecular graph G and the three vertex-deleted subgraphs obtained by removing one or both contact vertices. This is equivalent in chemical terms to the counting of non-bonding orbitals for the corresponding π systems. This gives a simple necessary and sufficient condition for conduction at the Fermi level, i.e. the conditions under which the right-hand side of Eq. (2.36) below vanishes. They are expressed entirely in terms of non-bonding orbitals by analysing the eigenvalue properties of the vertex-deleted subgraphs. The number of zero eigenvalues of the adjacency matrix of a graph (the nullity) is an invariant that is easily found without calculation of the full spectrum [6, 85]. Knowledge of the four nullities is all that is needed to decide whether $T(0)$ vanishes, except in the case that all four nullities are equal [70].

$$T(0) = \frac{4(u_0 t_0 - s_0 v_0) \tilde{\beta}^2}{(s_0 - \tilde{\beta}^2 v_0)^2 + (u_0 + t_0)^2 \tilde{\beta}^2} \quad (2.36)$$

where s_0 , t_0 , u_0 and v_0 are the values of the four characteristic polynomials at $E = 0$. In particular, they are the tail coefficients of the characteristic polynomials and each of them is zero if and only if the respective graph has at least one zero eigenvalue.

The determination of the selection rules works with the transmission function $T(E)$ in the limit of $E \rightarrow 0$. It is necessary to take limits, as the individual polynomials s , t , u and v may have $E = 0$ as a root.

Considering a general graph G , the four characteristic polynomials can be factored to display the zero roots explicitly, as

$$\begin{aligned} s(E) &= E^{g_s} s'(E) \\ t(E) &= E^{g_t} t'(E) \\ u(E) &= E^{g_u} u'(E) \\ v(E) &= E^{g_v} v'(E) \end{aligned} \quad (2.37)$$

where g_s , g_t , g_u , $g_v \geq 0$ are the multiplicities of the zero root and the remaining polynomials s' , t' , u' , v' take non-zero values s'_0 , t'_0 , u'_0 , v'_0 at $E = 0$.

By analysing the various combinations of g_s , g_t , g_u , g_v together with the vanishing of the opacity polynomial, the authors of [70] achieved a sufficient condition for the vanishing of $T(0)$. This leads to three cases at $E = 0$ depending on whether zero is a root of all or any of the four characteristic polynomials s , t , u and v . For the case when zero is a common root of all four of them, further investigation is required by taking into consideration the multiplicities of g_s , g_t , g_u , g_v . As stated in Section 3.1, Cauchy's Interlacing Theorem [86] imposes constraints on the range of values for the multiplicities of the vertex-deleted subgraphs g_t , g_u and g_v . These constraints and the parity restriction arising from the fact that the opacity polynomial is a

Case	g_s	g_t	g_u	g_v		$T(0)/(4\tilde{\beta}^2)$
1	g	$g+1$	$g+1$	$g+2$	All	0
2	g	$g+1$	$g+1$	g	All	$\frac{-s'_0 v'_0}{(s'_0 - \tilde{\beta}^2 v'_0)^2}$
3	g	$g+1$	g	$g+1$	Odd	0
4	g	$g+1$	g	g	Non	$\frac{-s'_0 v'_0}{(s'_0 - \tilde{\beta}^2 v'_0)^2 + (u'_0)^2 \tilde{\beta}^2}$
5	g	$g+1$	$g-1$	g	All	0
6	g	g	g	$g+1$	Non	$\frac{u'_0 t'_0}{(s'_0)^2 - (u'_0 + t'_0)^2 \tilde{\beta}^2}$
7	g	g	g	g	Non	$\frac{u'_0 t'_0 - s'_0 v'_0}{(s'_0 - \tilde{\beta}^2 v'_0)^2 + (u'_0 + t'_0)^2 \tilde{\beta}^2}$
8	g	g	$g-1$	$g-1$	Odd	0
9	g	$g-1$	$g-1$	g	All	$\frac{u'_0 t'_0}{(u'_0 + t'_0)^2 \tilde{\beta}^2}$
10	g	$g-1$	$g-1$	$g-1$	Non	$\frac{u'_0 t'_0}{((v'_0)^2 \tilde{\beta}^2 + (u'_0 + t'_0)^2) \tilde{\beta}^2}$
11	g	$g-1$	$g-1$	$g-2$	All	0

Table 2.1: Transmission and multiplicities of the zero eigenvalue. “Odd” refers to those cases where $u't' - s'v'$ has an odd number of zero roots. “All” refers to both bipartite and non-bipartite graphs. “Non” refers to non-bipartite graphs only [70].

square, lead to the 11 distinct cases listed by the authors of [70]. These cases are given in Table 2.1. If furthermore the graph G is bipartite, and we restrict attention specifically to eigenvalue zero, then the number of allowed combinations is reduced to five. Hence, as the authors of this study find [70], the general rule can be divided into four subrules according to whether the device is degenerate or non-degenerate, whether G is bipartite or non-bipartite, and whether counting is necessary or necessary and sufficient.

Their statement of the rules is as follows. Rule (i) states that for a bipartite graph, the system conducts at the Fermi level if and only if $g_s = g_v$ and $g_t = g_u$. If the graph is non-bipartite where G , $G - \bar{L}$, $G - \bar{R}$ and $G - \bar{L} - \bar{R}$ do not have the same number of zero eigenvalues, then the system conducts at the Fermi level if and only if $\min\{(g_s + g_v)/2, (g_t + g_u)/2\} = \min\{g_s, g_t, g_u, g_v\}$ – this is Rule (ii). In Rule (iii), G is non-bipartite with equal numbers of zero eigenvalues for all of G , $G - \bar{L}$, $G - \bar{R}$ and $G - \bar{L} - \bar{R}$, i.e., $g = g_t = g_u = g_v$ and the condition of Rule (ii) is automatically obeyed, and the system conducts at the Fermi level if and only if the opacity polynomial is non-vanishing, which, for $g = 0$, where all four graphs are non-singular, reduces to $u_0 t_0 - s_0 v_0 \neq 0$. Lastly, Rule (iv) states that for the degenerate *ipso* device, if G has zero eigenvalues, then $T(0) = 0$ for $g_t = g + 1$, $0 < T(0) < 1$ for $g_t = g$, and $T(0) = 1$ for $g_t = g - 1$, i.e. the device is opaque, conducting or completely transparent at the Fermi level, depending on whether $G - \bar{L} = G - \bar{R}$ has $g + 1$, g , or $g - 1$ zero eigenvalues, respectively. Hence, for the degenerate *ipso* device, the system conducts at the Fermi level if and only if $g_t \leq g$, which requires the connection vertex not to be an upper core-forbidden vertex (see Chapter 3).

The authors of [70] note that although the energy $E = 0$ is of most direct physical interest, the analysis applies for all roots ϵ of the Hückel problem, with replacement of E by $(E - \epsilon)$, and multiplicities g_s, \dots, g_v applying to the eigenvalue ϵ . Note that the reduction to five cases for bipartite graphs made in [87] applies only for eigenvalue zero as it relies on self-pairing of zero eigenvalue, under the Coulson–

Rushbrooke pairing theorem [5] (PWF personal communication). This helps to rationalise opacity features of the function $T(E)$ in the regions away from $E = 0$, although the possibility of accidental extra opacities must then be checked for any particular graphs. Fowler *et al.* [70] remark that the explicit expressions for $T(0)$ given in Table 2.1 can also be used to obtain simple conditions for perfect transparency at the Fermi level and relate them to counting of zero eigenvalues. The condition $T(0)$ will be equal to unity, independently of the value of the physical parameter $\tilde{\beta}$, if and only if $t'_0 = u'_0$ and $g_t = g_u = g_s - 1 = g_v - 1$. Restriction of the Fermi-level selection rule to bipartite graphs is considered in [87]. Essentially, the set of 11 distinct and 3 *ipso* cases reduces to 5 and 2, respectively. This is discussed in more detail in Chapter 5.

2.5 Conclusion

Ballistic transport of electrons through molecules can be modelled by a version of the standard tight-binding theory of conjugated hydrocarbons in the SSP model of MEDs in combination with Hückel approximations. In graph theoretical terms, the conventional problem is equivalent to determination of the spectrum of the adjacency matrix of the molecular graph, replaced in the SSP problem by a modified adjacency matrix that incorporates the scattering-type boundary conditions. This leads to a full analytic solution to determine r and T in terms of characteristic polynomials. The determination of T makes possible systematic explanation of the connection between structure and conduction of molecules. This leads to defining conditions for opacity and transparency. Moreover, through the selection rules achieved the approach is more qualitative and potentially useful since the number of zero eigenvalues of a graph is an invariant that is easily found without calculation of the full spectrum.

The rest of this thesis will deal with extensions and applications of the theory that exploit the close connections between the Hückel form of the SSP model and mathematical graph theory.

Chapter 3

Interlacing–extremal graphs

This chapter presents some of the main results that have been published in “Interlacing–extremal graphs” *Ars. Math. Comp.* **6**, 261–278, 2013, Sciriha, Debono, Borg, Fowler and Pickup [88]. This chapter is closely based on this reference, with some rewriting to incorporate new material and remove unnecessary repetitions of introductory material. As this was produced for publication in a Mathematical journal, the language is more formal than in later ‘chemical’ chapters, but the conclusions are still relevant to the theory of conduction. The main objective of this present chapter is to classify *devices* into different *kinds* and to identify two particular classes of graphs that correspond to different kinds: devices that have the *minimum* allowed value for the nullity of $G - \bar{L} - \bar{R}$ relative to that of G for all pairs of distinct vertices \bar{L} and \bar{R} of G , and those devices that have the nullity of $G - \bar{L}$ that reaches the *maximum* possible for all vertices \bar{L} in a graph G . The main focus is on devices of the latter kind and their implications for molecular conduction.

The structure of the chapter is as follows. Some basic definitions are given in Section 3.1. In Section 3.2 the characteristic polynomial of $\phi(G - \bar{L}, E)$ is expressed as the sum of terms in E^{g_s} and E^{g_s-1} with coefficients that are polynomials expanded in terms of the entries of the eigenvectors of adjacency matrix \mathbf{A} . By comparing the diagonal entries of the adjugate [89] of $(E\mathbf{I} - \mathbf{A})$ and of the spectral decomposition of $(E\mathbf{I} - \mathbf{A})^{-1}$ we obtain, in Section 3.3, an expression for $\phi(G - \bar{L} - \bar{R}, E)$ as the sum of three terms in E^{g_s} , E^{g_s-1} , E^{g_s-2} , respectively, again with polynomial coefficients. Jacobi’s identity is used to determine which kinds of device are not realised by any graph G . This gives a useful reformulation of the selection rule approach that appeared in the chemical literature in [70] and [87].

In Section 3.4, the vertices of a graph are partitioned into three subsets (*lower*, *middle* and *upper*), according to the vanishing or otherwise of the coefficients in the expansions of $\phi(G - \bar{L})$ and $\phi(G - \bar{L} - \bar{R})$, according to the vanishing or otherwise of their polynomial coefficients. By the Interlacing Theorem and Jacobi’s identity, exactly twelve *kinds* of device $(G - \bar{L} - \bar{R})$ exist, and they are partitioned into three main *varieties* (Sections 3.5 and 3.6). In Section 3.7 two classes of graphs that have extremal nullities are identified. These more formal results will be used in the next chapter, on omni–conduction.

3.1 The adjacency matrix and cores of singular graphs

The graphs we consider are *simple*, that is, without loops or multiple edges. We use $\mathbf{A}(G)$ or just \mathbf{A} when the context is clear, to denote the 0–1 *adjacency matrix* of a graph G , which is determined, up to isomorphism, by \mathbf{A} . If the adjacency matrix \mathbf{A} of a n -vertex graph G satisfies $\mathbf{A}\mathbf{x} = E\mathbf{x}$ for some non-zero vector \mathbf{x} then \mathbf{x} is said to be an *eigenvector* belonging to the *eigenvalue* E . There are n linearly independent eigenvectors. The eigenvalues of \mathbf{A} are said to be the *eigenvalues of G* and to form the *spectrum of G* . They are obtained as the roots of the *characteristic polynomial* $\phi(G, E)$ of the adjacency matrix of G , defined as the polynomial $\det(E\mathbf{I} - \mathbf{A})$ in E .

Cauchy's inequalities for a Hermitian matrix M place restrictions on the multiplicity of the eigenvalues of principal submatrices relative to those of M . When they are applied to graphs we have the Interlacing Theorem:

Theorem 3.1.1 *Let G be an n -vertex graph and $w \in V$. If the eigenvalues are E_1, E_2, \dots, E_n and those of $G - w$ are $\mu_1, \mu_2, \dots, \mu_{n-1}$ both in non-increasing order, then $E_1 \geq \mu_1 \geq E_2 \geq \mu_2 \geq \dots \geq \mu_{n-1} \geq E_n$.*

Thus, by the Interlacing Theorem [86] the eigenvalues of a vertex-deleted subgraph interlace the eigenvalues of the parent graph. As a consequence, the multiplicity (number of repetitions) of any one eigenvalue in the spectrum changes by at most one on deletion of a vertex.

We revise some definitions needed for discussing conduction in the graph theoretical SSP model. For the linear transformation \mathbf{A} , the *kernel*, or *nullspace*, $\ker(\mathbf{A})$ of \mathbf{A} is defined as the subspace of \mathbb{R}^n mapped to the zero vector by \mathbf{A} . A graph G is said to be *singular* of nullity g_s if the dimension of the nullspace $\ker(\mathbf{A})$ of \mathbf{A} is g_s and $g_s > 0$. If there exists a non-zero vector \mathbf{x} in the nullspace of the adjacency matrix \mathbf{A} , then \mathbf{x} is said to be a *kernel eigenvector* of the singular graph G and satisfies $\mathbf{A}\mathbf{x} = \mathbf{0}$. It is therefore an eigenvector of \mathbf{A} for the eigenvalue zero whose multiplicity g_s is also the number of roots of $\phi(G, E)$ equal to zero. A vertex corresponding to a non-zero entry of \mathbf{x} is said to be a *core vertex CV* of G . The core vertices corresponding to \mathbf{x} induce a subgraph of G termed the *core* of G with respect to \mathbf{x} . The core structure of a singular graph will be the basis of our classification of all graphs relative to g_s .

A *core graph* is a singular graph in which every vertex is a core vertex, for example, the four cycle is an example of a 4-vertex core graph of nullity two. A core graph of order at least three and nullity one is known as a *nut graph* and is connected and non-bipartite [90].

For singular graphs, the vertices can be partitioned into core-forbidden and core vertices. A *core-forbidden vertex* (CFV) corresponds to a zero entry in every kernel eigenvector. Otherwise, the vertex is a core vertex, CV, such that it lies on some core of G .

Let \bar{L} and \bar{R} be two distinct vertices of a graph G . By interlacing, when a vertex \bar{L} or \bar{R} is deleted from G , the nullity g_t or g_u , that is, the multiplicity of the eigenvalue zero of $G - \bar{L}$ or $G - \bar{R}$, respectively, may take one of three values from $g_s - 1$

to $g_s + 1$. If the two distinct vertices \bar{L} and \bar{R} are deleted, then the nullity g_v of $G - \bar{L} - \bar{R}$ may take values in the range from $g_s - 2$ to $g_s + 2$. Let a graph having two particular distinct vertices \bar{L} and \bar{R} be called a device (G, \bar{L}, \bar{R}) . The set of devices can be partitioned into three *varieties*: *variety 1* when both vertices are CV, *variety 2* when one vertex is a CFV and one a CV and *variety 3* when both vertices are CFVs. A device (G, \bar{L}, \bar{R}) is said to be of *kind* (g_s, g_t, g_u, g_v) . Since g_t and g_u can take three values each and g_v can take five values, there are potentially 45 *kinds* of graphs relative to g_s . Interlacing further restricts the values of g_v . Moreover, there are *kinds* of graphs that exclude certain combinatorial properties, such as that of being bipartite, as we shall see in Section 3.5.

3.2 Characteristic polynomials

First, some notation needs to be introduced. Associated with the $n \times n$ adjacency matrix \mathbf{A} of a n -vertex graph of nullity g_s , there is an *ordered orthonormal basis* \mathbf{x}^r , $1 \leq r \leq n$ for \mathbb{R}^n , consisting of eigenvectors of \mathbf{A} , with the g_s eigenvectors in the nullspace being labelled first. Let the $n \times 1$ column vector \mathbf{x}^r be $(x_{\bar{L}}^r)$, where for vertex \bar{L} , $1 \leq \bar{L} \leq n$. If

$$\mathbf{P} = \begin{pmatrix} x_1^1 & x_1^2 & \dots & x_1^n \\ x_2^1 & x_2^2 & \dots & x_2^n \\ \vdots & \vdots & \vdots & \vdots \\ x_n^1 & x_n^2 & \dots & x_n^n \end{pmatrix} \quad (3.1)$$

where the i^{th} column of \mathbf{P} is the eigenvector \mathbf{x}^i belonging to the eigenvalue E_i in the spectrum of \mathbf{A} , diagonalisation of \mathbf{A} is given by $\mathbf{P}^{-1}\mathbf{A}\mathbf{P} = \mathbf{D}[E_i]$, where $\mathbf{D}[E_i]$ is the diagonal matrix having E_i as the i^{th} entry on the main diagonal. Expressing \mathbf{A} in terms of \mathbf{D} and \mathbf{P} leads to the spectral decomposition theorem, which can also be applied to $(\mathbf{E}\mathbf{I} - \mathbf{A})^{-1}$. This leads to an expression for the characteristic polynomial of the adjacency matrix $\phi(G - \bar{L}, E)$ of $G - \bar{L}$ which is given explicitly in terms of eigenvector entries $\{x_{\bar{L}}^i\}$. Together with Jacobi's identity, it will serve as a basis for the characterisation of graphs according to those *kinds* that can exist.

Lemma 3.2.1

$$\phi(G - \bar{L}, E) = \sum_{i=1}^n \frac{(x_{\bar{L}}^i)^2}{(E - E_i)} \phi(G, E) \quad (3.2)$$

Proof: The characteristic polynomial of the adjacency matrix $\phi(G - \bar{L}, E)$ of $G - \bar{L}$ is the \bar{L}^{th} diagonal entry $(\text{adj}(\mathbf{E}\mathbf{I} - \mathbf{A}))_{\bar{L}\bar{L}}$ of the adjugate of $(\mathbf{E}\mathbf{I} - \mathbf{A})$. For arbitrary E , the matrix $(\mathbf{E}\mathbf{I} - \mathbf{A})$ is invertible and $\phi(G - \bar{L}, E) = ((\mathbf{E}\mathbf{I} - \mathbf{A})^{-1})_{\bar{L}\bar{L}} \phi(G, E)$. Since $\mathbf{P}^{-1}\mathbf{A}\mathbf{P} = \mathbf{D}[E_i]$, it follows that $\text{adj}(\mathbf{E}\mathbf{I} - \mathbf{A})/\phi(G, E) = (\mathbf{E}\mathbf{I} - \mathbf{A})^{-1} = \mathbf{P}\mathbf{D}[1/(E - E_i)]\mathbf{P}^{-1}$.

Taking the \bar{L}^{th} diagonal entry

$$\frac{\phi(G - \bar{L}, E)}{\phi(G, E)} = \begin{pmatrix} x_{\bar{L}}^1 & x_{\bar{L}}^2 & \dots & x_{\bar{L}}^n \end{pmatrix} \mathbf{D} \left[\frac{1}{E - E_i} \right] \begin{pmatrix} x_{\bar{L}}^1 \\ x_{\bar{L}}^2 \\ \vdots \\ x_{\bar{L}}^n \end{pmatrix} = \sum_{i=1}^n \frac{(x_{\bar{L}}^i)^2}{(E - E_i)} \quad (3.3)$$

■

For a graph G with adjacency matrix \mathbf{A} of nullity g_s , let $s(E)$ denote $\phi(G, E)$. If the spectrum of \mathbf{A} is E_1, E_2, \dots, E_n , starting with the zero eigenvalues (if any), we write

$$s(E) = \prod_{l=1}^n (E - E_l) = E^{g_s} s_0(E) \quad (3.4)$$

with $s_0(0) \neq 0$, where $s_0(E)$ is the product over the non-nullspace.

Partitioning the range of summation in Eq. (3.3),

$$\frac{\phi(G - \bar{L}, E)}{\phi(G, E)} = \sum_{k=1}^{g_s} (x_{\bar{L}}^k)^2 s_0(E) E^{g_s-1} + \sum_{k=g_s+1}^n \frac{(x_{\bar{L}}^k)^2 s_0(E) E^{g_s}}{E - E_k} \quad (3.5)$$

which we shall express as

$$\phi(G - \bar{L}, E) = f_b E^{g_s-1} + f_a E^{g_s} \quad (3.6)$$

3.3 Jacobi's identity

Relative to (G, \bar{L}, \bar{R}) , let us denote by $j(E)$, or j , the entry of the adjugate $\text{adj}(E\mathbf{I} - \mathbf{A})$ in the $\bar{L}\bar{R}$ position, obtained by taking the determinant of the submatrix of $(E\mathbf{I} - \mathbf{A})$ after deleting row \bar{L} and column \bar{R} and multiplying it by $(-1)^{\bar{L}+\bar{R}}$. We use the convention that $g_t \geq g_u$. Where the context is clear, s_0 may be written for $s_0(E)$, j for $j(E)$, *etc.*

Let $s(E), t(E), u(E), v(E)$, often referred to simply as s, t, u and v respectively, be the characteristic polynomials $\phi(G, E), \phi((G - \bar{L}), E), \phi((G - \bar{R}), E), \phi((G - \bar{L} - \bar{R}), E)$ of the graphs $G, G - \bar{L}, G - \bar{R}$ and $G - \bar{L} - \bar{R}$, respectively, that is, the determinants listed in Eq. (2.26).

From Lemma 3.2.1,

$$t(E) = \sum_{k=1}^n (x_{\bar{L}}^k)^2 \prod_{\ell \neq k} (E - E_\ell) \quad (3.7)$$

and

$$u(E) = \sum_{k=1}^n (x_{\bar{R}}^k)^2 \prod_{\ell \neq k} (E - E_\ell) \quad (3.8)$$

We shall see that the characteristic polynomial $v(E)$ of $G - \bar{L} - \bar{R}$ can also be expressed in terms of the eigenvector entries $\{x_{\bar{L}}^r\}$ and $\{x_{\bar{R}}^r\}$ associated with distinct vertices \bar{L} and \bar{R} .

Lemma 3.3.1 *For $\bar{L} \neq \bar{R}$, Jacobi's identity expresses the entry j of the adjugate of $E\mathbf{I} - \mathbf{A}$ in the $\bar{L}\bar{R}$ position, for a symmetric matrix \mathbf{A} , in terms of the characteristic polynomials s , u , t and v as $j^2 = ut - sv$ [83].*

Expressing Eqs (3.7) and (3.8) as in (3.6),

$$t(E) = \sum_{k=1}^{g_s} (x_{\bar{L}}^k)^2 s_0(E) E^{g_s-1} + \sum_{k=g_s+1}^n \frac{(x_{\bar{L}}^k)^2 s_0(E) E^{g_s}}{E - E_k} = t_b E^{g_s-1} + t_a E^{g_s} \quad (3.9)$$

and

$$u(E) = \sum_{k=1}^{g_s} (x_{\bar{R}}^k)^2 s_0(E) E^{g_s-1} + \sum_{k=g_s+1}^n \frac{(x_{\bar{R}}^k)^2 s_0(E) E^{g_s}}{E - E_k} = u_b E^{g_s-1} + u_a E^{g_s} \quad (3.10)$$

Now, considering pairs of vertices of G , since $\text{adj}(EI - A)/\phi(G, E) = (EI - A)^{-1} = PD[1/(E - E_i)]P^{-1}$,

$$j(E) = \sum_{k=1}^n (x_{\bar{L}}^k x_{\bar{R}}^k) \prod_{\ell \neq k} (E - E_\ell) \quad (3.11)$$

We can write

$$j(E) = \sum_{k=1}^{g_s} x_{\bar{L}}^k x_{\bar{R}}^k s_0(E) E^{g_s-1} + \sum_{k=g_s+1}^n \frac{x_{\bar{L}}^k x_{\bar{R}}^k s_0(E) E^{g_s}}{E - E_k} = j_b E^{g_s-1} + j_a E^{g_s} \quad (3.12)$$

The characteristic polynomial $v(E)$ can be written as $v(E) = (u(E)t(E) - j^2(E))/s(E)$, that is $v(E) = v_a E^{g_s} + v_b E^{g_s-1} + v_c E^{g_s-2}$, where

$$\begin{aligned}
v_c &= \frac{1}{s_0}(u_b t_b - j_b^2) = \frac{1}{2} s_0 \sum_{i=1}^{g_s} \sum_{\ell=1}^{g_s} (x_{\bar{R}}^i x_{\bar{L}}^\ell - x_{\bar{R}}^\ell x_{\bar{L}}^i)^2 \\
v_b &= \frac{1}{s_0}(u_a t_b + u_b t_a - 2j_a j_b) = s_0 \sum_{i=1}^{g_s} \sum_{\ell=g_s+1}^n \frac{(x_{\bar{R}}^i x_{\bar{L}}^\ell - x_{\bar{L}}^i x_{\bar{R}}^\ell)^2}{E - E_\ell} \\
v_a &= \frac{1}{s_0}(u_a t_a - j_a^2) = \frac{1}{2} s_0 \sum_{i=g_s+1}^n \sum_{\ell=g_s+1}^n \frac{(x_{\bar{L}}^i x_{\bar{R}}^\ell - x_{\bar{L}}^\ell x_{\bar{R}}^i)^2}{(E - E_i)(E - E_\ell)}
\end{aligned} \tag{3.13}$$

and in particular

$$j_a^2 = u_a t_a - s_0 v_a \tag{3.14}$$

$$j_a j_b = \frac{1}{2}(u_a t_b + u_b t_a - s_0 v_b) \tag{3.15}$$

$$j_b^2 = u_b t_b - s_0 v_c \tag{3.16}$$

3.4 The three vertex types

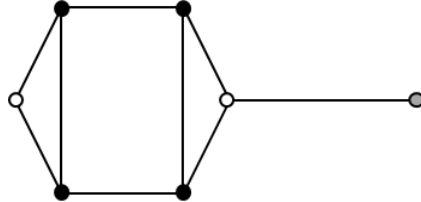


Figure 3.1: A chemical graph showing the different type of vertices. Core vertices are indicated with black-filled circles, upper core-forbidden vertices with white-filled circles, and middle core-forbidden vertices with grey-filled circles.

By interlacing, we can identify three types of vertex according to the effect on the nullity on deletion (see Fig. 3.1). A necessary and sufficient condition for the nullity to decrease on deletion of a vertex from a graph is that the deleted vertex is a CV. Therefore, by interlacing, deletion of a CFV either leaves the nullity unchanged or increases it by one. We call a vertex \bar{L} **lower**, **middle** or **upper** if the nullity of $G - \bar{L}$ is $g_s - 1$, g_s or $g_s + 1$, respectively. Other terms are also used in the literature: the CFV are referred to as peripheral vertices; upper vertices are variously termed maximal [91], Parter, or rank-strong vertices [92]; middle vertices are called intermediate [91] or rank-neutral [92]; and lower vertices are also called downer or rank-weak vertices [92]. Bipartite graphs do not have middle vertices (see Lemma 3.5.2). We shall distinguish among these three types of vertex (lower, middle and upper) according to the values of the functions f_a and f_b in Eq. (3.6).

vertex entries	eigenvector					
	x^1	\dots	x^{g_s}	x^{g_s+1}	\dots	x^n
x_1	*	\dots	*	*	\dots	*
x_2	*	\dots	*	*	\dots	*
\vdots	*	\dots	*	*	\dots	*
$x_{ CV }$	*	\dots	*	*	\dots	*
$x_{ CV +1}$	0	\dots	0	*	\dots	*
\vdots	\vdots	\vdots	\vdots	\vdots	\vdots	\vdots
x_n	0	\dots	0	*	\dots	*

Table 3.1: Ordered orthonormal basis of eigenvectors of \mathbf{A} with * representing a possibly non-zero entry.

In Table 3.1 we show the entries of the orthonormal eigenvectors $\{\mathbf{x}^r\}$ in an ordered basis for \mathbb{R}^n as presented in Section 3.2. We choose a vertex labelling such that the core vertices are labelled first. Note the zero submatrix corresponding to the CFVs.

We consider $\phi(G - \bar{L}, E)/(s_0 E^{g_s})$ from Eq. (3.5). It has poles at $E = \mu_i$, $1 \leq i \leq h$, where, for $1 \leq i \leq h$, the μ_i are the h distinct non-zero eigenvalues of G . Moreover,

the gradient of $\sum_{k=g_s+1}^n (x_{\bar{L}}^k)^2/(E - E_k)$ is less than 0 for all $E \neq \mu_i$. It follows that

$\phi(G - \bar{L}, E)/(s_0 E^{g_s})$ has at most $(h - 1)$ roots strictly interlacing the h distinct eigenvalues of \mathbf{A} . $\sum_{k=1}^{g_s} (x_{\bar{L}}^k)^2 = 0$ if and only if \bar{L} is a CFV. Thus at $E = 0$, f_b is

non-zero if \bar{L} is a CV and zero if it is a CFV. For a CFV \bar{L} , $\sum_{k=g_s+1}^n (x_{\bar{L}}^k)^2/(E - E_k)$

vanishes at $E = 0$ when \bar{L} is upper, and does not vanish when \bar{L} is middle. When $\sum_{k=1}^{g_s} (x_{\bar{L}}^k)^2 = 0$, one of the $(h - 1)$ interlacing roots may be zero.

Different cases occur depending on the vanishing or otherwise of the real constant $\sum_{k=1}^{g_s} (x_{\bar{L}}^k)^2$ and $\sum_{k=g_s+1}^n (x_{\bar{L}}^k)^2/(E - E_k)$ at $E = 0$. Eq. (3.5) and the above analysis lead

to the result that $g_s - 1 \leq g_t \leq g_s + 1$. This can be generalized for the multiplicity of any eigenvalue of G other than zero by replacing the cores and the nullspace of G by the μ_i -cores and μ_i -eigenspace of G (concepts introduced in [93]).

Proposition 3.4.1 *The values of f_b and f_a of Expression (3.6) for $\phi(G - \bar{L}, E)$ at $E = 0$ distinguish the three types of vertex as follows:*

Vertex \bar{L}	Status of \bar{L}	The values of f_b and f_a
Lower	CV	$f_b(0) \neq 0$
Middle	CFV	$f_b(0) = 0$ and $f_a(0) \neq 0$
Upper	CFV	$f_b(0) = 0$ and $f_a(0) = 0$

Proof: Let \bar{L} be a core vertex of a graph of nullity $g_s > 0$. There exists $x_{\bar{L}}^k \neq 0$ for some k , $1 \leq k \leq g_s$. Then $f_b(0) \neq 0$, which is a necessary and sufficient condition

for the multiplicity of the eigenvalue zero to be $g_s - 1$ for $G - \bar{L}$. It follows that a vertex is *lower* if and only if it is a CV.

If v is a CFV, then $f_b(0) = 0$. For $G - \bar{L}$, the multiplicity of the eigenvalue zero is at least g_s . If one of the roots of $\sum_{k=g_s+1}^n (x_{\bar{L}}^k)^2 / (E - E_k)$ is zero, then E divides

$\sum_{k=g_s+1}^n (x_{\bar{L}}^k)^2 / (E - E_k)$, the multiplicity of the eigenvalue zero is exactly $g_s + 1$ for $G - \bar{L}$ and the vertex \bar{L} is upper. Otherwise, the multiplicity of the eigenvalue zero remains g_s for $G - \bar{L}$ and the vertex \bar{L} is middle. ■

We consider three *varieties* of devices (G, \bar{L}, \bar{R}) with pairs (\bar{L}, \bar{R}) of vertices, namely *variety 1* with both \bar{L} and \bar{R} being CVs, *variety 2* with \bar{R} being a CV and \bar{L} a CFV and *variety 3* with both \bar{L} and \bar{R} being CFVs. Since a CFV can be upper or middle, *varieties 2* and *3* are subdivided further, as seen in Table 3.2.

From Proposition 3.4.1,

for *variety 1*, $u_b \neq 0$; $t_b \neq 0$;

for *variety 2*, $u_b \neq 0$; $j_b = t_b = v_c = 0$;

for *variety 3*: $u_b = j_b = t_b = v_b = v_c = 0$.

Some of these *varieties* can be further subdivided according to the values at $E = 0$ of v_c , v_b and v_a or j_a . From Proposition 3.4.1, $t_b(0) \neq 0$ if and only if \bar{L} is a core vertex. Similarly $u_b \neq 0$ if and only if \bar{R} is a core vertex. If at least one of \bar{R} or \bar{L} is core-forbidden, then $j_b(0) = 0$. However, there are ‘accidental’ cases where $j_b(0)$ vanishes when both \bar{R} and \bar{L} are CVs, if the vertices \bar{L} and \bar{R} are connected by an edge.

3.5 Restrictions on the nullity of $G - \bar{L} - \bar{R}$

It is possible to classify all graphs according to their *kind* defined by the quadruple (g_s, g_t, g_u, g_v) . This classification is given in Table 3.2.

3.5.1 Restrictions arising from interlacing

In a device (G, \bar{L}, \bar{R}) of *kind* (g_s, g_t, g_u, g_v) , interlacing restricts the values that g_v can take. The following result shows an instance when g_v is determined by interlacing alone.

Lemma 3.5.1 *For $(g_s, g_t, g_u, g_v) = (g_s, g_s + 1, g_s - 1, g_v)$, the nullity g_v of (G, \bar{L}, \bar{R}) is g_s .*

Hence, $(g_s, g_s + 1, g_s - 1, g_s)$ is the only *kind* where the nullities g_t and g_u differ by two. We say that it belongs to variety 2a.

In kinds where the nullities g_t and g_u differ by one, interlacing allows g_v to take either the value g_t or g_u . All three possible values of g_v are allowed by interlacing when $g_t = g_u$.

The symmetry about zero of the spectrum of a bipartite graph G [94] requires that the number of zero eigenvalues is $2k$, if G has an even number of vertices and $2k + 1$ if G has an odd number of vertices, for some $k \geq 0$. This implies that on deleting a vertex from a bipartite graph, the nullity changes parity. Therefore, if the nullity of a graph G and of its vertex-deleted subgraph $G - \bar{L}$ are the same, then G is not bipartite. Since on deleting a vertex a bipartite graph remains bipartite, it follows that a graph G of a *kind* where $g_s = g_t$ or $g_t = g_v$ cannot be bipartite.

Lemma 3.5.2 *If a vertex of a graph is middle, then the graph is not bipartite.*

Proof: By the Pairing Theorem [95], if the graph has an odd number of vertices, then its nullity is odd, whilst if the graph has an even number of vertices, then its nullity is even. Hence, on deleting a vertex there is a change of parity in both the number of vertices and nullity. Thus, the nullity does not remain the same as would be the case imposed by a middle CFV. ■

Fig. 3.2 shows a device (G, \bar{L}, \bar{R}) with a middle vertex \bar{R} which becomes upper in $G - \bar{L}$.



Figure 3.2: A graph with two middle vertices \bar{L} and \bar{R} .

3.5.2 Restrictions arising from Jacobi's identity

Lemma 3.3.1 requires that $j^2 = ut - sv$ has $2k$, $k \in \mathbb{Z}^+$, zero roots. Let g_f denote the number of zero roots of the real function f . Therefore, for kinds of graph that imply $g_{ut} = g_{sv} - 1$ and $g_u \neq g_t$, or, $g_{ut} = g_{sv} + 1$ and $g_u = g_t$, there is a contradiction and those *kinds* of graphs do not exist.

Lemma 3.5.3 *The following kinds of graphs do not exist:*

- (i) $(g_s, g_s, g_s - 1, g_s)$
- (ii) $(g_s, g_s + 1, g_s + 1, g_s + 1)$
- (iii) $(g_s, g_s, g_s, g_s - 1)$

Furthermore, if $g_{ut} = g_{sv}$ and g_{ut} is odd, then a graph of that *kind* exists if $ut - sv$ is zero at $E = 0$, otherwise j^2 would have an odd number of zeroes. Therefore, if $g_{ut} = g_{sv}$ and g_{ut} is odd, $j_b = 0$ at $E = 0$.

<i>Kind</i>	Characterisation	<i>Variety</i>	<i>G</i> bipartite
Two CVs		1	
$(g_s, g_t, g_u) = (g_s, g_s - 1, g_s - 1)$ $g_v = g_s - 2$	$v_c \neq 0 \ \& \ t_b \neq 0 \ \& \ u_b \neq 0$ $\& \ g_s \geq 2$	1(i)	Allowed
$g_v = g_s$	$v_c = 0 \ \& \ t_b \neq 0 \ \& \ u_b \neq 0$ $\& \ v_b(0) = 0 \ \& \ g_s \geq 1$	1(ii)	Allowed
$g_v = g_s - 1$	$v_c = 0 \ \& \ t_b \neq 0 \ \& \ u_b \neq 0$ $\& \ v_b(0) \neq 0 \ \& \ g_s \geq 1$	1(iii)	Forbidden
CV and CFV		2	
$(g_s, g_t, g_u) = (g_s, g_s + 1, g_s - 1)$ $g_v = g_s$	$v_c = 0 \ \& \ t_b = 0 \ \& \ u_b \neq 0$ $\& \ v_b(0) = 0 \ \& \ g_s \geq 1$	2a	Allowed
$(g_s, g_t, g_u, g_v) = (g_s, g_s, g_s - 1)$ $g_v = g_s - 1$	$v_c = 0 \ \& \ t_b = 0 \ \& \ u_b \neq 0$ $\& \ v_b(0) \neq 0 \ \& \ g_s \geq 1$	2b	Forbidden
Two CFVs		3	
$(g_s, g_t, g_u) = (g_s, g_s + 1, g_s + 1)$ $g_v = g_s$	$v_c = 0 \ \& \ t_b = 0 \ \& \ u_b = 0$ $\& \ v_b(0) = 0 \ \& \ t_a(0) = 0 \ \&$ $u_a(0) = 0 \ \& \ v_a(0) \neq 0$	3a 3a(i)	Allowed
$g_v = g_s + 2$	$v_c = 0 \ \& \ t_b = 0 \ \& \ u_b = 0$ $\& \ v_b(0) = 0 \ \& \ t_a(0) = 0 \ \&$ $u_a(0) = 0 \ \& \ v_a(0) = 0$	3a(ii)	Allowed
$(g_s, g_t, g_u) = (g_s, g_s + 1, g_s)$ $g_v = g_s + 1$	$v_c = 0 \ \& \ t_b = 0 \ \& \ u_b = 0$ $\& \ v_b(0) = 0 \ \& \ t_a(0) = 0 \ \&$ $u_a(0) \neq 0 \ \& \ v_a(0) = 0$	3b 3b(i)	Forbidden
$g_v = g_s$	$v_c = 0 \ \& \ t_b = 0 \ \& \ u_b = 0$ $\& \ v_b(0) = 0 \ \& \ t_a(0) = 0 \ \&$ $u_a(0) \neq 0 \ \& \ v_a(0) \neq 0$	3b(ii)	Forbidden
$(g_s, g_t, g_u) = (g_s, g_s, g_s)$ $g_v = g_s + 1$	$v_c = 0 \ \& \ t_b = 0 \ \& \ u_b = 0$ $\& \ v_b(0) = 0 \ \& \ t_a(0) \neq 0 \ \&$ $u_a(0) \neq 0 \ \& \ v_a(0) = 0$	3c 3c(i)	Forbidden
$g_v = g_s$	$v_c = 0 \ \& \ t_b = 0 \ \& \ u_b = 0$ $\& \ v_b(0) = 0 \ \& \ t_a(0) \neq 0 \ \&$ $u_a(0) \neq 0 \ \& \ v_a(0) \neq 0$	3c(ii)	Forbidden
$g_v = g_s \ \& \ j_a(0) \neq 0$	$v_c = 0 \ \& \ t_b = 0 \ \& \ u_b = 0$ $\& \ v_b(0) = 0 \ \& \ t_a(0) \neq 0 \ \&$ $u_a(0) \neq 0 \ \& \ v_a(0) \neq 0 \ \&$ $j_a(0) \neq 0$	3c(iiA)	Forbidden
$g_v = g_s \ \& \ j_a(0) = 0$	$v_c = 0 \ \& \ t_b = 0 \ \& \ u_b = 0$ $\& \ v_b(0) = 0 \ \& \ t_a(0) \neq 0 \ \&$ $u_a(0) \neq 0 \ \& \ v_a(0) \neq 0 \ \&$ $j_a(0) = 0$	3c(iiB)	Forbidden

Table 3.2: A characterisation of all devices (G, \bar{L}, \bar{R}) according to their *variety* and *kind* [88].

Lemma 3.5.4 *Graphs with $g_{ut} = g_{sv}$ and g_{ut} odd exist provided $j_b = 0$ at $E = 0$. They are non-bipartite and of one of the following kinds:*

- (i) $(g_s, g_s, g_s - 1, g_s - 1)$ (variety 2b)
- (ii) $(g_s, g_s + 1, g_s, g_s + 1)$ (variety 3b(i))

Lemma 3.5.5 *If (G, \bar{L}, \bar{R}) is a singular graph with $g_{ut} < g_{sv}$ and g_{sv} odd, then (G, \bar{L}, \bar{R}) is non-bipartite and of kind $(g_s, g_s - 1, g_s - 1, g_s - 1)$ (variety 1(iii)).*

Proof: If \bar{L} and \bar{R} are CVs, $g_{ut} < g_{sv}$, then (g_s, g_t, g_u, g_v) is

- (i) $(g_s, g_s - 1, g_s - 1, g_s)$ or
- (ii) $(g_s, g_s - 1, g_s - 1, g_s - 1)$.

Now if furthermore, g_{sv} is given to be odd, then $g_v = g_s - 1$. It follows that $g_t = g_u$. Therefore, G is not bipartite. ■

3.6 Kinds of graphs

In this section we determine the properties of a *kind* (g_s, g_t, g_u, g_v) within each of the three *varieties*.

3.6.1 Graphs of variety 1

Graphs of variety 1, are necessarily singular and therefore have at least one core. There are at least two vertices in a core (see for example Lemma 6.8.2 in Chapter 6).

Lemma 3.6.1 *For a device (G, \bar{L}, \bar{R}) of variety 1 and nullity one, $j_b(0) \neq 0$ for core vertices \bar{L} and \bar{R} .*

Proof: For $g_s = 1$, a non-zero column of the adjugate $\text{adj}(\mathbf{A})$ is a kernel eigenvector of G [96]. The non-zero entries occur only at core vertices. Therefore, $j_b(0) \neq 0$. ■

There are three types of pairs of vertices (CV, CV) for graphs of variety 1, depending on the nullity of $G - \bar{L} - \bar{R}$. Since $g_s \geq 1$ and $g_u = g_t = g_s - 1$, then the nullity g_v of $G - \bar{L} - \bar{R}$ can take any of the three values $g_s - 2$, g_s and $g_s - 1$, corresponding to *variety* 1(i), 1(ii) and 1(iii), respectively.

Theorem 3.6.1 *For a device (G, \bar{L}, \bar{R}) of variety 1(iii), $j(0) \neq 0$ for core vertices \bar{L} and \bar{R} .*

Proof: For nullity one the result follows from Lemma 3.6.1. Consider a graph with $g_s > 1$ of variety 1(iii), that is when $g_v = g_s - 1$. The number of zeroes g_{ut} of ut is $2g_s - 2$ and less than that of sv which is odd. If j^2 , which is $ut - sv$, is not to have an odd number of zeroes, it follows, from $j = j_b E^{g_s - 1} + j_a E^{g_s}$, that $j_b \neq 0$ at $E = 0$. ■

For variety 1(i), the vertices \bar{L} and \bar{R} are CVs. Moreover, without loss of generality, the vertex \bar{R} is a CV of the subgraph $G - \bar{L}$. Only for variety 1(i) is $v_c \neq 0$.

Definition 3.6.1 *The connected graphs G in the devices (G, \bar{L}, \bar{R}) with all pairs of vertices (\bar{L}, \bar{R}) being of variety 1(i) are said to form the class of **uniform–core graphs**.*

Equivalently, $g_v = g_s - 2$, that is \bar{R} is a CV of $G - \bar{L}$ for all vertex pairs (\bar{L}, \bar{R}) . It is clear that all vertices of a uniform–core graph are CVs, and that they remain so even in a vertex–deleted subgraph $G - \bar{L}$ for any vertex \bar{L} of G , but this is not the case in general; if \bar{L} and \bar{R} are two distinct core vertices of a graph G , then \bar{R} need not remain a core vertex of $G - \bar{L}$.

3.6.2 Graphs of variety 2

In a device (G, \bar{L}, \bar{R}) of variety 2, (\bar{L}, \bar{R}) is a mixed vertex pair, that is exactly one vertex \bar{R} of the pair (\bar{L}, \bar{R}) is a CV.

From Lemmas 3.5.1 and 3.5.3, the following result follows immediately:

Proposition 3.6.2 *In a device (G, \bar{L}, \bar{R}) of variety 2,*
(i) there is only one kind when \bar{L} is upper, namely kind $(g_s, g_s + 1, g_s - 1, g_s - 1)$ in variety 2a, and
(ii) only one kind when \bar{L} is middle, namely kind $(g_s, g_s, g_s - 1, g_s - 1)$ in variety 2b.

From Lemma 3.5.2, the graphs of variety 2b are non–bipartite.

Theorem 3.6.2 *In a device (G, \bar{L}, \bar{R}) of variety 2b, the term in E^{2g_s-1} of j^2 is identically equal to zero.*

Proof: In variety 2b, a graph is of kind $(g_s, g_s, g_s - 1, g_s - 1)$. The parameter v_c vanishes and $v_b(E) = u_b t_a / s_0 \neq 0$. The number of zeroes of ut is the same as that of sv . Therefore, $j^2 = ut - sv$ has at least $2g_s - 1$ zeroes. In variety 2b, the term in E^{2g_s-1} in its expansion is $u_b t_a - s_0 v_b$. Also v_c vanishes and $v_b(E) = u_b t_a / s_0 \neq 0$. Hence, $s_0 v_b = u_b t_a$ and the term in E^{2g_s-1} in the expansion of j^2 is identically equal to zero, as expected from the fact that j^2 is a perfect square. ■

The parameter v_b distinguishes between a graph in *variety 2a* and one in *variety 2b*.

Theorem 3.6.3 *For a graph in variety 2a, v_b vanishes at $E = 0$. For a graph in variety 2b, $v_b \neq 0$ at $E = 0$.*

Proof: For both *kinds* in *variety 2*, $u_b \neq 0$. For an upper vertex, $t_a = 0$ at $E = 0$ and for a middle vertex $t_a \neq 0$ at $E = 0$. Since $s_0 \neq 0$, it follows that for a graph in *variety 2a* $v_b = 0$ at $E = 0$ and, for a graph in *variety 2b*, $v_b \neq 0$ at $E = 0$. ■

3.6.3 Graphs of variety 3

We now consider variety 3 for (CFV, CFV) pairs, when t_b, u_b, j_b, v_b and v_c all vanish.

Interlacing provides three types of vertex pairs depending on whether a CFV in the pair (\bar{L}, \bar{R}) is upper or middle. When both vertices are upper (*variety 3a*), by Lemma 3.5.3 only *variety 3a(i)* for $g_v = g_s$ and *variety 3a(ii)*, when $g_v = g_s + 2$ are allowed. The values at $E = 0$ of v_a or j_a suffice to distinguish between graphs of *variety 3(i)* and *3(ii)*.

Theorem 3.6.4 *For variety 3a(i), both v_a and j_a are non-zero at $E = 0$. For variety 3a(ii), both v_a and j_a vanish at $E = 0$.*

Proof: For *variety 3*, $v_b = 0$. *Variety 3a(i)* is $(g_s, g_s + 1, g_s + 1, g_s)$. Since $v = v_a E^{g_s}$ and $g_v = g_s$, $v_a \neq 0$ at $E = 0$. Also $g_{j^2} = 2g_s$ so that $j_a \neq 0$ at $E = 0$. *Variety 3a(ii)* is $(g_s, g_s + 1, g_s + 1, g_s + 2)$. Since $g_v = g_s + 2$, E^2 divides v_a and E divides all of the functions t_a, u_a and j_a . ■

For *variety 3b*, one vertex is upper and one is middle. Interlacing allows only $g_v = g_s + 1$ and g_s , corresponding to *variety 3b(i)* and *variety 3b(ii)*, respectively. Both v_b and j_b vanish at $E = 0$. The value of j_a at $E = 0$ distinguishes between *variety 3b(i)* and *variety 3b(ii)*.

Theorem 3.6.5 *For variety 3b(i), j_a vanishes at $E = 0$. For variety 3a(ii), j_a is non-zero at $E = 0$.*

Proof: For *variety 3b(i)*, E divides j_a , as otherwise $ut - sv$ is not the perfect square j^2 . *Variety 3b(ii)* $g_v = g_s$ requires $j_a \neq 0$ at $E = 0$. ■

For *variety 3c*, both vertices are middle. The values at $E = 0$ of t_a and u_a are non-zero. By Lemma 3.5.3, $g_v = g_s + 1$ or g_s , corresponding to *variety 3c(i)* and *variety 3c(ii)*, respectively.

For *variety 3c(ii)*, when $g_v = g_s$, v_a is non-zero at $E = 0$. Two cases may occur. Either $j_a \neq 0$ at $E = 0$ or the number of zeroes of j_a is at least one. The former case is denoted by *variety 3c(iiA)*. The latter case is *variety 3c(iiB)* for which the terms in E^{2g_s-2} and in E^{2g_s-1} of j^2 vanish.

The remaining case is for *variety 3c(i)* when $g_v = g_s + 1$ and E divides v_a .

3.7 Graphs with analogous vertex pairs

In general, vertex pairs in a graph may be of different varieties and kinds. We can consider two classes of graphs with the same extremal nullity (allowed by interlacing) for all vertex-deleted subgraphs, where the classification of devices (G, \bar{L}, \bar{R}) depends on their *kind* (g_s, g_t, g_u, g_v) . A pair of vertices \bar{L} and \bar{R} for which $g_t = g_u$ is said to be an *analogous* vertex pair.

The first of these two classes consists of graphs G with the minimum possible nullity g_v for *all* pairs of distinct vertices \bar{L} and \bar{R} , (i.e., $g_s - 2$) and therefore also the minimum possible nullities g_t and g_u (i.e., $g_s - 1$). By Definition 3.6.1, these graphs form precisely the class of uniform–core graphs. The second of the two classes consists of graphs with the maximum possible nullity g_v , that is $g_s + 2$, for *some* pair of distinct vertices \bar{L} and \bar{R} , and therefore also the maximum possible nullities g_t and g_u (i.e., $g_s + 1$).

3.7.1 Uniform–core graphs

By Definition 3.6.1, each vertex pair in a uniform–core graph corresponds to a graph of variety 1(i). Since the nullity of a graph is non–negative, and $g_v = g_s - 2$ for all vertex pairs \bar{L} , \bar{R} of a uniform–core graph G , then the nullity of G is at least two. To understand better the core–structure of uniform–core graphs and be able to characterise them as a subclass of singular graphs, it is necessary to use their core structure with respect to a basis for their nullspace.

Let B be a basis for the g_s –dimensional nullspace of \mathbf{A} of a singular graph G (with no isolated vertices) of nullity $g_s \geq 1$. As seen in [97], *Hall’s Marriage* problem for sets guarantees a vertex–subset S of distinct vertex representatives to represent a system \mathcal{S}_{Cores} of cores corresponding to the vectors of B . This implies that deleting a vertex v representing a core F eliminates the core F from $G - v$, which will now have a new system of $g_s - 1$ cores. Also any $k \geq 1$ cores in a system \mathcal{S}_{Cores} of g_s cores cover at least $k + 1$ vertices.

Theorem 3.7.1 *A device (G, \bar{L}, \bar{R}) is of variety 1(i) if and only if the two vertices \bar{L} and \bar{R} do not lie in one core only, i.e. at least two cores are needed to cover the vertices \bar{L} and \bar{R} .*

Proof: Consider a basis B for the nullspace of \mathbf{A} . The vertices \bar{L} and \bar{R} lie on at least one core of G . There are two possibilities. Firstly, B has exactly one vector with non–zero entries at positions associated with \bar{L} and \bar{R} . In this case $g_v = g_t = g_s - 1$, which does not correspond to variety 1(i). Secondly, B has at least two vectors with non–zero entries at positions associated with \bar{L} or \bar{R} , when $g_v = g_t - 1 = g_s - 2$, which corresponds to variety 1(i). The two core vertices must represent two distinct cores in a system \mathcal{S}_{Cores} of g_s cores corresponding to a basis B for the nullspace [97]. ■

A subclass \mathcal{U} of uniform–core graphs can be constructed from nut graphs. A graph $G \in \mathcal{U}$ is obtained from a nut graph H on n vertices and m edges by duplicating each of the n vertices of H . Then G has $2n$ vertices and $4m$ edges. Fig. 3.3 shows the uniform–core graph $G \in \mathcal{U}$ obtained from the smallest nut graph H . The nullity of G is $|\mathcal{V}(G)|/2 + 1$. Deletion of any $|\mathcal{V}(G)|/2 + 1$ vertices reduces the graph to a non–singular graph.

Let the vertices of G be labelled $1, 2, \dots, n, 1', 2', \dots, n'$ where $\{1, 2, \dots, n\}$ are the vertices of the nut graph H and $\{1', 2', \dots, n'\}$ are the duplicate vertices of $\{1, 2, \dots, n\}$ in that order in G . Note that a vertex labelled r for $1 \leq r \leq n$ is adjacent to the original neighbours in H and also to precisely those primed vertices with the same

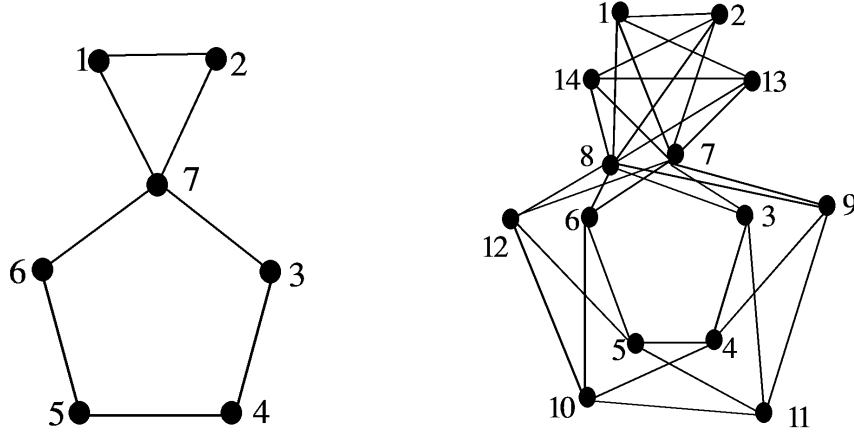


Figure 3.3: The smallest nut graph H and the uniform-core graph G derived from H . This construction is called the lexicographic product with empty graph on two vertices [98].

numeric label. The following result, expressing the adjacency matrix of $G \in \mathcal{U}$ in terms of the adjacency matrix of H , is immediate.

Theorem 3.7.2 *If \mathbf{H} is the adjacency matrix of the nut graph H , then the adjacency matrix of the uniform-core graph $G \in \mathcal{U}$ is $\begin{pmatrix} \mathbf{H} & \mathbf{H} \\ \mathbf{H} & \mathbf{H} \end{pmatrix}$. The spectrum of G consists of n eigenvalues equal in value to double the eigenvalues of H and an additional n zero eigenvalues corresponding to the n duplicate vertex pairs. If $(x_1, x_2, \dots, x_n)^T$ is an eigenvector of H for an eigenvalue μ , then $(x_1, x_2, \dots, x_n, x_1, x_2, \dots, x_n)^T$ is an eigenvector of G for an eigenvalue 2μ .*

We shall now characterise uniform-core graphs by requiring that a set of vertex representatives of a system \mathcal{S}_{Cores} of cores be an arbitrary subset of the vertices for all systems of cores.

Theorem 3.7.3 *A graph of nullity g_s is a uniform-core graph if and only if it is a singular graph such that the deletion of any subset of g_s vertices produces a non-singular graph.*

Proof: Let us relate the nullspace of \mathbf{A} to the vertices of a uniform-core graph G of nullity g_s . Let S be any subset of g_s vertices of G labelled $\{1, 2, \dots, g_s\}$ and let B be an ordered basis for the nullspace of \mathbf{A} . If all pairs of vertices give a graph of variety 1(i), then no two vertices lie in only one core of \mathcal{S}_{Cores} . Therefore, it is possible to obtain a new ordered basis B' for the nullspace of \mathbf{A} , by linear combination of the vectors in B , such that, for $1 \leq i \leq g_s$, only the vector i of B' has a non-zero entry at position i [97]. Removal of any vertex in S destroys precisely one eigenvector of B' reducing the nullity by one. Deletion of all the vertices in S destroys all the kernel eigenvectors and leaves a non-singular graph. ■

3.7.2 Non-singular graphs with a complete weighted inverse

We shall now look into the second class of devices where a graph G is a device (G, \bar{L}, \bar{R}) , of variety 3a(ii), for some pair of distinct vertices \bar{L} and \bar{R} . Can a graph G be a device (G, \bar{L}, \bar{R}) , of variety 3a(ii), for *all* vertex pairs $\{\bar{L}, \bar{R}\}$? The question amounts to determining whether it is possible to have g_v equal to the maximum allowed nullity relative to g_s , that is $g_s + 2$, for all vertex pairs $\{\bar{L}, \bar{R}\}$. The answer is in the negative.

Lemma 3.7.1 *It is impossible that a graph G is a device (G, \bar{L}, \bar{R}) of variety 3a(ii) for all pairs of distinct vertices \bar{L} and \bar{R} .*

Proof: Suppose G is a graph which is a device (G, \bar{L}, \bar{R}) of variety 3a(ii) for all pairs of distinct vertices \bar{L} and \bar{R} . This requires that each of the graphs $G - \bar{L}$ and $G - \bar{R}$ is singular and therefore has CVs. Deletion of a CV from $G - \bar{L}$, restores the nullity back to g_s . Hence it is impossible to achieve $g_v = g_s + 2$, for *all* vertex pairs $\{\bar{L}, \bar{R}\}$. ■

By Lemma 3.5.3, the kind $(g_s, g_t, g_u, g_v) = (g_s, g_s + 1, g_s, g_s + 1)$ is impossible. Hence the only devices (G, \bar{L}, \bar{R}) within the second class that have the maximum value of g_t relative to g_s , for all vertices \bar{L} , are of kind $(g_s, g_s + 1, g_s + 1, g_s)$. The focus is on the non-singular graphs of this kind having the inverse \mathbf{A}^{-1} equal to the adjacency matrix of the complete graph with real non-zero weighted edges and no loops.

The smallest candidate is K_2 . Indeed $\mathbf{A}(K_2) = (\mathbf{A}(K_2))^{-1} = \begin{pmatrix} 0 & 1 \\ 1 & 0 \end{pmatrix}$.

Definition 3.7.1 *Let G be a non-singular graph G with the off-diagonal entries of the inverse \mathbf{A}^{-1} of its adjacency matrix \mathbf{A} being non-zero and real, and all the diagonal entries of \mathbf{A}^{-1} being zero. Then G is said to be a nuciferous graph (meaning a nut-producing graph).*

Theorem 3.7.4 *G is a nuciferous graph if and only if G is either K_2 or each vertex-deleted subgraph $G - v$ is a nut graph.*

Proof: Let \mathbf{Q} be the $(n-1) \times n$ matrix obtained from \mathbf{A}^{-1} by suppressing the diagonal entry from each column. Therefore each entry of \mathbf{Q} is non-zero.

Let the i^{th} column of \mathbf{Q} be $\mathbf{q}_i := (q_{(1)i}, q_{(2)i}, \dots, q_{(i-1)i}, q_{(i+1)i}, q_{(i+2)i}, \dots, q_{(n)i})^T$ for $2 \leq i \leq n-1$. The first and last columns are $\mathbf{q}_1 := (q_{(2)1}, q_{(3)1}, \dots, q_{(n)1})^T$ and $\mathbf{q}_n := (q_{(1)n}, q_{(2)n}, \dots, q_{(n-1)n})^T$, respectively.

Since $\mathbf{A}\mathbf{A}^{-1}$ is the identity matrix \mathbf{I} , then $\mathbf{A}(G-i)\mathbf{q}_i = \mathbf{0}$ for all $1 \leq i \leq n$. Therefore, \mathbf{q}_i is a kernel eigenvector (with non-zero entries) of $G-i$ for all the vertices i . Hence $G-i$ is a core graph. By interlacing, it has nullity one. It follows that each vertex-deleted subgraph is a nut graph. ■

From Lemma 3.7.1, nuciferous devices (G, \bar{L}, \bar{R}) are not of type of variety 3a(ii) for all pairs of distinct vertices \bar{L} and \bar{R} . Moreover, from Theorem 3.7.4, for $G \neq K_2$, each vertex-deleted subgraph is a nut graph and therefore has nullity one. On deleting a vertex from a nut graph, the nullity becomes zero. Hence a candidate graph G cannot be of variety 3a(ii) for *any* pair of vertices \bar{L} and \bar{R} .

Theorem 3.7.5 *Let G be a nuciferous graph. If G is not K_2 , then*

(i) it has order at least eight;

(ii) the device (G, \bar{L}, \bar{R}) is of variety 3a(i) for all pairs of distinct vertices \bar{L} and \bar{R} ;

(iii) the graph G is not bipartite.

Proof: (i) Since nut graphs exist for order at least seven [90], it follows, from Theorem 3.7.4, that a nuciferous graph G that is not a K_2 , of order at least three, has at least eight vertices.

(ii) From the proof of Lemma 3.7.1, a nuciferous graph G is of *kind* $(g_s, g_s + 1, g_s + 1, g_s)$. Thus G is a device (G, \bar{L}, \bar{R}) of variety 3a(i) for all pairs of distinct vertices \bar{L} and \bar{R} .

(iii) From Theorem 3.7.4, $G - \bar{L}$ and $G - \bar{R}$ are nut graphs and therefore cannot be bipartite [90]. Hence G has odd cycles and cannot be bipartite. ■

There exists no graph on up to 10 vertices and no chemical graph on up to 16 vertices that satisfies Theorem 3.7.4, except K_2 . As a result, in [88], the following appeared:

Conjecture 3.7.2 *There are no graphs for which every vertex-deleted subgraph is a nut graph.*

Ghorbani disproves this conjecture in [99]. However, Sciriha and Farrugia show in [100] that there are no *chemical* graphs for which every vertex-deleted subgraph is a nut graph; that is the conjecture is true for chemical graphs, the graphs with vertex degree at most three. By calling K_2 the trivial case, Ghorbani conjectures that there are infinitely many non-trivial cases. Vertex transitive graphs on up to 31 vertices were investigated and 21 nuciferous graphs were found: 6 on 24, 3 on 28 and 12 on 30 vertices [99].

3.8 Chemical implications

In the graph theoretical version of the SSP model, the variation of electron transmission with energy is qualitatively modelled in terms of the characteristic polynomials of G , $G - \bar{L}$, $G - \bar{R}$, $G - \bar{L} - \bar{R}$, where G is the molecular graph and vertices \bar{L} and \bar{R} are in contact with wires. This motivated the definition of a *device* used in this chapter. As a consequence, the transmission at the Fermi level (corresponding here to $E = 0$) obeys selection rules couched in terms of the nullities g_s , g_t , g_u , and g_v [63]. Thus, the classification of devices into *kinds* and *varieties* is used to identify molecules (with carbon atoms, in particular) that conduct or else bar conduction at the Fermi level. In [70], conductors and insulators are classified into eleven cases that are essentially the twelve kinds of Table 3.2, with case 7 in [70] corresponding to kinds (g_s, g_s, g_s, g_s) in variety 3c(iiA) and (g_s, g_s, g_s, g_s) in variety 3c(iiB). These two varieties are distinguishable by the non-vanishing or otherwise of $j_a(0)$. In terms of the varieties defined here, prediction of conduction at the Fermi level for connection across the vertex pair (\bar{L}, \bar{R}) gives varieties 1(ii), 1(iii), 3a(i), 3b(ii), 3c(i) and 3c(iiA), and insulation occurs for varieties 1(i), 2a, 2b, 3a(ii), 3b(i) and 3c(iiB).

As regards the two interesting classes of graphs with the same extremal nullity, we can say that the first class, the *uniform-core graphs*, corresponds to insulation at the Fermi level for all two-vertex connections. On the other hand, the second class, the *nuciferous graphs*, corresponds to Fermi-level conducting devices (G, \bar{L}, \bar{R}) for all pairs of distinct vertices \bar{L} and \bar{R} , and it consists of devices corresponding to non-singular graphs that are Fermi-level insulators when $\bar{L} = \bar{R}$. Therefore, nuciferous graphs have no non-bonding orbital and are conductors for all distinct vertex connection pairs and insulators for all one vertex connections. In the language to be developed further in Chapters 4 and 5 uniform-core graphs are IC with $g_s > 1$ and nuciferous graphs are CI with $g_s = 0$.

3.9 Conclusion

We have shown how the concepts of variety and kind can give an interpretation of the selection rules governing conduction in the SSP model and in particular the utility of the core/core-forbidden and upper/middle/lower classification of vertices. Two limiting cases, in terms of the kind (g_s, g_t, g_u, g_v) , the uniform-core graphs and nuciferous graphs turn out to have clear connections to extremal conduction behaviour in the SSP model.

Chapter 4

Omni-conducting and omni-insulating molecules

The main results in this chapter have been published in “Omni-conducting and omni-insulating molecules” *The Journal of Chemical Physics* **140**, 054115, 2014, Fowler, Pickup, Todorova, Borg and Sciriha [84]. This chapter is closely based on this reference, with some rewriting to incorporate new material and remove unnecessary repetitions of introductory material. Work on the topic of omni-conduction began in late 2009 as a collaboration between the Sheffield and Malta groups, and some mathematical results were presented in a Master’s Thesis by the author [101]. Some of these are re-stated and/or rederived in this chapter, as noted below.

As already pointed out in Section 2.3, the Source and Sink Potential (SSP) model can be used to predict the existence of conduction/insulation. Here we take the idea further and look for molecular conjugated π systems that respectively support ballistic conduction or show insulation at the Fermi level, irrespective of the centres chosen as connections. These will be called omni-conductors and omni-insulators, respectively. *Distinct, ipso* and *strong* omni-conductors/omni-insulators show Fermi-level conduction/insulation for all *distinct* pairs of connections, for all connections via a *single* centre, and for *both*, respectively.

It will turn out that the class of conduction behaviour depends critically on the number of non-bonding orbitals (NBO) of the molecular system (corresponding to the nullity of the graph). Distinct omni-conductors have at most one NBO; distinct omni-insulators have at least two NBO; strong omni-insulators do not exist for any number of NBO. Distinct omni-conductors with a single NBO are all also strong and correspond exactly to the class of graphs known as *nut* graphs. Families of conjugated hydrocarbons corresponding to chemical graphs with predicted omni-conducting/insulating behaviour are identified. For example, most fullerenes are predicted to be strong omni-conductors [102].

4.1 Introduction

A molecule will be modelled by its *molecular graph* G , which represents the carbon skeleton of a conjugated π system. *Chemical graphs* are defined as graphs that

Omni-conductor	Omni-insulator
A molecular graph is said to be a <i>distinct omni-conductor</i> if $T(0) \neq 0$ for <i>all</i> distinct pairs of connecting vertices, \bar{L} and \bar{R} .	A molecular graph is said to be a <i>distinct omni-insulator</i> if $T(0) = 0$ for <i>all</i> distinct pairs of connecting vertices (terminals), \bar{L} and \bar{R} .
A molecular graph is said to be an <i>ipso omni-conductor</i> if $T(0) \neq 0$ for <i>all</i> choices of single-vertex connection, $\bar{L} = \bar{R}$.	A molecular graph is said to be an <i>ipso omni-insulator</i> if $T(0) = 0$ for <i>all</i> choices of single-vertex connection $\bar{L} = \bar{R}$.
A molecular graph is said to be a <i>strong omni-conductor</i> if it is both a <i>distinct</i> and an <i>ipso</i> omni-conductor.	A molecular graph is said to be a <i>strong omni-insulator</i> if it is both a <i>distinct</i> and an <i>ipso</i> omni-insulator.

Table 4.1: The six classes of molecular graphs and the devices related to them.

are connected and have maximum degree at most three; their vertices represent unsaturated carbon centres and their edges represent the σ -bond framework. Setting aside the dependence of transmission on energy by considering conduction to take place at the Fermi level (corresponding to the zero of energy in the Hückel/SSP model) and considering the molecule to be connected to similar left and right wires via its atoms \bar{L} and \bar{R} , the question asked is whether conjugated molecular structures exist for which there is conduction (non-zero transmission) at the Fermi level for *all* choices of connections \bar{L} and \bar{R} , and similarly, for the case of insulation (zero transmission).

There can be two types of connection of the wires to ‘terminal’ vertices \bar{L} and \bar{R} in the molecular graph: either the connecting vertices are *distinct*, which is the relevant case for most applications, or they coincide, which is the so-called ‘*ipso*’ case. The fractional transmission of a ballistic electron at the Fermi level for a given connection pair (\bar{L}, \bar{R}) , which is here calculated within the SSP model, will be denoted $T(0)$. As mentioned in Chapter 3, the combination of a graph G and a pair of contact vertices, not necessarily distinct, is called a *device*. Thus, there are in principle six classes of molecular graphs and the devices related to them (Table 4.1).

It will be proved that the class of strong omni-insulators is empty. All the other classes include molecular graphs of chemical interest.

A molecule with non-bonding orbitals corresponds to a *singular* graph, and the number of non-bonding orbitals is equal to the *nullity*, the number of zero eigenvalues of the adjacency matrix of the graph. It has already been shown that the numbers of non-bonding levels of molecular graphs and subgraphs are important in defining selection rules for Fermi-level conduction of given connection pairs in general [70], and for graphene-related molecular graphs in particular [87]. The nullity is also a crucial factor in characterising omni-conductors and omni-insulators. Specifically, it will be proved here that *all* distinct omni-conductors have at most one non-bonding orbital whereas *all* distinct omni-insulators have at least two, and will give a complete characterisation of the nullity-one distinct omni-conductors.

A brief summary of the SSP model and graph theoretical background is given in Section 4.2. A unified treatment of the selection rules for Fermi-level conduction/insulation of individual devices in terms of characteristic polynomials, nullity

of graphs and vertex types is given by Sections 4.3 and 4.4. It leads to existence and characterisation results for the six classes of omni-conductors and insulators (Section 4.4). In Section 4.5, explicit calculations for large numbers of graphs in various chemically interesting classes and infinite families are presented, with statistical information about the distribution of the different classes, leading to the conclusion (Section 4.6) that omni-conduction at the Fermi level could be a widely occurring phenomenon.

4.2 Background

4.2.1 The SSP model

The SSP model, already discussed thoroughly in Chapter 2, can be used, as a simple model of ballistic conduction of electrons through a conjugated molecule [62, 69, 103]. In the tight-binding approximation, calculation of the fractional transmission of an electron with given energy reduces to the solution of the Hückel problem under scattering boundary conditions, and hence to an essentially graph theoretical question, as conduction is determined by functions of the characteristic polynomials of four graphs [63, 70, 87, 104, 105].

To recapitulate, in the SSP model, the transmission function for a molecule that has a carbon skeleton with graph G connected to similar left and right wires via molecular vertices \bar{L} and \bar{R} , is given by [63]

$$T(E) = \frac{4 \sin^2 q (ut - sv) \tilde{\beta}^2}{\left| e^{-2iq} s - e^{-iq} (u + t) \tilde{\beta} + v \tilde{\beta}^2 \right|^2} \quad (4.1)$$

where E is the reduced electron energy, defined as a scale factor where the unit is the molecular resonance integral $|\beta|$, and the zero is the molecular Coulomb integral α , which is taken here as the Fermi level. Coulomb integrals are assumed to be equal throughout the device, and the parameter $\tilde{\beta}$ is defined by the values of resonance integrals within wires ($\beta_L = \beta_R$) and between molecule and wire ($\beta_{L\bar{L}} = \beta_{R\bar{R}}$), in units of the molecular resonance integral β , (which is the unit for all energies occurring in the model): $\tilde{\beta} = \beta_{L\bar{L}}/\beta_L = \beta_{R\bar{R}}/\beta_R$. Typically, $\tilde{\beta}^2 \simeq 1/2$ [63, 69]. The $4 \sin^2 q$ factor in Eq. (4.1) acts to confine transmission to the conduction band of the wires. In Eq. (4.1) q is the wavenumber of the electron wave (defined by $E = 2 \cos q$, with energy in units of $|\beta|$). The quantities s, t, u, v are the characteristic polynomials $\phi(G, E)$, $\phi(G - \bar{L}, E)$, $\phi(G - \bar{R}, E)$, $\phi(G - \bar{L} - \bar{R}, E)$ of the graphs G , $G - \bar{L}$, $G - \bar{R}$ and $G - \bar{L} - \bar{R}$, respectively, i.e., they are the determinants (refer to Eq. (2.26)). G must be a connected graph if it is to represent a conjugated π system; deletion of vertices as in $G - \bar{L}$, $G - \bar{R}$, and $G - \bar{L} - \bar{R}$ may result in a disconnected graph. Another quantity that is important in the determination of transmission is the combination $ut - sv$, which is equal to a squared polynomial [106]

$$j^2(E) = u(E)t(E) - s(E)v(E) = (|\mathbf{EI} - \mathbf{A}(G)|^{\bar{L}, \bar{R}})^2. \quad (4.2)$$

It can be shown that $j(E)$ is the entry at position \bar{L}, \bar{R} of the adjugate matrix $\text{adj}(E\mathbf{I}-\mathbf{A})$ and, if the matrix $(E\mathbf{I}-\mathbf{A})$ is invertible, then at any energy E , $j(E)$ is proportional to the \bar{L}, \bar{R} entry in the inverse $(E\mathbf{I}-\mathbf{A})^{-1}$, with constant of proportionality equal to the determinant of the matrix (Appendix 2 in [83]). The usual *distinct* case for a molecular device has $\bar{L} \neq \bar{R}$. In the *ipso* case, where both wires contact a single atom, $\bar{L} = \bar{R}$, polynomials t and u are identical, and v is deleted from the equations.

As $E = 2 \cos q$ [69], expanding the denominator and making trigonometric substitutions, to give the full energy dependence of the transmission (4.1)

$$T(E) = \frac{(4 - E^2)j^2\tilde{\beta}^2}{[(s - v\tilde{\beta}^2)^2 + (u + t)^2\tilde{\beta}^2] - E(s + v\tilde{\beta}^2)(u + t)\tilde{\beta} + E^2sv\tilde{\beta}^2} \quad (4.3)$$

and for transmission of electrons at the Fermi level, the limit is taken according to:

$$T(0) = \lim_{E \rightarrow 0} T(E).$$

In the analysis that follows, we assume that $\tilde{\beta}^2 \neq 0$ and that $(s - v\tilde{\beta}^2)^2 \neq 0$ at the energy of interest. Thus, effectively, questions about the vanishing of $(s - v\tilde{\beta}^2)^2$ can be answered by inspection of $s^2 + v^2$. Physically, the claim is that even if $\tilde{\beta}$ happens to take one of the special values, there will always be a ‘nearby’ device where it does not, and to which our generic conclusions will apply.

It is straightforward to show that the zero-energy limit of Eq. (4.3) is equivalent to the simpler expression

$$T(0) = \lim_{E \rightarrow 0} \frac{4j^2\tilde{\beta}^2}{[(s - v\tilde{\beta}^2)^2 + (u + t)^2\tilde{\beta}^2]} \quad (4.4)$$

The question for a qualitative treatment is whether $T(0)$ is zero, or not. It has been shown [70] that the answer to this question for a given connection pattern can be decided in almost all cases simply by counting the zero eigenvalues of the graph and of its vertex-deleted subgraphs, which leads to a set of ‘selection-rules’ for conduction. In order to exploit this insight further, and make a systematic investigation of the questions of omni-conduction and insulation, it is necessary to understand how the outcome depends on the intrinsic properties of the connecting vertices relative to the nullspace vectors.

4.2.2 Characteristic polynomials

An expression for $T(E)$ can now be assembled, and its limit taken using the numerator and denominator terms from Eq. (4.4). As in Chapter 3, we expand the structural polynomials:

$$\begin{aligned}
t(E) &= t_b E^{g_s-1} + t_a E^{g_s} \\
u(E) &= u_b E^{g_s-1} + u_a E^{g_s} \\
j(E) &= j_b E^{g_s-1} + j_a E^{g_s} \\
v(E) &= v_c E^{g_s-2} + v_b E^{g_s-1} + v_a E^{g_s}
\end{aligned} \tag{4.5}$$

Explicit expressions are given in Chapter 3 Section 3.3. The numerator of Eq. (4.4) is then expressed as

$$4\tilde{\beta}^2 j^2 = 4\tilde{\beta}^2 (j_a^2 E^2 + 2j_a j_b E + j_b^2) E^{2g_s-2} \tag{4.6}$$

and the denominator of Eq. (4.4) is

$$\begin{aligned}
(s - \tilde{\beta}^2 v)^2 + (u + t)^2 \tilde{\beta}^2 = & \\
& \{E^4[(s_0 - \tilde{\beta}^2 v_a)^2 + (u_a + t_a)^2 \tilde{\beta}^2] \\
& + E^3[-2v_b(s_0 - v_a \tilde{\beta}^2) + 2(u_a + t_a)(u_b + t_b)] \tilde{\beta}^2 \\
& + E^2[v_b^2 \tilde{\beta}^2 - 2v_c(s_0 - v_a \tilde{\beta}^2) + (u_b + t_b)^2] \tilde{\beta}^2 \\
& + E[2v_b v_c] \tilde{\beta}^4 + v_c^2 \tilde{\beta}^4\} E^{2g_s-4}
\end{aligned} \tag{4.7}$$

(This corrects a minor typo in Eq. (23) of [84].)

As both numerator and denominator may vanish at $E = 0$, it is not sufficient simply to examine whether j vanishes to determine the conduction or insulation behaviour of a device with a given pair of contacts. In general, it is necessary to delve more deeply into the cancellation behaviour of the numerator and denominator as E approaches zero.

The advantage of the present formulation for $T(E)$ is that the conductive properties of all devices based on a given molecular graph can be determined from a simple calculation of the eigenvectors and eigenvalues of G alone. No separate calculations on the n vertex-deleted graphs $G - w$ or the $n(n - 1)/2$ double-deleted graphs $G - w - z$ are required. This gives the basis for an efficient computational scheme for identifying omni-conductors and omni-insulators. Conditions for insulation or conduction for a distinct pair of contact vertices in a graph with a particular nullity are easily deduced (Tables 4.2 and 4.3); analogous conditions for *ipso* connections are derived by setting $v_a = v_b = v_c = 0$, $u_a = t_a$ and $u_b = t_b$. (These versions follow [107], where a misprint in [84] is corrected.)

4.3 Devices and varieties

In principle, there are 64 types of device, depending on which of the six parameters u_b , t_b , v_b , v_c , j_a and j_b vanish at $E = 0$, but not all combinations are possible, because of the Interlacing Theorem, and not all are independent, as \bar{L} and \bar{R} play

$g_s = 0$	$j_a = 0$
$g_s = 1$	$\left\{ \begin{array}{l} j_b = 0 \text{ and } j_a = 0 \\ \text{or} \\ j_b = 0 \text{ and } j_a \neq 0 \end{array} \right\} \left\{ \begin{array}{l} u_b + t_b \neq 0 \\ \text{or} \\ v_b \neq 0 \end{array} \right.$
$g_s > 1$	$\left\{ \begin{array}{l} v_c \neq 0 \\ \text{or} \\ v_c = 0 \end{array} \right\} \left\{ \begin{array}{l} j_b = 0 \text{ and } j_a \neq 0 \text{ and } v_b \neq 0 \text{ or } u_b + t_b \neq 0 \\ \text{or} \\ j_b = 0 \text{ and } j_a = 0 \end{array} \right.$

Table 4.2: The seven conditions for insulation.

$g_s = 0$	$j_a \neq 0$
$g_s = 1$	$\left\{ \begin{array}{l} j_b \neq 0 \\ \text{or} \\ j_b = 0 \text{ and } j_a \neq 0 \text{ and } u_b + t_b = 0 \text{ and } v_b = 0 \end{array} \right\} \left\{ \begin{array}{l} u_b + t_b \neq 0 \\ \text{or} \\ v_b \neq 0 \end{array} \right.$
$g_s > 1$	$\left\{ \begin{array}{l} v_c = 0 \text{ and } j_b \neq 0 \\ \text{or} \\ v_c = 0 \text{ and } j_b = 0 \text{ and } j_a \neq 0 \text{ and } u_b + t_b = 0 \text{ and } v_b = 0 \end{array} \right\} \left\{ \begin{array}{l} u_b + t_b \neq 0 \\ \text{or} \\ v_b \neq 0 \end{array} \right.$

Table 4.3: The seven conditions for conduction.

symmetrical roles. A device with distinct connections ($\bar{L} \neq \bar{R}$) falls under one of three categories leading to the definition of six main varieties of connection pairs, as mentioned in Section 3.4:

- Variety 1: two CV connections,
- Variety 2a: one CV connection and one CFV middle,
- Variety 2b: one CV connection and one CFV upper,
- Variety 3a: two CFV upper connections,
- Variety 3b: one CFV middle connection and one CFV upper,
- Variety 3c: two CFV middle connections.

Varieties 1 and 2 are characterised by $t_b(0) \neq 0$ and/or $u_b(0) \neq 0$. Recall that $t_b(0) \neq 0$ if and only if \bar{L} is a CV, and $u_b(0) \neq 0$ if and only if \bar{R} is a CV. The varieties can be further subdivided into types distinguished by the behaviour at $E = 0$ of t , u , v or j . A further subdivision of varieties can be based on the relative nullities of G , $G - \bar{L}$, $G - \bar{R}$, and $G - \bar{L} - \bar{R}$, which in turn are restricted by the operation of the Interlacing Theorem.

The final set of twelve device varieties is summarised in Table 4.4 (a reformulation of Table 3.2), where details of the properties of the characteristic polynomials at

$E = 0$, and the conclusions that can be drawn about their conduction/insulation behaviour, are also listed.

Kind	(g_s, g_t, g_u, g_v)	Variety	Case [70]	Conduction?
Two CVs		1		
	$(g_s, g_s - 1, g_s - 1, g_s - 2)$	1(i)	D11	Insulation
	$(g_s, g_s - 1, g_s - 1, g_s)$	1(ii)	D9	Conduction
	$(g_s, g_s - 1, g_s - 1, g_s - 1)$	1(iii)	D10	Conduction
CV and CFV		2		
	$(g_s, g_s + 1, g_s - 1, g_s)$	2a	D5	Insulation
	$(g_s, g_s, g_s - 1, g_s - 1)$	2b	D8	Insulation
Two CFVs		3		
	$(g_s, g_s + 1, g_s + 1, g_s)$	3a(i)	D2	Conduction
	$(g_s, g_s + 1, g_s + 1, g_s + 2)$	3a(ii)	D1	Insulation
	$(g_s, g_s + 1, g_s, g_s + 1)$	3b(i)	D3	Insulation
	$(g_s, g_s + 1, g_s, g_s)$	3b(ii)	D4	Conduction
	$(g_s, g_s, g_s, g_s + 1)$	3c(i)	D6	Conduction
	(g_s, g_s, g_s, g_s) and $j_a(0) \neq 0$	3c(iiA)	D7	Conduction
	(g_s, g_s, g_s, g_s) and $j_a(0) = 0$	3c(iiB)	D★7	Insulation

Table 4.4: A characterisation of *distinct* devices (G, \bar{L}, \bar{R}) . The nullity signature (g_s, g_t, g_u, g_v) lists the numbers of zero eigenvalues of the graphs G , $G - \bar{L}$, $G - \bar{R}$ and $G - \bar{L} - \bar{R}$. The 12 varieties defined from the nullity signature in the present chapter are correlated with the 11 cases defined in the earlier treatment of the nullity selection rules [70]; the variety/case marked 3c(iiB) and D★7 corresponds to the so-called accidental situation, where all four graphs have equal nullity and $j_a(0)^2 = u_a(0)t_a(0) - s_0(0)v_a(0) = 0$, but the terms $u_a(0)t_a(0)$ and $s_0(0)v_a(0)$ are individually non-zero.

Every variety is realised in some chemical graph, and a single molecular graph may have connection pairs of several varieties. The table also gives the correspondence with the 11 cases previously used to derive the nullity-based selection rules for molecular conduction [70]. Devices with distinct connections conduct or not, depending on four selection rules based on the quantities g_s, g_t, g_u, g_v , which are the numbers of zero roots of the four characteristic polynomials s, t, u and v , respectively. We write $s(0) = s_0 E^{g_s}$, $t(0) = t_0 E^{g_t}$, $u(0) = u_0 E^{g_u}$ and $v(0) = v_0 E^{g_v}$, where s_0, t_0, u_0 and v_0 are all non-zero. The selection rules are then those as mentioned in Section 2.4 [70].

The full set of 11 selection rules is relevant in molecular conduction, as examples of all cases occur for small molecular graphs. Fig. 4.1 shows the smallest examples of devices based on chemical graphs that require invocation of each selection rule.

The extra utility of thinking about classification of vertices by CV and CFV types is that it gives a different way of detecting when and why certain cases can occur. It also leads to the possibility of deriving ‘super selection rules’ for omni-conductors and omni-insulators that deal simultaneously with all devices based on given graphs, as will be demonstrated in Section 4.4. Some relationships that link the types of the connection vertices with the conduction behaviour of the device and are easily proved include the following:

Proposition 4.3.1 *A device with two core vertices as connections (Variety 1) is an insulator at $E = 0$ if and only if it is of Variety 1(i), i.e., has $g_v = g_s - 2$.*

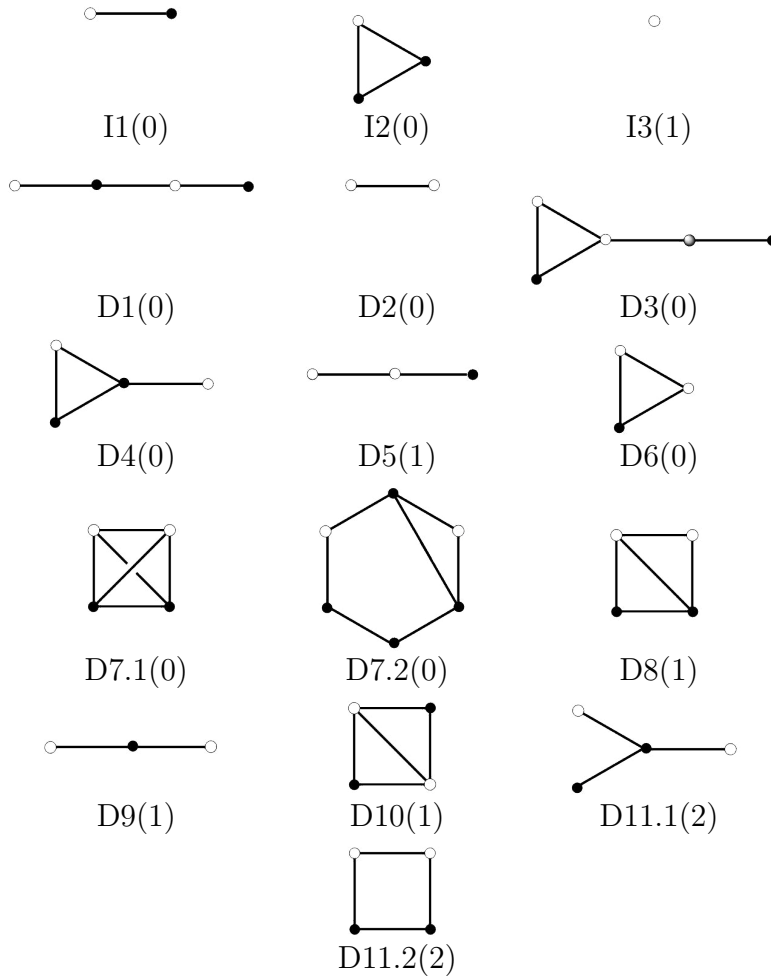


Figure 4.1: Smallest examples of the 11 selection rules for *ipso* and *distinct* devices based on chemical graphs, named by case and nullity listed in brackets. The subcases of Cases 7 and 11 are distinguished by values of g_j , the number of roots of the j polynomial, which will turn out to be of significance later. White-filled circles show the pair of connection vertices satisfying the case. Where there are possibilities that are not equivalent by symmetry, a device satisfying the case is found by taking the metallic-shaded vertex with any one of the white-filled circles.

Proposition 4.3.2 *For Variety 2 connections, i.e., with one CV and one CFV, there is no conduction at $E = 0$.*

Connections of Variety 3, where both are CFV, yield more mixed results. In Variety 3c(ii), $g_v = g_s$, v_a is non-zero at $E = 0$, and two cases may occur: either $j_a \neq 0$ at $E = 0$, or j_a has more than one zero. The first case is Variety 3c(iiA), and the device conducts. The second is Variety 3c(iiB), and the device is an insulator. Both varieties are included under a single ‘Case 7’ in the classification by nullity signature that was used in the previous treatment [70]; in the present case, 3c(iiB) corresponds to the ‘accidental’ subcase of Case 7, where $u_0 t_0 - s_0 v_0$ vanishes. This ‘accident’ occurs often in practice (see Fig. 4.2).

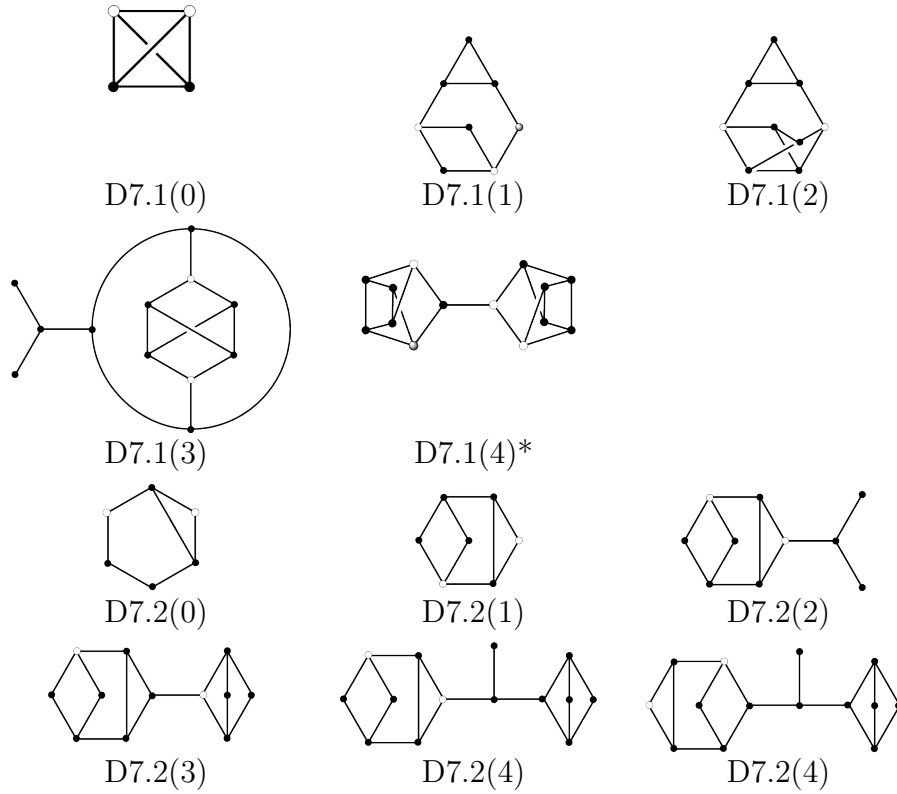


Figure 4.2: Examples of Case 7 selection rules for devices based on chemical graphs, named by case and nullity, $g_s \neq 0$. The labelling convention is as in Fig. 4.1. In the graph labelled * the central pair of cut-vertices also satisfy the case, and thus there are in total four non-isomorphic devices of type D7.1(4) for this graph.

4.4 Implications for omni-conductors and omni-insulators

The considerations of Section 4.3 lead to some general conclusions based on the types of connection vertex. These can be assembled to give a global picture of the classes of omni-conductors and omni-insulators. The existence of omni-conductors could be expected, as the systems under study are conjugated, with extensive delocalisation of electrons, but the fact that omni-insulators exist is more surprising, as an omni-insulator has mobile, delocalised electrons and yet by definition it does not conduct at the Fermi level, no matter which connection vertices are chosen.

4.4.1 Deductions by device type: distinct connections

4.4.1.1 Graphs of nullity $g_s = 0$

A simple criterion emerges for non-singular graphs, namely that Fermi insulation or conduction across \bar{L} and \bar{R} depends only on whether j_a vanishes at $E = 0$, since the denominator in Eq. (4.4) does not vanish for $g_s = 0$. Furthermore, for nullity $g_s = 0$, the entry in position \bar{L}, \bar{R} of $(E\mathbf{I} - \mathbf{A})^{-1}$ is equal to $j_a(E)$ divided by the determinant $|E\mathbf{I} - \mathbf{A}|$ [83]. Therefore:

Theorem 4.4.1 *A necessary and sufficient condition for conduction at $E = 0$ of a non-singular graph with connection vertices \bar{L}, \bar{R} is that $(\mathbf{A}^{-1})_{\bar{L}, \bar{R}} \neq 0$.*

As the determinant $|\mathbf{A}|$ is non-zero for a non-singular graph, we could equally well test the corresponding element of the adjugate $\text{adj}(\mathbf{A})$.

Some deductions follow:

Corollary 4.4.2 *A non-singular graph ($g_s = 0$) is a strong omni-conductor if and only if the inverse matrix \mathbf{A}^{-1} is full (i.e., has no zero elements) (See also [101] Theorem 7.2.4).*

The isolated-pentagon C_{60} is one of many fullerene examples of strong omni-conductors of this type.

Corollary 4.4.3 *A non-singular graph ($g_s = 0$) is a distinct omni-conductor if and only if the off-diagonal part of the inverse matrix \mathbf{A}^{-1} is full (See also [101] Theorem 7.2.3).*

Families of non-singular graphs that are distinct omni-conductors include the complete graphs K_r , $r \geq 2$ and the cycles C_{2k+1} , $k \geq 1$.

Corollary 4.4.4 *A non-singular graph ($g_s = 0$) is an ipso omni-conductor if and only if the inverse matrix \mathbf{A}^{-1} has a full diagonal.*

Corollaries 4.4.2 and 4.4.4 can be interpreted as saying that for a non-singular graph to be an *ipso* omni-conductor, each vertex must be a middle CFV (a core-forbidden vertex whose deletion does not change the nullity).

Corollary 4.4.5 *There are no non-singular distinct omni-insulators (and hence no non-singular strong omni-insulators) (See also [101] Theorem 7.3.1).*

This last corollary follows since, as if \mathbf{A}^{-1} is diagonal, then \mathbf{A} is diagonal too, implying that the graph G has no edges and hence is not connected. Non-singular *ipso* omni-insulators exist, and in fact *all ipso* omni-insulators are non-singular, with each vertex being an upper CFV (a core-forbidden vertex whose deletion increases the nullity). For example, any non-singular bipartite graph consists entirely of *upper* core-forbidden vertices and hence is an *ipso* omni-insulator: this class includes all Kekulean benzenoids (a benzenoid is Kekulean if it has a perfect matching (Kekulé structure)). A curious observation is that a graph may be *ipso* omni-insulating but *distinct* omni-conducting (a so-called *nuciferous* graph [88]).

4.4.1.2 Graphs of nullity $g_s = 1$

For graphs of nullity one, there is an analogous but weaker condition for conductivity, based on the adjugate matrix:

Theorem 4.4.6 *A sufficient condition for conduction at $E = 0$ of a device based on a graph of nullity one with connection vertices \bar{L} and \bar{R} is that \bar{L} and \bar{R} are core vertices and $\text{adj}(\mathbf{A})_{\bar{L},\bar{R}} \neq 0$ (See also [101] Theorem 7.2.7).*

As the entry in $\text{adj}(\mathbf{A})$ is non-zero for every core-core pair in a graph with nullity one, this implies that *all* core-core pairs are conducting for graphs with $g_s = 1$. Moreover, it is straightforward to show from Table 4.4 that, for $g_s = 1$, when the pair \bar{L}, \bar{R} consists of one core and one core-forbidden vertex (hence $g_t = g_s - 1$ and $g_v = g_s$ or $g_v = g_s - 2$), the device is insulating. This case can be recognised from the adjugate, since for a CV/CFV pair the off-diagonal entry $\text{adj}(\mathbf{A})_{\bar{L}\bar{R}}$ is zero and exactly one of $\text{adj}(\mathbf{A})_{\bar{L}\bar{L}}$ and $\text{adj}(\mathbf{A})_{\bar{R}\bar{R}}$ is non-zero, with the non-zero entry corresponding to the core vertex [96]. Behaviour of devices where *both* \bar{L} and \bar{R} are core-forbidden depends on the combinations of upper and middle types, as detailed by the selection rules (Table 4.4).

From Theorem 4.4.6, we have the following corollaries:

Corollary 4.4.7 *The distinct omni-conductors with $g_s = 1$ are exactly the nut graphs.*

This follows easily from the fact that a singular graph has core vertices. If the graph has any core-forbidden vertex, there is at least one insulating device. Hence, any distinct omni-conductor must contain *only* core vertices. A graph that has only core vertices and nullity 1 is a nut graph by definition. Nut graphs are also *ipso* omni-conductors.

Corollary 4.4.8 *The strong omni-conductors with $g_s = 1$ are exactly the nut graphs (See also [101] Theorem 7.2.15).*

The nut graphs are only a subset of the *ipso* omni-conductors with nullity 1. For example, the isolated-pentagon fullerene C_{70} has $g_s = 1$, is not a nut graph, but is an *ipso* omni-conductor [102].

Corollary 4.4.9 *There are no strong omni-insulators with $g_s = 1$ (See also [101] Theorem 7.3.2).*

This follows from the fact that any graph with $g_s = 1$ has at least two core vertices, but clearly cannot have $g_v = g_s - 2$; there is at least *one* conducting device with distinct connections, and at least *two* with *ipso* connections, all based on the same graph.

4.4.1.3 Graphs of nullity $g_s > 1$

When the nullity is larger, the situation for core–core pairs is more complicated, but we do have one useful statement:

Theorem 4.4.10 *A device where both \bar{L} and \bar{R} are core vertices and $g_s \geq 2$ is insulating if the nullity of $G - \bar{L} - \bar{R}$ is $g_s - 2$, i.e., if \bar{L} is a core vertex of $G - \bar{R}$ and \bar{R} is a core vertex of $G - \bar{L}$.*

The significance of this technical statement derives from the fact that *all* graphs with $g_s > 1$ have at least one such core–core pair. The existence of this pair is easily proved using the idea of *vertex representatives* of the nullspace of a graph [97, 108]. The essential idea is that for $g_s > 1$ it is always possible to construct g_s independent (not necessarily orthogonal or normalised) kernel eigenvectors such that when these vectors are written out as rows with core vertices occurring first, the entries for the first g_s vertices form a $g_s \times g_s$ identity matrix. A consequence of taking this special form of the vectors is that removal of any two of the chosen core vertices leads to a graph with nullity $g_v = g_s - 2$. Hence, *every* graph with $g_s > 1$ gives rise to at least one device with distinct connections that is insulating at the Fermi level.

It is possible to find graphs with $g_s > 1$ where every vertex is a CV and hence every pair of connections \bar{L} and \bar{R} leads to insulation. Graphs of this type have been called *uniform-core* graphs. They are extremal in the opposite way to nuciferous graphs [88].

From Theorem 4.4.10:

Corollary 4.4.11 *There are no distinct (and no strong) omni-conductors of nullity $g_s > 1$.*

We can remark that *ipso* omni-conductors with $g_s > 1$ exist: they may contain core vertices only, or consist of a mixture of core and middle vertices. An example is the ‘carbon cylinder’ isolated-pentagon isomer of fullerene C_{84} , 84:24 [109], which has $g_s = 3$.

Corollary 4.4.12 *There are no ipso (and hence no strong) omni-insulators of nullity $g_s > 1$.*

The proof is the same as for $g_s = 1$. Taken with Corollary 4.4.9, this implies that all *ipso* omni-insulators are non-singular. However, singular distinct omni-insulators exist. They must contain only core vertices and each of the pairs of core vertices must give $g_v = g_s - 2$, implying $g_s > 1$.

4.4.2 Deductions by device type: *ipso* connections

For *ipso* connections, the formula for transmission, Eq. (4.4), reduces to a single form, irrespective of the nullity of the graph:

$$T(E) = \frac{4\tilde{\beta}^2 t^2}{s_0^2 + 4\tilde{\beta}^2 t^2}. \quad (4.8)$$

If $t_b \neq 0$ the device conducts. If $t_b = 0$ then either $t_a \neq 0$, giving conduction, or $t_a = 0$, giving insulation. *Ipso* devices follow a set of selection rules embodied in Table 4.5. The equivalents for *ipso* devices of the various statements made in the Section 4.4.1 about distinct devices are as follows.

Kind	(g_s, g_t)	Case [70]	Conduction?
CFV upper	$(g_s, g_s + 1)$	I1	Insulation
CFV middle	(g_s, g_s)	I2	Conduction
CV	$(g_s, g_s - 1)$	I3	Conduction

Table 4.5: A characterisation of *ipso* devices (G, y, z) . The nullity signature (g_s, g_t) lists the numbers of zero eigenvalues of the graphs $G, G - \bar{L}$.

Theorem 4.4.13 *A necessary and sufficient condition for conduction at $E = 0$ of a non-singular graph with connection vertices $\bar{L} = \bar{R}$ is that $(\mathbf{A}^{-1})_{\bar{L}, \bar{L}} \neq 0$.*

For non-singular graphs $t = t_a$, so the device conducts at the Fermi level if and only if $t_a \neq 0$. For singular graphs, the CVs and CFVs are distinguished by the value of t_b . Moreover, the value of t_a distinguishes between *ipso* connections at middle and upper vertices, for which there is conduction and insulation, respectively.

Theorem 4.4.14 *For an ipso connection in a singular graph, there is conduction at $E = 0$ when the connecting vertex v is a CV or a middle CFV, and conversely, insulation when the connecting vertex is an upper CFV.*

4.4.3 Deductions by conduction class

The results listed in this section so far show that nullity one is an important dividing line between conducting and insulating regimes. Four global statements emphasising this special role of non-bonding orbitals in conduction, all of which follow from the above, are as follows:

Corollary 4.4.15 *All distinct and strong omni-conductors have nullity $g_s \leq 1$.*

Corollary 4.4.16 *For nullity $g_s = 1$, all distinct or strong omni-conductors are nut graphs.*

Corollary 4.4.17 *All distinct omni-insulators have nullity $g_s > 1$.*

Corollary 4.4.18 *There are no strong omni-insulators.*

Table 4.6 reports the main theoretical conclusions as a summary of the distribution of conduction and insulation behaviour across the six classes and three nullity regimes. It can be seen that nine of the 18 combinations are impossible and nine are realisable, of which two are characterised exactly as the nut graphs. This classification is explored further in Chapter 5, where it is illustrated by a Venn-like diagram showing how the classes may combine (Fig. 5.1). Significantly, we have examples of chemical graphs for all of the realisable combinations. Conjugated π systems with the various predicted omni-conduction or omni-insulation properties are in fact very common in chemistry.

	Non-singular	Nullity one	Nullity \geq two
Distinct omni-conductor	SOME	NUT	NONE
<i>Ips</i> o omni-conductor	SOME	SOME	SOME
Strong omni-conductor	SOME	NUT	NONE
Distinct omni-insulator	NONE	NONE	SOME
<i>Ips</i> o omni-insulator	SOME	NONE	NONE
Strong omni-insulator	NONE	NONE	NONE

Table 4.6: Classification of omni-conductors and omni-insulators by class and nullity. NONE indicates classes unrealisable by connected graphs. Of the nine realisable classes, two are precisely the class of nut graphs (denoted NUT). Other realisable classes are simply marked SOME.

4.5 Results

4.5.1 Statistics of conduction of molecular graphs

Calculations implementing the rules embodied in Tables 4.2 and 4.3 were carried out for various sets of graphs in order to check for the abundance of omni-conductors and omni-insulators amongst conjugated systems, and identify families that show these properties. Generators geng (part of the nauty software written by B. D. McKay and available at <http://cs.anu.edu.au/~bdm/>), plantri [110], CaGe [111], fullgen [112], and our own in-house programs were used to construct general families of graphs.

The generated datasets include chemical graphs (connected graphs with maximum degree ≤ 3), chemical trees (acyclic chemical graphs), benzenoids (subgraphs of the hexagonal tessellation of the plane with all internal faces hexagonal and without holes or handles), cubic polyhedra (planar, 3-connected graphs), fullerenes (cubic polyhedra with face sizes restricted to 5 and 6), general graphs (connected graphs without limitation of maximum degree), and general trees (acyclic general graphs). Note that our definition of a chemical tree is that it is a tree with maximum degree ≤ 3 , i.e. it is a chemical graph in our case. Some authors [113] allow degree 4 for chemical trees, for the purpose of counting alkanes. Here we are concerned with unsaturated carbon frameworks.

For all sets, conductors and insulators were enumerated. Summaries of the results are given in Tables 4.7 to 4.11. In the tables, we count ‘pure’ cases of each type; pure *ipso* or distinct omni-insulators/conductors are respectively *ipso* or distinct but not strong.

n	$N(n)$	Insulators		Conductors			N_{nut}
		N_{ipso}^i	N_{distinct}^i	N_{ipso}^c	N_{distinct}^c	N_{strong}^c	
2	1	1	0	0	1	0	0
3	2	0	0	0	0	1	0
4	6	1	1	2	0	1	0
5	10	0	0	1	0	1	0
6	29	6	1	4	0	2	0
7	64	0	1	2	0	5	0
8	194	24	0	15	0	8	0
9	531	0	1	26	0	14	1
10	1733	132	2	88	5	48	0
11	5524	0	2	210	0	85	8
12	19430	902	3	665	9	342	9
13	69322	0	6	2034	0	885	27
14	262044	7669	10	7055	151	3744	23
15	1016740	0	22	26946	73	10788	414
16	4101318	77056	45	95539	2311	50770	389

Table 4.7: Distribution of omni-insulators and omni-conductors amongst chemical graphs with $n \leq 16$. $N(n)$ is the total number of chemical graphs, N_{ipso}^i is the number of pure *ipso* omni-insulators, N_{distinct}^i is the number of pure distinct omni-insulators. N_{ipso}^c is the number of pure *ipso* omni-conductors, N_{distinct}^c is the number of pure distinct omni-conductors and N_{strong}^c is the number of strong (*ipso* + distinct) omni-conductors. N_{nut} counts the chemical graphs that are also nut graphs.

n	$N(n)$	Insulators		Conductors			N_{nut}
		N_{ipso}^i	N_{distinct}^i	N_{ipso}^c	N_{distinct}^c	N_{strong}^c	
2	1	1	0	0	1	0	0
3	2	0	0	0	0	1	0
4	6	1	1	2	0	1	0
5	21	0	1	4	0	3	0
6	112	7	2	21	0	7	0
7	853	0	7	136	0	38	3
8	11117	129	20	1352	0	496	13
9	261080	0	107	32575	31	10132	560
10	11989762	15356	938	1429875	406	783928	12551

Table 4.8: Distribution of omni-insulators and omni-conductors amongst general graphs with $n \leq 10$. $N(n)$ is the total number of connected graphs, N_{ipso}^i is the number of pure *ipso* omni-insulators, N_{distinct}^i is the number of pure distinct omni-insulators. N_{ipso}^c is the number of pure *ipso* omni-conductors, N_{distinct}^c is the number of pure distinct omni-conductors and N_{strong}^c is the number of strong (*ipso* + distinct) omni-conductors. N_{nut} counts the general graphs that are also nut graphs. This is a corrected version of a table that appeared in the published paper [84]; Mr Aidan Birkinshaw is thanked for pointing out some misplaced entries.

n	$N(n)$	N_{ipso}^i	$N_{\text{distinct}}^i (\eta)$	n	$N(n)$	N_{ipso}^i	$N_{\text{distinct}}^i (\eta)$
2	1	1	0	14	552	96	0
3	1	0	0	15	1132	0	0
4	2	1	1 (2)	16	2410	319	6 (6)
5	2	0	0	17	5098	0	0
6	4	2	0	18	11020	1135	0
7	6	0	1 (3)	19	23846	0	13 (7)
8	11	4	0	20	52233	4150	0
9	18	0	0	21	114796	0	0
10	37	11	2 (4)	22	254371	15690	31 (8)
11	661	0	0	23	565734	0	0
12	135	30	0	24	1265579	60506	0
13	265	0	3 (5)	25	2841632	0	73 (9)

Table 4.9: Distribution of omni-insulators amongst chemical trees with $n \leq 25$. $N(n)$ is the total number of chemical trees with n vertices N_{ipso}^i is the number of pure *ipso* omni-insulators, N_{distinct}^i is the number of pure distinct omni-insulators and η is the nullity of (all) the distinct omni-insulating chemical trees on n vertices.

n	$N(n)$	N_{ipso}^i	$N_{\text{distinct}}^i (\eta)$
2	1	1	0
3	1	0	0
4	2	1	1 (2)
5	3	0	1 (3)
6	6	2	1 (4)
7	11	0	2 (5,3)
8	23	5	3 (6,4)
9	47	0	4 (7,5)
10	106	39	7 (8,6,4)

Table 4.10: Distribution of omni-insulators amongst all trees with $n \leq 10$. $N(n)$ is the total number of trees with n vertices, N_{ipso}^i is the number of pure *ipso* omni-insulators, N_{distinct}^i is the number of pure distinct omni-insulators and η is the set of nullities achieved by distinct omni-insulating trees on n vertices, e.g., nullities 8, 6 and 4 for the 7 distinct omni-insulators with 10 vertices.

If extrapolation from small numbers can be trusted, omni-conductors and omni-insulators, though numerous, constitute only a small fraction of the rapidly increasing numbers of chemical graphs and general graphs. In chemical graphs, the proportion appears to oscillate around a relative decrease with increasing n . Subject to the caveat about small numbers, pure *ipso* omni-conductors are more numerous than strong omni-conductors, which in turn are more numerous than pure distinct omni-conductors. For insulators, strong omni-insulators do not exist (Corollary 4.4.18), and pure *ipso* omni-insulators appear to outnumber pure distinct omni-insulators. All nut graphs are strong omni-conductors (Corollary 4.4.8), but constitute only a small fraction of the total set of strong omni-conductors. Fig. 4.3 shows the smallest chemical nut graph.

Tables 4.7 and 4.8 suggest that *ipso* omni-insulators with odd n are either rare or do not exist. The question is open, but, it is apparent (Corollaries 4.4.9 and 4.4.12) that all *ipso* omni-insulators are non-singular, with all vertices of CFV (upper)

n	$N(n)$	N_{ipso}^i	N_{ipso}^c	N_{distinct}^c	N_{nut}^c
4	1	0	0	1	0
6	1	0	1	0	0
8	2	1	0	0	0
10	5	0	1	4	0
12	14	0	9	4	2
14	50	1	8	17	0
16	233	2	80	125	0
18	1249	0	327	708	285
20	7595	7	1343	3925	0

Table 4.11: Distribution of omni-insulators and omni-conductors amongst the cubic polyhedra with $n \leq 20$. $N(n)$ is the total number of cubic polyhedra, N_{ipso}^i is the number of pure *ipso* omni-insulators, N_{ipso}^c is the number of pure *ipso* omni-conductors, N_{strong}^c is the number of strong omni-conductors, and N_{nut}^c is the number of cubic polyhedra that are also nut graphs. In the range, there are neither pure distinct omni-insulators nor pure distinct omni-conductors, but the fullerenes provide examples of larger cubic polyhedra that are pure distinct omni-conductors [102].

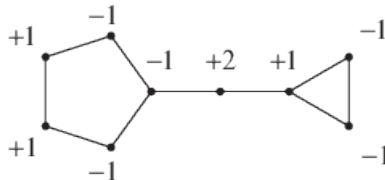


Figure 4.3: The smallest nut graph that is also a chemical graph. Relative values of the entries in the unique nullspace eigenvector are shown on the diagram.

type (Theorem 4.4.14). Thus, if *ipso* omni-insulators with odd n exist, they are non-bipartite (odd bipartite graphs have odd $\eta \geq 1$) and must have at least *two* disjoint odd cycles, since deletion of any vertex leaves a graph with even order but $\eta = 1$, implying a non-bipartite graph. Furthermore, a construction for reducing *ipso* omni-insulators [114] (Algorithm 36 in that paper) implies that the smallest such graph has no pendant edge.

Tables 4.9 and 4.10 deal with chemical and general trees. From the results, it appears that there are no *ipso* (and hence no strong) omni-conducting trees, that there are no *ipso* omni-insulating trees with odd numbers of vertices, and that K_2 is the only distinct omni-conducting tree. These three observations are all general, as shown by the following arguments. For the first observation, note that every tree has at least one CFV (upper) vertex. Hence by Theorems 4.4.13 and 4.4.14 there is at least one *ipso*-insulating vertex in every tree. For the second, note that an *ipso* omni-insulator is non-singular, but trees with odd numbers of vertices are all singular. For the third observation the chain of reasoning is longer. Distinct omni-conductors are either nut graphs or non-singular. No tree on $n > 1$ vertices is a nut graph. For non-singular distinct omni-conductors, off-diagonal entries in the inverse matrix \mathbf{A}^{-1} are all non-zero (Theorem 4.4.1). Hence each vertex-deleted subgraph arising from a putative distinct omni-conducting tree would have to be a nut graph [88] and also a tree, yielding a contradiction unless the starting tree is K_2 . Hence, we have the following theorem:

Theorem 4.5.1

- (i) No tree is an *ipso* omni-conductor;
- (ii) no tree with an odd number of vertices is an *ipso* omni-insulator; and
- (iii) the only tree that is a distinct omni-conductor is K_2 .

In the range $2 \leq n \leq 25$ distinct omni-insulating chemical trees are rare, appearing only at $n = 3k + 4$, and interestingly these examples also have $g_s = k + 2$. There is a structural explanation for this observation, in terms of vertex fusion of S_3 graphs (stars with 3 peripheral vertices), which in turn suggests an explanation for the counts for general trees and a conjecture for all chemical graphs. Amongst chemical trees, the trend appears to be towards a smaller fraction of pure distinct omni-conductors with increasing n .

Benzenoid graphs give results that do not need a table: Kekulean (non-singular) benzenoids are all *ipso* omni-insulators (all vertices of a non-singular bipartite graph are CFV upper). In the range $1 \leq h \leq 12$, where h is the number of hexagonal faces, no Kekulean benzenoids belong to any other class of omni-conductors or omni-insulators, and no non-Kekulean benzenoids have any omni-conducting or omni-insulating properties.

Cubic (3-regular) polyhedral graphs (which are good candidates for carbon cages) (Table 4.11) show a bias to strong omni-conduction: for example, of the 7595 cubic polyhedra with $n = 20$ vertices, 3925 are strong omni-conductors. Interestingly, these graphs appear to include neither distinct omni-insulators nor pure distinct omni-conductors. Restriction to the fullerene subclass of cubic polyhedra gives an even greater pre-dominance of strong omni-conductors [102]. The data for the small cases in Table 4.11 might be taken to suggest that no cubic polyhedra are pure distinct omni-conductors, but this is disproved by the counterexample of fullerenes on, e.g., $n = 54$ vertices [102].

4.5.2 Some families of omni-conductors

Observations from constructions suggest several general families of omni-conductors: all complete graphs K_n with $n > 2$ are strong omni-conductors, as are all nut graphs, all cycles C_{4N+1} and C_{4N+3} , bi-cycles formed by fusion of an odd cycle and an aromatic $(4N + 2)$ cycle, bowtie graphs consisting of two odd cycles linked by a chain of any length, and all $[p]$ prisms with odd $p \not\equiv 0 \pmod{3}$ (see Fig. 4.4).

Pure *ipso* omni-conductors include the anti-aromatic cycles C_{4N} , bi-cycles formed by fusion of odd cycles C_p and C_q with $p - q \not\equiv 0 \pmod{4}$, and $[p]$ prisms for all odd p and all $p \equiv 0 \pmod{6}$.

The preceding observations can be proved using theorems given earlier (e.g., Theorem 4.4.14). For example, the complete graph K_n ($n > 1$) has all vertices of CFV (middle) type, and hence the graph is an *ipso* omni-conductor. Also, for $n > 2$, two deletions of vertices in K_n lead to a smaller complete graph, K_{n-2} , and we therefore have case 3c(iiA)/7 of Table 4.4, with $g_s = 0$ and $j^2 = ut - sv = E + 1$, and hence a strong omni-conductor.

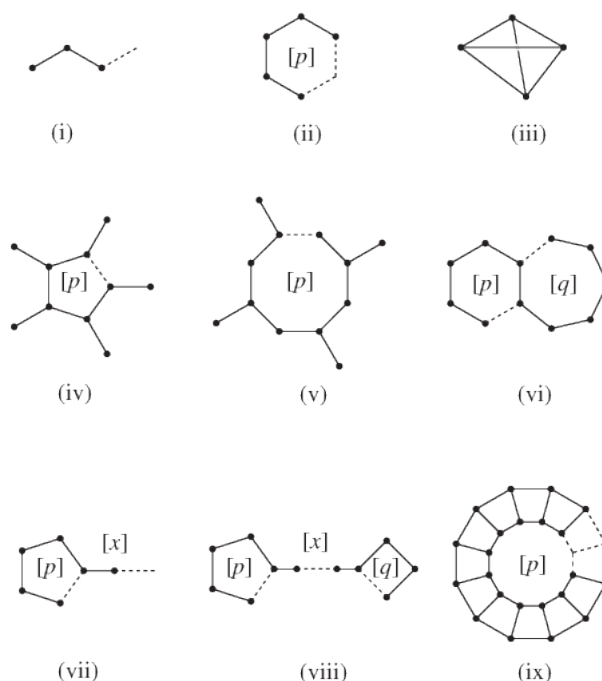


Figure 4.4: Families of chemical graphs with interesting conduction and insulation behaviour. Those illustrated are: (i) paths ($n = p$, $m = p - 1$, $p \geq 2$); (ii) cycles ($n = m = p$, $p \geq 3$); (iii) complete graphs ($n = p$, $m = p(p - 1)/2$, $p \geq 2$); (iv) radialenes ($n = p$; $m = 2p$, $p \geq 3$); (v) semi-radialenes ($n = m = 3p/2$, $p \geq 4$); (vi) bi-cycles ($n = p + q - 2$, $m = p + q - 1$, $p, q \geq 3$); (vii) tadpoles ($n = m = p + x$, $p \geq 3$, $x \geq 1$); (viii) bowties ($n = p + q + x$, $m = n + 1$, $p, q \geq 3$, $x \geq 0$); (ix) prisms ($n = 2p$, $m = 3p$, $p \geq 3$).

4.5.3 Some families of omni-insulators

Construction of families of graphs leads to a number of observations about omni-insulators that can be proved from the theorems in the Section 4.4. For example, *ipso* omni-insulators are common in some families.

Examples of families of *ipso* omni-insulators include even paths P_{2N} , aromatic cycles C_{4N+2} , all radialenes, tadpoles with an aromatic cycle and an even number of vertices in the tail, bi-cycles formed by fusion of two even rings, bowties with two aromatic rings and an even number of vertices in the intervening chain, $[p]$ prisms with p even and $\neq 0 \pmod 6$ (see Fig. 4.4 for the definitions of these commonly used names for families of conjugated systems). As for the omni-conductors, all the above observations about insulators can be proved straightforwardly.

Families of distinct omni-insulators are also found amongst the chemical graphs: for example, all semi-radialenes with more than 6 vertices, belong to this class, as do the subset of chemical trees mentioned in Section 4.5. A common substructure appears in these and other examples. A construction that often but not invariably leads from a parent chemical graph to a chemical graph that is a distinct omni-insulator is an operation we call ‘starification’. In this construction each vertex of a parent graph G is replaced by a three-pointed star S_3 , and pairs of stars corresponding to edges of G are fused by superposition of a terminal vertex of each (see Fig. 4.5). In other words, $Star(G)$ is obtained from G by first forming the subdivision of G (obtained from G by inserting a vertex in every edge) and then adding two pendant edges to original end vertices (of degree one) and one pendant edge to each original

vertex of degree two. Given that S_3 has three peripheral vertices, as the starting graph is chemical (i.e., connected and with maximum degree ≤ 3) with n vertices and m edges, the derived graph $Star(G)$ has $4n - m$ vertices, and $3n$ edges, of which $3n - 2m$ are leaves connecting central vertices of stars to vertices of degree 1. If G has adjacency eigenvalues $\{\mu_i\}$, the graph $Star(G)$ has $2n$ eigenvalues given by $\pm\sqrt{3 + \mu_i}$, with all other eigenvalues equal to zero. Precisely in the case that G is cubic and bipartite, $Star(G)$ has two zero eigenvalues arising from $\mu_n = -3$ of G . Hence, the total number of zero eigenvalues of $Star(G)$ is $2n - m + 2$ zeroes for cubic bipartite G and $2n - m$ for all other chemical graphs.

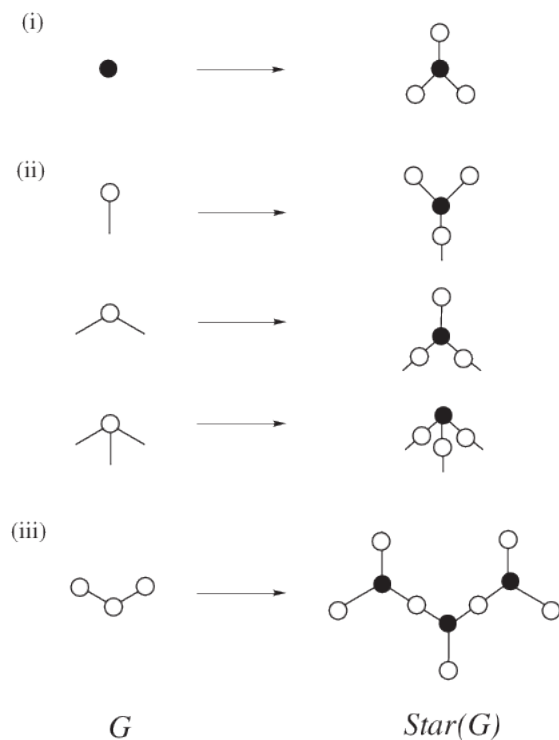


Figure 4.5: The starification construction. Starting from a parent G , (i) each vertex is replaced by a star graph S_3 ; (ii) stars that are neighbours along an original edge of G are fused at a peripheral vertex, leaving $(3-d)$ pendant vertices per star replacing the original vertex of degree d .

The eigenvalues of the star of the graph can be deduced to be $\pm\sqrt{3 + \mu_i}$ by taking a local view on the three possible degrees that a vertex of a chemical graph can have. Fig. 4.6 shows the original vertices of the parent graph G labelled with capital letters and indicated with black-filled circles, whereas the inserted vertices are labelled with small letters and indicated with white-filled circles. Considering Fig. 4.6 (i), if A is an entry of an eigenvector corresponding to an end vertex and B is associated with its unique neighbour in the same eigenvector for the parent graph, then

$$\mu A = B \tag{4.9}$$

Similarly if the entries of an eigenvector are a , b and c , then

$$\begin{aligned}
\lambda a &= A \\
\lambda b &= A \\
\lambda c &= A + B \\
\lambda A &= a + b + c
\end{aligned}
\tag{4.10}$$

Substituting for a , b and c from the first three equations of Eq. 4.10 in the last equation gives

$$(\lambda^2 - 3)A = B \tag{4.11}$$

Hence, by matching the multipliers in Eqs (4.9) and (4.11), the relationship between the eigenvalues of the parent graph G and its star is

$$\mu = \lambda^2 - 3 \Rightarrow \lambda = \pm\sqrt{3 + \mu} \tag{4.12}$$

The same process may be applied to vertices of degree 2 and 3 in the parent graph G as shown in Fig. 4.6 (ii) and (iii), yielding the same relation in Eq. (4.12). Thus, the set of equations of the form given in Eq. (4.9), of which there are n in all, whatever the degree of the vertex, Eq. (4.12) holds. Note that Eq. (4.12) suffices to give all the eigenvalues of $Star(G)$ from the eigenvalues of G . (See also the discussion about Fig. 8.4 in Subsection 8.1.2.)

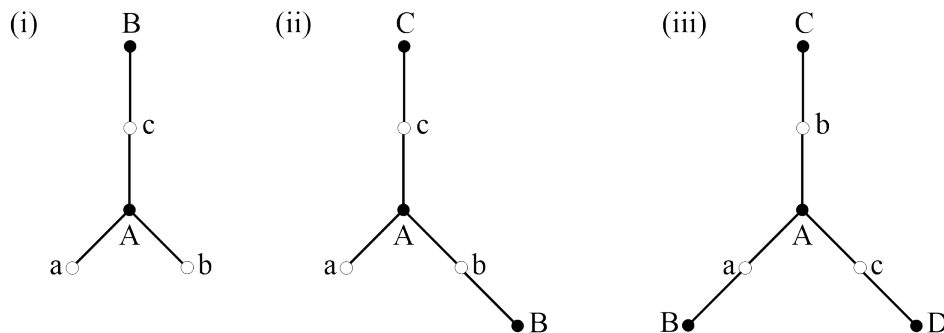


Figure 4.6: A local starification construction. Original vertices are indicated with black-filled circles, and inserted vertices with white-filled circles where the original vertex has degree 1 in (i), degree 2 in (ii) and degree 3 in (iii).

Application of the starification operation to all chemical graphs with $2 \leq n \leq 14$ indicates that ‘nearly all’ $Star(G)$ for chemical parents G are distinct omni-insulators. The ‘exceptions’ ($Star(G)$ that are not distinct omni-insulators) are comparatively rare: for parents with $n = 2, \dots, 14$, there are only 0, 0, 1, 1, 4, 4, 14, 23, 73, 166, 533, 1504, 5061, ... exceptions (to be compared with the much larger total numbers of chemical graphs listed in Table 4.7). Features common to the exceptions are under investigation and some conjectures are listed in Section 8.1. For example, some but not all cubic graphs G lead to exceptions, whereas all chemical trees G on n vertices lead to distinct omni-insulators $Star(G)$ with $3n + 1$ vertices (see also the further discussion in Section 8.1).

It is intriguing to ask exactly ‘why’ the omni-insulating chemical trees have their characteristic property, and ‘why’ in general insulation should be associated with

high nullity. A hint comes from observations on calculated transmission in so-called cross-conjugated systems [61, 67, 81]: a connection across a cross-conjugated junction in model systems leads to strong reduction in transmission [67] at energies that are associated with the eigenvalues of the intervening side chain [81]. Within the graph-theoretical version of the SSP model [63], this corresponds to a theorem that can be derived straightforwardly from the previous work on composite systems presented in [105].

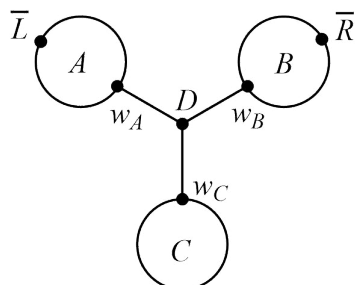


Figure 4.7: Three fragments A, B and C connected via a single three-coordinate vertex D to form a Y-junction.

Theorem 4.5.2 *Let three fragments A, B and C be connected via a single three-coordinate vertex D to form a Y-junction (see Fig. 4.7). The vertices adjacent to D in A, B, C are w_A , w_B and w_C , respectively. If a device is constructed with \bar{L} in A and \bar{R} in B, the opacity polynomial of the device, $j^2 = ut - sv$, is $j^2(ABC) = j^2(A)j^2(B)\phi^2(C)$, where $j^2(A)$ is the opacity polynomial for a device consisting of A alone with connections \bar{L} and w_A , $j^2(B)$ is the opacity polynomial for a device consisting of B alone with connections \bar{R} and w_B , and $\phi(C)$ is the characteristic polynomial of the whole graph C.*

Proof is by combination of Theorems 6 and 7 from the earlier paper “Fragment analysis of single-molecule conduction” [105]. Our omni-conducting trees include multiple copies of such Y-junctions, and the denominator of the transmission $T(E)$ will therefore contain zeroes at $E = 0$ arising from the many leaves on these particular trees, as will the characteristic polynomial of the tree itself. This is suggestive of a more general connection between nullity, cross conjugation, and omni-insulation.

4.6 Conclusion

In this chapter it has been shown that the graph theoretical SSP model leads naturally to the definition of omni-conductors and omni-insulators, that membership of the various categories is crucially dependent on graph nullity (number of non-bonding orbitals) and is governed by a number of general theorems, and that many families of chemically relevant molecular graphs omni-conduct. For example, many bicyclic π -systems, and almost all fullerenes [102] are strong omni-conductors.

In the following two chapters, the global classification of molecular devices into omni-conductors, omni-insulators and others will be further refined, to cover the case of devices that have ‘limited’ omni-conduction and insulation.

Chapter 5

Near omni-conductors and insulators in the SSP model

The results presented here have been published in “Near omni-conductors and insulators: alternant hydrocarbons in the SSP model of ballistic conduction” *The Journal of Chemical Physics* **147**, 164115, 2017, Fowler, Sciriha, Borg, Seville and Pickup [107]. This chapter is closely based on this reference, with some rewriting to incorporate new material and remove unnecessary repetitions of introductory material. This chapter takes forward the classification of omni-conduction from the last chapter, showing how an extended version can cover a chemically relevant (although not omni-conducting) class of molecules. This chapter will show that: a complete characterisation can be obtained within the source-and-sink-potential model for the conduction behaviour of *alternant* π -conjugated hydrocarbons (conjugated hydrocarbons without odd cycles). Alternant hydrocarbons, molecular graphs that are bipartite, cannot be full omni-conductors or full omni-insulators, but may conduct or insulate within well-defined subsets of vertices (unsaturated carbon centres). This leads to the definition of ‘near omni-conductors’ and ‘near omni-insulators’. We show that of 81 conceivable classes of conduction behaviour for alternants, only 14 are realisable. Of these, nine are realised by more than one chemical graph. Conduction of all Kekulean benzenoids (nanographenes) is described by two classes. In particular, the catafused benzenoids (benzenoids in which no carbon atom belongs to three hexagons) *conduct* when connected to leads *via* one starred and one unstarred atom, but otherwise *insulate*, corresponding overall to conduction type CII in the near-omni classification scheme.

5.1 Introduction

The simple ‘empty-molecule’ version of the SSP approach, in which the ballistic electron has no interaction with the molecular electrons, has already given rise to useful generalisations such as derivations of classes of equi-conductors [104], omni-conductors and omni-insulators [84], and the construction of selection rules for conduction/insulation at the Fermi level that depend on counting zero roots of the structural polynomials [70, 87]. Many conjugated π systems are alternant hydrocarbons, and hence have bipartite molecular graphs (graphs for which the vertices fall into two disjoint sets such that any edges include a vertex from each set). It

Kind	Rule	g_t	g_u	g_v	g_j	$T(0)$
CFV+CFV	D1	g_s+1	g_s+1	g_s+2	$\geq g_s+1$	$= 0$
	D2	g_s+1	g_s+1	g_s	g_s	$\neq 0$
CFV+CV	D5	g_s+1	g_s-1	g_s	$\geq g_s$	$= 0$
CV+CV	D9	g_s-1	g_s-1	g_s	g_s-1	$\neq 0$
	D11.1	g_s-1	g_s-1	g_s-2	g_s-1	$= 0$
	D11.2	g_s-1	g_s-1	g_s-2	$\geq g_s$	$= 0$
CFV	I1	g_s+1			$g_s + 1$	$= 0$
CV	I3	g_s-1			$g_s - 1$	$\neq 0$

Table 5.1: Selection rules for Fermi-level conduction of distinct and *ipso* molecular devices based on bipartite graphs with nullity g_s . Combinations of CV and CFV describe the (\bar{L}, \bar{R}) pair in terms of core and core-forbidden vertices. Each signature $\{g_t, g_u, g_v, g_j\}$ leads to a prediction about transmission at the Fermi level, $T(0)$, as either $\neq 0$ (conduction), or 0 (insulation). Rules are labelled D for *distinct* devices ($\bar{L} \neq \bar{R}$) and I for *ipso* devices ($\bar{L} = \bar{R}$).

follows, for example, that significant classes of conjugated hydrocarbons, such as the Kekulean benzenoids, *cannot* be distinct omni-conductors [84]. Hence, it is natural to ask how closely an alternant hydrocarbon can approach omni-conductor or omni-insulator status. The present chapter gives a systematic answer to this question by defining *near* omni-conduction and insulation and showing that there are only a very few possible cases needed to describe real π systems.

So far, two approaches have been used for obtaining information about systematics of conduction in the SSP model. One is suitable for formal algebraic proofs, and the other for numerical calculation. The first approach is via *selection rules*, where conduction at the Fermi level is defined by a set of selection rules based on the numbers of zero roots of the five polynomials s , t , u , v and j , denoted by g_s , g_t , g_u , g_v and g_j . The second is through *spectral expansions*. Devices fall into 14 cases, which reduce to the eight possibilities listed in Table 5.1 when the graph G is bipartite [84,87]. Assignment of cases to conduction or insulation at the Fermi level according to Table 5.1 can be made through computation of terms in the expansions at $E = 0$.

The structure of this chapter is as follows. Section 5.2 defines a two-letter code classification of omni-conductors and omni-insulators, in which every alternant or non-alternant graph appears in exactly one of eight categories. This is refined in Section 5.3 to give a systematic classification of conduction/insulation behaviour of alternants in terms of a three-letter acronym (TLA) for ‘near-omni’ systems. We prove that of 81 conceivable cases, only 14 are realisable. Sections 5.4 – 5.7, supported by Section 5.10, show how this reduction is achieved, and give families of chemical examples (Fig. 5.4 and Table 5.4). Section 5.8 describes the startlingly simple restriction of the full classification for benzenoids, and Section 5.9 states the overall conclusions. The end result is a complete description of ballistic conduction at the Fermi level as predicted within the ‘empty-molecule’ SSP model.

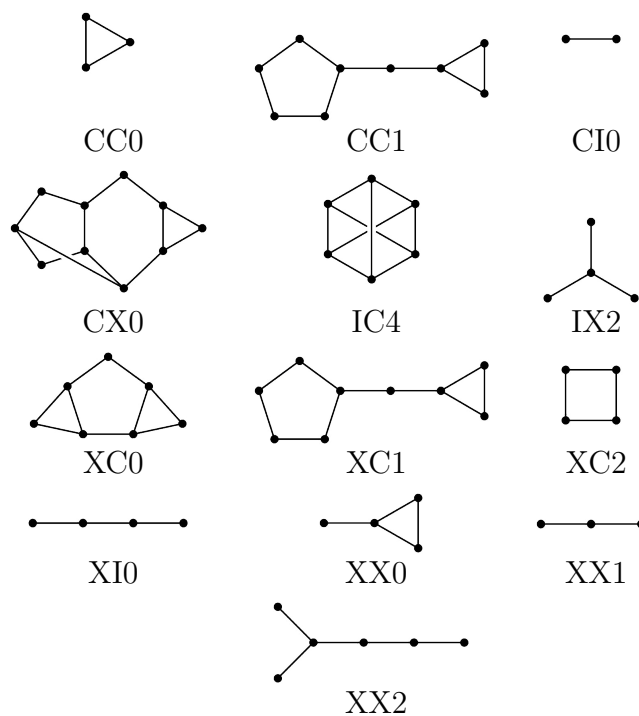


Figure 5.2: Smallest non-trivial chemical graph for each region in the Venn-like diagram (Fig. 5.1). In each case the two-letter code is given followed by the nullity. Only 13 cases are possible (refer to Section 5.5).

Code	Nullity		
	0	1	> 1
CC	Some	Nut	None
CI	Some	None	None
CX	Some	None	None
IC	None	None	Some
II	None	None	None
IX	None	None	Some
XC	Some	Some	Some
XI	Some	None	None
XX	Some	Some	Some

Table 5.2: Full classification of conduction behaviour by nullity for general connected graphs. Conventions as in Table 4.6.

fact, as will be proved later, only five two-letter codes apply to bipartite graphs (XI ($g_s = 0$), XC, XX ($g_s \geq 1$), IC, IX ($g_s > 1$)). The main aim here is to work out how to translate the restrictions imposed by bipartivity into a full classification of Fermi-level conduction behaviour of bipartite molecular graphs (alternant π systems).

5.3 A classification scheme for alternant hydrocarbons

Evidently, a more refined classification is needed to capture the conduction behaviour of devices based on alternant hydrocarbons. The molecular graph of an alternant hydrocarbon is *bipartite*. By definition, the vertices of a bipartite graph can be split into two disjoint partite sets, which we may call starred and unstarred, and denote by V_1 and V_2 , respectively, with $|V_1| \geq |V_2|$. K_1 is trivially bipartite, with V_2 empty. Each edge of the graph connects a starred and an unstarred vertex. Bipartite graphs are precisely those graphs that contain no odd cycles. Conduction behaviour is affected by these properties.

The classification adopted here concentrates on behaviour within and between partite sets. The *distinct/ipso/strong* classification for general graphs is replaced by a set of three-letter acronyms (TLA). The alphabet is $\{C, I, X\}$, as with the two-letter codes, and the three sets of interest for bipartite graphs are indicated by position: the first letter refers to *inter* devices (one starred and one unstarred connection vertex), the second to *intra* (two starred or two unstarred connection vertices) and the third to *ipso* (connection via a single vertex). X is interpreted as ‘neither C nor I’, so that it can also be used when the set in question is empty, as for *intra* and *inter* sets for K_1 , and the *intra* set for K_2 .

Thus, for example, a TLA of IXC would imply omni-insulation for all distinct pairs $\bar{L} \neq \bar{R}$ from opposite sets, mixed conduction/insulation for distinct devices $\bar{L} \neq \bar{R}$ in the same set, and omni-conduction for all *ipso* devices.

There are 27 three-letter codes to be considered, from CCC to XXX. Guided again by the significance of nullity in classification for general graphs, we distinguish cases with nullities $g_s = 0, 1, > 1$, leading to a total of 81 combinations of TLA code and nullity. We check each of these to decide whether a given combination of TLA and nullity is possible (by finding a small bipartite graph example), or can be proved to be impossible.

5.4 Calculations

As a preliminary, assessments were carried out for sets of graphs using the numerical approach for calculation of spectral expansions of the structural polynomials. Complete sets of bipartite graphs on up to 10 vertices, bipartite chemical graphs (connected bipartite graphs with maximum degree 3) on up to 12 vertices, and benzenoids on up to 12 hexagons, all available from previous work [84], were tested. These calculations provided examples for 14 of the 81 TLA/nullity combinations. Fig. 5.3 shows the smallest graphs for each of the 14 combinations. In all but one case these are chemical graphs (skeletons of possible alternant hydrocarbons). This approach was used systematically to obtain the results described in the rest of this chapter.

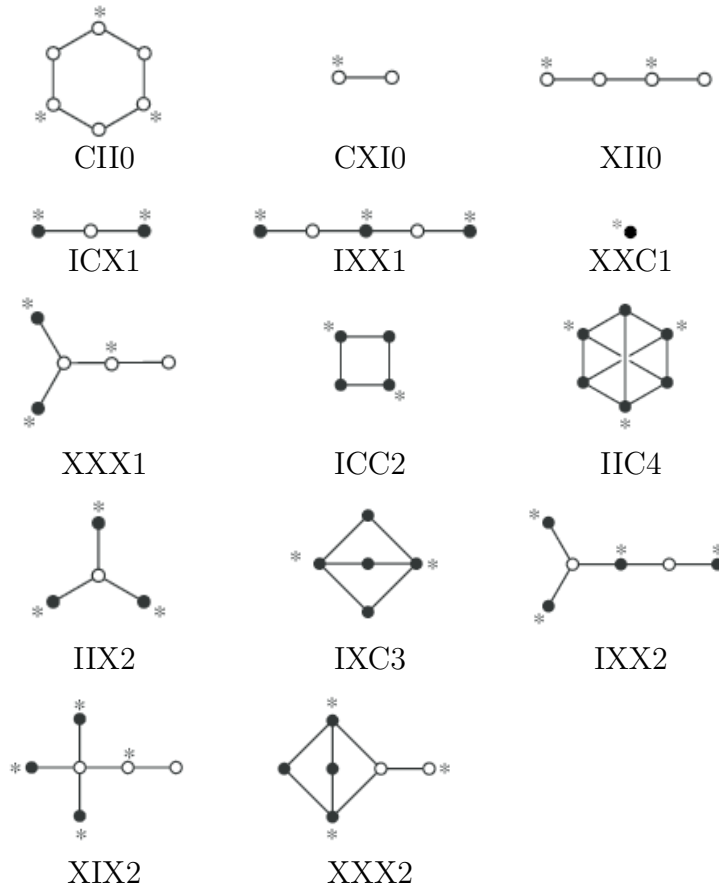


Figure 5.3: Smallest examples of the 14 conduction types for devices based on bipartite graphs, named by three-letter acronym and nullity. Vertices in the partite sets V_1 and V_2 are shown as starred and unstarred, respectively. Core vertices are indicated with black-filled circles, and core-forbidden vertices with white-filled circles. Case XIX2 is the non-chemical Latin cross graph.

5.5 Elimination of remaining cases

The grid of 81 combinations is shown in Table 5.3. We begin by populating the table with the cases where we have an example from exhaustive search of small graphs. These cells are filled with the string ‘Some’. The focus of the theoretical work is then to eliminate as many as possible of the remaining cells. The conjecture is that all other cells correspond to combinations that are impossible for bipartite graphs.

We can immediately eliminate some combinations using the old broad classification of possible and impossible cases for general graphs. Strong omni-insulators are not possible [84]. Hence type III can be ruled out for bipartite graphs. Similarly, as distinct and strong omni-conductors for nullity one are identical with the class of nut graphs [90] (graphs with $n > 1$ and $g_s = 1$ in which the eigenvector of zero eigenvalue has no zero entries), and as nut graphs are not bipartite [90], types CCC and CCI are ruled out for nullity one. Knowing that a distinct omni-conductor exists if the graph has a nullity less than 2, that is, either 1 or 0 [84], then the remaining possible case for CCC is that the graph is a distinct omni-conductor having a nullity of 0. In this case, we can divide the distinct pairs into inter and intra sets.

1. Since the graph is bipartite, its nullity and number of vertices have the same parity by the Pairing Theorem [95] and the graph has an even number of vertices.
2. A bipartite graph without a perfect matching has a nullity which is not 0 and so is singular. This is a consequence of a result of Frobenius [7] and the Hall Marriage Theorem [8].
3. Let G be a non-singular bipartite graph. Removal of an intra pair \bar{L} , \bar{R} gives $G - \bar{L} - \bar{R}$ with no perfect matching. Hence, the two vertex-deleted subgraph has a nullity which is not 0, and is in fact 2.

This is Variety 3a (ii) Case D1 of the selection rules [70], which gives insulation. Hence, no bipartite graph having a nullity of 0 is a distinct omni-conductor.

Impossibility proofs for all those combinations left open by the computer search are briefly indicated in Section 5.10. The results of the proof procedure are summarised in Table 5.3, from which it is evident that the conjecture was correct: we do now have the *complete* classification of possibilities.

As an essentially graph-theoretical approach, the SSP model gives predictions for general classes of alternant hydrocarbons. Fig. 5.4 illustrates representative families of bipartite molecular graphs. Table 5.4 lists the SSP predictions for their conduction behaviour.

5.6 Rare cases

Some cases in Table 5.3 correspond to a very small number of graphs.

5.6.1 Cases XXC, CXI and ICX

Types XXC, CXI and ICX have only one example each within the test sets; the only graph found for XXC is K_1 , the molecular graph of a single unsaturated carbon centre; CXI is K_2 , the complete graph on two vertices and the molecular graph of ethene; the only graph found for ICX is P_3 , the path on three vertices, the molecular graph of the allyl radical. As shown in Section 5.10, these three graphs are the unique examples of their respective conduction types.

5.6.2 Case IIC

The search found only one example amongst chemical graphs for type IIC, although it found others amongst non-chemical graphs. The sole chemical graph is $K_{3,3}$. This is a *complete bipartite graph*. It has three starred and three unstarred vertices, and all starred are joined to all unstarred vertices; it appears in mathematical puzzles as the ‘Utility Graph’. In a complete bipartite graph, $K_{p,q}$, each of the p vertices in V_1 is joined by an edge to each of the q vertices in V_2 . $K_{3,3}$ is famously non-planar

Case	Nullity, g_s		
	0	1	> 1
CCC	1, 2	4, 6	10, 11
CCI	2	4, 6	8, 10
CCX	1, 2	6, 7	9, 10
CIC	1	4, 5, 6	10, 11
CII	Some	4, 5, 6	8, 10
CIX	1	5, 6	10
CXC	1, 2	4, 6	10, 11
CXI	K_2	4, 6	8, 10
CXX	1, 2	3	10
ICC	1, 2	4	Some
ICI	2	4	1, 8
ICX	1, 2	P_3	9
IIC	1	4, 5	Some
III	3	4, 5	8
IIX	1	5	Some
IXC	1, 2	4	Some
IXI	2	4	8
IXX	1, 2	Some	Some
XCC	1, 2	4	11
XCI	2	4	8
XCX	1, 2	7	9
XIC	1	4, 5	11
XII	Some	4, 5	8
XIX	1	5	Some
XXC	1, 2	K_1	11
XXI	2	4	8
XXX	1, 2	Some	Some

Table 5.3: Conduction behaviour of alternant π -conjugated hydrocarbons, showing the existence status of all 81 conceivable combinations of *inter-intra-ipsa* device behaviour with nullity of the molecular graph. Entries ‘Some’ indicate that at least one example has been found. Entries x with $x = 1$ to 11 refer to the theorems 5.10. x that can be used to rule out a given case. Cases CXI ($g_s = 0$), XXC and ICX ($g_s = 1$) and IIC ($g_s > 1$) are each realised by only one chemical graph. These are the stars $K_2 \equiv K_{1,1}$, K_1 , $P_3 \equiv K_{2,1}$ and $K_{3,3}$, respectively. Case IIC also has non-chemical realisations; no chemical realisation has been found so far for case XIX.

(cannot be drawn in the plane without edges crossing). Molecular realisation of this graph seems unlikely. In chemistry it appears as the graph of the discarded Claus proposal for the structure for benzene, where antipodal carbon atoms were connected by extra single bonds [116].

The small examples of non-chemical graphs in IIC are also complete bipartite graphs, $K_{p,q}$ with $p \geq 3, q \geq 3$. It is easy to show that all such $K_{p,q}$ are of type IIC. $K_{p,q}$ ($p, q > 0$) has nullity $p + q - 2$ and consists entirely of core vertices. Deletion

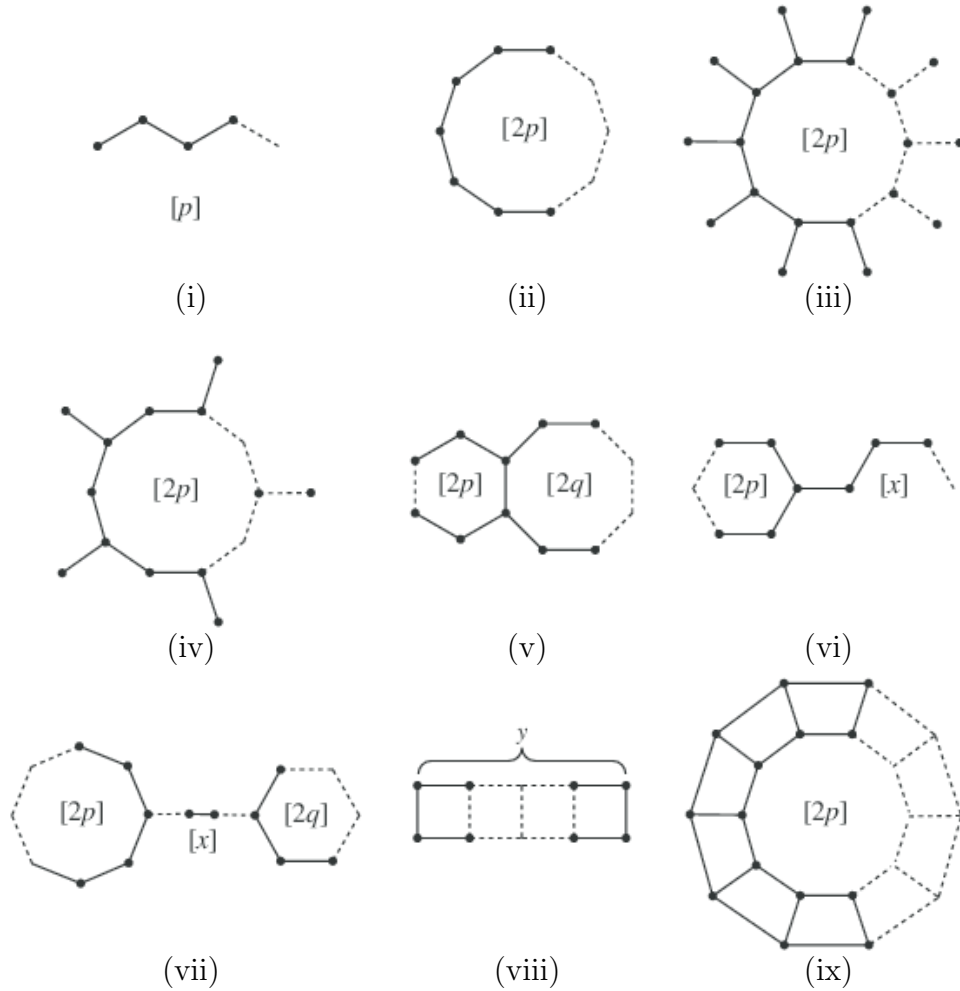


Figure 5.4: Families of bipartite graphs with systematic conduction behaviour in the SSP model. The families are: (i) paths (linear polyenes); (ii) cycles (annulenes); (iii) radialenes; (iv) semi-radialenes; (v) bi-cycles (fused annulenes); (vi) tadpoles; (vii) bowties; (viii) ladders; (ix) prisms. Cycle sizes in bipartite graphs are even, and denoted here by $2p$ or $2q$; x is the number of atoms in a chain connected to a cycle, not counting vertices common to the chain and a cycle; y is the number of squares in the ladder. See Table 5.4 for the results.

of one vertex in $K_{p,q}$ ($p, q \geq 3$) yields $K_{p-1,q}$ or $K_{p,q-1}$ and deletion of two vertices gives $K_{p-2,q}$, $K_{p-1,q-1}$ or $K_{p,q-2}$. These combinations correspond to rule D11 (g_s , $g_s - 1$, $g_s - 1$, $g_s - 2$), and hence insulation.

However, the graphs $K_{p,q}$ do not exhaust the type IIC. A family of IIC graphs can be constructed by using the adjacency matrix of a *uniform core graph*, as introduced in [88]. A uniform core graph is a core graph such that removal of any vertex leaves a core graph. A uniform core graph satisfies rule D11 for every distinct device. As all vertices are CV, all *ipso* devices based on uniform core graphs satisfy rule I3. A bipartite graph G can be constructed from *any* uniform core graph H , with adjacency matrix

$$\mathbf{A}(G) = \begin{pmatrix} \mathbf{0} & \mathbf{A}(H) \\ \mathbf{A}(H) & \mathbf{0} \end{pmatrix},$$

where $\mathbf{A}(H)$ is the adjacency matrix of H . One construction that yields a uniform

Family	Sub-family	g_s	TLA
Path	K_1	1	XXC
	K_2	0	CXI
	P_3	1	ICX → ICci
	Even path, $n > 2$	0	XII
	Odd path, $n > 3$	1	IXX → Icici
Cycle	$2p = 4N + 2$	0	CII
	$2p = 4N$	2	ICC
Radialene	all p	0	XII
Semi-radialene	$2p = 4$	2	IXX → Iixci
	$2p > 4$	p	IIX → IIci
Bi-cycle	$2p = 4N + 2, 2q = 4N' + 2$	0	CII
	all others	0	XII
Tadpole	$2p = 4N + 2, x = 2N'$	0	XII
	$2p = 4N + 2, x = 2N' + 1$	1	IXX → Icici
	$2p = 4N, x = 2N'$	2	IXX → Ixcxcx
	$2p = 4N, x = 2N' + 1$	1	XXX → Xixix
Bowtie	$2p = 4N + 2, 2q = 4N' + 2, x = 2N''$	0	XII
	$2p = 4N + 2, 2q = 4N' + 2, x = 2N'' + 1$	1	IXX → Icici
	$2p = 4N + 2, 2q = 4N', x = 2N''$	2	IXX → Ixcxcx
	$2p = 4N + 2, 2q = 4N', x = 2N'' + 1$	1	XXX → Xixix
	$2p = 4N, 2q = 4N', x = 2N''$	2	XXX
Ladder	$2p = 4N, 2q = 4N', x = 2N'' + 1$	3	IXX → Ixcxcx
	$y = 3N + 1, N > 1$	2	IXX
Prism	$y \neq 3N + 1$	0	XII
	$2p = 6N$	4	IXC
	$2p \neq 6N$	0	CII

Table 5.4: Conduction behaviour for families of bipartite molecular graphs. n is the number of vertices; p , q and x are as defined in Fig. 5.4, where $2p$ and $2q$ are the cycle sizes and x is the length of a chain of vertices that are not in any cycle. Three-letter acronyms are defined in Section 5.3; expanded five-letter acronyms in Section 5.7.

core graph [88] gives $\mathbf{A}(H)$ as

$$\mathbf{A}(H) = \begin{pmatrix} \mathbf{A}(N) & \mathbf{A}(N) \\ \mathbf{A}(N) & \mathbf{A}(N) \end{pmatrix},$$

where $\mathbf{A}(N)$ is the adjacency matrix of a nut graph, N .

The graph H constructed in this way has N as a subgraph, and therefore is not bipartite [90]. The construction doubles the vertex degrees of the starting nut graph (which were all greater than 1 [90]) and so cannot generate a chemical graph. When a vertex is deleted from G the subgraph obtained remains a core graph. The graphs G are therefore examples of IIC bipartite graphs that are neither chemical graphs

nor complete bipartite.

5.6.3 Case XIX

Another rare case is XIX. In the computer search, no chemical graph was found for this type, although non-chemical graphs such as the six-vertex Latin cross are found in this class (See the entry for XIX in Fig. 5.3).

5.7 Refining the TLA description

The three-letter classification can be further refined in some cases. In the *intra* and *ipso* positions of the TLA, a letter X could signify conduction within one partite set and insulation within the other, or conduction or insulation in one set and mixed possibilities in the other, and so on. In some cases, further reasoning allows the letter X to be replaced by a more detailed specification, and we use two lower-case letters such as ci, cx, ix to indicate the behaviour within V_1 and V_2 . The core and core-forbidden classification of vertices used earlier is also useful here.

For graphs with nullity zero, all vertices are CFV, *inter* and *intra* pairs (if any) are all of kind CFV-CFV, and no new interesting cases arise from distinguishing V_1 and V_2 .

5.7.1 Singular bipartite graphs with $g_s = 1$

For graphs with nullity one, all core vertices are in the larger partite set V_1 , and the interesting case is when V_1 is ‘full’, i.e. when every member of V_1 is CV. V_2 is ‘empty’ in the sense that every vertex in V_2 is CFV. A graph with this distribution of CV and CFV is a *half-core*. If G is a half-core with $g_s = 1$, the *intra* pairs in V_1 are CV/CV and satisfy D9. For *intra* pairs in V_2 we have CFV/CFV, and potentially Rule D1 or D2. However, repeated removal of vertices raises the nullity at each step, as the difference $||V_1| - |V_2||$ increases by one at each step. Hence, the CFV/CFV pairs are insulating, by Rule D1. Therefore, the expanded code has ci instead of X in the *intra* position. The *ipso* entry is also ci (by I1 and I3), whereas the *inter* pairs are all insulating, by D5. Hence, all half-cores with $g_s = 1$ have TLA IXX and expanded code Icici.

5.7.2 Singular bipartite graphs with $g_s > 1$

For graphs with nullity greater than one, the potentially interesting cases are half-cores, defined as above, and *cores*, in which all vertices are CV so that both V_1 and V_2 are full.

If the graph is a *half-core* with $g_s > 1$, the *ipso* entry X is equivalent to ci. The *inter* entry is I (all *inter* pairs fall under Rule D5). Therefore the conduction types of interest are IIX or IXX. The type IIX is simply expanded to IICI, and hence is

resolved. However, experimentation shows that graphs in IXX can be Ixici, so this type is not fully resolved.

If the graph is a *core* with $g_s > 1$, the *ipso* entry is C (all vertices are CV), and hence the only unresolved entry is IXC. Some small graphs can be found that correspond to IxxC, so this case is unresolved.

In summary, the expanded codes give complete resolution for $g_s = 1$ but only partial resolution for $g_s > 1$.

5.8 Benzenoids

Calculations on all benzenoids on up to twelve hexagonal rings are summarised in Table 5.5. Here, benzenoids are taken to be simply-connected subgraphs of the graphene plane composed of hexagonal rings only. In a *catafused* benzenoid all vertices are in the perimeter, i.e. no vertices belong to three hexagons. Conversely, all *perifused* benzenoids have at least one such ‘internal’ vertex. The table reveals some interesting patterns of predicted conduction behaviour between these classes of benzenoids. It turns out that only four TLA are needed to describe the conduction behaviour of all benzenoids in the range that we searched, two for those with Kekulé structures, and two for those without.

N_{hex}	$g_s = 0$		$g_s = 1$			$g_s > 1$		N_{tot}
	CII	CII	XII	IXX	XXX	IXX	XXX	
1	1							1
2	1							1
3	2				1			3
4	5		1	1				7
5	12	1	2	5	2			22
6	36	7	8	27	1	2		81
7	118	33	39	121	13	7		331
8	411	160	193	586	33	52		1435
9	1489	787	947	2776	181	322	3	6505
10	5572	3756	4779	13097	927	1931	24	30086
11	21115	17557	24207	61627	5419	11096	208	141229
12	81121	81314	122483	290133	30726	62247	1560	669584

Table 5.5: Conduction behaviour of benzenoids, classified by nullity. For the non-singular benzenoids ($g_s = 0$), the first CII column corresponds to catafused benzenoids; the second CII and first XII columns correspond to Kekulean perifused benzenoids. All benzenoids with $g_s > 0$ are perifused. N_{tot} is the total number of benzenoids with N_{hex} rings.

Table 5.5 lists the conduction behaviour of benzenoids classified by nullity. The class CII at $g_s = 0$ is more populated than that of XII. Also, such benzenoids at this nullity are *ipso* omni-insulators. The smallest examples of a non-catafused Kekulean benzenoid is shown in Fig. 5.5, which also shows the smallest perifused non-Kekulean benzenoid. At $g_s = 1$, the IXX class is more populated than that of the XXX class. The same is true for $g_s > 1$, but the XXX class is even more empty

for smaller N_{hex} , the number of hexagonal rings. We do not exclude the possibility that for $g_s > 1$ there might exist some other larger benzenoid that gives a different TLA code. However, up to now there has been found no benzenoid that is a core graph. This is seen from Table 5.5 since none of the TLA codes have a C in the *ipso* position.

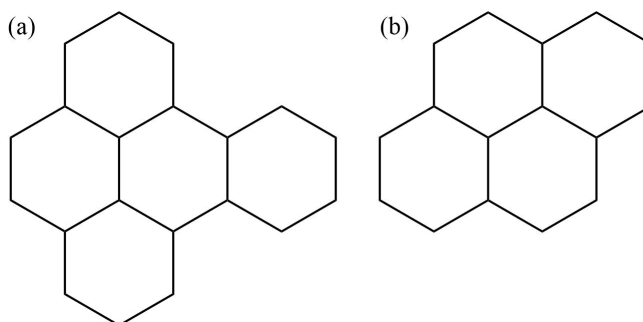


Figure 5.5: (a) The smallest perifused Kekulean benzenoid for the CII code. (b) Pyrene is the smallest perifused Kekulean benzenoid for the XII code.

5.8.1 Kekulean benzenoids

A benzenoid is *Kekulean* if it has a perfect matching (Kekulé structure). A benzenoid is Kekulean if and only if it is non-singular ($g_s = 0$) [117]. The perimeter of a catafused benzenoid is a Hamiltonian circuit (a circuit of edges that visits every vertex exactly once) and therefore every catafusene has at least two perfect matchings. Hence, all catafused benzenoids are Kekulean. In contrast, perifused benzenoids may be either Kekulean or non-Kekulean.

Kekulean benzenoids fall into conduction types CII and XII (Table 5.3), as they are non-singular bipartite graphs $G \neq K_2$. However, the numbers in Table 5.5 suggest a further conjecture, that *all* catafused benzenoids correspond to type CII, whereas perifused Kekulean benzenoids may belong to *either* CII or XII.

This conjecture is straightforwardly proved. First, *ipso* and *intra* entries in the TLA for a catafused benzenoid G are both I, by Theorems 5.10.1 and 5.10.2 (Section 5.10). The *inter* entry of the TLA is fixed by the analysis illustrated in Fig. 5.6. An *inter* pair of connection vertices has one vertex in V_1 , say \bar{L} , and one, say \bar{R} in V_2 (Fig. 5.6(a)). The two vertices are connected along the perimeter by two paths that consist of an odd number of edges (Fig. 5.6(b)). Choose one of the paths and call it P_1 . Now choose the matching of the perimeter circuit in which P_1 has two terminal double bonds, and call that matching M_1 . The complementary perimeter matching is M_2 , with terminal double bonds in the other path, P_2 (Fig. 5.6(c)). Now delete vertices \bar{L} and \bar{R} . The path $P_1 - \bar{L} - \bar{R}$ has a perfect matching when its edges are chosen as in M_2 , as does path $P_2 - \bar{L} - \bar{R}$ when its edges are chosen as in M_1 (see Fig. 5.6(d)). Hence the graph $G - \bar{L} - \bar{R}$ has a perfect matching in which any remaining chordal edges carry single bonds. As any internal face remaining in this two-vertex-deleted graph is still of size $4N + 2$, the existence of this perfect matching implies nullity zero [117–119]. Therefore, all *inter* pairs of a catafused benzenoid obey Rule D2, and the conduction type is CII. This proof also applies to catafused helicenes. In contrast, non-singular perifused benzenoids may be either CII or XII; the smallest examples of each type are illustrated in Fig. 5.7(a) and (b).

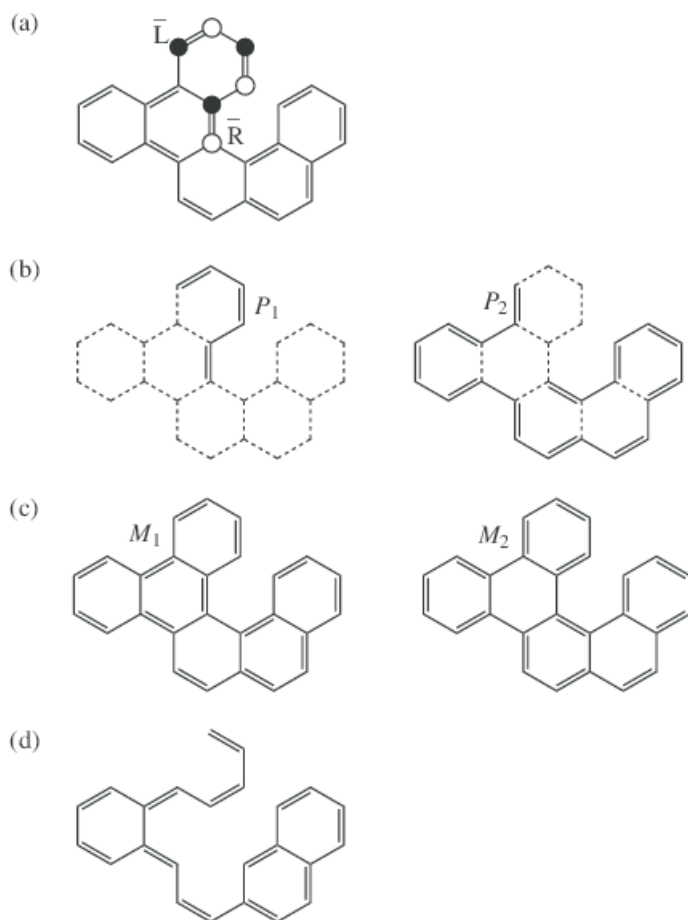


Figure 5.6: Pictorial proof that catafused benzenoids all belong to conduction type CII. (a) A catafusene G with an *intra* pair of connections \bar{L} and \bar{R} ; (b) Two perimeter paths P_1 and P_2 connecting \bar{L} and \bar{R} ; (c) The pairs of perimeter perfect matchings M_1 and M_2 , chosen to give terminal double bonds in paths P_1 and P_2 , respectively; (d) Matching of the vertex-deleted graph $G - \bar{L} - \bar{R}$, proving that the device is a conductor by Rule D2.

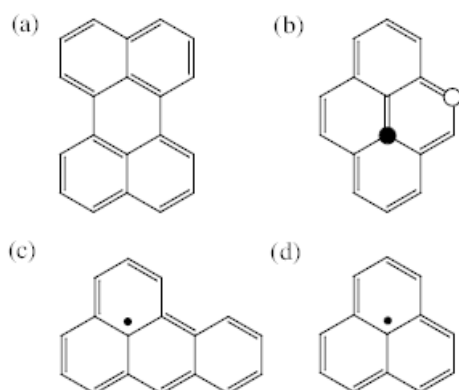


Figure 5.7: Smallest perifused benzenoids of each conduction type identified in the search. They are: (a) perylene (CII), (b) pyrene (XII), (c) benzophenalenyl radical (IXX), (d) phenalenyl radical (XXX). The two marked vertices in pyrene are a conducting *inter* pair; apart from symmetry images of this pair, all *inter* pairs are insulating.

5.8.2 Non–Kekulean benzenoids

The remaining columns of Table 5.5 deal with non–Kekulean benzenoids. Benzenoids with $g_s \geq 1$ are found in conduction types IXX and XXX, as they must be, since P_3 is not a benzenoid. However, the same two TLAs apparently suffice also for benzenoids with $g_s > 1$: specifically, the five other types available to general bipartite graphs (ICC, IIC, IIX, IXC, XIX) are not found for benzenoids in the range of the search. This may be an effect of small numbers; we are not aware of a proof of the sufficiency of the two classes for benzenoids with $g_s > 1$.

We note that a half–core benzenoid is of type Icici (hence also IXX). All IXX entries in the table for $g_s = 1$ and for $g_s > 1$ correspond to half–cores; it would be interesting to know if this observation generalises.

Fig. 5.7(c) and (d) show the smallest examples of benzenoids with $g_s = 1$. The smallest benzenoid with $g_s = 1$ is the radical derived from benzophenylene (Fig. 5.7(c)); the central vertex carries entry zero in the NBO, leading to conduction type XXX (Xixix). The smallest half–core with $g_s = 1$ is phenalene (Fig. 5.7(d)).

Phenalene is also the smallest of the triangulenes, which as the name suggests consist of a triangular array of hexagons and hence of $1, 3, 6, \dots, a(a+1)/2$ hexagons, where a is the number of rows and $a(a+1)/2$ is the total number of hexagons. As neutral molecules, and in a high–spin ground state, the triangulenes with $a > 1$ would have g_s unpaired spins distributed over vertices of set V_1 . For $a > 2$, $g_s > 1$ the system is a half–core, and hence of type IXX (in fact, Iixix). The case $a = 2$, $g_s = 1$ (phenalene) is special in having a CFV in the V_1 set: the unique non–bonding orbital is antisymmetric with respect to each of the three σ_v mirror planes of the D_{3h} group, and hence must have zero entry on the central vertex of the molecular graph; as there are no other non–bonding orbitals, this zero entry cannot be compensated by a mirror–symmetric partner orbital, as it would be in similar cases for $g_s > 1$. In spite of the difficulties of conventional synthesis [38, 120, 121], the triangulenes are of great interest as possible examples of giant organic molecular magnets and for applications in quantum electronic devices [38, 122, 123]. In a recent development, individual molecules of triangulene itself ($a = 3$) have been assembled on Xe, NaCl and Cu surfaces [124].

5.9 Conclusion

The SSP model allows a complete classification of conduction devices based on bipartite and non–bipartite graphs.

A general scheme for distinct–*ipso*–strong omni–conduction of devices based on bipartite or non–bipartite graphs has been constructed. All types except strong omni–insulators have some chemical representatives.

For bipartite graphs, the available types in the general scheme are fewer, but can be classified more finely. The result is: for devices based on a bipartite graph G with $n \geq 4$ vertices and nullity g_s , the possible *inter–intra–ipso* omni–conduction types are: ($g_s = 0$) CII, XII; ($g_s = 1$) IXX, XXX; ($g_s > 1$) ICC, IIC, IIX, IXC, IXX, XIX, XXX.

The three connected bipartite graphs with $n < 4$ each uniquely realise a conduction type: XXC is apparently possible only for K_1 (isolated vertex); CXI only for K_2 (ethene); ICX only for P_3 (allyl).

Of the nine types possible for $n \geq 4$, two appear to be sparsely represented amongst chemical graphs: so far, only one chemical graph has been found for IIC (non-planar $K_{3,3}$), and no chemical graph for XIX.

This global picture of conduction behaviour can be used to make predictions that can be tested against more sophisticated calculations for specific devices based on systems of chemical interest, such as the benzenoids or ‘nanographenes’ [125].

For the most important set of bipartite chemical graphs, the benzenoids, the SSP model gives an even simpler conclusion: all catafused benzenoids belong to type CII (they conduct for *all* distinct *inter* pairs of vertices, and otherwise insulate) and perifused Kekulean benzenoids are either CII or XII (they conduct for *some* distinct *inter* pairs). Benzenoids with nullity one also fit into two conduction types, IXX and XXX.

The theme of conduction in bipartite systems will be taken up again in Chapter 7 Section 7.6.

5.10 Appendix: Theorems for case-by-case proofs

We list some theorems that are useful in eliminating cases from the grand list of 81 TLA. We note that for a bipartite graph, all vertices are either core (CV), in which case deletion lowers g_s by 1, or core-forbidden (CFV) and *upper*, in which case deletion raises g_s by 1; i.e. a bipartite graph has no *middle* vertices (for which deletion would leave nullity unchanged). The two disjoint vertex subsets of a bipartite graph are V_1 and V_2 , with $|V_1| \geq |V_2|$, and the adjacency matrix may be written in block form (with the vertex sets ordered (V_1, V_2)) as

$$\mathbf{A} = \begin{pmatrix} \mathbf{0} & \mathbf{B} \\ \mathbf{B}^T & \mathbf{0} \end{pmatrix}.$$

5.10.1 Non-singular molecular graphs ($g_s = 0$)

Theorem 5.10.1 *For a bipartite graph G with $g_s = 0$, the ipso entry of the TLA is I.*

Proof: No vertices of G are CV, so all are CFV upper, and all *ipso* devices insulate (Rule I1). ■

Theorem 5.10.2 *For a bipartite graph G with $g_s = 0$ either the intra entry of the TLA is I or the class of intra pairs is empty (and then $G = K_2$, with intra entry X).*

Proof: For $g_s = 0$, $|V_1| = |V_2| = n/2$. Let \bar{L} be in V_2 . Then $G - \bar{L}$ has $g_s = 1$ and since deletion of all V_2 vertices gives $g_s = n/2$, $G - \bar{L} - \bar{R}$ (with \bar{L} and \bar{R} in V_2 of G) must have $g_s = 2$. Therefore there is no conduction for *intra* pairs (Rule D1): either the *intra* entry in the TLA is I or there are no *intra* pairs. The only graph with $n > 1$ vertices but no *intra* pairs is K_2 , consisting of two vertices joined by a single edge. ■

Application of Theorems 5.10.1 and 5.10.2 leaves only the TLA III undecided for $g_s = 0$. This case is settled by:

Theorem 5.10.3 *There are no strong omni-insulators with $g_s = 0$.*

Proof: For a device with $g_s = 0$, a distinct \bar{L} , \bar{R} is conducting if and only if the entry in the inverse, $(\mathbf{A}^{-1})_{\bar{L},\bar{R}}$ is non-zero [84]. For a distinct omni-insulator G , \mathbf{A}^{-1} is a diagonal matrix, hence \mathbf{A} is also a diagonal matrix, implying that G is not connected. As distinct omni-insulators with $g_s = 0$ are impossible, then strong omni-insulators with $g_s = 0$ are also impossible. (In fact, strong omni-insulators with $g_s \neq 0$ are impossible too [84].) ■

5.10.2 Singular molecular graphs with $g_s = 1$

Theorem 5.10.4 *For a bipartite graph G with $g_s = 1$, the ipso entry of the TLA is X.*

Proof: As G has some CV, some cases of *ipso* conduction occur by Rule I3. Assume that G has $n > 1$ vertices: since G is bipartite it is not a nut graph and hence has some CFV, which give *ipso* insulation by Rule I1. (N.B. If instead G has $n = 1$, the *ipso* entry is C and the whole TLA is XXC as both sets of distinct pairs are empty.) ■

Theorem 5.10.5 *For a bipartite graph G with $g_s = 1$, the intra entry of the TLA is not I.*

Proof: For a bipartite graph with $g_s = 1$, all CV are in the larger subset of vertices, V_1 (the unique NBO is concentrated on the starred vertices of the molecular graph [6]). As G is connected, \mathbf{A} is not empty but has a zero eigenvalue, so contains at least two CV in V_1 . A CV/CV pair is either D9 or D11, but D11 is impossible for $g_s < 2$ and hence the CV pair conducts, by D9. ■

Theorem 5.10.6 *For a bipartite graph G with $g_s = 1$, the inter entry of the TLA is not C.*

Proof: At least one CV/CFV *inter* pair exists, as all CV are in V_1 , and this is insulating, by D5, so the *inter* entry is I or X. ■

Application of theorems 5.10.4 to 5.10.6 leaves only case XCX undecided. This is settled by:

Theorem 5.10.7 For a bipartite graph G with $g_s = 1$, an *intra* entry of C in the TLA implies entries I for *inter* and X for *ipso*.

Proof: For $g_s = 1$, all CV are in V_1 . If the *intra* entry is C then V_1 must consist entirely of CV as a CV/CFV pair would insulate. Then *ipso* is X by I1 and I3 and *inter* is I by D5. ■

Theorems 5.10.4 to 5.10.7 rule out XCX. A singular bipartite graph with $g_s = 1$ belongs to one of three types: ICX, IXX or XXX. Furthermore, the TLA ICX is realised by exactly one graph, which is P_3 . To see this, observe that $g_s = 1$ implies $|V_1| - |V_2| = 1$ and since all vertices in V_2 are CFV, we cannot have more than one CFV in V_2 (otherwise it would give an insulating pair by D1). Hence G has one CFV and is a star. The only star with $g_s = 1$ and $n > 1$ is P_3 .

5.10.3 Singular molecular graphs with $g_s > 1$

Theorem 5.10.8 For a bipartite graph G with $g_s > 1$, the *ipso* entry of the TLA is not I .

Proof: Since G has at least one CV, at least one *ipso* device is conducting. ■

Theorem 5.10.9 For a bipartite graph G with $g_s > 1$ if the *intra* entry in the TLA is C , then the *ipso* entry is not X .

Proof: Suppose the *intra* entry is C and the *ipso* entry is X . G must have at least one CFV and at least one CV. If they form an *intra* pair we have insulation by D5 and the *intra* entry is not C . If there is no CV/CFV *intra* pair, then V_1 is all CV and V_2 is all CFV and the *intra* V_2 pairs are insulating by D1, giving a contradiction. ■

Theorem 5.10.10 For a bipartite graph G with $g_s > 1$, the *inter* entry is not C .

Proof: Choose \bar{L} as a CV in V_1 . Choose \bar{R} in V_2 . Either we have a CV/CFV pair and insulation by D5 or we have a CV/CV pair. In that case, \bar{R} remains a core vertex in $G - \bar{L}$ and we have $g_s - 2$ for the nullity of $G - \bar{L} - \bar{R}$, hence insulation by D11. To see that \bar{R} is CV in $G - \bar{L}$, observe that the CV in each vector in a basis for the nullspace of G can be concentrated in one or other of V_1 and V_2 ; removal of \bar{L} in V_1 reduces nullity by 1 but all restricted vectors corresponding to CVs in V_2 remain in the nullspace of $G - \bar{L}$. ■

Theorem 5.10.11 For a bipartite graph G with $g_s > 1$, with *ipso* entry C in the TLA, the *inter* entry is I .

Proof: If the *ipso* entry is C , all vertices are CV by I3. For *inter* pairs, we have either D9 or D11, but by the argument used in the proof of Theorem 5.10.10, if \bar{L} is in V_1 and \bar{R} is in V_2 , then \bar{R} is a CV in $G - \bar{L}$ and we have rule D11, and insulation for all *inter* pairs. ■

A corollary to Theorems 5.10.6 and 5.10.10 could be:

Corollary 5.10.1 C in the *inter* position implies that the nullity is zero where benzenoids are some examples within this class.

Chapter 6

A complete classification: the d -omni-conductors

This chapter contains a manuscript that has been prepared for publication by the author of this thesis in collaboration with Prof. P.W. Fowler, Prof. B.T. Pickup and Prof. I. Sciriha. The title of the intended publication is “Molecular graphs and molecular conduction: the d -omni-conductors”.

6.1 Abstract

Ernzerhof’s source-and-sink-potential (SSP) model for ballistic conduction in conjugated π systems predicts transmission of electrons in a two-wire device in terms of the characteristic polynomials of the molecular graph and three subgraphs based on the pattern of connections. We present here a complete classification of conduction properties of all molecular graphs within the SSP model. An *omni-conductor/omni-insulator* is a molecular graph that conducts/insulates at the Fermi level (zero of energy) for *all* connection patterns. We define d -omni-conduction/insulation in terms of Fermi conduction/insulation for all devices with graph distance d between connections. This gives a natural generalisation to all graphs of the concept of *near-omni-conduction/insulation* previously defined only for bipartite graphs. Every molecular graph can be assigned a nullity class and a compact three-letter code defining conduction behaviour: there are three nullity classes, as each graph has 0, 1, >1 zero eigenvalues (non-bonding molecular orbitals), and three letters drawn from {C, I, X} indicating conducting, insulating or mixed behaviour within the sets of devices with connection vertices at odd, even and zero distances d . Examples of graphs, in 28 cases chemical, are given for 35 out of 81 possible combinations of nullity and three-letter code, and proofs of non-existence are given for 42 combinations, leaving four cases unresolved.

6.2 Introduction

The SSP (source-and-sink-potential) model was introduced by Ernzerhof *et al.* [55, 58, 62, 69, 81, 103, 126–133] as a simple but effective description of ballistic molecular

conduction. In its graph theoretical (Hückel) incarnation [63, 68, 70, 82, 84, 87, 102, 104, 105, 107, 134], it predicts the transmission as a function of energy for a two-wire device from an expression involving a functional of four characteristic polynomials: those of the molecular graph and three subgraphs. Devices are either *distinct*, with leads connected to a pair of graph vertices, or *ipso*, with both leads connected to a single vertex. The graph theoretical SSP formulation leads to ‘selection rules’ for conduction at the Fermi level, couched in terms of nullities of the molecular graph and the subgraphs (i.e., the numbers of non-bonding π orbitals of the corresponding molecules) [70, 88]. Response of the molecular device is thereby specified in terms of the underlying molecule and the pattern of connections to the leads.

A natural question relates to *omni-conduction* and *omni-insulation*: are there molecular graphs that are predicted in the ‘empty-molecule’ SSP picture to conduct/insulate at the Fermi level for *all* connection patterns? Such graphs would be respectively omni-conductors or omni-insulators [84]. Various types of omni-behaviour can be defined in terms of consistent behaviour within *distinct*, *ipso* or *all* devices: these lead to definition of *distinct*, *ipso* and *strong* omni-conductors/insulators. Nullity again plays a key role [84].

This variety of behaviour can be captured using a simple classification system. Division into nullity classes 0, 1, and >1 , combined with conduction (C), insulation (I) or mixed (X) behaviour for distinct and ipso devices leads to a classification of molecular devices into at most 27 categories, each labelled by a *two-letter* acronym and nullity class, which can be proved to reduce to only 13 that are realisable by general graphs [107].

Bipartite molecular graphs cannot have full omni-conduction, for well understood mathematical reasons [107], but we can still ask how closely they approach it. *Near-omni* systems support as many conducting devices as mathematically possible within some imposed restriction. Restriction to bipartite graphs (graphs of alternant hydrocarbons) allows a *three-letter* acronym (TLA) for each nullity class. In the three-letter formulation, devices are characterised by their *intra*, *inter* and *ipso* behaviour, further distinguished by nullity. Intra and inter devices are those that have distinct connection vertices belonging respectively to the same or different partite sets (i.e. the sets of starred and unstarred atoms of alternant hydrocarbons [6]). It can be proved that the 81 conceivable classes reduce to just 14 [107]. This perspective gives richer detail for possible *near-omni*-conduction patterns for families of graphs. In the present context, it also points to a generalisation for *non-bipartite* graphs.

The central idea used to realise this final generalisation is a partitioning of conduction, insulation and mixed behaviour according to *graph-theoretical distance*, d , between the connection vertices. This leads to the definition of d -omni-conductors and insulators and a new interpretation of the three-letter acronyms used in the near-omni conduction formalism [107] that applies to *all* graphs, whether bipartite or not, and hence now covers all conjugated hydrocarbons.

Specifically, we imagine incorporation of a molecular graph into a circuit through connections chosen via a pair of calipers with a fixed-jaw opening (see Fig. 6.1). For simplicity, we suppose that the calipers span a fixed *graph-theoretical* distance: the calipers touch contact vertices separated by a fixed distance d (length in edges of a shortest path between connection vertices \bar{L} and \bar{R} in the molecular graph, G)

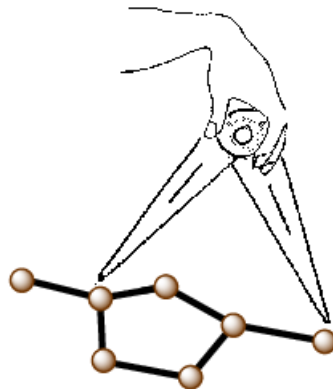


Figure 6.1: Schematic of the d -conductor: here, connection vertices at fixed distance $d = 3$ are chosen for attachment to wires in a set of devices.

drawn from the set $\{d\} = \{0, 1, \dots, D\}$ (where D is the *diameter* of the graph). We can then ask the omni-conduction/insulation question for each d , leading to a $(D + 1)$ -dimensional code for each graph. Condensation to three categories (odd- d , non-zero even- d , and zero- d) then gives a three-letter short code that maps smoothly onto the *inter* (odd d), *intra* (even $d \neq 0$) and *ipso* ($d = 0$) cases for bipartite graphs, so that all bipartite graphs keep the same label as before. The classification again gives a maximum of 81 cases when C, I, X are combined with nullity classes $g_s = 0, 1, >1$, of which some will turn out to be empty.

In the present chapter, we explore the possibilities for d -omni and near- d -omni conductors and insulators, show that the 81 cases reduce to a significantly smaller number, and we discuss systematics for long and short codes in various families of bipartite and non-bipartite graphs of interest in chemistry.

We therefore arrive at a compact, universal scheme for classification of Fermi-level conduction within the graph theoretical SSP approach.

6.3 Background

6.3.1 The SSP model

In the graph-theoretical version of the SSP approach [63], a device is represented as a molecular graph G attached by internal vertices (atoms) \bar{L} and \bar{R} to *source* (L) and *sink* (R) vertices that represent the effect of semi-infinite wires, which respectively deliver and remove a fraction T of an electron in steady-state ballistic conduction. The transmission is a function of electron energy, E . The $(n + 2)$ -vertex *device* incorporating molecular and distinct source and sink vertices is illustrated in Fig. 6.2.

Usefully, it turns out that $T(E)$ depends on E through s , t , u and v , the characteristic polynomials of the four graphs G , $G - \bar{L}$, $G - \bar{R}$ and $G - \bar{L} - \bar{R}$. At energy $E = 0$ (the Fermi energy) the transmission is given by the limit of a ratio of high-order polynomials [84]:

$$T(0) = \lim_{E \rightarrow 0} \frac{4j^2 \tilde{\beta}^2}{[(s - v\tilde{\beta}^2)^2 + (u + t)^2 \tilde{\beta}^2]}. \quad (6.1)$$



Figure 6.2: A molecular device in the SSP model. M is a molecule with a conjugated π system and its molecular graph has n vertices, of which \bar{L} and \bar{R} are connected to semi-infinite leads. (\bar{L} and \bar{R} coincide in an *ipso* device.) Each lead is replaced by a non-molecular vertex: source (L) or sink (R), respectively. The whole device $\{G, \bar{L}, \bar{R}\}$ is modelled by an $(n+2)$ -vertex graph, with complex weights on source and sink vertices, and real weights representing Hückel Coulomb and resonance integrals, α and β , on internal vertices and edges.

where j^2 is the determinantal combination $ut - sv$, and $\tilde{\beta}$ is a device parameter determined by relative magnitudes of resonance integrals for wire-to-molecule and intra-molecule contacts [105].

6.3.2 Selection rules

Selection rules [70, 88] for Fermi-level conduction of devices $\{G, \bar{L}, \bar{R}\}$ follow from Eq. (6.1) by considering the nullities of the graphs G , $G - \bar{L}$, $G - \bar{R}$ and $G - \bar{L} - \bar{R}$, or equivalently the numbers of zero roots of the characteristic polynomials s , t , u and v . The Cauchy Interlacing Theorem [86] leads to a small set of possibilities, as listed in Table 6.1, predicting Fermi-level conduction or insulation of a device according to 11 distinct and 3 *ipso* cases.

6.3.3 Vertex types

The Interlacing Theorem allows partition of the vertices of the molecular graph into three subsets: *lower*, or *core* vertices (CV) and two types of core-forbidden vertices (CFV), *middle* and *upper* [84, 91, 92]. Deletion of a CV lowers nullity by 1, deletion of a middle CFV leaves it unchanged, and deletion of an upper CFV increases the nullity by 1. Bipartite graphs have no middle vertices. The CV/CFV notation comes about because the vertices that lower the nullity on deletion are exactly those that have a non-zero entry in some vector within the graph nullspace, i.e. are ‘within the core’ of the graph. In chemical terms, core vertices are those with a non-zero contribution to the charge/spin density resulting from half/full occupation of the set of non-bonding orbitals in the π system. Conversely, the core-forbidden vertices all make zero contribution in these cases.

One simple consequence of these definitions is that if a vertex has one CV neighbour, then it must have at least two, as the neighbourhood of every vertex i in a kernel vector obeys a zero-sum rule for entries on the neighbours j of i .

Furthermore, it is useful to note that the distance between a pair of CV neighbours of a middle CFV might be 1 or 2 if G contains triangles. This awkward fact can complicate the construction of non-existence proofs.

Rule	g_s	g_t	g_u	g_v	g_j	$T(0)$
D1	g_s	g_s+1	g_s+1	g_s+2	$\geq g_s+1$	$= 0$
D2	g_s	g_s+1	g_s+1	g_s	g_s	$\neq 0$
D3	g_s	g_s+1	g_s	g_s+1	$\geq g_s+1$	$= 0$
D4	g_s	g_s+1	g_s	g_s	g_s	$\neq 0$
D5	g_s	g_s+1	g_s-1	g_s	$\geq g_s$	$= 0$
D6	g_s	g_s	g_s	g_s+1	g_s	$\neq 0$
D7.1	g_s	g_s	g_s	g_s	g_s	$\neq 0$
D7.2	g_s	g_s	g_s	g_s	$\geq g_s+1$	$= 0$
D8	g_s	g_s	g_s-1	g_s-1	$\geq g_s$	$= 0$
D9	g_s	g_s-1	g_s-1	g_s	g_s-1	$\neq 0$
D10	g_s	g_s-1	g_s-1	g_s-1	g_s-1	$\neq 0$
D11	g_s	g_s-1	g_s-1	g_s-2	$\geq g_s-1$	$= 0$
I1	g_s	g_s+1				$= 0$
I2	g_s	g_s				$\neq 0$
I3	g_s	g_s-1				$\neq 0$

Table 6.1: Selection rules for Fermi-level conduction of molecular devices based on graphs with nullity g_s . Each signature $\{g_t, g_u, g_v, g_j\}$ for nullities of the subgraphs and zero roots of the combination $|j| = \sqrt{ut - sv}$ leads to a prediction of $T(0) \neq 0$ (conduction), or $T(0) = 0$ (insulation). Devices are labelled D for *distinct* ($\bar{L} \neq \bar{R}$) and I for *ipso* ($\bar{L} = \bar{R}$).

6.3.4 Calculations

Use of a spectral representation and the corresponding Laurent expansion allows calculation of all the various required nullities needed for the selection rules directly from the eigenvectors and eigenvalues of the adjacency matrix of G alone [84, 107], and hence assignment of cases D1 to D11 and I1 to I3 and prediction of conduction or insulation, device by device. This is readily turned into a method for detection of omni-conduction/insulation behaviour across the whole family of devices based on a particular graph. This is the toolkit that was used to find two-letter and three-letter acronyms, and is employed here again to make the d -omni classification.

6.4 Classification of conduction behaviour

6.4.1 Two-letter codes (all graphs)

We take devices based on a given graph G (chemical or not) to be either *distinct* or *ipso*. For each class of devices we assign a letter from $\{C, I, X\}$ to denote respectively a class for which all devices conduct at the Fermi level, a class where all insulate, or a class that is empty or has mixed behaviour. We further label the classes by nullity of G , g_s , with $g_s = 0$, $g_s = 1$ and $g_s > 1$.

Of the 27 class labels consisting of two letters and a nullity, it can be proved [107] that 13 correspond to realisable devices $\{G, \bar{L}, \bar{R}\}$ and the others are labels for empty classes (impossible devices). A special case is the acronym II, which is unrealisable for all nullities (see Table IV of [84] and Table 4.6). Fig. 6.3 shows the realisable combinations of two-letter labels and nullities. Another way of representing these data is as eight two-letter pairs, with four nullity restrictions. This is illustrated by the shading scheme in the figure, each colour of which is common to all regions of the diagram that have the same nullity class.

6.4.2 Three-letter codes (bipartite graphs)

At the next level of classification we treat only bipartite graphs, and partition the distinct devices into inter and intra, according to whether connections \bar{L} and \bar{R} belong to different or identical partite sets. Again, we use an alphabet of three letters $\{C, I, X\}$ for omni-conducting, omni-insulating, and mixed or non-existent sets. The nine two-letter combinations then split into 27 three-letter combinations, as shown in Table 6.2.

If G is bipartite, it can be proved [107] that only 14 out of the 27×3 combinations of letters and nullities are possible. The allowed classes of bipartite devices having *inter-intra-ipso* omni-conduction types, for graphs with $n \geq 4$ vertices and nullity

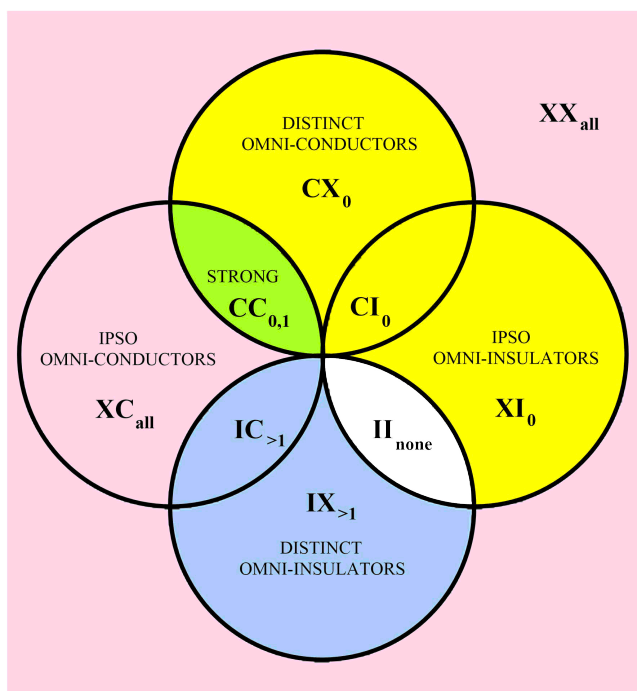


Figure 6.3: Venn-like diagram showing the two-letter (distinct/*ipso*) classification of conduction behaviour in the SSP model of all possible molecular graphs where C, I and X stand for conduction, insulation and mixed, and subscripts denote the nullity classes (0, 0 and 1, >1, none, all) for which the two-letter code applies.

g_s are:

$$\begin{aligned}
 g_s = 0 & \quad \text{CII, XII;} \\
 g_s = 1 & \quad \text{IXX, XXX;} \\
 g_s > 1 & \quad \text{ICC, IIC, IIX, IXC, IXX, XIX, XXX.}
 \end{aligned}$$

The three connected bipartite graphs with $n < 4$ each uniquely realise a conduction type: K_1 (isolated vertex) is apparently the only bipartite graph with type XXC , though other non-bipartite examples exist (see below); CXI appears only for K_2 (ethene); ICX only for P_3 (allyl).

The main types are well populated: for example, the class CII ($g_s = 0$) covers all catafused benzenoids [107]. For further details, see the statistical Tables 6.3 to 6.8.

6.4.3 Three-letter codes (all graphs)

What happens if we use an alternative subdivision of distinct devices? Distinct devices have \bar{L} and \bar{R} at non-zero graph theoretical distance, d . We make a subdivision into distinct devices with odd- d , and even- d , respectively. For brevity, we will sometimes call these *odd* and *even* devices, respectively. For bipartite graphs G , the odd/even dichotomy maps exactly onto the inter, intra subdivision, so bipartite graphs retain their old codes, but now non-bipartite graphs G are also included in the same scheme. In the following section we investigate how many of the 27×3

Nullity	2-LA	→	TLA
0, 1	CC	→	CCC
0	CI	→	CCI
0, 1	CX	→	CCX
>1	IC	→	IIC
none	II	→	III
>1	IX	→	IIX
0, 1, >1	XC	→	CIC, CXC, ICC, IXC, XCC, XIC, XXC
0	XI	→	CII, CXI, ICI, IXI, XCI, XII, XXI
0, 1, >1	XX	→	CIX, CXX, ICX, IXX, XCX, XIX, XXX

Table 6.2: Conversion of two- to three-letter acronyms. Each two-letter combination is labelled with allowed nullity values from the set $\{0, 1, >1\}$ [107]. Note that $II \rightarrow III$ would be a strong omni-insulator, a combination that is not possible for any graph [84].

= 81 combinations of three letters and nullity type are possible for chemical and general, bipartite and non-bipartite graphs.

6.5 Method

As in previous work we adopt a two-pronged approach. First, we check large sets of examples to find which classes (combinations of a three-letter acronym and nullity type) have examples amongst small graphs. Then we attempt to prove the emptiness of the remaining classes.

Assignment of conduction behaviour was carried out by taking sets of graphs from various graph generators, and using the previously developed [84] conduction/insulation decision-tree screens based on the selection rules. The screens use numerical eigenvectors of the adjacency matrix of G to compute coefficients in Laurent expansions of scaled structural polynomials $\hat{t} = t/s$, $\hat{u} = u/s$, $\hat{v} = v/s$ and $\hat{j} = j/s$, and use them to assign conduction or insulation.

The datasets of graphs were generated with *nauty* [135] (general and chemical graphs), *plantri* [110] (cubic polyhedra), *fullgen* [112] and *CaGe* [111] (for fullerenes and benzenoids). We also searched databases of larger vertex-transitive and two-orbit graphs, kindly provided by Gordon Royle (personal communication to P.W. Fowler). All graphs considered here are simple (with no loops or multiple edges) and connected.

Case	g_s	Vertex count													
		1	2	3	4	5	6	7	8	9	10	11	12	13	14
CC	0			1	1	1	2	5	8	13	48	77	333	858	3721
CI	0		1												
CX	0										5		9		151
XC	0						1	4	11	25	108	270	1178	3553	
XI	0			1		6		24		132		902		7669	
XX	0			1	2	7	17	71	177	707	1904	8762	25469	126365	
CC	1									1		8	9	27	23
XC	1	1		1		2		10	7	42	54	285	539	2773	
XX	1			1		6	3	35	27	261	322	2660	3963	32252	55733
IC	>1					1									
IX	>1			1			1		1	2	2	3	6	10	
XC	>1			1	1	1	1	1	8	21	48	110	317	729	
XX	>1					7	4	49	52	429	663	4784	8676	61317	
Total count		1	1	2	6	10	29	64	194	531	1733	5524	19430	69322	262044

Table 6.3: Distribution over allowed classes (defined by the alphabet C, I, X and nullity) for two-letter codes of chemical graphs on $n \leq 14$ vertices.

6.6 Results

6.6.1 Allowed d -omni codes

A search of chemical graphs (connected graphs with maximum degree ≤ 3) with vertex counts $n \leq 14$, general graphs with $n \leq 11$, and vertex-transitive and two-orbit graphs with $n \leq 24$ already supplies examples of 35 of the 81 conceivable combinations of TLA and nullity class.

Tables 6.3 to 6.8 show some statistics on occurrence of two and three-letter codes derived from these searches. Throughout the tables, cases not listed are forbidden, or have smallest examples outside the range of n (CCI, $g_s = 0$, CIC $g_s = 0$, IXC $g_s > 1$), or are unresolved (CIC $g_s = 0$, ICC $g_s = 1$, IXC $g_s = 1$, ICX $g_s > 1$). An exhaustive search of all 1,006,700,565 graphs on 11 vertices adds only IXC $g_s > 1$ to the list of exemplified cases obtained for $n \leq 10$.

One interesting case is that of the *nuciferous graphs* (or *nucifers*), which are non-singular graphs that are conducting for all distinct devices but insulating for all *ipso* devices, i.e. with code CCI for graphs where inter, intra and *ipso* classes of device are all non-empty. K_2 is the trivial nucifer with no intra devices, and unique TLA CXI. All non-trivial nucifers are non-chemical [100]; vertex-transitive examples are known with $n \geq 24$ [99], and we were able to find smaller examples, with $n \geq 18$, by considering graphs with two orbits of vertices. Hence, the class CCI with $g_s = 0$ is in fact populated, though not by chemical graphs.

Figs 6.4 – 6.6 show small examples for the 35 cases (chemical where we have one, and in other cases, bipartite and non-bipartite where we have both).

Next we concentrate on eliminating impossible combinations. Limitations imposed by the unrealisable subset of two-letter/nullity codes [84] can be used to rule out

Case	g_s	Vertex count									
		1	2	3	4	5	6	7	8	9	10
CC	0			1	1	3	7	35	483	9572	771377
CI	0		1								
CX	0								31	406	46839
XC	0						4	39	388	16341	795546
XI	0				1		7		129		15356
XX	0				1	5	34	268	4693	114744	6231077
CC	1							3	13	560	12551
XC	1	1			1	1	8	46	591	10663	499908
XX	1			1		7	34	291	3090	80431	2300210
IC	>1						1	2	3	7	24
IX	>1				1	1	1	5	17	100	914
XC	>1				1	3	8	49	370	5564	134397
XX	>1						22	101	1823	22178	908372
Total count		1	1	2	6	20	126	839	11631	260566	11716571

Table 6.4: Distribution over allowed classes (defined by the alphabet C, I, X and nullity) for two-letter codes of general graphs on $n \leq 10$ vertices.

Case	g_s	Vertex count													
		1	2	3	4	5	6	7	8	9	10	11	12	13	14
CII	0						1	2		4		11		47	
CXI	0		1												
XII	0				1		4	18		96		605		4691	
ICX	1			1											
IXX	1				1		4		12		62		366		
XXC	1	1													
XXX	1				2		10		61		413		3311		
ICC	>1				1			1				2		2	
IIC	>1						1								
IIX	>1				1			1	1	2	2	3	6	10	
IXC	>1					1			1	3	3	5	5	13	
IXX	>1						4	3	17	21	85	141	530	1014	3904
XXX	>1						2	14	5	105	80	918	934	8585	
Total count		1	1	1	3	4	12	18	52	101	295	701	2074	5636	17252

Table 6.5: Distribution over allowed classes (defined by the alphabet C, I, X and nullity) for three-letter codes of chemical bipartite graphs on $n \leq 14$ vertices.

Case	g_s	Vertex count													
		1	2	3	4	5	6	7	8	9	10	11	12	13	14
CCC	0					1	2	5	8	13	48	77	333	858	3721
CCX	0										5		9		151
CII	0						1		2		4		11		47
CXC	0		1	1				1		2	1	11	9	65	87
CXI	0	1													
CXX	0						1	1	6			7	33	49	157
XCC	0									3	4	29	20	214	205
XCX	0			1				1			8	18	14	59	291
XII	0			1		5		19			105		658		5079
XIX	0				1		1	1	5	1	23	5	153		21
XXC	0								4	6	20	68	241	899	3261
XXI	0								3		23		233		2543
XXX	0				1	7	15	68	166	698	1856	8710	25208	125896	
CCC	1									1		8	9	27	23
ICX	1		1												
IXX	1				1		5			18		93		552	
XCC	1			1							1				2
XCX	1				1					1				1	
XXC	1	1				2		10	7	41	54	285	539	2771	
XXX	1				4	3	30	27	242	322	2567	3963	31699	55733	
ICC	>1			1				1					2		2
IIC	>1					1									
IIX	>1			1			1		1	2	2	3	6	10	
IXC	>1				1					1	3	4	6	6	15
IXX	>1					5	3	22	26	118	200	807	1643	6709	
XIC	>1					1							7		
XXC	>1						1			7	18	44	95	311	712
XXX	>1					2	1	27	26	311	463	3977	7033	54608	
Total count		1	1	2	6	10	29	64	194	531	1733	5524	19430	69322	262044

Table 6.6: Distribution over allowed classes (defined by the alphabet C, I, X and nullity) for three-letter codes of chemical graphs on $n \leq 14$ vertices.

Case	g_s	Vertex count										
		1	2	3	4	5	6	7	8	9	10	
CII	0						1		3		16	
CXI	0		1									
XII	0				1		4		32		597	
ICX	1			1								
IXX	1					1		5		40		
XXC	1	1										
XXX	1					2		17		823		
ICC	>1				1				1		2	
IIC	>1						1	1	2	2	3	
IIX	>1				1	1	1	3	7	19	73	
IXC	>1					1	1	2	5	15	47	
IXX	>1							5	11	56	198	1204
XIX	>1						2	2	17	29	249	
XXX	>1						2	3	59	144	841	
Total count		1	1	1	3	5	17	44	182	730	4032	

Table 6.7: Distribution over allowed classes (defined by the alphabet C, I, X and nullity) for three-letter codes of bipartite graphs on $n \leq 10$ vertices.

some three-letter/nullity codes. This removes 25 of the 81 cases.

A further simple argument about non-zero entries in the inverse adjacency matrix removes all codes of type I** with $g_s = 0$, hence eliminating a further six cases.

Appendix 6.8 lists these and other theorems that can be used to prune the possibilities still further. Table 6.10 shows the state of play, where 35 classes have examples and 42 are provably empty. At present, we have 4 stubborn classes that are undecided, with neither an example nor a proof that there can be no example.

The populations of the various classes for small numbers of vertices vary considerably. As might be expected, type XXX, where there is no regularity in conduction behaviour, predominates. Other types have very few representatives, e.g. IC $g_s > 1$ apparently contains only $K_{3,3}$ amongst the chemical graphs. Chemical graphs are well represented, occurring in nearly all (at least 28) of the 35 resolved classes.

Incidentally, Table 6.10 in its present form constitutes an alternative proof of the sufficiency of 13 2-letter codes to describe all graphs. Theorem 6.8.1 rules out 13 cases, and another, CX with $g_s = 1$, is ruled out by theorem 6.8.3 or by the simpler argument that for this nullity, C* implies a nut graph, but a nut graph implies *C.

6.6.2 Expanded d -omni codes

Useful though the short three-letter acronyms are in labelling families of bipartite and non-bipartite graphs, it is interesting to explore the more detailed information afforded by the full d -omni approach.

We can define the *long code* for a molecular graph as a string of $(D + 1)$ letters drawn from the alphabet {C, I, X}, where each letter refers to the conduction behaviour of

Case	g_s	Vertex count									
		1	2	3	4	5	6	7	8	9	10
CCC	0					2	6	34	482	9571	771376
CCX	0								31	406	46839
CII	0						1		3		16
CXC	0			1	1	1	1	12	19	2141	50904
CXI	0		1								
CXX	0							4	28	966	51389
XCC	0						1	13	55	2874	78503
XCX	0				1	2	5	16	101	1766	88254
XIC	0						1	1	2	5	8
XII	0				1		5		38		700
XIX	0					1	1	8	15	94	190
XXC	0						2	14	313	11322	666132
XXI	0						1		88		14640
XXX	0					2	28	240	4549	111918	6091244
CCC	1							3	13	560	12551
ICX	1			1							
IXX	1				1		14		514		
XCC	1				1	1	3	6	20	115	1178
XCX	1					1	1	2	6	30	184
XXC	1	1					5	40	571	10548	498730
XXX	1					6	19	289	2570	80401	2300026
ICC	>1				1	1	1	1	2	1	3
IIC	>1						1	2	3	7	24
IIX	>1				1	1	1	5	17	100	914
IXC	>1					1	2	6	27	142	1076
IXX	>1						9	29	281	2211	51805
XCC	>1						1	1	4	7	37
XCX	>1							1	1	3	7
XIC	>1					1	3	6	30	142	980
XIX	>1						4	18	112	864	10789
XXC	>1						1	35	307	5272	132301
XXX	>1						9	53	1429	19100	845771
Total count		1	1	2	7	20	126	839	11631	260566	11716571

Table 6.8: Distribution over allowed classes (defined by the alphabet C, I, X and nullity) for three-letter codes of graphs on $n \leq 10$ vertices.

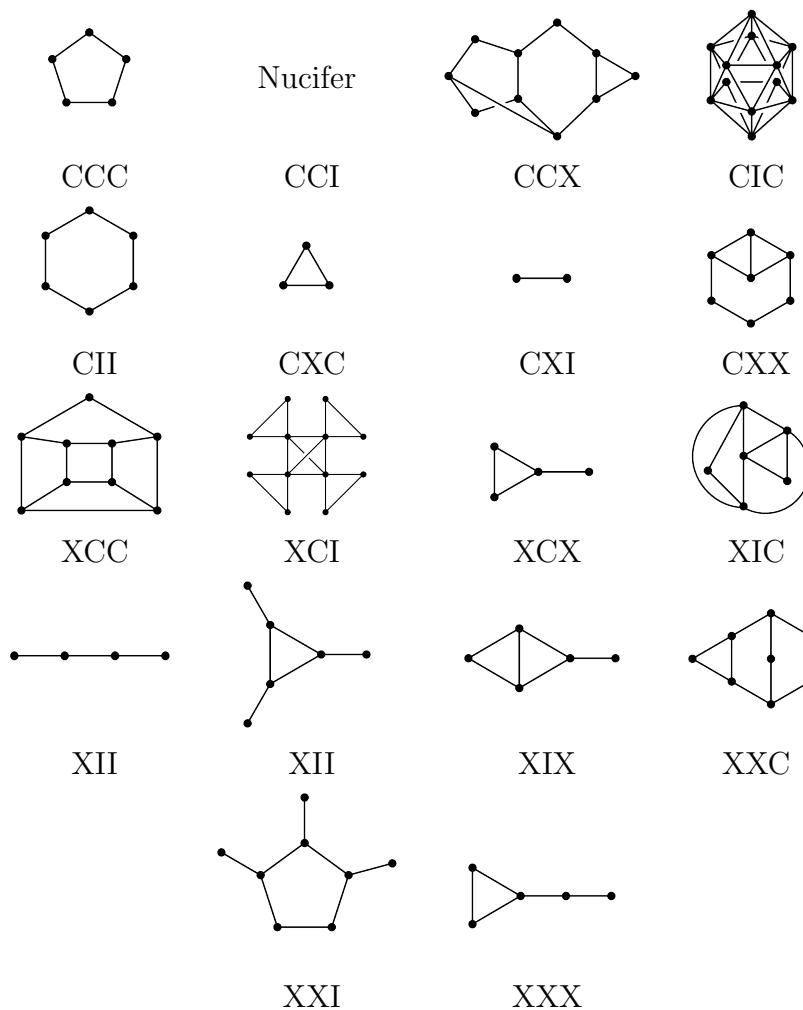


Figure 6.4: Realisation of d -omni-conduction types classified by three-letter acronym showing the cases for $g_s = 0$, and the entry ‘Nucifer’ is a placeholder for the smallest example of class CCI. The graph for category CIC is the skeleton of the icosahedron. In each case, a chemical example is given if we have one, and otherwise bipartite and non-bipartite examples are given, where we have both.

devices with a fixed value of d , drawn from the available range $d = 0, 1, \dots, D$, where D is the diameter of the graph. Notice that the entries in the long code are ordered strictly by increasing d , with alternating even and odd devices starting from *ipso* $d = 0$. The TLA has *ipso* at the final position, for consistency with the previous usage [107].

Some long codes are obvious, determined entirely by a three-letter acronym that contains no X in the first two positions. Table 6.9 analyses long codes for the graph families defined in Fig. 6.7.

6.7 Conclusions

An important advantage of the SSP (Source and Sink Potential) model for ballistic conduction is its essentially graph theoretical nature, which enables qualitative predictions (selection rules) for conduction or insulation at the Fermi level. These allow

Family		Short code	Long code		Notes
Paths, P_n	n even	XII	(IX) ^a IC	$a = (n - 2)/2$	CXI for $n = 2$
	n odd	IXX	(XI) ^a C	$a = (n - 1)/2$	ICX for $n = 3$
Cycles, C_n	$n = 4N + 2$	CII	(IC) ^a	$a = (n - 2)/2$	
	$n = 4N$	ICC	(CI) ^a C	$a = n/4$	
	n odd	CCC	(C) ^a	$a = (n + 1)/2$	CXC for $n = 3$
Radialenes, R_n	$n = 2N$	XII	IXIX(I) ^a	$a = \lfloor N/2 \rfloor - 1$	IXIC for $N = 3$
Semiradialenes, $n = 3p$	$2p = 4N + 2$	XII	(XI) ^a	$a = (N + 2)/2$	XIIIC for $n = 4$
	$2p = 4N$	XII	(XI) ^a	$a = (N + 4)/2$	
Bi-cycles, p, q	$p = 4N + 2,$ $q = 4N' + 2$	CII	(IC) ^a	$a = N + N' + 1$	
	$p = 4N,$ $q = 4N', p \geq q$	XII	(IX) ^a (IC) ^b	$a = N,$ $b = N'$	
	$p = 4N + 2,$ q odd	CCC	(C) ^a	$a = (p + q - 1)/2$ $= (n + 1)/2$	
	$p = 4N,$ q odd	XXX	(X) ^a	$a = (p + q - 1)/2$ $= (n + 1)/2$	
	p, q odd, $p + q = 4N + 2$	XXC	C(X) ^a C	$a = (p + q - 4)/2$ $= 2N - 1$	XCC for $p = q = 3$
	p, q odd, $p + q = 4N$	XXX	(X) ^a C	$a = (p + q - 2)/2$ $= 2N - 1$	

Table 6.9: Full d -omni codes for Fermi-level conduction of chemical families of molecular devices, defined in Fig. 6.7.

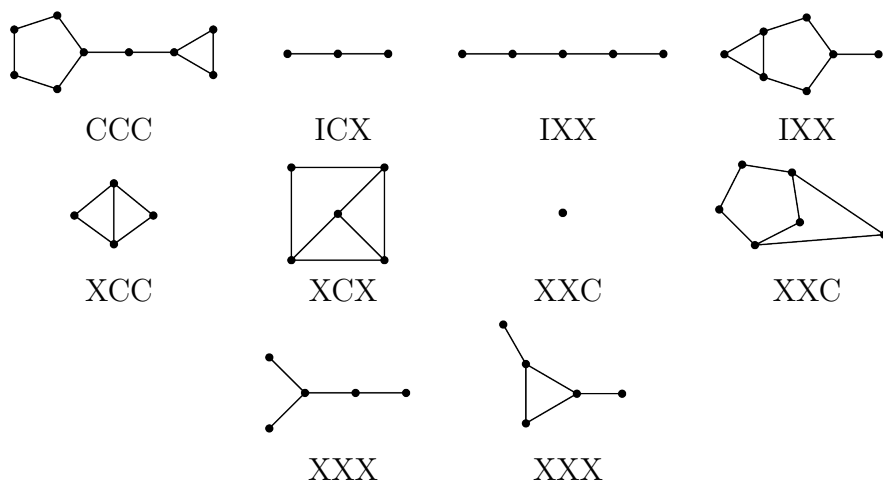


Figure 6.5: Realisation of d -omni-conduction types classified by three-letter acronym showing the cases for $g_s = 1$. In each case, a chemical example is given if we have one, and otherwise bipartite and non-bipartite examples are given, where we have both.

classification of the whole to a set of devices associated with different patterns of connection of wires to a given molecular structure. The concepts of omni-conduction and omni-insulation have been successively refined to describe systematics of conduction within chemically significant subsets of these devices. This chapter has presented a new classification scheme based on graph distance that can deal with the molecular graph of any conjugated π system. Seventy seven of the 81 hypothetical conduction types have been resolved: 35 are realised by some small graph; 42 are unrealisable by any graph, leaving 4 cases open. Of the 35 realised cases, at least 28 are exemplified by a chemical graph representative of conjugated π system. The new scheme is compatible with the previous classification of bipartite graphs but now applies to all π systems, alternant and non-alternant.

6.8 Appendix: Theorems for d -omni codes

The tripartite classification of vertices into lower, middle and upper types will be used repeatedly in this section. Also, in this section, wildcard characters are used to stand for arbitrary letters drawn from the $\{C, I, X\}$ alphabet. Hence, A^*B indicates a code with behaviour A at odd d , B at zero d and any of C, I or X at even d .

A remark on notation may be useful. The dual use of the letter X to signify either the absence of devices in a class or the presence of mixed conduction/insulation for device in a class requires some care when comparing two- and three-letter acronyms. For example, the complete graph K_n for $n > 2$ is a strong omni-conductor. The two-letter acronym for $K_{n>2}$ is CC but the TLA is CXC , as $d \leq 1$ for any complete graph on $n > 1$ vertices, so the class of devices with even distance $d \geq 2$ is empty. For $2 \leq n \leq 6$ the code CXC applies in this sense to complete graphs; from $n \geq 7$ there are graphs with the same TLA code, but now with the X standing for mixed behaviour for distinct devices with even distance between the connections. This distinction is obvious from the long code, or just from the graph diameter, but needs to be kept in mind when looking at how two- and three-letter acronyms are

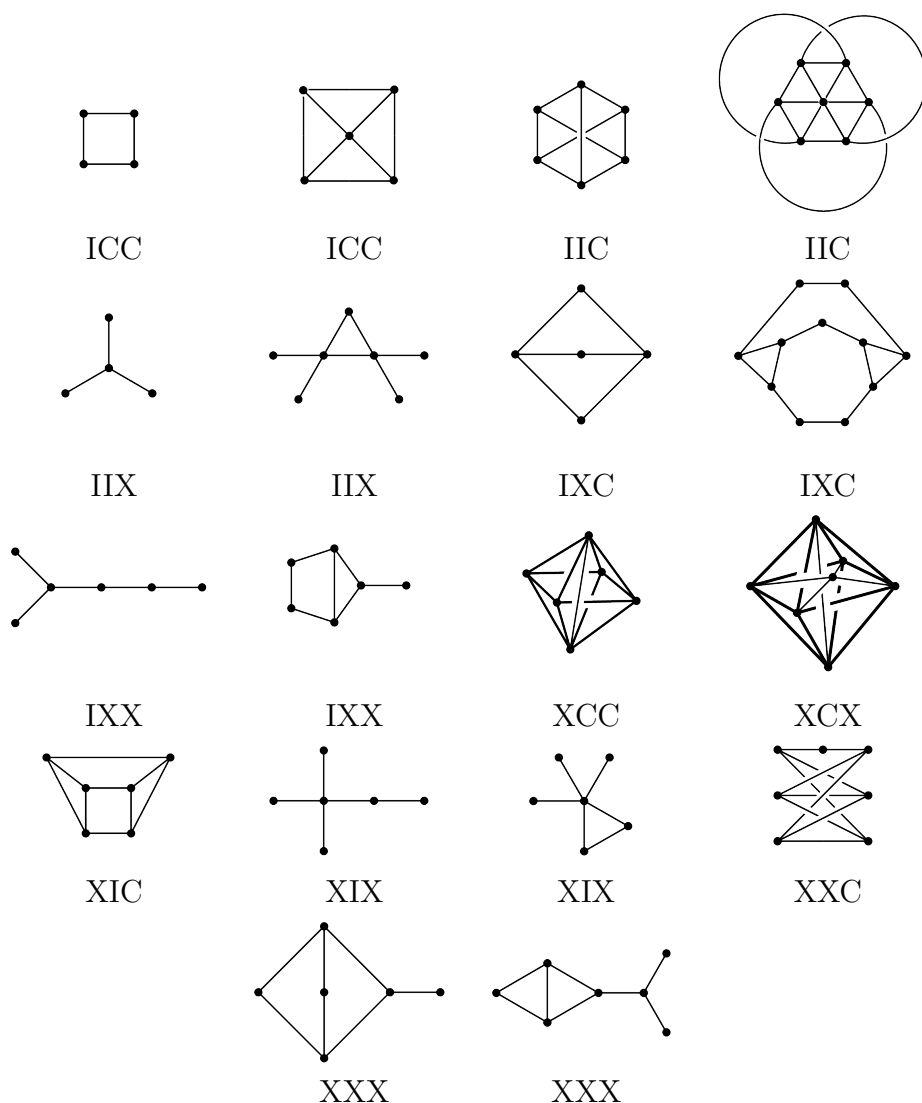


Figure 6.6: Realisation of d -omni-conduction types classified by three-letter acronym showing the cases for $g_s > 1$, and case IIC is the ‘Utility Graph’, $K_{3,3}$ and appears to be the only chemical in this class. In each case, a chemical example is given if we have one, and otherwise bipartite and non-bipartite examples are given, where we have both.

correlated.

In deriving rules for exclusion of cases, we begin by noting the combinations forbidden by previous results. From the set of theorems proved in [84], 25 of the 81 TLA can be ruled out immediately.

Theorem 6.8.1 *The following 25 cases are not realisable by any graph.*

$g_s = 0$ IIC, III, IIX

$g_s = 1$ CCI, CII, CXI, ICI, IIC, III, IIX, IXI, XCI, XII, XXI

$g_s > 1$ CCC, CCI, CCX, CII, CXI, ICI, III, IXI, XCI, XII, XXI

Furthermore, a simple argument based on linear algebra eliminates more classes for

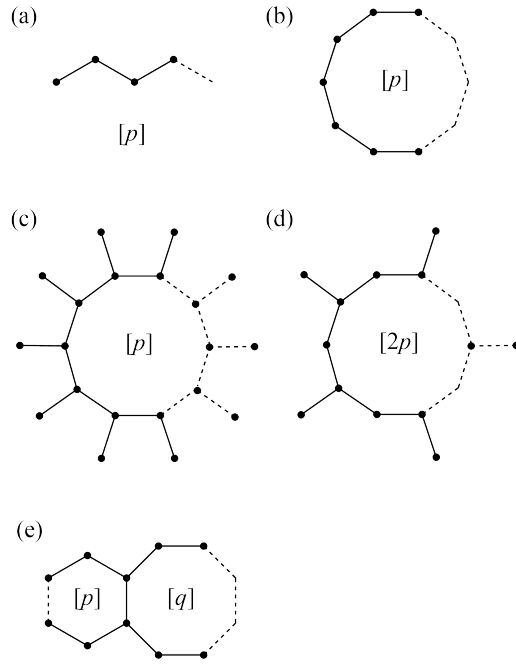


Figure 6.7: Families of graphs with interesting long codes describing their conduction behaviour: (a) paths, (b) cycles, (c) radialenes, (d) semiradialenes, (e) bi-cycles. The parameters $[p]$ and $[q]$ in (a) to (e) may take both odd and even values.

$g_s = 0$. The key result is [84]:

Theorem 6.8.2 *For $g_s = 0$, a device with connections \bar{L} and \bar{R} is conductive at the Fermi level if and only if the corresponding off-diagonal element in the inverse of the adjacency matrix of the graph is non-zero.*

Proof: The letter I in the first position implies that all devices with odd d insulate, and hence that all devices with \bar{L} and \bar{R} adjacent insulate. However, definition of the inverse requires

$$\sum_j (A)_{ij} (A^{-1})_{ji} = \mathbf{I}_{ii} = 1 \quad (6.2)$$

for all i . The only non-zero entries in the adjacency matrix, \mathbf{A} , are for pairs i, j connected by an edge, but the corresponding entries in the inverse, \mathbf{A}^{-1} , are zero, by hypothesis. Hence we have a contradiction. ■

The consequence is that all codes \mathbf{I}^{**} for $g_s = 0$ are unrealisable. This adds a further six to the list of unrealisable cases listed in Theorem 6.8.1

Corollary 6.8.1 *TLA \mathbf{I}^{**} is not realisable by any non-singular connected graph.*

An easy consequence of Eq. (6.2) is that every vertex \bar{L} of a non-singular connected graph G is part of at least one conducting device where \bar{R} is a neighbour of \bar{L} . There are at least $\lceil n/2 \rceil$ such edgewise-conducting devices. All leaves $u - w$ in G define a conducting device (G, u, w) .

Another straightforward observation is:

Case	Nullity, g_s		
	0	1	> 1
CCC	Some	Some	6.8.1
CCI	Some	6.8.1	6.8.1
CCX	Some	6.8.3	6.8.1
CIC	Some	6.8.4	6.8.5
CII	Some	6.8.1	6.8.1
CIX	*	6.8.3	6.8.3
CXC	Some	6.8.4	6.8.5
CXI	Some	6.8.1	6.8.1
CXX	Some	6.8.3	6.8.3
ICC	6.8.2	*	Some
ICI	6.8.2	6.8.1	6.8.1
ICX	6.8.2	Some	*
IIC	6.8.1	6.8.1	Some
III	6.8.1	6.8.1	6.8.1
IIX	6.8.1	6.8.1	Some
IXC	6.8.2	*	Some
IXI	6.8.2	6.8.1	6.8.1
IXX	6.8.2	Some	Some
XCC	Some	Some	Some
XCI	Some	6.8.1	6.8.1
XCX	Some	Some	Some
XIC	Some	6.8.6	Some
XII	Some	6.8.1	6.8.1
XIX	Some	6.8.6	Some
XXC	Some	Some	Some
XXI	Some	6.8.1	6.8.1
XXX	Some	Some	Some

Table 6.10: Conduction behaviour of π -conjugated hydrocarbons, i.e molecules that have molecular graphs which are chemical, showing the existence status of the 81 conceivable combinations of *odd-even-ipso* device behaviour with nullity of the molecular graph. Entries ‘Some’ indicate that at least one example has been found. An entry in the form 6.8.number refers to the first theorem that can be used to rule out a given case (see Section 6.8 for details). Cases marked with a star are unresolved.

Lemma 6.8.1 *X in the ipso position implies that both middle and upper vertices are present (for $g_s = 0$), and at least upper and lower vertices are present (for $g_s \geq 1$).*

This is used to prove:

Theorem 6.8.3 *C*X with $g_s \geq 1$ is not realisable.*

Proof: By Lemma 6.8.1, X in the *ipso* position implies vertices CV and upper CFV are present in G . Middle CFV vertices may also be present. As the graph is

connected it must have at least one edge ($d = 1$) connecting a CV and either an upper or a middle CFV, which are Cases D5 and D8, respectively, and insulating, contradicting the claimed conduction for all devices with odd d . ■

This eliminates a further five cases.

Lemma 6.8.2 *All graphs with $g_s \geq 1$ on $n > 2$ vertices have at least two core vertices.*

Proof: For $g_s = 1$, the nullspace contains a unique eigenvector. Either the graph has only core vertices and $|\text{CV}| = n$ and by hypothesis $n > 1$, or there is a core-forbidden vertex v adjacent to a core vertex u and the zero-sum rule for entries in the eigenvector on the neighbourhood of v demands at least one additional neighbour of v to be a core vertex.

For $g_s > 1$, the nullspace contains g_s independent eigenvectors and a given core vertex u can be assigned a zero entry in at least one vector by taking a linear combination, but again by the zero-sum rule for the neighbourhood of each vertex, this vector must contain at least one non-zero entry, and so $|\text{CV}| \geq 2$. ■

Lemma 6.8.3 *If $g_s \geq 1$ then there exist at least two CVs therefore some ipso conduction exists, and **I is impossible.*

Lemma 6.8.4 *If $g_s \geq 1$ and the TLA code is **C, then the graph has no upper CFV vertices.*

Theorem 6.8.4 *CIC and CXC with $g_s = 1$ are not realisable.*

Proof: The TLA code with C in the *ipso* position can mean two things: either the graph G has only core vertices and it is a nut graph with the TLA code CCC. Or else, G must have core vertices and middle CFV. Since G is connected, there exists an insulating CV–CFV edge (Case 8) contradicting the C in the first position of the TLA codes CIC and CXC. ■

Hence, two further combinations are eliminated.

Theorem 6.8.5 *CIC and CXC with $g_s > 1$ are not realisable.*

Proof: C in the *ipso* position implies that G has CV and possibly middle vertices. However, there can be no CV–middle edge, as this would imply insulation for at least one device with $d = 1$ device, and in the TLA we have C for all odd d . Hence there are no middle vertices, and G is a core.

Consider a CV–CV edge pair u, v . Choose a kernel vector that has non-zero entries at positions u and v . The device $\{G, u, v\}$ is not Case 11, because this would be an insulator, in contradiction of the C entry in the first position of the TLA. Hence, all other vectors in the kernel space must have zero entries at position u and position v , as otherwise we would have a Case 11 (insulating edge). G is connected, so

by induction on edge pairs it is possible to choose a kernel eigenvector with *all* entries non-zero, forcing all other kernel vectors to be filled by zeroes. This is a contradiction of the claim that G has $g_s > 1$.

Note that CCC is already proved impossible for $g_s > 1$ by Theorem 6.8.2, which follows from Theorem 4.3 of [84], so in fact we have that C*C is impossible for $g_s > 1$. ■

Theorem 6.8.6 *XIC and XIX with $g_s = 1$ are not realisable.*

Proof: First note that G is not a nut graph (as the TLA code is not CCC). Taking the first part of the theorem, the TLA code XIX implies that G has at least 2 CVs and at least one middle CFV, because it is an *ipso* omni-conductor that is not a nut. Therefore, there exists Case 8 insulation for a CV–middle CFV pair that are either at odd or even distance apart. XIX allows both.

All CV–CV pairs give conduction since Case 11 cannot occur (owing to $g_s = 1$). As the TLA implies that all pairs with d even must give insulation, it follows that all CV–CV pairs are odd distances apart.

Case 1: All CVs induce a core which is the union of cliques (K_p , $p > 1$). This gives a contradiction since the core has to induce a singular graph. (Note that complete graphs are not singular, for $p > 1$.)

Case 2: There exist CVs that form an independent set such that each pair is at distance 3, 5, *etc.* apart. Each middle CFV adjacent to a CV must be adjacent to at least 2 CVs, by the zero-sum rule. Hence, either there exists an edge between the two CVs and so a middle CFV and its two adjacent CVs are on a triangle, or else, there is no edge between the 2 CVs that are adjacent to the middle CFV. In the former case where there is an edge between the 2 CVs, then the CVs are not independent and so give rise to a clique that is non-singular. In the latter case where there is no edge between the 2 CVs, these 2 CVs are an even distance apart and these can only give rise to conduction by Case 9 or 10. Thus, in either of these two cases, a contradiction results for XIX.

For the second part of the proof, the reasoning for XIX can be adapted to exclude XIX also. The TLA code XIX implies that with X in the *ipso* position the vertices of G are CV and CFV, with upper CFV for sure and possibly middle CFV. G also has at least 2 CVs. The argument follows the same course as listed for Case 1 and Case 2, but now uses a general CFV instead of a middle CFV. ■

The combination of Theorems 6.8.1 and 6.8.6, shows that XI* with $g_s = 1$ is not realisable. Thus, the codes CIX with $g_s = 0$, ICC and IXC with $g_s = 1$ and ICX with $g_s > 1$ are the only codes left either to be proved unrealisable or furnished with an example.

Chapter 7

A molecular orbital view of the SSP method

The main results described here have been published in “A new approach to the method of source–sink potentials for molecular conduction” *The Journal of Chemical Physics* **143**, 191405, (2015), Pickup, Fowler, Borg and Sciriha [82]. This chapter is closely based on this reference, with some rewriting to incorporate new material and remove unnecessary repetitions of introductory material. In earlier work, both in the literature [55, 58, 62, 69, 81, 103, 126–133] and reported in this thesis it has been shown that the graph–theoretical formulation of the SSP model can lead to general qualitative conclusions about molecular conduction. This work was based on an atomic–orbital formalism. In the present chapter the tight–binding SSP equations for ballistic conduction through conjugated molecular structures are re–derived in an inhomogeneous form that avoids singularities. The re–derivation gives new results for families of molecular devices in terms of eigenvectors and eigenvalues of the adjacency matrix of the molecular graph, i.e., molecular orbitals and orbital energies. The present chapter defines the transmission of electrons through individual molecular orbitals (MO) and through MO shells. Conduction near eigenvalues is dominated by the transmission curves of nearby shells of orbitals, which may be inert or active. An inert shell does not conduct at any energy, not even at its own eigenvalue. Conduction may occur at the eigenvalue of an inert shell, but is then carried entirely by other shells. If a shell is active, it carries all of the conduction at its own eigenvalue.

7.1 A rederivation of the SSP equations

Our starting point is the SSP device defined with general (unsymmetrical) leads. The SSP expression for the transmission of such a device is

$$T(E) = \mathcal{B}(q_L, q_R) \frac{j^2}{|D|^2} \quad (7.1)$$

where

$$\mathcal{B}(q_L, q_R) = (2\beta_L \sin q_L)(2\beta_R \sin q_R)\beta_{LL}^2\beta_{RR}^2 \quad (7.2)$$

is a ‘bandpass’ function ensuring that the electron energy is within the conduction band of each lead, $j^2 = ut - sv$, and

$$D(E) = \beta_L e^{-iq_L} \beta_R e^{-iq_R} s - \beta_R e^{-iq_R} \beta_{LL}^2 t - \beta_L e^{-iq_L} \beta_{RR}^2 u + \beta_{LL}^2 \beta_{RR}^2 v \quad (7.3)$$

This expression applies equally to systems for which weighted graphs are appropriate, such as systems displaying π -distortivity [136,137], or doped with hetero-atoms. All applications of the SSP model in the present chapter are based on devices with one-dimensional leads attached to single atoms of the molecule. More complicated leads and connection patterns can be accommodated by modification of the contents of the blocks of the device matrix (see Eqs (7.22) and (7.29)). Examples of SSP treatments of multichannel devices are given in [138] and [133].

The new feature of the approach used here is that it is based on qualitative molecular-orbital theory as we believe that such models allow ‘for a transparent interpretation of molecular conductance in terms of discrete eigenstates’ [69]. The use of orbitals and orbital densities gives an opportunity for using familiar chemical concepts to give insight [103, 130, 139, 140].

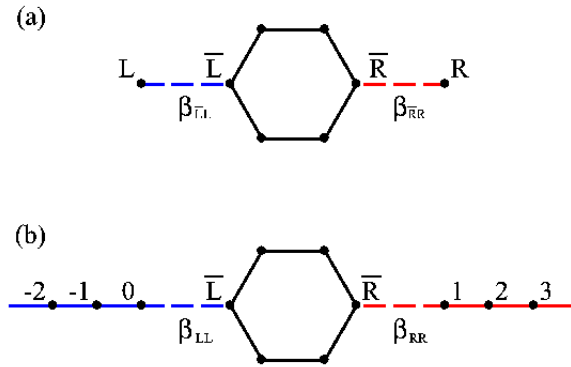


Figure 7.1: (a) An SSP molecular device comprising a molecule attached to source and sink atoms L and R via contacts \bar{L} and \bar{R} , respectively. (b) A molecule attached to infinite left- and right-hand wires, showing the numbering scheme adopted for the atoms in the wires.

Fig. 7.1 replicates the SSP device and consists of the molecule with two attached infinite wires. The normalisation of the wavefunctions for the full device connected to infinite wires, where the numbering scheme for atoms in Fig. 7.1(b) is designed to simplify the algebra that follows by elimination of the unnecessary phase factors that have confused previous derivations [62, 63, 103].

In what follows, p, q, \dots will be used for atoms, labels k, k', \dots for molecular orbitals, and K for shells.

7.1.1 Flux normalisation

The target in an SSP theory is the device wavefunction. This consists of lead and molecule parts. The wavefunctions ψ^{left} , ψ^{right} in left- and right-hand wires, respectively, are written in the tight-binding (Hückel) approximation as linear combinations

$$\begin{aligned}\psi^{\text{left}} &= \sum_{p=-\infty}^0 c_p^{\text{left}} \phi_p \\ \psi^{\text{right}} &= \sum_{p=1}^{\infty} c_p^{\text{right}} \phi_p\end{aligned}\quad (7.4)$$

where the ϕ_p are basis functions on the atoms of left and right wires, and the Hückel Coulomb and resonance parameters for each wire are α_L, β_L , and α_R, β_R , respectively. As in Chapter 2, coefficients for the left and right wires are given by

$$\begin{aligned}c_p^{\text{left}} &= \frac{1}{N_L} (e^{iq_L p} + r e^{-iq_L p}) \\ c_p^{\text{right}} &= \frac{1}{N_R} \tau e^{iq_R p}\end{aligned}\quad (7.5)$$

for the specified boundary conditions, where the left-hand wavefunction is a combination of a forward-travelling wave (e^{iq_L}) and a backward-travelling component (e^{-iq_L}) with a reflection coefficient, r . The molecule acts as a potential barrier that produces a reflected wave in the left wire and a forward transmitted wave (e^{iq_R}) in the right wire, with a transmission coefficient, τ . This corresponds to a flux of electrons with energy E , satisfying both the dispersion relations below and the Hückel Schrödinger equation for infinite wires, in terms of the wavevectors q_L and q_R .

$$E = \alpha_L + 2\beta_L \cos q_L = \alpha_R + 2\beta_R \cos q_R \quad (7.6)$$

The normalisation factors N_L and N_R have been introduced in Eq. (7.5) to obtain the requisite unit electron flux. Hence, the current density [141] from atom $(p-1)$ to atom p in the left wire, using the standard Hückel formulation is

$$\begin{aligned}J_{(p-1) \rightarrow p}^{\text{left}} &= \frac{1}{i} \left(\langle \phi_{p-1} | \hat{H} | \phi_p \rangle c_{p-1}^{\text{left}*} c_p^{\text{left}} - \text{c.c.} \right) \\ &= \frac{2\beta_L \sin q_L}{N_L^2} (1 - |r|^2)\end{aligned}\quad (7.7)$$

where we have used $\langle \phi_{p-1} | \hat{H} | \phi_p \rangle = \beta_L$. This expression is independent of the index p , showing that a constant current flows down the wire. This current is required to be equal to the transmission probability, $T(E)$. Hence, we deduce that the correct flux normalisation is achieved by setting

$$N_L^2 = 2\beta_L \sin q_L \quad (7.8)$$

and using an analogous derivation for the right-hand wire

$$N_R^2 = 2\beta_R \sin q_R \quad (7.9)$$

7.1.2 The SSP equations in the atomic orbital basis

We now look for the portion of the wavefunction that lies within the molecule and represent it in AO form. The secular equations of the device shown in Fig. 7.1(b) for atom 0 in the left-hand wire and for atom 1 in the right-hand wire are

$$\begin{aligned}\beta_L c_{-1}^{\text{left}} + (\alpha_L - E) c_0^{\text{left}} + \beta_{LL} c_{\bar{L}} &= 0 \\ \beta_{RR} c_{\bar{R}} + (\alpha_R - E) c_1^{\text{right}} + \beta_{RC_2}^{\text{right}} &= 0\end{aligned}\quad (7.10)$$

where β_{LL}, β_{RR} are resonance parameters for the connections from the wires to the molecule. We wish to replace the left wire by a single source atom, L , sited at atom 0 and creating a flux of electrons corresponding to the wavefunction ψ^{left} in Eqs (7.4) and (7.5). Similarly, we wish to replace the right wire by a single sink atom, R sited at atom 1 and removing the transmitted flux. This requires the definition of *complex* potentials, Θ_L, Θ_R , on these source and sink atoms to replace the effects of atoms to the left of atom 0, and to the right of atom 1, respectively [62].

Hence, we define

$$\begin{aligned}\beta_L c_{-1}^{\text{left}} &= \Theta_L c_0^{\text{left}} \\ \beta_{RC_2}^{\text{right}} &= \Theta_R c_1^{\text{right}}\end{aligned}\quad (7.11)$$

These complex potentials, Θ_L, Θ_R , are the same as the quantities denoted by Σ in Ernzerhof's original derivation of the SSP equations [62]. The potentials can now be derived by using the expressions from Eq. (7.5) for the orbital coefficients

$$\begin{aligned}\Theta_L &= \beta_L \frac{c_{-1}^{\text{left}}}{c_0^{\text{left}}} = \beta_L \frac{(e^{-iqL} + r e^{iqL})}{(1+r)} \\ \Theta_R &= \beta_R \frac{c_2^{\text{right}}}{c_1^{\text{right}}} = \beta_R e^{iqR}\end{aligned}\quad (7.12)$$

In the standard SSP formalism [63, 103, 126] these potentials are used directly in the SSP secular equations. However, when the reflection coefficient, r , becomes equal to -1 , the potential Θ_L becomes infinite. A more satisfactory approach, avoiding this singularity, is obtained by substituting the explicit form of c_{-1}^{left} into Eq. (7.10) to give

$$\frac{\beta_L}{N_L} (e^{-iqL} + r e^{iqL}) + (\alpha_L - E) c_L + \beta_{LL} c_{\bar{L}} = 0\quad (7.13)$$

and noting from Eq. (7.5) that

$$c_L \equiv c_0^{\text{left}} = \frac{1+r}{N_L}\quad (7.14)$$

we deduce that

$$r = N_L c_L - 1\quad (7.15)$$

Substituting for r in Eq. (7.13), we obtain

$$\begin{aligned}(\beta_L e^{iqL} + \alpha_L - E) c_L + \beta_{LL} c_{\bar{L}} &= \frac{2i\beta_L \sin qL}{N_L} \\ &= iN_L\end{aligned}\quad (7.16)$$

where we have placed the inhomogeneity on the right-hand side. We can carry out the same procedure using c_1^{right} from Eq. (7.5) in Eq. (7.10) to give

$$c_R \equiv c_1^{\text{right}} = \frac{\tau}{N_R} e^{iq_R} \quad (7.17)$$

and hence

$$c_2^{\text{right}} = e^{2iq_R} \frac{\tau}{N_R} = e^{iq_R} c_R \quad (7.18)$$

Substitution of this expression into Eq. (7.10) gives

$$\beta_{\bar{R}R} c_{\bar{R}} + (\alpha_R - E + \beta_R e^{iq_R}) c_R = 0 \quad (7.19)$$

which does not contain an inhomogeneity.

With these modifications to the boundary conditions, the wavefunction for the model device can be found. The wavefunction

$$\psi_{\text{SSP}} = \sum_{p=1}^n c_p^{\text{AO}} \phi_p + c_L \phi_L + c_R \phi_R \quad (7.20)$$

is the solution to the SSP equations in the AO formalism. The ϕ_p here are basis functions on the atomic centres, and ϕ_L, ϕ_R are basis functions on source and sink atoms. The $(n+2)$ -dimensional SSP equations for the SSP device depicted in Fig. 7.1(a) can now be written in matrix form as

$$\mathbf{P}_{\text{AO}} \begin{pmatrix} \mathbf{c}^{\text{AO}} \\ c_L \\ c_R \end{pmatrix} = \begin{pmatrix} \mathbf{0} \\ -iN_L \\ 0 \end{pmatrix} \quad (7.21)$$

where the *device matrix* is

$$\mathbf{P}_{\text{AO}} = \begin{pmatrix} E\mathbf{1} - \mathbf{A} & -\mathbf{b}_L & -\mathbf{b}_R \\ -\tilde{\mathbf{b}}_L & E - \alpha_L - \beta_L e^{iq_L} & 0 \\ -\tilde{\mathbf{b}}_R & 0 & E - \alpha_R - \beta_R e^{iq_R} \end{pmatrix} \quad (7.22)$$

and where for our single-atom-contact configurations the *connection matrix* elements are

$$\begin{aligned} (\mathbf{b}_L)_p &= \delta_{p\bar{L}} \beta_{\bar{L}L} \\ (\mathbf{b}_R)_p &= \delta_{p\bar{R}} \beta_{\bar{R}R} \end{aligned} \quad (7.23)$$

and the source and sink matrix elements are

$$\begin{aligned} E - \alpha_L - \beta_L e^{iq_L} &= \beta_L e^{-iq_L} \\ E - \alpha_R - \beta_R e^{iq_R} &= \beta_R e^{-iq_R} \end{aligned} \quad (7.24)$$

Here the dispersion relations Eq. (7.6) were used to remove E from source and sink matrix elements.

7.1.3 The SSP equations in the MO basis

The form of the SSP matrix equations in the molecular orbital (MO) representation is useful for analysing the behaviour of the solution at the eigenvalues of the isolated molecule. The Hückel MOs

$$\psi_k = \sum_{p=1}^n \phi_p U_{pk} \quad (7.25)$$

diagonalise the secular matrix of the isolated molecule, *i.e.*,

$$\sum_{q=1}^n A_{pq} U_{qk} = U_{pk} \epsilon_k \text{ for } p = 1, 2, \dots, n, \quad (7.26)$$

Assuming the $n \times n$ -dimensional adjacency matrix \mathbf{A} is real and symmetric, the matrix \mathbf{U} can be considered to be orthogonal. Hence, we can define an augmented $(n+2) \times (n+2)$ -dimensional orthogonal matrix

$$\begin{pmatrix} \mathbf{U} & \mathbf{0} & \mathbf{0} \\ \mathbf{0} & 1 & 0 \\ \mathbf{0} & 0 & 1 \end{pmatrix} \quad (7.27)$$

which can be used to transform the AO-based SSP secular equations (Eq. (7.10)) to give the MO-based version

$$\mathbf{P}_{\text{MO}} \begin{pmatrix} \mathbf{c}^{\text{MO}} \\ c_L \\ c_R \end{pmatrix} = \begin{pmatrix} \mathbf{0} \\ -iN_L \\ 0 \end{pmatrix} \quad (7.28)$$

where the SSP device matrix in the MO basis is

$$\mathbf{P}_{\text{MO}} = \begin{pmatrix} \mathbf{p} & -\mathbf{u}_L & -\mathbf{u}_R \\ -\tilde{\mathbf{u}}_L & \beta_L e^{-iq_L} & 0 \\ -\tilde{\mathbf{u}}_R & 0 & \beta_R e^{-iq_R} \end{pmatrix} \quad (7.29)$$

and the diagonal MO-MO block has

$$\mathbf{p}_{kk'} = \delta_{kk'} p_k = (E - \epsilon_k) \quad (7.30)$$

The connection matrix in the MO basis is more complicated than in the AO form, *i.e.*,

$$\begin{aligned} (\mathbf{u}_L)_k &= (\tilde{\mathbf{U}}\mathbf{b}_L)_k = \beta_{LL} U_{Lk} \\ (\mathbf{u}_R)_k &= (\tilde{\mathbf{U}}\mathbf{b}_R)_k = \beta_{RR} U_{Rk} \end{aligned} \quad (7.31)$$

and the MO expansion coefficients are related to those in the AO basis by

$$\mathbf{c}^{\text{MO}} = \tilde{\mathbf{U}}\mathbf{c}^{\text{AO}} \quad (7.32)$$

The SSP wavefunction, the solution to Eq. (7.28), is then

$$\psi_{\text{SSP}} = \sum_{k=1}^n c_k^{\text{MO}} \psi_k + c_L \phi_L + c_R \phi_R \quad (7.33)$$

where now the ψ_k are MOs of the molecule, the coefficients c_L, c_R are identical in Eqs (7.20) and (7.33), and the MO and AO coefficients are related as in Eq. (7.32).

The two mathematically equivalent expansions of the wavefunction ψ_{SSP} , *i.e.*, Eqs (7.20) and (7.33), correspond to physically different models of the conduction process, as illustrated in Fig. 7.2 for the example of an end-to-end connected allyl chain. In one, the electron hops from AO to AO along edges of the molecular graph; in the other, the MOs act as parallel channels for conduction of electrons.

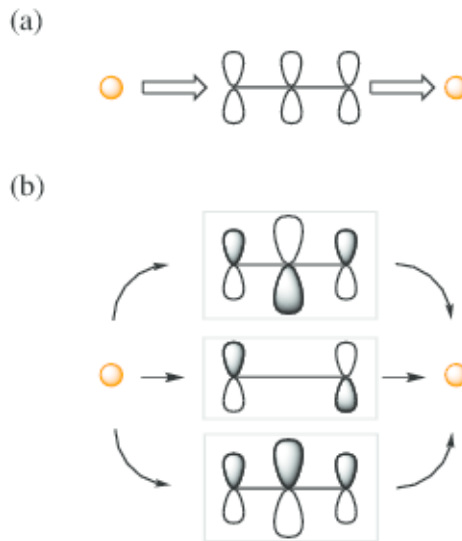


Figure 7.2: Alternative schematic representations of ballistic conduction in a source-sink model device: (a) in the AO basis, where conduction between source and sink takes place via bonds between atoms carrying single basis functions; (b) in the MO basis, where the molecular orbitals act as parallel conducting channels between source and sink.

All coefficients $c_L, c_R, \mathbf{c}^{\text{MO}}$ and \mathbf{c}^{AO} are in general complex, but the transformation matrix \mathbf{U} refers to the unperturbed molecule and can always be chosen to be real. It may sometimes be convenient to use complex \mathbf{U} for degenerate eigenvalues, but it is never necessary.

7.2 A mathematical toolkit

This section is a mathematical investigation of the structural polynomials and related quantities used for derivation and analysis of the solutions of the SSP equations.

7.2.1 Structural polynomials in the MO basis

The aim here is to re-express the structural polynomials that have been discussed in earlier chapters (Chapters 3 and 4) in terms of the eigenvectors and eigenvalues of the adjacency matrix defined in Eq.(7.26). Hence,

$$s(E) = \det(E\mathbf{1} - \mathbf{A}) = \prod_k (E - \epsilon_k) = \prod_k p_k \quad (7.34)$$

using the notation of Eq. (7.30), and the product runs over the whole molecular spectrum. We shall consider the general structural polynomials

$$\begin{aligned} j_{rs} &= (-1)^{r+s} \det(E\mathbf{1} - \mathbf{A})^{[r,s]} \\ v_{pqrs} &= (-1)^{p+q+r+s} \det(E\mathbf{1} - \mathbf{A})^{[pq,rs]} \end{aligned} \quad (7.35)$$

which subsumes all the definitions in Eq. (2.26), namely,

$$t = j_{\bar{L}\bar{L}}, \quad u = j_{\bar{R}\bar{R}}, \quad j = j_{\bar{L}\bar{R}}, \quad v = v_{\bar{L}\bar{R}\bar{L}\bar{R}} \quad (7.36)$$

It can be shown that [142]

$$sv_{pqrs} = \{j_{pr}j_{qs}\}_- \quad (7.37)$$

which has been defined using the notation for the anti-symmetrised product

$$\{X_{pr}X_{qs}\}_- = X_{pr}X_{qs} - X_{ps}X_{qr} \quad (7.38)$$

Eq. (7.37) is a more general form of the Jacobi–Sylvester relation given in Eq. (4.2).

The ‘hat’ symbol will indicate that a quantity is divided by the polynomial s , and will be referred to as a ‘reduced’ structural polynomial.

$$\hat{X} = \frac{X}{s} \quad (7.39)$$

These can be shown to be matrix elements of the inverse of the characteristic matrix by using the well-known Cramer’s rule [76] result

$$\hat{j}_{rs} = (-1)^{r+s} \frac{\det(E\mathbf{1} - \mathbf{A})^{[r,s]}}{\det(E\mathbf{1} - \mathbf{A})} = (E\mathbf{1} - \mathbf{A})_{rs}^{-1} \quad (7.40)$$

The spectral representation of the polynomial follows directly as

$$\hat{j}_{rs} = \sum_k \frac{U_{rk}U_{sk}}{E - \epsilon_k} \quad (7.41)$$

Defining the quantities

$$\begin{aligned} s_k &= \frac{s}{p_k} \\ s_{kk'} &= \frac{s}{p_k p_{k'}} \end{aligned} \quad (7.42)$$

we see that all the (real) characteristic polynomials of the device, Eq. (2.26), can

be expressed in terms of these factors as

$$\begin{aligned} j_{rs}(E) &= \sum_k U_{rk} U_{sk} s_k \\ v_{pqrs}(E) &= \sum_{k>k'} \{U_{pk} U_{qk'}\}_- \{U_{rk} U_{sk'}\}_- s_{kk'} \end{aligned} \quad (7.43)$$

where Eqs (7.37) and (7.40) have been used to deduce the formula for v .

7.2.2 Expansion of the reduced structural polynomials

It will prove useful to expand solutions of the SSP equations as a series around molecular eigenvalues. The degeneracy, g , of such eigenvalues needs to be taken into account. The degenerate space is referred to as a ‘shell’, and capital Roman indices are used to label such shells. The individual MOs in the shell space, K , will then be ψ_k for $k \in K$. (Strictly, g is g_K , but the K dependence will be suppressed when there is no ambiguity.) To understand more fully what happens when the electron energy is at a shell eigenvalue, ϵ_K , we need to explore the behaviour of the reduced structural polynomials near that eigenvalue. For the most general reduced structural polynomial shown in Eq. (7.35), we have

$$\begin{aligned} \hat{j}_{rs}(E) &= \sum_{k \in K} \frac{U_{rk} U_{sk}}{E - \epsilon_K} + \sum_{a \notin K} \frac{U_{ra} U_{sa}}{E - \epsilon_a} \\ &= \sum_k \frac{U_{rk} U_{sk}}{p_K} + \sum_a \frac{U_{ra} U_{sa}}{\epsilon_K - \epsilon_a + p_K} \end{aligned} \quad (7.44)$$

The summation indices k, k', \dots , label MOs inside the degenerate shell K , and indices a, b, \dots , label MOs that are ‘off-shell’, without explicitly indicating the summation ranges. Within the radius of convergence, each reduced structural polynomial can be expanded in a Laurent series around the point $E = \epsilon_K$. We use $p_K = E - \epsilon_K$ as the expansion parameter. It is easy to deduce that

$$\hat{j}_{rs}(E) = \frac{\hat{j}_{rs,-1}}{p_K} + \hat{j}_{rs,0} + \hat{j}_{rs,1} p_K + O(p_K^2) \quad (7.45)$$

where *all* dependence upon E is through powers of p_K , and the expansion coefficients are

$$\begin{aligned} \hat{j}_{rs,-1} &= \sum_k U_{rk} U_{sk} \\ \hat{j}_{rs,0} &= \sum_a \frac{U_{ra} U_{sa}}{(\epsilon_K - \epsilon_a)} \\ \hat{j}_{rs,1} &= - \sum_a \frac{U_{ra} U_{sa}}{(\epsilon_K - \epsilon_a)^2} \end{aligned} \quad (7.46)$$

A similar derivation, using Eq. (7.37) in the form $\hat{v}_{pqrs} = \{\hat{j}_{pr} \hat{j}_{qs}\}_-$, produces

$$\begin{aligned} \hat{v}_{pqrs}(E) &= p_K^{-2} \hat{v}_{pqrs,-2} + p_K^{-1} \hat{v}_{pqrs,-1} \\ &\quad + \hat{v}_{pqrs,0} + \hat{v}_{pqrs,1} p_K + O(p_K^2) \end{aligned} \quad (7.47)$$

where

$$\begin{aligned}
\hat{v}_{\text{pqrs},-2} &= \sum_{k>k'} \{U_{\text{pk}}U_{\text{qk}'}\}_- \{U_{\text{rk}}U_{\text{sk}'}\}_- \\
\hat{v}_{\text{pqrs},-1} &= \sum_{k,a} \frac{\{U_{\text{pk}}U_{\text{qa}}\}_- \{U_{\text{rk}}U_{\text{sa}}\}_-}{(\epsilon_K - \epsilon_a)} \\
\hat{v}_{\text{pqrs},0} &= \sum_{a>b} \frac{\{U_{\text{pa}}U_{\text{qb}}\}_- \{U_{\text{ra}}U_{\text{sb}}\}_-}{(\epsilon_K - \epsilon_a)(\epsilon_K - \epsilon_b)} - \sum_{k,a} \frac{\{U_{\text{pk}}U_{\text{qa}}\}_- \{U_{\text{rk}}U_{\text{sa}}\}_-}{(\epsilon_K - \epsilon_a)^2}
\end{aligned} \tag{7.48}$$

The terms $\hat{j}_{\text{rs},-1}$ (and hence \hat{t}_{-1} , \hat{u}_{-1} , and \hat{j}_{-1}) and $\hat{v}_{\text{pqrs},-2}$, $\hat{v}_{\text{pqrs},-1}$ (and hence \hat{v}_{-2} , \hat{v}_{-1}), are all traces over the degenerate shell. These are therefore *invariant* to unitary transformations amongst the MOs *within* the shell subspace.

In later parts of this chapter we will need definitions of restricted structural polynomials that depend only upon ‘off-shell’ orbitals, *i.e.*,

$$\begin{aligned}
s_A(E) &= \prod_a p_a \\
\hat{j}_{A,\text{rs}}(E) &= \sum_a \frac{U_{\text{ra}}U_{\text{sa}}}{E - \epsilon_a} \\
\hat{v}_{\text{pqrs},A}(E) &= \sum_{a>b} \frac{\{U_{\text{pa}}U_{\text{qb}}\}_- \{U_{\text{ra}}U_{\text{sb}}\}_-}{(E - \epsilon_a)(E - \epsilon_b)}
\end{aligned} \tag{7.49}$$

where ‘A’ denotes *all* eigenvectors associated with eigenvalues $\epsilon_a \neq \epsilon_K$. These definitions are exactly analogous to those in Section 7.2.1. It can be seen from Eqs (7.44, 7.45, 7.47, 7.48), that the whole energy-dependence of the structural polynomials can be expressed as

$$\begin{aligned}
p_K \hat{j}_{\text{rs}}(E) &= \hat{j}_{\text{rs},-1} + p_K \hat{j}_{A,\text{rs}}(E) \\
p_K^2 \hat{v}_{\text{pqrs}}(E) &= \hat{v}_{\text{pqrs},-2} + p_K \hat{v}_{\text{pqrs},-1} + p_K^2 \hat{v}_{A,\text{pqrs}}(E)
\end{aligned} \tag{7.50}$$

In earlier work [70, 84] (see Chapter 4) conduction and insulation properties have been linked to the interlacing properties of the eigenvalues of a graph. Since

$$s(E) = p_K^g s_A(E) \tag{7.51}$$

we deduce that the polynomials are written *exactly* in terms of the degeneracy as

$$\begin{aligned}
j_{\text{rs}}(E) &= p_K^{g-1} s_A(E) [\hat{j}_{\text{rs},-1} + p_K \hat{j}_{A,\text{rs}}(E)] \\
v_{\text{pqrs}}(E) &= p_K^{g-2} s_A(E) [\hat{v}_{\text{pqrs},-2} + p_K \hat{v}_{\text{pqrs},-1} + p_K^2 \hat{v}_{A,\text{pqrs}}(E)]
\end{aligned} \tag{7.52}$$

The Laurent expansion about the shell eigenvalue equivalent to these expressions is

$$\begin{aligned}
j_{\text{rs}}(E) &= p_K^{g-1} s_A(E) (\hat{j}_{\text{rs},-1} + \hat{j}_{\text{rs},0} p_K + \hat{j}_{\text{rs},1} p_K^2 + \dots) \\
v_{\text{pqrs}}(E) &= p_K^{g-2} s_A(E) (\hat{v}_{\text{pqrs},-2} + \hat{v}_{\text{pqrs},-1} p_K + \hat{v}_{\text{pqrs},0} p_K^2 + \hat{v}_{\text{pqrs},1} p_K^3 + \dots)
\end{aligned} \tag{7.53}$$

The structural polynomial $t = j_{\bar{L}\bar{L}}$, is the characteristic polynomial for the $(n-1)$ -vertex graph derived by removing vertex \bar{L} from the original molecular graph. We can read the degeneracy, g_t , for eigenvalue ϵ_K in the spectrum of this vertex-deleted

graph directly from the lowest non-vanishing coefficient of the expansion of t in Eq. (7.53). Hence, if $\hat{t}_{-1} \neq 0$, then $g_t = g - 1$, *etc.* Similar deductions can be made for the graphs corresponding to polynomials u and v .

This machinery can be applied (see Section 7.5.4) to the case of transmission at $E = \epsilon_K$, to give a simple link to previous results deduced using interlacing [70] and reported in Chapter 4.

7.2.3 The expansion of $D(E)$

We can also use the expansion of the structural polynomials in Eq. (7.50) together with an expansion of the denominator from Eq. (7.3) to give

$$\hat{D} = \frac{D}{s} = p_K^{-2} \hat{D}_{-2} + p_K^{-1} \hat{D}_{-1} + \hat{D}_0 + O(p_K) \quad (7.54)$$

where the expansion terms

$$\begin{aligned} \hat{D}_{-2} &= \beta_{LL}^2 \beta_{RR}^2 \hat{v}_{-2} \\ \hat{D}_{-1} &= \beta_{LL}^2 \beta_{RR}^2 \hat{v}_{-1} \\ &\quad - \beta_L e^{-iq_L} \beta_{RR}^2 \hat{u}_{-1} - \beta_R e^{-iq_R} \beta_{LL}^2 \hat{t}_{-1} \\ \hat{D}_0 &= \beta_L e^{-iq_L} \beta_R e^{-iq_R} + \beta_{LL}^2 \beta_{RR}^2 \hat{v}_0 \\ &\quad - \beta_L e^{-iq_L} \beta_{RR}^2 \hat{u}_0 - \beta_R e^{-iq_R} \beta_{LL}^2 \hat{t}_0 \end{aligned} \quad (7.55)$$

are deduced directly from Eq. (7.3). The values of the wire momenta, q_L and q_R in Eq. (7.55), are to be evaluated at the eigenvalue ϵ_K and should also be expanded in powers of p_K . The leading term in this expansion is $O(1)$, and is just the momentum evaluated at the eigenvalue. The higher terms in p_K do not contribute to any expressions we derive. Of course, the \hat{D}_0 term in Eq. (7.55) will contain a contribution arising from the expansion of the momenta in \hat{D}_{-1} . These extra terms are unimportant for our purposes, since they vanish in all the cases where \hat{D}_0 is the leading term in the expansion of \hat{D} .

We can also use Eqs (7.51) and (7.54) to write $D(E)$ in the form of Eq. (7.50) as

$$D(E) = p_K^{g-2} s_A(E) \left\{ \hat{D}_{-2} + p_K \hat{D}_{-1} + p_K^2 \hat{D}_A(E) \right\} \quad (7.56)$$

This expression can be used to deduce the values of E at which $D(E)$ vanishes. In particular, it is clear that $D(E)$ may have a root at $E = \epsilon_K$, with a multiplicity that depends on which (if any) of the terms \hat{D}_{-2} , or \hat{D}_{-1} is non-zero, and on the degeneracy g . The ‘off-shell’ quantity \hat{D}_A is defined as

$$\hat{D}_A = \beta_L \beta_R e^{-i(q_L+q_R)} - \beta_R \beta_{LL}^2 e^{-iq_R} \hat{t}_A(E) - \beta_L \beta_{RR}^2 e^{-iq_L} \hat{u}_A(E) + \beta_{LL}^2 \beta_{RR}^2 \hat{v}_A(E) \quad (7.57)$$

7.3 Solution of the SSP model in the AO basis

Eq. (7.21) has a unique solution provided the $(n+2)$ -dimensional SSP characteristic matrix, \mathbf{P}_{AO} , on the left-hand side of Eq. (7.21) has an inverse, *i.e.*, iff

$$\det \mathbf{P}_{\text{AO}} = \det \mathbf{P}_{\text{MO}} = D(E) \neq 0 \quad (7.58)$$

where $D(E)$ is given by Eq. (7.3). The matrix may be singular in cases where E matches an eigenvalue of the isolated molecule, depending on fulfilment of some conditions on the rank of a related matrix (see Section 7.5.3 and Eq. (7.56)). It is useful, however, first to assume that the inverse exists, and only later to examine separately the cases where it does not. The first line of the AO SSP matrix equation, Eq. (7.21), can then be rearranged to give

$$\mathbf{c}^{\text{AO}} = (E\mathbf{1} - \mathbf{A})^{-1} (\mathbf{b}_L c_L + \mathbf{b}_R c_R) \quad (7.59)$$

provided E is not an eigenvalue of \mathbf{A} . In components, this is the two-term formula

$$\begin{aligned} c_p^{\text{AO}} &= (E\mathbf{1} - \mathbf{A})_{p\bar{L}}^{-1} \beta_{\bar{L}L} c_L + (E\mathbf{1} - \mathbf{A})_{p\bar{R}}^{-1} \beta_{\bar{R}R} c_R \\ &= \hat{j}_{p\bar{L}} \beta_{\bar{L}L} c_L + \hat{j}_{p\bar{R}} \beta_{\bar{R}R} c_R \end{aligned} \quad (7.60)$$

The source-and-sink equations from Eqs (7.21) and (7.22) are

$$\begin{aligned} -\tilde{\mathbf{b}}_L \mathbf{c}^{\text{AO}} + \beta_L e^{-iq_L} c_L &= -iN_L \\ -\tilde{\mathbf{b}}_R \mathbf{c}^{\text{AO}} + \beta_R e^{-iq_R} c_R &= 0 \end{aligned} \quad (7.61)$$

The secular equations, Eq. (7.61), can be simplified by substituting for \mathbf{c}^{AO} from Eq. (7.59), and noting that the products $\tilde{\mathbf{b}}(E\mathbf{1} - \mathbf{A})^{-1}$ reduce to single entries in the inverse, which can in turn be expressed as ratios of determinants by Cramer's Rule, giving

$$\begin{aligned} \hat{F}_L c_L - \beta_{\bar{L}L} \beta_{\bar{R}R} \hat{j} c_R &= -iN_L \\ -\beta_{\bar{L}L} \beta_{\bar{R}R} \hat{j} c_L + \hat{F}_R c_R &= 0 \end{aligned} \quad (7.62)$$

as a 2×2 matrix equation for c_L and c_R . The new quantities used in Eq. (7.62) are \hat{F}_L and \hat{F}_R ,

$$\begin{aligned} \hat{F}_L &= \beta_L e^{-iq_L} - \beta_{\bar{L}L}^2 \hat{t} \\ \hat{F}_R &= \beta_R e^{-iq_R} - \beta_{\bar{R}R}^2 \hat{u} \end{aligned} \quad (7.63)$$

given in terms of the *reduced* structural polynomials defined previously. The solution to Eq. (7.62) gives the source and sink coefficients in the wavefunction as

$$\begin{aligned} c_L &= -iN_L \frac{\hat{F}_R}{\hat{D}} = -iN_L \frac{F_R}{D} \\ c_R &= -iN_L \beta_{\bar{L}L} \beta_{\bar{R}R} \frac{\hat{j}}{\hat{D}} = -iN_L \beta_{\bar{L}L} \beta_{\bar{R}R} \frac{J}{D} \end{aligned} \quad (7.64)$$

where $D = D(E) = s\hat{D}(E)$ is given by Eq. (7.3).

7.3.1 Transmission

We are now in a position to derive the expression Eq. (7.1) for the total transmission, using Eqs (7.17) and (7.64), as

$$T = |\tau|^2 = (\beta_{\bar{L}L}\beta_{\bar{R}R}N_LN_R)^2 \frac{j^2}{|D|^2} = \mathcal{B}(q_L, q_R) \frac{j^2}{|D|^2} \quad (7.65)$$

which is, of course, identical to that derived previously [63].

The current from the source to the left contact in the molecule is

$$\begin{aligned} J_{L \rightarrow \bar{L}}^{\text{AO}} &= \frac{1}{i} \left(\langle \phi_L | \hat{H} | \phi_{\bar{L}} \rangle c_L^* c_{\bar{L}}^{\text{AO}} - c.c. \right) \\ &= -i\beta_{\bar{L}L} (c_L^* c_{\bar{L}}^{\text{AO}} - c.c.) \end{aligned} \quad (7.66)$$

and since from Eq. (7.60)

$$c_{\bar{L}}^{\text{AO}} = \beta_{\bar{L}L} \hat{t} c_L + \beta_{\bar{R}R} \hat{j} c_R \quad (7.67)$$

it follows that

$$\begin{aligned} (c_L^* c_{\bar{L}}^{\text{AO}} - c.c.) &= (\beta_{\bar{L}L} \hat{t} |c_L|^2 + \beta_{\bar{R}R} \hat{j} c_L^* c_R - c.c.) \\ &= \hat{j} \beta_{\bar{R}R} (c_L^* c_R - c_L c_R^*) \end{aligned} \quad (7.68)$$

Substitution of Eq. (7.68) into Eq. (7.66) gives

$$\begin{aligned} J_{L \rightarrow \bar{L}}^{\text{AO}} &= -i\beta_{\bar{L}L}^2 \beta_{\bar{R}R}^2 \frac{N_L^2}{|D|^2} \frac{j^2}{s} (F_R^* - F_R) \\ &= -i\beta_R \beta_{\bar{L}L}^2 \beta_{\bar{R}R}^2 N_L^2 \frac{j^2}{|D|^2} (e^{iq_R} - e^{-iq_R}) \\ &= \mathcal{B}(q_L, q_R) \frac{j^2}{|D|^2} \end{aligned} \quad (7.69)$$

which is the same expression as that given for the gross transmission $T(E)$ in Eqs (7.1) and previously [63], as it must be, since there is a single edge connection between \bar{L} and L through which all current must pass. It is easy to derive the analogous expression for the current in the right-hand link, and to show that likewise

$$J_{\bar{R} \rightarrow R}^{\text{AO}}(E) = J_{L \rightarrow \bar{L}}^{\text{AO}}(E) = T(E) \quad (7.70)$$

In the next section we shall partition these expressions for total current.

7.3.2 Bond currents

Currents between atoms within the molecule will be referred to as *bond* or *edge* currents. They are

$$\begin{aligned} J_{p \rightarrow q}^{\text{AO}} &= \frac{1}{i} \left(\langle \phi_p | \hat{H} | \phi_q \rangle c_p^{\text{AO}*} c_q^{\text{AO}} - c.c. \right) \\ &= -i\beta_{pq} (c_p^{\text{AO}*} c_q^{\text{AO}} - c.c.) \end{aligned} \quad (7.71)$$

Using Eqs (7.60) and (7.64), we can deduce that

$$\begin{aligned} J_{p \rightarrow q}^{\text{AO}} &= \mathcal{B}(q_L, q_R) \beta_{pq} \frac{J}{|D|^2} \frac{\{J_{p\bar{L}} J_{q\bar{R}}\}}{s} \\ &= \mathcal{B}(q_L, q_R) \beta_{pq} \frac{J}{|D|^2} v_{pq\bar{L}\bar{R}} \end{aligned} \quad (7.72)$$

where the final equality uses the definition Eq. (7.37).

The bond current, $J_{p \rightarrow q}^{\text{AO}}$, vanishes when $c_L = c_R = 0$. This is implied by Eq. (7.60) and Eq. (7.71). This fact will be used in the discussion of behaviour of transmission quantities at molecular eigenvalues.

The bond currents satisfy a sum rule. Hence, using the first line of Eq. (7.71) and the p^{th} secular equation from Eq. (7.21)

$$\begin{aligned} \sum_q J_{p \rightarrow q}^{\text{AO}}(E) &= \delta_{p\bar{L}} \frac{\beta_{\bar{L}\bar{L}}}{i} (c_p^{\text{AO}} c_L^* - c_p^{\text{AO}*} c_L) \\ &\quad + \delta_{p\bar{R}} \frac{\beta_{\bar{R}\bar{R}}}{i} (c_p^{\text{AO}} c_R^* - c_p^{\text{AO}*} c_R) \end{aligned} \quad (7.73)$$

and substitution of Eq. (7.60) in Eq. (7.73) gives

$$\begin{aligned} \sum_q J_{p \rightarrow q}^{\text{AO}}(E) &= \frac{\beta_{\bar{L}\bar{L}} \beta_{\bar{R}\bar{R}}}{i} (c_L^* c_R - c_R^* c_L) \\ &\quad \times (\delta_{p\bar{L}} \hat{J}_{p\bar{R}} - \delta_{p\bar{R}} \hat{J}_{p\bar{L}}) \end{aligned} \quad (7.74)$$

After substitution of Eq. (7.64) we obtain the final result

$$\sum_q J_{p \rightarrow q}^{\text{AO}}(E) = T(E) (\delta_{p\bar{L}} - \delta_{p\bar{R}}) \quad (7.75)$$

Eq. (7.75) says that the sum of currents out of *any* vertex is zero. The term $\delta_{p\bar{L}}$ on the right-hand side of Eq. (7.75) arises because the vertex \bar{L} has a current *in* from the source L to balance its outward currents. A similar remark can be made for the vertex \bar{R} .

7.3.3 A physical corollary for *ipso* devices

An important result follows from Eq. (7.72). It is clear from the structure of the equation that

$$J_{p \rightarrow q}^{\text{AO}} = 0 \text{ when } \bar{L} = \bar{R} \quad (7.76)$$

because the term in v_{pqrs} vanishes when $r = s$ (see Eqs (7.37) and (7.38)), *i.e.*, in the case of an *ipso* connection there are no internal molecular currents. Conduction can only take place for *ipso* devices, if at all, through the directly connected links $L\bar{L}$ and $\bar{L}R$.

The physical interpretation of this mathematical fact is also clear. In an *ipso* device the net flow into the rest of the molecule from the single contact atom $\bar{L} = \bar{R}$ is $J_{L \rightarrow \bar{L}}^{\text{AO}}(E) = J_{\bar{L} \rightarrow R}^{\text{AO}}(E) = T(E)$, so any putative flow of current within the molecule

would consist of a set of self-cancelling closed circulations of arbitrary direction. It makes physical sense that these should have zero amplitude.

7.4 General solutions of the SSP equations in the MO basis

For solution of the SSP equations in the MO basis, we first study the equations for energies away from molecular eigenvalues.

7.4.1 Solutions away from eigenvalues

The solution of the SSP equations, assuming that E is not an eigenvalue, proceeds in the same way as for the AO case. For the SSP coefficients, c_k^{MO} , we find, from Eq. (7.28) with $E \neq \epsilon_K$ and hence $p_K \neq 0$,

$$c_k^{\text{MO}} = p_K^{-1} (c_L \beta_{\bar{L}L} U_{\bar{L}k} + c_R \beta_{\bar{R}R} U_{\bar{R}k}) \quad (7.77)$$

The equations for c_L and c_R are identical in MO and AO representations. However, the interpretations of the solutions in the two cases are different.

A new possibility arises from Eq. (7.77), of obtaining an expression for the current from ϕ_L into a given MO ψ_k , *via*

$$J_{L \rightarrow k}^{\text{MO}} = \frac{1}{i} \left[\langle \phi_L | \hat{H} | \psi_k \rangle c_L^* c_k^{\text{MO}} - \text{c.c.} \right] \quad (7.78)$$

and, since

$$\langle \phi_L | \hat{H} | \psi_k \rangle = \beta_{\bar{L}L} U_{\bar{L}k} \quad (7.79)$$

it follows that

$$\begin{aligned} J_{L \rightarrow k}^{\text{MO}} &= -i \beta_{\bar{L}L} \beta_{\bar{R}R} \frac{U_{\bar{L}k} U_{\bar{R}k}}{p_k} (c_L^* c_R - c_L c_R^*) \\ &= \mathcal{B}(q_L, q_R) U_{\bar{L}k} U_{\bar{R}k} s_k \frac{J}{|D|^2} \end{aligned} \quad (7.80)$$

Using Eq. (7.43) we can see that there is a simple sum rule

$$\sum_k J_{L \rightarrow k}^{\text{MO}}(E) = T(E) \quad (7.81)$$

as we would expect, and of course the sum over *all* orbitals ψ_k of contributions $J_{L \rightarrow k}^{\text{MO}}$ recovers the total current. The n molecular orbitals in the molecule provide n channels over which the total current is distributed (*c.f.* Fig. 7.2).

If the spectrum of the molecular graph has degeneracies, the choice of orthonormal MOs within each eigenspace (shell) is arbitrary, and it is sensible to sum currents

over degenerate sets to give

$$J_{L \rightarrow K}^{\text{MO}} = \mathcal{B}(q_L, q_R) \hat{j}_{-1} \frac{\hat{j}}{|\hat{D}|^2} \quad (7.82)$$

where we have divided numerator and denominator by s^2 , and used the shell invariant $\hat{j}_{-1} = \hat{j}_{\bar{L}\bar{R}, -1}$ defined in Eq. (7.46). The shell current is a fraction of the total current, given formally by

$$J_{L \rightarrow K}^{\text{MO}} = \frac{\hat{j}_{-1}}{\hat{j}} T \quad (7.83)$$

This ‘fraction’ may be positive or negative, and indeed may be greater than 1.

A similar derivation for the current from ψ_k to the sink atom, R can be derived. This gives a simple conservation law,

$$J_{k \rightarrow R}^{\text{MO}}(E) = J_{L \rightarrow k}^{\text{MO}}(E). \quad (7.84)$$

as there can be no current *between* MOs, since

$$\langle \phi_k | \hat{H} | \psi_{k'} \rangle = 0$$

when $k \neq k'$.

7.4.2 Active and inert orbitals and shells

A final feature revealed by Eq. (7.80) is that some MOs may be insulating at *all* electron energies, *i.e.*, they can be *inert*. This property occurs when either or both of $U_{\bar{L}k}$ or $U_{\bar{R}k}$ are zero for the particular choice of the MO and the device connections. Hence, it is a joint property of the molecule (construction of the eigenspaces) and the device (placement of the connections relative to possible nodes in the eigenvectors). Orbitals that are not inert are *active*.

Inert orbitals or shells are merely bystanders in the conduction of the molecular device. Rules for prediction of the occurrence of inert shells can be deduced from case-by-case analysis (refer to Sections 7.5.4 and 7.5.5).

7.5 Solutions of the SSP equations in the MO basis at molecular eigenvalues

In this section we study the nature of solutions of the SSP equations at a particular eigenvalue ϵ_K which we assume to have degeneracy, $g = g_K \geq 1$.

7.5.1 Shell partitioning of the SSP equations

We can partition the SSP equations into three parts: ‘on-shell’ (g equations with block label K), ‘off-shell’ ($n - g$ equations with block label A), and ‘source-sink’

(two equations). The SSP matrix in Eq. (7.29) is then given more explicitly by

$$\mathbf{P}_{\text{MO}} = \begin{pmatrix} p_K \mathbf{1} & 0 & -\mathbf{u}_{\text{KL}} & -\mathbf{u}_{\text{KR}} \\ 0 & \mathbf{p}_A & -\mathbf{u}_{\text{AL}} & -\mathbf{u}_{\text{AR}} \\ -\tilde{\mathbf{u}}_{\text{KL}} & -\tilde{\mathbf{u}}_{\text{AL}} & \beta_L e^{-iq_L} & 0 \\ -\tilde{\mathbf{u}}_{\text{KR}} & -\tilde{\mathbf{u}}_{\text{AR}} & 0 & \beta_R e^{-iq_R} \end{pmatrix} \quad (7.85)$$

so that the SSP equations become

$$\mathbf{P}_{\text{MO}} \begin{pmatrix} \mathbf{c}_K^{\text{MO}} \\ \mathbf{c}_A^{\text{MO}} \\ c_L \\ c_R \end{pmatrix} = \begin{pmatrix} \mathbf{0} \\ \mathbf{0} \\ -iN_L \\ 0 \end{pmatrix} \quad (7.86)$$

As $E \rightarrow \epsilon_K$, then $(\mathbf{p}_A)_{ab} \rightarrow \delta_{ab}(\epsilon_K - \epsilon_a) \neq 0$. Since $p_a \neq 0$, we have

$$c_a^{\text{MO}} = p_a^{-1} (c_L \beta_{\bar{L}L} U_{\bar{L}a} + c_R \beta_{\bar{R}R} U_{\bar{R}a}) \quad (7.87)$$

for the off-shell block. This step cannot in itself be used to solve the equations for the shell orbitals because p_K vanishes at the shell eigenvalue.

However, the SSP equations derived from the matrix in Eq. (7.85) can now be used in exactly the same way as in the previous derivation (*cf.* Eqs (7.59–7.62)), by substituting Eq. (7.87) into L and R equations in Eq. (7.85) to produce a set of $(g+2)$ SSP equations with the ‘off-shell’ components folded into the L, R block, and the degenerate shell handled explicitly. The result is

$$\mathbf{P}'_{\text{MO}} = \begin{pmatrix} p_K \mathbf{1} & -\mathbf{u}_{\text{KL}} & -\mathbf{u}_{\text{KR}} \\ -\tilde{\mathbf{u}}_{\text{KL}} & \hat{F}_{\text{AL}} & -\beta_{\bar{L}L} \beta_{\bar{R}R} \hat{J}_A \\ -\tilde{\mathbf{u}}_{\text{KR}} & -\beta_{\bar{L}L} \beta_{\bar{R}R} \hat{J}_A & \hat{F}_{\text{AR}} \end{pmatrix} \quad (7.88)$$

for the device matrix and

$$\mathbf{P}'_{\text{MO}} \begin{pmatrix} \mathbf{c}_K^{\text{MO}} \\ c_L \\ c_R \end{pmatrix} = \begin{pmatrix} \mathbf{0} \\ -iN_L \\ 0 \end{pmatrix} \quad (7.89)$$

for the SSP equation. The 2×2 source-sink terms are defined by analogy with Eq. (7.63), *viz.*,

$$\begin{aligned} \hat{F}_{\text{AL}}(E) &= \beta_L e^{-iq_L} - \beta_{\bar{L}L}^2 \hat{t}_A \\ \hat{F}_{\text{AR}}(E) &= \beta_R e^{-iq_R} - \beta_{\bar{R}R}^2 \hat{u}_A \end{aligned} \quad (7.90)$$

The ‘off-shell’ polynomials appearing in Eq. (7.90) were defined in Eqs (7.49).

7.5.2 The shell connection matrix, rank and the echelon representation

A key to understanding Eqs (7.90) is the $(g \times 2)$ -dimensional *shell connection matrix* between the source-sink and degenerate shell, K, blocks

$$\mathbf{B}_K^{\text{con}} = (\mathbf{u}_{KL} \quad \mathbf{u}_{KR}) = \begin{pmatrix} \beta_{\bar{L}\bar{L}}U_{\bar{L}1} & \beta_{\bar{R}\bar{R}}U_{\bar{R}1} \\ \beta_{\bar{L}\bar{L}}U_{\bar{L}2} & \beta_{\bar{R}\bar{R}}U_{\bar{R}2} \\ \vdots & \vdots \\ \beta_{\bar{L}\bar{L}}U_{\bar{L}g} & \beta_{\bar{R}\bar{R}}U_{\bar{R}g} \end{pmatrix} \quad (7.91)$$

As the first diagonal block of Eq. (7.88) is proportional to the unit matrix, we are free to make any suitable orthogonal transformation amongst the orbitals within the shell, K. In particular, we can use a sequence of 2×2 rotations to bring the matrix $\mathbf{B}_K^{\text{con}}$ to *row echelon* form

$$\mathbf{B}_K^{\text{con}} = \begin{pmatrix} a & b \\ 0 & d \\ 0 & 0 \\ \vdots & \vdots \end{pmatrix} \quad (7.92)$$

where $a = \beta_{\bar{L}\bar{L}}U'_{\bar{L}1}$, $b = \beta_{\bar{R}\bar{R}}U'_{\bar{R}1}$, and $d = \beta_{\bar{L}\bar{L}}U'_{\bar{R}2}$, are expressed in terms of the only non-zero \bar{L} and \bar{R} components of the orbitals after the operation of the sequence of orthogonal transformations leading to this *echelon* representation of the degenerate shell. The echelon representation is different, in principle, for each possible device, *i.e.*, for each possible choice of \bar{L}, \bar{R} .

We can use the fact that the coefficients $\hat{t}_{-1}, \hat{u}_{-1}, \hat{j}_{-1}$, and \hat{v}_{-2} defined in Eqs (7.46) and (7.48) are *invariant* to orthogonal transformations amongst the shell orbitals to obtain simple expressions for the coefficients a, b , and d . These are

$$\begin{aligned} a^2 &= \beta_{\bar{L}\bar{L}}^2 \hat{t}_{-1} \\ b^2 + d^2 &= \beta_{\bar{R}\bar{R}}^2 \hat{u}_{-1} \\ ab &= \beta_{\bar{L}\bar{L}} \beta_{\bar{R}\bar{R}} \hat{j}_{-1} \\ a^2 d^2 &= \beta_{\bar{L}\bar{L}}^2 \beta_{\bar{R}\bar{R}}^2 \hat{v}_{-2} \end{aligned} \quad (7.93)$$

Treatment of these equations depends on the rank of the shell connection matrix. The rank of a square matrix is the difference between the order of the matrix and its nullity. The necessary and sufficient conditions for the connection matrix to be of rank 0 are that $a = b = d = 0$, which imply that $\hat{t}_{-1} = \hat{u}_{-1} = \hat{v}_{-2} = 0$, and hence that

$$U_{\bar{L}k} = U_{\bar{R}k} = 0, \text{ for } k = 1, \dots, g \quad (7.94)$$

in which case the quantities $\hat{j}_{-1}, \hat{v}_{-1}$ also vanish.

Necessary and sufficient conditions for the shell connection matrix to have rank 1 are now obvious, *i.e.*, that *either* $d = 0$, *or* $a = 0$. In each case it follows that

$$\hat{v}_{-2} = 0 \iff \{U_{\bar{L}k}U_{\bar{R}k'}\} = 0 \forall k, k' \in K \quad (7.95)$$

In all other cases, the rank is 2. The rank, r_K , of the transformed $\mathbf{B}_K^{\text{con}}$ matrix must

be $r_K \leq \min(g, 2)$, and hence

$$p_K c_k = 0 \text{ for } k = r_K + 1, \dots, g \quad (7.96)$$

We now turn to the dependence of the solutions to the SSP equations, i.e. the set of coefficients of molecular orbitals c_k , on the energy in the region of an eigenvalue, i.e. where p_K is small. We concentrate on the case where the orbitals within shell K have been put in Echelon form, as above.

These $g - r_K$ equations have solution $c_k^{\text{MO}} = 0$ when $E \neq \epsilon_K$. When the energy is equal to the eigenvalue, ϵ_K , we have a case where the SSP matrix in Eq. (7.85) has no inverse, and the solution in the $(g - r_K)$ -dimensional manifold is undetermined. We can use *continuity*, however, to argue that it makes no physical sense for an insulating orbital suddenly to become conducting at its own eigenvalue. We can, therefore, take $c_k^{\text{MO}} = 0$ for all values of E . Hence, as shown in Subsection 7.5.4, we need to consider only solutions of the SSP equations in the $(r_K + 2)$ -dimensional manifold determined by the first r molecular orbitals and the source and sink atoms.

7.5.3 Shell and bond currents in the echelon representation

An advantage of the Echelon representation is that it makes it easy to show that the whole of the shell current $J_{L \rightarrow K}^{\text{MO}}$, from the source L to shell K, if any, passes through the first orbital of the shell. This follows from the association of parameters a , b and d with the scaled coefficients $\beta_{\bar{L}\bar{L}} U'_{\bar{L}1}$, $\beta_{\bar{R}\bar{R}} U'_{\bar{R}1}$ and $\beta_{\bar{R}\bar{R}} U'_{\bar{R}2}$. By the definition of an inert orbital orbitals $2, \dots, k$ are already inert and orbital 1 is active if and only if the product ab is non-zero.

From Eq. (7.80), we have

$$\begin{aligned} J_{L \rightarrow 1}^{\text{MO}}(E) &= \mathcal{B}(q_L, q_R) U'_{\bar{L}1} U'_{\bar{R}1} \frac{\hat{J}}{|\hat{D}|^2} \\ &= \mathcal{B}(q_L, q_R) \hat{J}_{-1} \frac{\hat{J}}{|\hat{D}|^2} = J_{L \rightarrow K}(E) \end{aligned} \quad (7.97)$$

We can also examine the behaviour of currents along bonds (graph edges) by looking at the quantity $J_{p \rightarrow q}^{\text{AO}}(\epsilon_K)$ (*cf.* Eq. (7.72)) in the ‘hatted’ form

$$J_{p \rightarrow q}^{\text{AO}} = \mathcal{B}(q_L, q_R) \beta_{pq} \frac{\hat{J}}{|\hat{D}|^2} \hat{v}_{pq\bar{L}\bar{R}} \quad (7.98)$$

To explore the behaviour of the bond currents at the shell eigenvalue we have to expand the antisymmetric quantity in Eq. (7.98) using Eq. (7.50). The expansion of \hat{v} contains the coefficients $\hat{v}_{pqrs,-2}$, $\hat{v}_{pqrs,-1}$ and $\hat{v}_{pqrs,0}$ defined in Eq. (7.48). Note that the quantity $\hat{v}_{pq\bar{L}\bar{R},-2}$ contains factors $\{U_{\bar{L}k} U_{\bar{R}k'}\}$. The leading term in the expansion of $J_{p \rightarrow q}^{\text{AO}}$, therefore, is determined by the rank of the connection matrix, $\mathbf{B}_K^{\text{con}}$. Ranks 2, 1, and 0 give, in principle, leading terms $\hat{v}_{pq\bar{L}\bar{R},-2}$, $\hat{v}_{pq\bar{L}\bar{R},-1}$, and $\hat{v}_{pq\bar{L}\bar{R},0}$, respectively.

7.5.4 The eleven canonical molecular conduction cases for a shell with eigenvalue ϵ_K

r_K	Case	g_t	g_u	g_v	g_j	$T(\epsilon_K)$	$J_{p \rightarrow q}^{\text{AO}}(\epsilon_K)$	$J_{L \rightarrow K}^{\text{MO}}(E)$
0	1	$g+1$	$g+1$	$g+2$	$\geq g+1$	0	0	0
	2	$g+1$	$g+1$	g	g	T_a	T_b	0
	3	$g+1$	g	$g+1$	$\geq g+1$	0	0	0
	4	$g+1$	g	g	g	T_a	T_b	0
	6	g	g	$g+1$	g	T_a	T_b	0
	7.1	g	g	g	g	T_a	T_b	0
	7.2	g	g	g	$\geq g+1$	0	0	0
1	5	$g+1$	$g-1$	g	$\geq g$	0	0	0
	8	g	$g-1$	$g-1$	$\geq g$	0	0	0
	9	$g-1$	$g-1$	g	$g-1$	T_c	T_d	$\neq 0$
	10	$g-1$	$g-1$	$g-1$	$g-1$	T_c	T_d	$\neq 0$
2	11.1	$g-1$	$g-1$	$g-2$	$g-1$	0	0	$\neq 0$
	11.2	$g-1$	$g-1$	$g-2$	$\geq g$	0	0	0

Table 7.1: Patterns of conduction for *non-ipso* molecular devices, showing the total transmission, $T(\epsilon_K)$, the bond currents $J_{p \rightarrow q}^{\text{AO}}(\epsilon_K)$ calculated at the shell eigenvalue ϵ_K , and the shell current $J_{L \rightarrow K}^{\text{MO}}(E)$ at *any* energy. The non-zero quantities $T_a = \mathcal{B}(q_L, q_R) \hat{j}_0^2 / |\hat{D}_0|^2$, $T_b = \mathcal{B}(q_L, q_R) \beta_{pq} \hat{j}_0 \hat{v}_{pq \bar{L} \bar{R}, 0} / |\hat{D}_0|^2$, $T_c = \mathcal{B}(q_L, q_R) \hat{j}_{-1}^2 / |\hat{D}_{-1}|^2$, and $T_d = \mathcal{B}(q_L, q_R) \beta_{pq} \hat{j}_{-1} \hat{v}_{pq \bar{L} \bar{R}, -1} / |\hat{D}_{-1}|^2$, are evaluated using Eq. (7.55), subject to conditions implied by g_t , g_u , and g_v in the particular case.

Here we make a connection with the previous work [70, 84] which uses graph theoretical concepts, where the Interlacing Theorem was used to show the transmission at the Fermi level in molecular devices. However, the Interlacing Theorem alone does not give access to full information about g_j but the table included here does so, enabling some new sub-cases to be distinguished. The cases (11 in all) were previously stated in terms of the Fermi energy, but the analysis can be extended to the whole eigenvalue spectrum of G [93].

By re-examining these eleven canonical cases in detail in Section 7.10 Appendix according to the rank of the connection matrix, $\mathbf{B}_K^{\text{con}}$, it can be shown that the eight possibilities for the construction of $\mathbf{B}_K^{\text{con}}$ in the echelon representation map onto the eleven cases for distinct-device conduction determined by interlacing. The results of this process are given in Table 7.1, showing *total* transmission, T , and bond currents $J_{p \rightarrow q}^{\text{AO}}$, both evaluated at the shell eigenvalue, ϵ_K , and the shell current, $J_{L \rightarrow K}^{\text{MO}}$, for *any* energy. The property of inertness or activity of the shell can be read off from the final column of the table. An entry ' $\neq 0$ ' means that the shell is active, and '0' means that it is inert. Overall conduction or insulation of the device is given by the

entry in column 7 of the table.

The rank-0 cases in Table 7.1 possess the important property that for all these cases the shell is insulating at *all* energies, *i.e.*, is inert. As far as conduction is concerned, it is as if the shell were not present. Any conduction at the eigenvalue predicted in that rank-0 case must, therefore, be carried through ‘off-shell’ orbitals. This is very different from the normal behaviour, where an ‘active’ shell carries all the transmission at its own shell eigenvalue.

The property of inertness is not particularly unusual nor is it restricted to degenerate shells. Indeed, Table 7.1 shows that all cases but three (9, 10, and 11.1) of the possible eigenvalue combinations imply an inert shell.

Two further remarks can be made about the applicability of this extended table, compared to that of Tables I in [70] and [84] and Table 4.6 which were limited to describing behaviour at the Fermi level for devices based on general and bipartite graphs, respectively. The first is about the interpretation of the present table for the case when all quantities are evaluated at a value, E , that is not an eigenvalue of G , *i.e.*, when $g = 0$. The formally allowed cases in Table 7.1 are then those with $\min\{g_t - g, g_u - g, g_v - g\} \geq 0$, *i.e.*, the cases of rank $r_K = 0$. In such cases the generic statements about overall transmission (column 7) and bond currents (column 8) hold, provided all the quantities are evaluated by taking the structural polynomials at E . The shell current, $J_{L \rightarrow K}^{\text{MO}}(E)$ (column 9), has no meaning in this case.

The second remark is about the use of the extended table for devices based on bipartite graphs. When the table referred only to $\epsilon_K = 0$, it was possible to use the special property that the nullity and order of a bipartite graph have the same parity to reduce the number of cases from 11 to 5 (or from 13 to 6 in the finer classification used in the present chapter). When ϵ_K is a general eigenvalue, the link between nullity and order is broken; deletion of a vertex of a bipartite graph may leave the degeneracy of a given eigenvalue unchanged or increased or decreased by one, and hence, any of the cases in Table 7.1 may apply.

7.5.5 Conduction in *ipso* devices

r_K	Case	g_t	$T(\epsilon_K)$	$J_{p \rightarrow q}^{\text{AO}}(\epsilon_K)$	$J_{L \rightarrow K}^{\text{MO}}(E)$
0	I1	$g+1$	0	0	0
	I2	g	T_a	0	0
1	I3	$g-1$	T_b	0	$\neq 0$

Table 7.2: Patterns of conduction for *ipso* molecular devices, showing the total transmission $T(\epsilon_K)$, the bond currents $J_{p \rightarrow q}^{\text{AO}}(\epsilon_K)$ calculated at the shell eigenvalue ϵ_K , and the shell current $J_{L \rightarrow K}^{\text{MO}}(E)$ at *any* energy. The non-zero quantities $T_a = \mathcal{B}(q_L, q_R) \hat{t}_0^2 / |\hat{D}_0|^2$ and $T_b = \mathcal{B}(q_L, q_R) \hat{t}_{-1}^2 / |\hat{D}_{-1}|^2$ are evaluated using Eq. (7.99) for the particular case.

Devices where the external links are connected to the *same* internal atom are termed *ipso* devices, where $t = u = j$, and $v \equiv 0$, and the connection matrix can have rank 0

or 1 only. The parameters $\beta_L, \beta_{\bar{L}L}$, and $\beta_R, \beta_{\bar{R}R}$ have the same values as for *non-ipso* devices. The expansion of \hat{D} becomes

$$\begin{aligned}\hat{D}_{-2} &= 0 \\ \hat{D}_{-1} &= -(\beta_L e^{-iq_L} \beta_{\bar{R}R}^2 + \beta_R e^{-iq_R} \beta_{\bar{L}L}^2) \hat{t}_{-1} \\ \hat{D}_0 &= \beta_L e^{-iq_L} \beta_R e^{-iq_R} - (\beta_L e^{-iq_L} \beta_{\bar{R}R}^2 + \beta_R e^{-iq_R} \beta_{\bar{L}L}^2) \hat{t}_0\end{aligned}\quad (7.99)$$

\hat{D}_{-2} vanishes because $v \equiv 0$.

There are only three possible cases (*cf.* Table 7.2) depending on the allowed g_t values for the graph with vertex \bar{L} removed. There is no restriction on the value of g . The cases exhibit all possible combinations of device conduction/insulation and shell character.

1. Case I1 ($g_t = g+1$)

This case has a rank-0 connection matrix because $\hat{t}_{-1} = \hat{t}_0 = 0$. The numerator in c_R is $O(p_K)$, whereas \hat{D}_0 is the leading term in the denominator. Hence $c_R = 0$ at the eigenvalue; there is device insulation and the shell is inert.

2. Case I2 ($g_t = g$)

This case also has rank 0 because $\hat{t}_{-1} = 0$. As $\hat{t}_0 \neq 0$, and \hat{D}_0 is the leading term in the denominator, there is device conduction at the eigenvalue. However, the shell is inert, so conduction at this eigenvalue is carried entirely by orbitals from other shells.

3. Case I3 ($g_t = g-1$)

This case has a rank-1 connection matrix, and is the equivalent of the *non-ipso* case 11. We have $\hat{t}_{-1} \neq 0$, and so $\hat{D}_{-1} \neq 0$. The numerator and denominator have the same order in p_K , and device conduction occurs at the eigenvalue. The shell is active and carries all the current at the shell eigenvalue.

7.5.6 A difference between conduction of *ipso*- and *non- ipso* devices

The remaining feature of *ipso* devices is that the expressions for currents and total transmission depend upon the behaviour of a single structural polynomial. For this reason, the transmission $T(E)$ has zeroes every time that $\hat{t}(E)$ vanishes. From the definition, Eq. (7.40), it is easy to see that $\hat{t}(E)$ is a piecewise continuous curve with asymptotes at the molecular eigenvalues, and the gradient is always negative. It follows that there will be a zero of $\hat{t}(E)$ between each molecular eigenvalue (*cf.* Fig. 7.3). Consequently, *ipso* transmission curves typically look very different from the curves for *non-ipso* devices based on the same molecule, *cf.* Section 7.7.

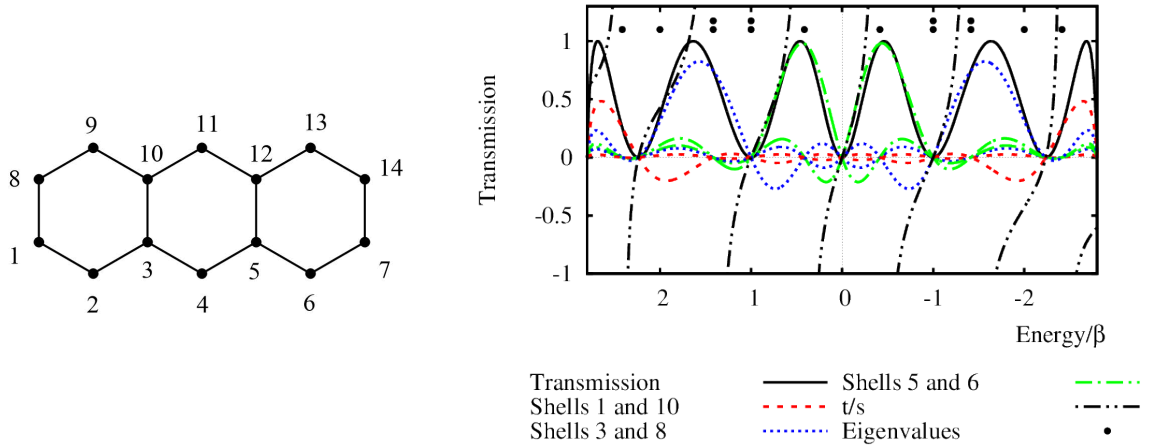


Figure 7.3: Anthracene shell currents and transmission for a symmetrical *ipso* device connected to atom 4, as shown on the graph of the molecule on the left. The structural polynomial $\hat{t} = t/s$ is also shown.

7.6 Conduction in molecules with bipartite graphs

An alternant molecule has a bipartite molecular graph containing two disjoint sets of nodes (atoms) and in which edges (bonds) connect only members of the two sets. We shall call these two sets \mathcal{S}_o and \mathcal{S}_* . If we number the members of the sets contiguously, then we can write the adjacency matrix in the form

$$\mathbf{A} = \begin{pmatrix} 0 & \mathbf{B} \\ \tilde{\mathbf{B}} & 0 \end{pmatrix} \quad (7.100)$$

where we have placed the n_o un-starred vertices in the first block, and the n_* starred vertices in the second, and we assume that $n_o \leq n_*$. The dimension of the matrix \mathbf{B} is, therefore, $n_o \times n_*$.

A simple two-component SSP approach to conductivity in bipartite molecules has been developed [103, 143] for the case $E = 0$. In this section we derive rules that apply to such molecules at general values of E .

7.6.1 The Coulson–Rushbrooke theorem

For convenience, we present a compact derivation of this well-known [144] theorem in a formalism that is useful for our study of conduction.

We can solve the eigenvector problem for the positive semi-definite matrix $\mathbf{B}\tilde{\mathbf{B}}$ of dimension $n_o \times n_o$ and of rank $r \leq n_o$, in the form [89]

$$\begin{aligned} \mathbf{B}\tilde{\mathbf{B}}\mathbf{V}_k &= \mathbf{V}_k\sigma_k^2 \text{ for } k = 1, \dots, r \\ \mathbf{B}\tilde{\mathbf{B}}\mathbf{V}_k &= 0 \text{ for } k = r + 1, \dots, n_o \end{aligned} \quad (7.101)$$

where the $n_o \times n_o$ matrix, \mathbf{V} , formed from the n_o columns \mathbf{V}_k is an orthogonal transformation with $n_o - r$ null-space eigenvectors. We can also consider the n_* -dimensional eigenvalue problem

$$\begin{aligned}\tilde{\mathbf{B}}\mathbf{B}\mathbf{W}_k &= \mathbf{W}_k\sigma_k^2 \text{ for } k = 1, \dots, r \\ \tilde{\mathbf{B}}\mathbf{B}\mathbf{W}_k &= 0 \text{ for } k = r + 1, \dots, n_*\end{aligned}\quad (7.102)$$

which has r identical positive eigenvalues, a null-space of dimension $n_* - r$, and the matrix \mathbf{W} is orthogonal. We can write the *singular value decomposition* [89] of \mathbf{B} as

$$\begin{aligned}\mathbf{B}\mathbf{W} &= \mathbf{V}\Sigma \\ \text{or} \\ \tilde{\mathbf{B}}\mathbf{V} &= \mathbf{W}\tilde{\Sigma}\end{aligned}\quad (7.103)$$

where the $n_o \times n_*$ matrix, Σ , is in principle rectangular, with a diagonal containing the *positive* numbers $\sigma_1 \geq \sigma_2 \geq \dots \geq \sigma_r > 0$.

We can now construct an $(n_o + n_*)$ -dimensional orthogonal transformation

$$\begin{pmatrix} \mathbf{V} & 0 \\ 0 & \mathbf{W} \end{pmatrix}\quad (7.104)$$

that when applied to the adjacency matrix of Eq. (7.100) gives rise, for each of the r terms having $\sigma_k > 0$, to a series of 2×2 interacting blocks of the form

$$\begin{pmatrix} 0 & \sigma_k \\ \sigma_k & 0 \end{pmatrix}\quad (7.105)$$

These blocks are each diagonalised by the same 2-dimensional orthogonal transformation

$$\begin{pmatrix} 1/\sqrt{2} & 1/\sqrt{2} \\ 1/\sqrt{2} & -1/\sqrt{2} \end{pmatrix}\quad (7.106)$$

The appropriate combination of Eqs (7.104) and (7.106) solves the original eigenvalue problem by providing r paired solutions $\psi_k, \psi_{\bar{k}}$ having eigenvalues $+\sigma_k$ and $-\sigma_k$, respectively, and constructed from columns of the orthogonal matrices \mathbf{V} and \mathbf{W} . They are

$$\begin{aligned}\psi_k &= \frac{1}{\sqrt{2}} \left(\sum_{p \in \mathcal{S}_o} V_{pk} \phi_p + \sum_{p \in \mathcal{S}_*} W_{pk} \phi_p \right) \\ \psi_{\bar{k}} &= \frac{1}{\sqrt{2}} \left(\sum_{p \in \mathcal{S}_o} V_{pk} \phi_p - \sum_{p \in \mathcal{S}_*} W_{pk} \phi_p \right)\end{aligned}\quad (7.107)$$

for $k = 1, \dots, r$, and the nullspace is

$$\begin{aligned}\psi_k &= \sum_{p \in \mathcal{S}_o} V_{pk} \phi_p \text{ for } k = r + 1, \dots, n_o \\ \psi_{\bar{k}^*} &= \sum_{p \in \mathcal{S}_*} W_{pk} \phi_p \text{ for } k^* = r + 1, \dots, n_*\end{aligned}\quad (7.108)$$

Hence, there are $2r$ eigenvalues in pairs related to each other by a change of sign, and a nullspace of dimension $n_o + n_* - 2r$. This is the content of the Coulson–Rushbrooke pairing theorem [5, 145, 146], which is usually derived in an *ad hoc* way from the Hückel secular equation. We now derive an extension for conduction properties.

7.6.2 Structural polynomials for bipartite graphs

For bipartite graphs (alternant molecules), we can obtain structural polynomials from the above formulae for the eigenvectors and eigenvalues, together with the spectral expansions given earlier. Hence, after some algebra,

$$\begin{aligned}\hat{t} &= E \sum_{k=1}^r \frac{V_{\bar{L}k}^2}{E^2 - \sigma_k^2} + \frac{1}{E} \sum_{k=r+1}^{n_o} V_{\bar{L}k}^2 \text{ for } \bar{L} \in \mathcal{S}_o \\ \hat{t} &= E \sum_{k=1}^r \frac{W_{\bar{L}k}^2}{E^2 - \sigma_k^2} + \frac{1}{E} \sum_{k=r+1}^{n_*} W_{\bar{L}k}^2 \text{ for } \bar{L} \in \mathcal{S}_*\end{aligned}\quad (7.109)$$

The formulae for \hat{u} are easily obtained by analogy. It is seen that

$$\begin{aligned}\hat{t}(-E) &= -\hat{t}(E) \\ \hat{u}(-E) &= -\hat{u}(E)\end{aligned}\quad (7.110)$$

so that both functions are *odd*, as expected from parity arguments. The equations for \hat{j} are more complicated, as there are two cases, depending on whether indices \bar{L}, \bar{R} belong to the same or different sets. When $\bar{L} \in \mathcal{S}_o$ and $\bar{R} \in \mathcal{S}_o$,

$$\hat{j} = E \sum_{k=1}^r \frac{V_{\bar{L}k} V_{\bar{R}k}}{E^2 - \sigma_k^2} + \frac{1}{E} \sum_{k=r+1}^{n_o} V_{\bar{L}k} V_{\bar{R}k}\quad (7.111)$$

which is an odd function of E . When $\bar{L} \in \mathcal{S}_o$ and $\bar{R} \in \mathcal{S}_*$,

$$\hat{j} = \sum_{k=1}^r \sigma_k \frac{V_{\bar{L}k} W_{\bar{R}k}}{E^2 - \sigma_k^2}\quad (7.112)$$

which is even. From the formula $\hat{v} = \hat{u}\hat{t} - \hat{j}^2$, it is clear that $\hat{v}(E) = \hat{v}(-E)$, regardless of the nature of \bar{L} and \bar{R} .

7.6.3 Conduction properties of alternant molecules

We now consider the transmission properties of molecules with bipartite graphs for unbiased devices, *i.e.*, those for which $\alpha_L = \alpha_R = 0$, under the transformation $E \rightarrow -E$. This transformation affects the momenta (*cf.* Eq. (7.6)) through $q_L \rightarrow \pi - q_L$ and $q_R \rightarrow \pi - q_R$. It follows that $\exp(-iq_L) \rightarrow -\exp(iq_L)$, and $\sin q_L \rightarrow -\sin q_L$. The terms in q_R behave in an identical manner. From the discussion of the transformation properties of these quantities, it is obvious from Eq. (7.3) that

$$D(-E) = D(E)^*\quad (7.113)$$

and hence

$$T(-E) = T(E) \quad (7.114)$$

so that the total transmission is symmetric about $E = 0$ for unbiased devices.

We can also look at the symmetry properties of the MO currents by writing Eq. (7.80) in terms of the hatted polynomials

$$J_{L \rightarrow k}^{\text{MO}}(E) = \mathcal{B}(q_L, q_R) \frac{U_{\bar{L}k} U_{Rk}}{E - \epsilon_k} \frac{\hat{j}(E)}{|\hat{D}(E)|^2} \quad (7.115)$$

Putting this equation into the context of the current section: for the paired orbitals, $\psi_k, \psi_{\bar{k}}$, we recognise that the eigenvectors for the paired MOs satisfy

$$\begin{aligned} U_{pk} &= U_{p\bar{k}} \text{ for } p \in \mathcal{S}_o \\ U_{pk} &= -U_{p\bar{k}} \text{ for } p \in \mathcal{S}_* \end{aligned} \quad (7.116)$$

and

$$J_{L \rightarrow k}^{\text{MO}}(E) = J_{L \rightarrow \bar{k}}^{\text{MO}}(-E) \quad (7.117)$$

The paired orbitals have currents that are reflections of each other about the line $E = 0$. It is also obvious that Eq. (7.117) for $g \geq 2$ extends also to shells, so that

$$J_{L \rightarrow K}^{\text{MO}}(E) = J_{L \rightarrow \bar{K}}^{\text{MO}}(-E) \quad (7.118)$$

It can be shown that bond currents in bipartite molecules also display the same symmetry

$$J_{p \rightarrow q}^{\text{AO}}(E) = J_{p \rightarrow \bar{q}}^{\text{AO}}(-E) \quad (7.119)$$

7.6.4 Conduction at the Fermi level for bipartite graphs

The conduction properties of the shell at $\epsilon_k = 0$ can be discussed in a very simple manner using the eigenspaces listed in Eqs (7.107) and (7.108), and the connection matrix in Eqs (7.28) and (7.31).

For molecular graphs that possess a nullspace, we have a single shell with $\epsilon_K = 0$ and degeneracy $g = n_o + n_* - 2r$. There are two possibilities:

1. Contact atoms in different sets, *e.g.* $\bar{L} \in \mathcal{S}_o$ and $\bar{R} \in \mathcal{S}_*$.

In this case the structure of the *null-space* connection vector is

$$\mathbf{u}_L = \beta_{\bar{L}\bar{L}} \begin{pmatrix} V_{\bar{L}r+1} \\ \vdots \\ V_{\bar{L}n_o} \\ 0 \\ \vdots \\ 0 \end{pmatrix}, \quad \mathbf{u}_R = \beta_{\bar{R}\bar{R}} \begin{pmatrix} 0 \\ \vdots \\ 0 \\ W_{\bar{R}r+1} \\ \vdots \\ W_{\bar{R}n_*} \end{pmatrix} \quad (7.120)$$

The formula for MO currents, Eq. (7.80), shows that current is proportional to a product of \bar{L} and \bar{R} MO coefficients from the connection vectors. The

structure of the vectors in Eq. (7.120) implies that this product is identically zero. The shell carries no current and is inert regardless of the rank of the connection matrix.

2. Contact atoms in the same set, *e.g.* $\bar{L} \in \mathcal{S}_\circ$ and $\bar{R} \in \mathcal{S}_\circ$.

In this case the structure of the *null-space* connection vector is

$$\mathbf{u}_L = \beta_{\bar{L}\bar{L}} \begin{pmatrix} V_{\bar{L}r+1} \\ \vdots \\ V_{\bar{L}n_\circ} \\ 0 \\ \vdots \\ 0 \end{pmatrix}, \mathbf{u}_R = \beta_{\bar{R}\bar{R}} \begin{pmatrix} V_{\bar{R}r+1} \\ \vdots \\ V_{\bar{R}n_\circ} \\ 0 \\ \vdots \\ 0 \end{pmatrix} \quad (7.121)$$

The $n_* - r$ molecular orbitals from the starred space are all *inert*, but the MOs from the un-starred space are not necessarily inert. The shell may therefore still be active, depending on the case to which the shell belongs (*cf.* Table 7.1).

For cases where $E = 0$ is *not* an eigenvalue, the present reasoning makes a connection with a ‘symmetry rule’ (actually a graph-theoretical rule) for *non-ipso* conduction at the Fermi level for closed-shell alternant molecules [140,147]. It was observed that the predicted Fermi-level conduction of a molecule with bipartite molecular graph and a non-zero HOMO-LUMO gap (specifically a Kekulean benzenoid) is large when both HOMO and LUMO have entries of large magnitude on both connection vertices (our \bar{L} and \bar{R}) and the product of entries is of opposite sign for HOMO and LUMO. By the Pairing theorem this latter requirement implies that the connection vertices are in different partite sets.

This rule has a straightforward interpretation in terms of shell contributions. HOMO and LUMO shells of a bipartite graph have mirror conduction curves, so are either both active or both inert. For active shells, both shell conduction curves will be close to local maxima in the vicinity of the Fermi level. If the connection vertices are in opposite sets, the curves will contribute equal amounts to the total conduction at the Fermi level. (Other active shells will typically also contribute. Such contributions may be positive or negative.) If the connection vertices belong to the same partite set, however, we have nullity signature $g = 0$, $g_t = g_u = 1$, $g_v = 2$ and insulation at the Fermi level [70].

7.7 Some illustrative examples

In this section we shall see that every molecular graph has at least one active shell and give some analytical examples for chains and rings and some examples of numerical calculations. The algebraic computations reported in this paper were all performed by using Maple 18 [148] written by Prof. B.T. Pickup. Computations for the figures were carried out using unbiased ($\alpha_L = \alpha_R = 0$), and symmetric devices ($\beta_L = \beta_R$), with specific values $\beta_L = 1.4\beta$ and $\beta_{\bar{L}\bar{L}} = \beta_{\bar{R}\bar{R}} = \beta$.

7.7.1 Molecular conduction of LOMO and HUMO shells

Every π system with a connected molecular graph G has a non-degenerate lowest-lying π level. Mathematically, the eigenvector corresponding to the largest positive eigenvalue of G , ϵ_{\max} , *i.e.*, the lowest occupied π molecular orbital (LOMO), has specific implications for the conduction properties. This maximum eigenvalue is known in mathematics as the Perron eigenvalue [2]; it has multiplicity one for a connected graph, and the associated eigenvector has a non-zero entry of the same sign on every vertex [149]. Deletion of any vertex in a connected graph leads to a decrease in the maximum eigenvalue; deletion of a second vertex may lead to a further decrease or may leave the maximum eigenvalue unchanged (only if removal of the first vertex had disconnected the graph).

Hence, the LOMO always constitutes an active shell, belonging to case 10. A proof based on interlacing is straightforward. Whilst the Perron eigenvalue of graph G has degeneracy $g = 1$, degeneracies g_t and g_u are both 0, as the maximum eigenvalue falls on vertex deletion. Whether the graph $G - \bar{L} - \bar{R}$ is disconnected or not, the maximum eigenvalue of this graph is strictly less than ϵ_{\max} , and so $g_v = 0$, and we have case 10, which is active (*c.f.* Table 7.1).

The LOMO typically contributes some conduction at all energies that are not eigenvalues, and so will have a (small) contribution at the Fermi level if G is non-singular. If G is connected and bipartite, then it has a unique eigenvalue ϵ_{\min} , and the conduction properties of the corresponding ‘anti-Perron’ eigenvector (the highest unoccupied molecular orbital, or HUMO) also follow case 10, and in particular will have a conduction peak near the eigenvalue. For a non-singular molecular graph this will reinforce the contribution of the LOMO at the Fermi level.

7.7.2 Conduction in chains

We gave explicit analytical formulae for the total transmission in chains and rings, based on full electron delocalisation, in earlier work [63]. Here we concentrate on the conditions for inert orbitals and shells.

The molecular graph of the general linear polyene C_nH_{2n+2} is the path on n vertices, P_n . All eigenvalues of P_n are non-degenerate, and so the set of cases for exploration is 1 to 10 (connection matrix of rank 1 or 0), and shells are active if they belong to cases 9 or 10. Both of these cases occur.

An orbital is inert whenever \bar{L} or \bar{R} , or both, is at a node. The k^{th} vector ($k = 1, \dots, n$) has entry [83]

$$U_{pk} = \sqrt{2/(n+1)} \sin(pk\pi/(n+1)) \quad (7.122)$$

on vertex p , such that $p = 1, \dots, n$. Hence, there are nodes at $kp = \mathcal{P}(n+1)$, where \mathcal{P} is a non-zero integer and shell k is inert, therefore, if $k\bar{L} = \mathcal{P}(n+1)$ and/or $k\bar{R} = \mathcal{P}(n+1)$. For example, all odd chains connected *via* their central vertex ($p = (n+1)/2$) have inert orbitals at all even k (implying $\mathcal{P} = k$).

Given that both k and p are less than $n+1$, a small general observation follows for even chains: if $n+1$ is prime, the chain has *no* inert shells, since kp cannot contain $n+1$ as a factor. Hence, chains with $n = 2, 4, 6, 10, 12, 16, \dots$ have no inert shells.

7.7.3 Conduction in rings

A device based on a $C_n H_n$ ring has connections $\bar{L} = 1$, $\bar{R} - \bar{L} = p$ ($0 \leq p \leq n - 1$). The spectrum of the cycle is [83]

$$\epsilon_k = 2 \cos(2\pi k/n) \quad (7.123)$$

with $k = 0, 1, \dots, \lfloor n/2 \rfloor$ and degeneracies $g = 1$ for $k = 0$ (Perron) and $k = n/2$ (anti-Perron, for even n only), but $g = 2$ for all other values of k . The shells with $\epsilon_k = +2$ (and -2 for even n) are active, by the arguments given above for the Perron eigenvalue.

Deletion of any vertex of the cycle C_n yields the path P_{n-1} , and so $g_t = g_u = 1$ for all shells with $g = 2$. Therefore, all *ipso* devices based on the cycle are of type I3 (Table 7.2) and all shells are active. For *non-ipso* devices, the possible cases for inertness/activity are limited to 9, 10, 11.1 and 11.2 of Table 7.1, and hence all shells are active except those that fall under case 11.2 ($g_v = 0$, $g_j \geq 2$). Detection of inert shells can be done in several ways. One route is via the connection matrix. For a degenerate shell of the cycle, the matrix $\mathbf{B}_K^{\text{con}}$ is

$$\begin{aligned} \mathbf{B}_K^{\text{con}} &= \begin{pmatrix} \beta_{\bar{L}\bar{L}} U_{\bar{L}1} & \beta_{\bar{R}\bar{R}} U_{\bar{R}1} \\ \beta_{\bar{L}\bar{L}} U_{\bar{L}2} & \beta_{\bar{R}\bar{R}} U_{\bar{R}2} \end{pmatrix} \\ &= \begin{pmatrix} \sqrt{\frac{2}{n}} \beta_{\bar{L}\bar{L}} \cos\left(\frac{2\pi k \bar{L}}{n}\right) & \sqrt{\frac{2}{n}} \beta_{\bar{R}\bar{R}} \cos\left(\frac{2\pi k \bar{R}}{n}\right) \\ \sqrt{\frac{2}{n}} \beta_{\bar{L}\bar{L}} \sin\left(\frac{2\pi k \bar{L}}{n}\right) & \sqrt{\frac{2}{n}} \beta_{\bar{R}\bar{R}} \sin\left(\frac{2\pi k \bar{R}}{n}\right) \end{pmatrix} \end{aligned} \quad (7.124)$$

in the sine/cosine representation of the eigenspace and with $k = 1, \dots, \lfloor n/2 \rfloor$.

For case 11.2 we must have $\hat{v}_{-2} \neq 0$ and $\hat{j}_{-1} = 0$ (to give $g_v = g - 2$ and $g_j = g - 1$). Now, with our definition of $\bar{R} - \bar{L} = p$, by Eq. (7.43),

$$\begin{aligned} \hat{v}_{-2} &= \frac{4\beta_{\bar{L}\bar{L}}^2 \beta_{\bar{R}\bar{R}}^2}{n^2} \sin^2(2\pi k p/n), \\ \hat{j}_{-1} &= \frac{2\beta_{\bar{L}\bar{L}} \beta_{\bar{R}\bar{R}}}{n} \cos(2\pi k p/n). \end{aligned} \quad (7.125)$$

The expression for \hat{j}_{-1} vanishes for $4kp = (2q + 1)n$, with integer q . This condition is sufficient to ensure that $\hat{v}_{-2} \neq 0$, and hence that we are in case 11.2.

Clearly, if n is *odd*, $4kp$ cannot be the product of two odd integers, and so *no* shells of an odd cycle are inert.

Equally, if n is of the form $4N + 2$, $2kp$ cannot be the product of two odd integers, and so *no* shells of a $(4N + 2)$ cycle are inert.

The remaining case is where n is of the form $4N$. Devices based on C_{4N} cycles have inert shells whenever the shell index k and the pathlength p between connection vertices obey $kp = (2q + 1)N$. For example, C_8 has inert shells with $k = 1, 3$ for $p = 2$, but $k = 2$ for $p = 1$ and $p = 3$. Likewise, C_{20} has inert shells at $k = 5$ for $p = 1, 3, 5, 7, 9$ and at $k = 1, 3, 5, 7, 9$ for $p = 5$.

There is a particular implication for conduction at the Fermi level through devices based on $4N$ cycles. Note that even/odd values of p correspond to devices with \bar{L}

and \bar{R} in the same/opposite partite sets. Therefore, the shell at $\epsilon = 0$ ($k = 2N$), is active (case 9) when \bar{L} and \bar{R} are in the same partite set, and inert (case 11.2) when they are in opposite sets. The cycles C_{4N+2} are also bipartite, but do not have $\epsilon = 0$ as an eigenvalue.

7.7.4 An alternant molecule with a space of non-bonding orbitals

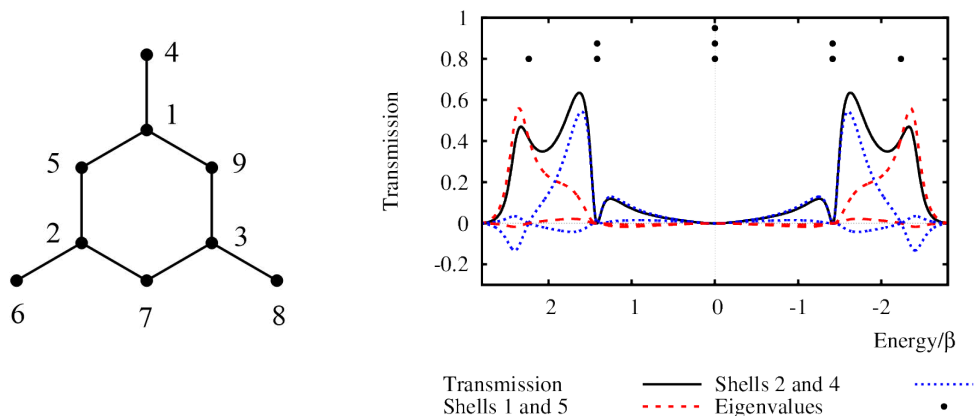


Figure 7.4: The shell currents for a device connected to atoms 1 and 8 of the molecule depicted on the left showing the labelling schemes of the atom.

Fig. 7.4 has 9 conjugated centres with $n_* = 3$, and $n_o = 6$. The device treated in this example has connections via atoms 1 and 8. The (3×6) -dimensional matrix \mathbf{B} in Eq. (7.100) has rank 3, and there are three nullspace vectors, concentrated on the unstarred set of atoms. Shells 1 and 5 are case 10, whilst shells 2 and 4 are case 11.2. It can be seen from Fig. 7.4 that the triply-degenerate nullspace (shell 3) is inert. This shell is an example of case 5, which is also insulating. The inert character of the null shell arises from the special eigenvector structure for a bipartite molecule, as outlined in Section 7.6.

7.8 Inertness/activity and core/core-forbidden vertex sets

The inertness/activity property has a simple interpretation in terms of nodal character. This is nicely expressed in terms of the notation of core and core-forbidden vertex sets [108], which is usually used for the nullspace of a graph, but has a natural extension for any shell [93]. In this extended sense, the vertices in the core set for a given shell are those with a non-zero sum of amplitudes of entries when summed over the shell. In chemical terms, they have non-zero partial π charges for occupation of the shell. Vertices outside the core are *core-forbidden vertices* (CFV): they are nodal points in all possible representations of the degenerate set of orbitals. A shell is inert in a given device if one (or both) of the connection atoms \bar{L} and \bar{R} corresponds to vertices in the *core-forbidden* set for that shell.

CFV can in some cases be identified by symmetry arguments. If vertex r is a CFV for the eigenspace K , the eigenvector entry U_{rk} vanishes and the local adjacency condition $\sum_{s \sim r} U_{sk} = 0$ applies for all $k \in K$. If r is at a special point of the point group, the vanishing of U_{rk} may be enforced by the symmetry spanned by the eigenspace (the set of degenerate orbitals). For example, if r lies in a mirror plane and all vectors in the eigenspace are antisymmetric with respect to reflection in that plane, r must be a CFV for shell K . Thus, for example, the central vertex of an odd path is always CFV for even k (*c.f.* Section 7.7.2). More typical is the situation for a doubly degenerate shell where it will often be possible to choose one symmetric and one antisymmetric vector with respect to a given plane, and r is therefore not a CFV. This is the case for all degenerate shells of the cycle.

The language of CFVs also gives an alternative view of the effects of side-chains on conduction, more usually expressed in terms of quantum interference [54, 61, 81, 150, 151]. In this analysis, quantisation conditions for side-chains force a node at the junction with the backbone, *i.e.* a CFV that kills conduction [105]. Nodal positions are robust to improvements in the level of theory if they are determined by symmetry; if instead they result from a cancellation within the Hückel model, they may shift with improvements, but the qualitative prediction of zero shell conduction may still be an indicator of a low contribution to conduction.

7.9 Conclusions

A new analysis of the SSP model has been presented. The strengths (and the limitations) of the model stem from its graph-theoretical form. The connection with spectral graph theory gives a new and chemically informative way to think about ballistic conduction in terms of orbital contributions. To do this, first a re-derivation of the SSP equations was presented in a manner that gives easier access to quantities of interest and elucidates behaviour in special circumstances.

Current through molecules can be discussed in terms of transmission through a series of bonds, *i.e.*, bond currents. These bond currents can go with or against the main direction of current flow, and strong cancellation occurs frequently near energies at which there is overall insulation. There is not always an obvious interpretation of these currents [55]. In the bond current picture, intramolecular interference effects are inevitable [20].

Current through molecules can also be discussed in terms of parallel channels corresponding to molecular orbitals and shells of molecular orbitals. These currents can be negative, but typically behave in a more stable fashion than do bond currents, and at every energy they add up to the total transmission, $T(E)$.

Transmission has been partitioned into orbital contributions in other computational schemes, using projection techniques [152–155]. The scheme followed here gives shell contributions naturally and uniquely within the tight-binding approach.

Shell currents turn out to have some interesting general properties governing their contributions to transmission across the range of accessible energies. It has been shown previously that total transmission at eigenvalues can be classified in terms of 11 cases derived by use of the Interlacing Theorem. The new SSP equations give a

finer classification, splitting two cases to give a total of 13 possibilities for behaviour in terms of insulation and conduction both at and between eigenvalues.

Shell currents are classified in terms of the same set of cases, which reveal specific behaviour at eigenvalues and a global property of activity/inertness. It turns out that some shells are *inert*. That is to say, they are insulating at all values of E . Shells that conduct at some energy E are *active*.

Only three cases (9, 10, and 11.1) out of the 13 represent active shells. A practical application of this classification scheme is that transmission near the Fermi energy is dominated by frontier-shell contributions. If any of these shells are inert, the conductivity of the molecule will be greatly decreased.

Finally, the viewpoint based on orbital rather than bond current contributions should be especially useful when further refinements of the SSP model beyond the scope of this thesis are considered. Molecular-orbital contributions to transmission could be derived by similar methods for more complex, multi-channel devices such as those treated in the extended SSP model by Dumont [138]. They will be at their most useful when considering the proper inclusion of electron repulsion.

7.10 Appendix: Detailed analysis of the 11 canonical cases

We shall assume that the rank of the SSP equations, (*cf.* Eqs (7.88) and (7.89)), in the echelon representation is 2. The general solution in the linearly independent space to the SSP equations for any energy, $E \neq \epsilon_K$, in this case of rank 2 is given by

$$\begin{pmatrix} c_1^{\text{MO}} \\ c_2^{\text{MO}} \\ c_L \\ c_R \end{pmatrix} = -\frac{iN_L}{\hat{\Delta}} \begin{pmatrix} -ad^2 + p_K (a\hat{F}_{\text{AR}} + b\beta_{\text{LL}}\beta_{\text{RR}}\hat{J}_A) \\ d(ab + p_K\beta_{\text{LL}}\beta_{\text{RR}}\hat{J}_A) \\ p_K(-b^2 - d^2 + p_K\hat{F}_{\text{AR}}) \\ p_K(ab + p_K\beta_{\text{LL}}\beta_{\text{RR}}\hat{J}_A) \end{pmatrix} \quad (7.126)$$

where

$$\begin{aligned} \hat{\Delta}(E) = & a^2d^2 - p_K[a^2\hat{F}_{\text{AR}} + (b^2 + d^2)\hat{F}_{\text{AL}} \\ & + 2ab\beta_{\text{LL}}\beta_{\text{RR}}\hat{J}_A] \\ & + p_K^2(\hat{F}_{\text{AR}}\hat{F}_{\text{AL}} - \beta_{\text{LL}}^2\beta_{\text{RR}}^2\hat{J}_A^2) \end{aligned} \quad (7.127)$$

When $p_K \neq 0$, the solutions given for c_L and c_R in Eq. (7.126) reduce to those already shown in Section 7.4, as they must, and it can be shown that c_L, c_R are identical to those in Eq. (7.64). The expressions for c_1^{MO} and c_2^{MO} are not those derived previously, since they refer particularly to orbitals in the echelon representation.

We shall consider the eight possibilities arising from Eq. (7.92), depending upon whether the constants, a, b , and d are zero or non-zero. Eqs (7.126) and (7.127) are in a form which is robust enough to cover each of the eight cases, so long as $p_K \neq 0$.

We have shown that it is possible to use Eq. (7.64) for a derivation of SSP solutions

at an eigenvalue. We now need to take these solutions for quantities such as c_R , T , *etc.*, and then take the limit $E \rightarrow \epsilon_K$.

The leading term in the expansion (*cf.* Eqs (7.54) and (7.55)) of \hat{D} is determined entirely by the rank of the connection matrix, $\mathbf{B}_K^{\text{con}}$. Hence, rank 2, gives \hat{D}_{-2} as the leading term. Ranks 1 and 0 have \hat{D}_{-1} , and \hat{D}_{-0} , as leading terms, respectively.

We now consider the different ranks in turn.

7.10.1 Devices with rank–2 connection matrices

We note that this is only possible when $g \geq 2$. In such a case, a rank–2 connection matrix can be achieved in just two different ways out of the eight possibilities for the choice of a , b , and d .

(i) $a \neq 0$, $b \neq 0$, $d \neq 0$

In this case it is evident from Eq. (7.93) that $\hat{t}_{-1} \neq 0$, $\hat{u}_{-1} \neq 0$, $\hat{v}_{-2} \neq 0$, and $\hat{j}_{-1} \neq 0$, so that $g_t = g_u = g_j = g-1$, and $g_v = g-2$. This corresponds with case 11 of our previous work in [70, 84]. Solution of the linear equations at $p_K = 0$ gives a unique SSP vector

$$\begin{pmatrix} c_1^{\text{MO}} \\ c_2^{\text{MO}} \\ c_L \\ c_R \end{pmatrix} = \frac{iN_L}{a} \begin{pmatrix} 1 \\ -b/d \\ 0 \\ 0 \end{pmatrix} \quad (7.128)$$

The vanishing of c_L and c_R , implies that $r = -1$, and $\tau = 0$, and hence $T(\epsilon_K) = 0$. This particular value of the reflection factor (*cf.* Eq. (7.15)) is an explicit example of the singularity sometimes present in the original version of the SSP formalism [62, 63]. This case is labelled 11.1 in Table 7.1.

We can also see, from Eq. (7.97), that the shell is *active*, *i.e.*, the current through shell K at general values of E is non–zero for case 11.1, because of the non–vanishing \bar{L} – and \bar{R} –components of the first echelon orbital.

The bond currents, $J_{p \rightarrow q}^{\text{AO}}$, vanish at ϵ_K because $c_L = c_R = 0$, as noted in section 7.3.2.

(ii) $a \neq 0$, $b = 0$, $d \neq 0$

We also have $\hat{t}_{-1} \neq 0$, $\hat{u}_{-1} \neq 0$, and $\hat{v}_{-2} \neq 0$, so that $g_t = g_u = g-1$, and $g_v = g-2$. This also conforms with the specification of case 11 [70, 84]. The unique solution to the SSP equations at $p_K = 0$ is

$$\begin{pmatrix} c_1^{\text{MO}} \\ c_2^{\text{MO}} \\ c_L \\ c_R \end{pmatrix} = \frac{iN_L}{a} \begin{pmatrix} 1 \\ 0 \\ 0 \\ 0 \end{pmatrix} \quad (7.129)$$

and implies that $T(\epsilon_K) = 0$, as before.

The sole change between this and the previous type occurs because $\hat{j}_{-1} = ab = 0$, which means that $g_j \geq g$, and hence the shell is *inert*. We distinguish this as case 11.2.

The bond currents also all vanish, as $c_L = c_R = 0$.

7.10.2 Devices with rank–1 connection matrices

There is no restriction on degeneracy for a rank–1 connection matrix, the necessary and sufficient condition for which is that $\hat{v}_{-2} = 0$. This can occur in five ways out of the eight possibilities for the choices of a , b , and d . These are:

(iii) $a = 0, b \neq 0, d \neq 0$ This does not lead to a real example, since an additional 2×2 rotation of the first two orbitals would lead to possibility (v).

(iv) $a = 0, b = 0, d \neq 0$

Thus, $\hat{t}_{-1} = \hat{j}_{-1} = \hat{v}_{-2} = 0$, and $\hat{u}_{-1} \neq 0$. This implies that $g_t \geq g$, $g_u = g-1$, $g_j \geq g$, and $g_v \geq g-1$, so that this corresponds to cases 5 and 8.

The solution to the SSP equations is

$$\begin{pmatrix} c_2^{\text{MO}} \\ c_L \\ c_R \end{pmatrix} = -\frac{iN_L}{\hat{F}_{AL}} \begin{pmatrix} \beta_{\bar{L}L}\beta_{\bar{R}R}\hat{j}_A/d \\ -1 \\ 0 \end{pmatrix} \quad (7.130)$$

where we have left out the undetermined coefficient, c_1^{MO} , which can be considered to be zero by continuity with the solution at $p_K \neq 0$. We note also that $c_R = 0$ implies that $T(\epsilon_K) = 0$. The condition $\hat{v}_{-2} = 0$ implies, from Eq. (7.95), that the bond currents also vanish. The condition $\hat{j}_{-1} = 0$ implies that the shell must be *inert*.

(v) $a = 0, b \neq 0, d = 0$

Again $g_t \geq g$, $g_u = g-1$, $g_j \geq g$, and $g_v \geq g-1$, which is another example of cases 5 and 8. The (non–unique) solution for the SSP vector

$$\begin{pmatrix} c_1^{\text{MO}} \\ c_L \\ c_R \end{pmatrix} = -\frac{iN_L}{\hat{F}_{AL}} \begin{pmatrix} -\beta_{\bar{L}L}\beta_{\bar{R}R}\hat{j}_A/b \\ 1 \\ 0 \end{pmatrix} \quad (7.131)$$

where the arbitrary c_2^{MO} component has been left out of the equations. Analysis of the conduction properties is identical to (iv).

(vi) $a \neq 0, b = 0, d = 0$

This requires $g_t = g-1$, $g_u \geq g$, $g_j \geq g$, and $g_v \geq g-1$, which is another example of cases 5 and 8 in which the rôles of g_t and g_u have been swapped. The solution is

$$\begin{pmatrix} c_1^{\text{MO}} \\ c_L \\ c_R \end{pmatrix} = \frac{iN_L}{a} \begin{pmatrix} 1 \\ 0 \\ 0 \end{pmatrix} \quad (7.132)$$

with c_2^{MO} again arbitrary, and conduction properties as described in (iv).

(vii) $a \neq 0, b \neq 0, d = 0$

The values of the constants imply that $\hat{t}_{-1} \neq 0, \hat{u}_{-1} \neq 0$, and $\hat{v}_{-2} = 0$, but $\hat{j}_{-1} \neq 0$, so that $g_t = g_u = g_j = g - 1$, and $g_v \geq g - 1$. Hence, this corresponds to cases 9 and 10. The SSP solution is

$$\begin{pmatrix} c_1^{\text{MO}} \\ c_L \\ c_R \end{pmatrix} = \frac{iN_L}{\hat{D}_{-1}} \begin{pmatrix} a\hat{F}_{AR} + b\beta_{\bar{L}L}\beta_{\bar{R}R}\hat{J}_A \\ -b^2 \\ ab \end{pmatrix} \quad (7.133)$$

where

$$\hat{D}_{-1} = a^2\hat{F}_{AR} + 2ab\beta_{\bar{L}L}\beta_{\bar{R}R}\hat{J}_A + b^2\hat{F}_{AL}$$

The coefficient c_2^{MO} is not determined by the equations, but no current can be carried by this MO as $d = 0$. The values of c_L and c_R are, however, uniquely determined, and the total transmission is

$$T(\epsilon_K) = \mathcal{B}(q_L, q_R) \frac{\hat{j}_{-1}^2}{|\hat{D}_{-1}|^2} \quad (7.134)$$

At least some bond currents will be non-zero, and the shell is *active*.

It is clear from their entries in Table 7.1 that cases 5 and 8 share the feature that $\hat{j}_{-1} = 0$, which implies that both lead to inert shells. This same feature ensures that the j -factor in the numerator of the expression for c_R is $O(1)$ in the series expansion in powers of p_K . The denominator is clearly $O(p_K^{-1})$ for both cases because of the presence of non-zero terms in \hat{D}_{-1} in Eq. (7.55). It follows that $c_R = 0$, and hence $T(\epsilon_K) = 0$.

Cases 9 and 10 have a non-zero value of \hat{j}_{-1} . This leads to an *active* shell, and $T(\epsilon_K) \neq 0$.

It is not possible to distinguish between cases 5 and 8, or between 9 and 10, on the basis of the quantities a, b , and d , and indeed because of the similarity of behaviour of these pairs, it does not seem necessary to do so.

7.10.3 Devices with rank-0 connection matrices

This is the last of the eight choices of the quantities a, b , and d .

(viii) $a = 0, b = 0, d = 0$

The quantities $\hat{t}_{-1} = \hat{u}_{-1} = \hat{j}_{-1} = 0$. This implies that $g_t \geq g, g_u \geq g, g_j \geq g$, and $g_v \geq g$. The vanishing of \hat{t}_{-1} and \hat{u}_{-1} means, that all \bar{L} and \bar{R} components of the shell wavefunctions vanish, and hence $\hat{v}_{-1} = 0$. The SSP solution is

$$\begin{pmatrix} c_L \\ c_R \end{pmatrix} = \frac{iN_L}{\hat{F}_{AL}\hat{F}_{AR} - \beta_{\bar{L}L}^2\beta_{\bar{R}R}^2\hat{J}_A^2} \begin{pmatrix} \hat{F}_{AR} \\ \beta_{\bar{L}L}\beta_{\bar{R}R}\hat{J}_A \end{pmatrix} \quad (7.135)$$

with c_L and c_R uniquely determined, and both MO coefficients, c_1^{MO} and c_2^{MO} arbitrary, but set to zero using continuity.

The various cases in Table 7.1 cannot be distinguished on the basis of the behaviour of the orbitals of the echelon representation. We can conclude immediately, however, that the shell is inert in all of these cases because $\hat{j}_{-1} = 0$.

Table 7.1 indicates that four of the cases conduct at the eigenvalue. It is obvious that such conduction can only occur through other shells. All of these cases have values of g_t , g_u , and g_v that are greater than or equal to g , so that each of the ‘hatted’ structural polynomials has an expansion with a leading term in p_K of $O(1)$ or greater. It follows directly that the leading term in the expansion of \hat{D} is \hat{D}_0 . (cf. Eq. (7.55)). The decision as to whether or not the various cases conduct at the eigenvalue hinges on the expansion of \hat{j} . We will make a few remarks about each case.

Case 1 ($g_t = g+1$, $g_u = g+1$, $g_v = g+2$)

The leading terms in the \hat{u} , \hat{t} and \hat{v} expansions are \hat{t}_1 , \hat{u}_1 and \hat{v}_2 , respectively. Since the 0th term in the j -expansion, when $\hat{j}_{-1} = 0$, can be expressed as

$$\hat{j}_0^2 = \hat{u}_0 \hat{t}_0 - \hat{v}_0 + \hat{t}_{-1} \hat{u}_1 + \hat{t}_1 \hat{u}_{-1} \quad (7.136)$$

the leading term in \hat{j} is \hat{j}_1 . The numerator in the expression for c_R is $O(p_K)$ whilst \hat{D} is $O(1)$. We conclude that $T(\epsilon_K) = 0$.

Case 2 ($g_t = g+1$, $g_u = g+1$, $g_v = g$)

The fact that $\hat{v}_0 \neq 0$ implies that the leading term in \hat{j} is \hat{j}_0 . This implies conduction at the eigenvalue.

Case 3 ($g_t = g+1$, $g_u = g$, $g_v = g+1$)

It is possible to deduce that $\hat{j}_0 = 0$, so that

$$\hat{j}_1^2 = \hat{u}_1 \hat{t}_1 - \hat{v}_2 \quad (7.137)$$

and hence \hat{j}_1 would be the lowest possible leading term in the \hat{j} expansion. We conclude that $T(\epsilon_K) = 0$. It is possible, however, for

$$\hat{u}_1 \hat{t}_1 = \hat{v}_2 \quad (7.138)$$

in which case \hat{j}_2 is the leading term. This makes no difference to the insulation properties.

Case 4 ($g_t = g+1$, $g_u = g$, $g_v = g$)

The leading terms in \hat{t} , \hat{u} and \hat{v} series are $O(p_K)$, $O(1)$ and $O(1)$, respectively, and hence

$$\hat{j}_0^2 = -\hat{v}_0 \quad (7.139)$$

So the order in p_K in numerator and denominator of the expression for c_R are the same. This leads to conduction at the eigenvalue.

Case 6 ($g_t = g$, $g_u = g$, $g_v = g+1$)

The leading terms in the \hat{t} , \hat{u} and \hat{v} series are $O(1)$, $O(1)$ and $O(p_K)$, respectively. Hence,

$$\hat{j}_0^2 = \hat{u}_0 \hat{t}_0 \quad (7.140)$$

and there is conduction at the eigenvalue.

Case 7 ($g_t = g, g_u = g, g_v = g$)

The leading terms in the \hat{u} and \hat{t} series are \hat{u}_0 and \hat{t}_0 , respectively, whilst the \hat{v} expansion also leads with \hat{v}_0 . We conclude that

$$\hat{j}_0^2 = \hat{u}_0 \hat{t}_0 - \hat{v}_0, \quad (7.141)$$

with implication that, in general, conduction occurs. However, as in case 3, there can be a cancellation inside Eq. (7.141) that would lead to the leading term in \hat{j} being \hat{j}_1 . This would be non-conducting. For case 7, there are conducting (7.1) and non-conducting (7.2) variants, as noted previously [70], depending on the value of g_j . Case (7.2) was described as an accident in the sense that it is not predicted from $g_t, g_u,$ and g_v alone.

Chapter 8

New developments in applications of graph theory to MEDs

This thesis has presented a development of the SSP approach using general graph theoretical arguments to devise chemical conclusions about MEDs, such as that omni-conduction occurs for molecular graphs with no NBOs or only one, and omni-insulation occurs for molecular graphs that have a large number of NBOs. It includes energy dependence of transmission, the rules for conduction or insulation at the Fermi level, the classification of the MEDs by conduction classes, from simple division into omni-conductors and omni-insulators of various types, to the comprehensive division by odd, even and zero distance between connection points. The initial AO-basis formulation of the SSP model has been extended to a singularity-free MO formulation, implying a graph-theoretical model of eigenvector channels for conduction.

The present chapter summarises some more recent activity in the field and points out some directions for both mathematical and chemical exploration. Three preliminary accounts of research projects within the group are given. These are a further investigation of the starification construction that was proposed in Chapter 4; the first stage of an investigation of the effects of distortivity and non-trivial topology on conduction of carbon nano-frameworks; a discussion of the effects of Pauli spin statistics on ballistic conduction, which again turns out to have a graph theoretical dimension. Some indications are given of directions for future research.

8.1 The starification construction

Starification is a process in which vertices of a graph are formally replaced by stars, with increasing consequences for conduction properties. In Section 4.5.3, it was mentioned that when chemical graphs with $2 \leq n \leq 14$ are starified “nearly” all stars of the parent chemical graphs are distinct omni-insulators. However, there exist cases where the star of the parent chemical graph is not a distinct omni-insulator. These cases seem to be rare and are counted in Table 8.1 for $n \leq 10$.

A vertex of degree one or two of the original graph corresponds to a core-forbidden vertex in the star. This is because a pendant vertex on a leaf puts a zero on its

$n(\text{Parent})$	2	3	4	5	6	7	8	9	10
$N(\text{Parent})$	1	2	6	10	29	64	194	531	1733
$N(\text{distinct omni-insulator})$	1	2	5	9	25	60	180	508	1660
$N(\text{other})$	0	0	1	1	4	4	14	28	73

Table 8.1: A count for the stars of a parent graph that lead to distinct omni-insulators ($N(\text{distinct omni-insulator})$) and other cases ($N(\text{other})$), where $n(\text{Parent})$ is the number of vertices in the parent chemical graph and $N(\text{Parent})$ is the number of graphs on $n(\text{Parent})$ vertices.

neighbouring vertex. Then this vertex puts a zero on all vertices connected to it in the parent graph. As the parent graph is a connected graph, then all original vertices are core-forbidden. On the other hand, if one original vertex in the star is core, then all are, by the same connectedness argument. We may also remark the following. A well known result often used when determining the nullity of a given graph is that the nullity remains unchanged when deleting an end-vertex and its neighbour. Here we give our proof. Moreover, when an end vertex together with its neighbour is removed, the type of vertex remains unchanged within the vertex-deleted subgraph.

Lemma 8.1.1 *Let G be a graph with an end vertex \bar{L} and neighbour \bar{R} . Then the nullity of $G - \bar{L} - \bar{R}$ is equal to the nullity of G . Also, the core vertices in $G - \bar{L} - \bar{R}$ are exactly the same as in G .*

Proof: Let the adjacency matrix be labelled such that the end vertex and its neighbour are labelled last.

$$\left(\begin{array}{ccc|cc} & & & * & 0 \\ & & & \vdots & \vdots \\ & G - \bar{L} - \bar{R} & & * & 0 \\ \hline * & \dots & * & 0 & 1 \\ 0 & \dots & 0 & 1 & 0 \end{array} \right) \begin{pmatrix} x \\ \dots \\ y \\ z \end{pmatrix} = \begin{pmatrix} 0 \\ \vdots \\ 0 \\ 0 \\ 0 \end{pmatrix} \quad (8.1)$$

If G is a graph that has an end vertex then removing this end vertex and its neighbour leaves $G - \bar{L} - \bar{R}$. From Eq. (8.1) y is 0 and $(G - \bar{L} - \bar{R})x = 0$. Moreover the nullity of $G - \bar{L} - \bar{R}$ is equal to the nullity of G . This is because there is a 1-1 correspondence between the kernel eigenvectors in $G - \bar{L} - \bar{R}$ and the kernel eigenvectors in G , and whatever z is, this 1-1 correspondence holds. So the number of linearly independent vectors in the nullspace of G is equal to the number of linearly independent vectors \mathbf{x} in the nullspace of $G - \bar{L} - \bar{R}$. Also, on removing the end vertex and its neighbour, the non-zero entries of x for $G - \bar{L} - \bar{R}$ will be the same as in G . Hence, the core and core-forbidden vertices in $G - \bar{L} - \bar{R}$ are the same as those in G . ■

8.1.1 The rare cases

In all examples found so far the rare cases where the star of a parent chemical graph is not a distinct omni-insulator results from the parent chemical graph belonging

to the family of the cubic graphs and their decorations by subdivision of a triangle edge, addition of paths on a triangle edge, and subdivision of disjoint triangle edges on addition of some other motifs on edges. These graphs have conduction taking place when the selected vertices \bar{L} and \bar{R} of a device are non-adjacent in the star and both are inserted vertices of the star (Fig. 8.1).

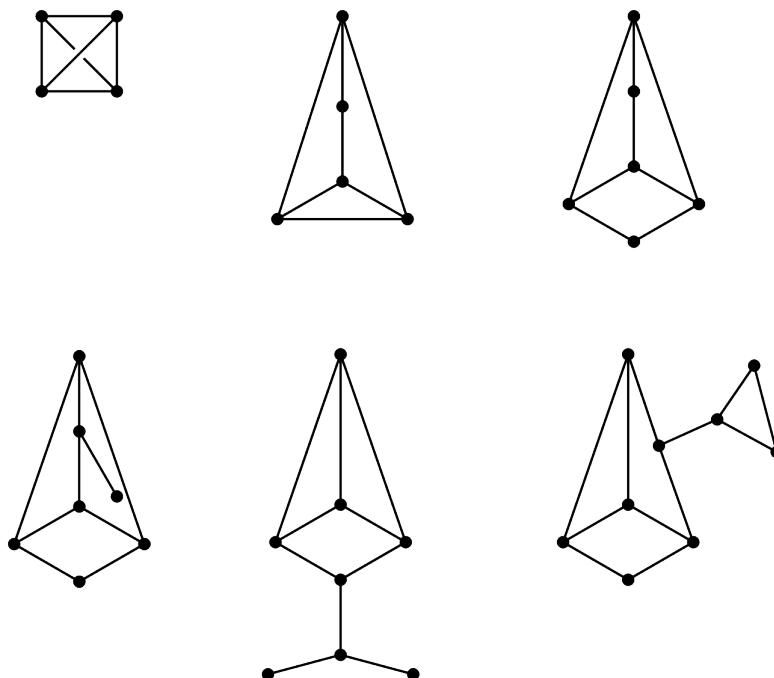


Figure 8.1: A selection of parent chemical graphs that have stars which are not distinct omni-insulators.

However, further investigation via computational tests showed that there are 19 cubic graphs on 10 vertices and only 14 of these give exceptions, that is, five of them follow the general conjecture that their star is a distinct omni-insulator. These are shown in Fig. 8.2.

It also results that $K_{3,3}$, the complete bipartite graph on 6 vertices, is an insulator and its star is not a distinct omni-insulator. This means that *some* of its devices conduct. This conduction takes place when selecting the device in such a way that both \bar{L} and \bar{R} are original vertices in the star of $K_{3,3}$. This also happens for the stars of the graphs shown in Fig. 8.3.

These sporadic observations do not immediately lend themselves to formal proof, but one area where it has been possible to find mathematical proofs is in the study of starified trees.

8.1.2 Trees and their stars

In graph theory, a tree is an undirected graph in which any two vertices are connected by exactly one path. Is a tree an omni-conductor or an omni-insulator? From Theorem 4.5.1, we have that no tree is an *ipso* omni-conductor, and no tree with an odd number of vertices is an *ipso* omni-insulator. The only tree that is a distinct omni-conductor is K_2 . Other quantitative results are presented in Tables 4.9 and

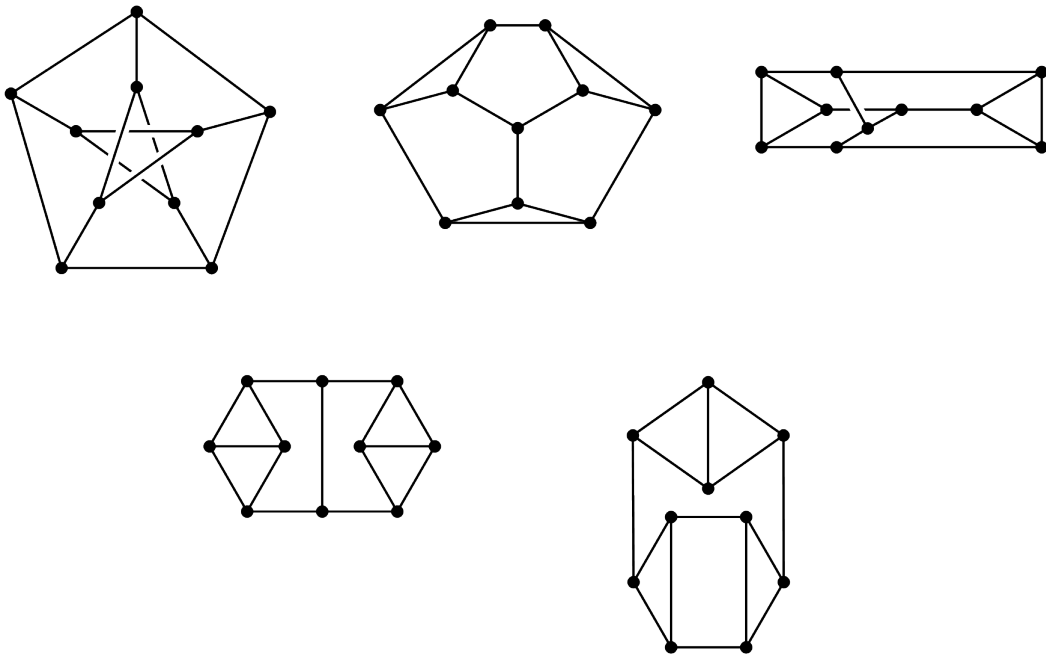


Figure 8.2: The five cubic parent chemical graphs that give distinct omni-insulators when starified.

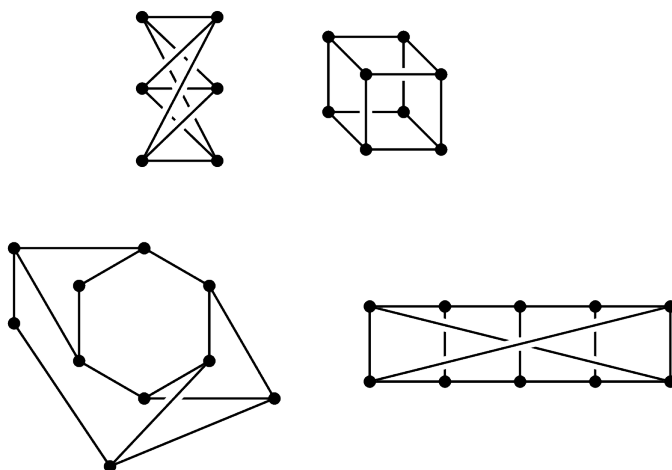


Figure 8.3: Some other examples of graphs that do not have a distinct omni-insulator star.

4.10 in Section 4.5.1. Trees have pendant edges and so Lemma 8.1.1 proves to be very useful.

If a tree has n vertices of which p are pendant vertices, then the number of vertices of the star of a tree is $3n + 1$, and the number of duplicate pendant vertex pairs is p . What is interesting is that the star of a tree is a distinct omni-insulator, but a mixed *ipso* device, i.e. 2LA IX. The latter case can easily be proved, since the star of a tree is a bipartite graph whose vertices are core vertices or upper core-forbidden vertices, that is, no vertex is a middle core-forbidden vertex (proof of this is given in Section 3.5.1). The star of a tree has both of these types of vertices, and core vertices give rise to conduction and upper core-forbidden vertices give rise to insulation in an *ipso* device. Hence, in the TLA code introduced in Section 5.3 this will be ****X**. We can also prove the following for a star of a tree.

Theorem 8.1.1 *The original vertices of a star of a tree are all upper core-forbidden vertices.*

Proof: In a star, there are two leaves adjacent to each original leaf. Thus, at the position of an original leaf there exists an upper core-forbidden vertex as obtained by considering the zero-sum rule for each row of $\mathbf{Ax} = \mathbf{0}$. A subdivided edge exists between a pair of original vertices. Thus, both original vertices are upper core-forbidden vertices. By propagation and using the zero-sum rule, all original vertices are upper core-forbidden. ■

Theorem 8.1.2 *The inserted vertices of a star of a tree are all core vertices.*

Proof: We claim that the nullity of the star of a tree decreases when an inserted vertex is removed. There are fewer original vertices than inserted ones. Each of the pendant vertices is adjacent to a neighbour which is an original vertex of the tree. Deleting both vertices of a pendant edge successively as they appear in the resulting subgraph, creates $n + 1$ isolated vertices, all of which were core vertices in the star. Indeed, when deleting pendant vertices and their neighbours, as they appear in this process, all original vertices are removed, leaving $(3n+1)-(2n)$ which gives the nullity. ■

To obtain the signature of a device for all possible pairs of distinct vertices from a star of a tree results in the following possibilities, taking into consideration the allowed cases for bipartite graphs:

1. An edge where the vertices are a pendant inserted vertex (CV) and a neighbouring original vertex (CFV_{upp}): Case D5 Insulation
2. An edge where the vertices are a non-pendant inserted vertex (CV) and a neighbouring original vertex (CFV_{upp}): Case D5 Insulation
3. A non-edge where the vertices are a pendant inserted vertex (CV) and a non-neighbouring original vertex (CFV_{upp}): Case D5 Insulation
4. A non-edge where the vertices are a non-pendant inserted vertex (CV) and a non-neighbouring original vertex (CFV_{upp}): Case D5 Insulation

5. A non–edge where the vertices are an original vertex (CFV_{upp}) and a non-neighbouring original vertex (CFV_{upp}): Case D1 Insulation or Case D2 Conduction
6. A non–edge where the vertices are an inserted vertex (CV) and a non-neighbouring inserted vertex (CV): Case D11 Insulation or Case D9 Conduction

Hence, it remains to show that for the stars of trees to follow the TLA code IIX and qualify as distinct omni–insulators but mixed *ipso* devices, Cases D2 and D9 are non–realisable, as we now show. First we need to present a simple way of determining a basis for the nullspace of \mathbf{A} .

Proposition 8.1.2 *For a degree one vertex v adjacent to a unique neighbour i , $\alpha_i = 0$, where α_i is the i th entry of the kernel eigenvector.*

Proof: From $\mathbf{Ax} = \mathbf{0}$, select the row corresponding to vertex v which has degree one and is adjacent to a unique neighbour i . Then

$$e_v^T Ax = 0 \Rightarrow \left(0 \quad \dots \quad 0 \quad 1 \quad 0 \quad \dots \quad 0 \right) \begin{pmatrix} \alpha_1 \\ \vdots \\ \alpha_n \end{pmatrix} = \begin{pmatrix} 0 \\ \vdots \\ 0 \end{pmatrix} \quad (8.2)$$

Hence,

$$\alpha_i = 0 \quad (8.3)$$

where the neighbourhood of v is $N(v) = \{i\}$. ■

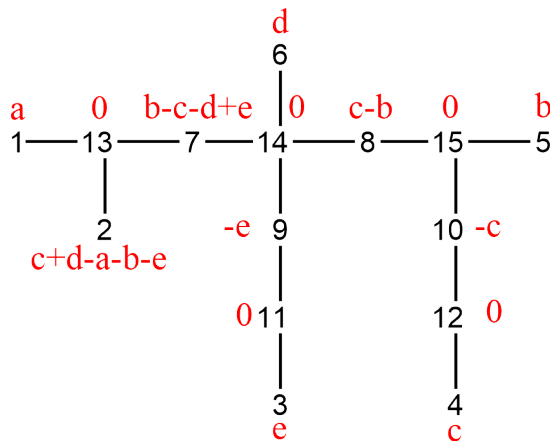


Figure 8.4: A general tree on 15 vertices. The black labelling refers to the vertices. The red labelling refers to the weighting set on each vertex which are the entries of a generalised eigenvector.

The zero–sum rule is a technique used to generate the generalised kernel eigenvector. This gives the basis for the nullspace, $\ker A$, and yields the nullity as well. For g_s , a

generalised eigenvector is a linear combination of g_s parameters (degrees of freedom) obtained using $\mathbf{Ax} = \mathbf{0}$. The g_s linearly independent eigenvectors can be obtained by setting one parameter equal to one and the rest zero. Fig. 8.4 shows a graph on 15 vertices. Vertices 11, 12, 13, 14 and 15 are given a zero entry as they are adjacent to a pendant vertex (vertices 1, 2, 3, 4, 5 and 6). Each of the pendant vertices, except vertex 2, is given a weighting a , b , c , d and e , respectively. The labels on the other vertices are listed in such a way that the zero-sum rule is obeyed. For example, vertex 10 has a labelling of $-c$ since vertex 4 is labelled with c . When combined together, they give zero as a sum on vertex 12. With this labelling, the generalised eigenvector of the graph in Fig. 8.4 is:

$$\begin{pmatrix} a \\ c + d - a - b - e \\ e \\ c \\ b \\ d \\ b + e - c - d \\ c - b \\ -e \\ -c \\ 0 \\ 0 \\ 0 \\ 0 \\ 0 \end{pmatrix}$$

This means that the graph has a nullity of five and so has five linearly independent eigenvectors, one of which is:

$$\begin{pmatrix} 1 \\ -1 \\ 0 \\ 0 \\ 0 \\ 0 \\ 0 \\ 0 \\ 0 \\ 0 \\ 0 \\ 0 \\ 0 \\ 0 \\ 0 \end{pmatrix}$$

by setting $a = 1$ and $b = c = d = e = 0$. The other four eigenvectors can be generated in a similar way.

We can now show that cases D2 and D9 are not realisable.

Theorem 8.1.3 *Case D2 is non-realizable for a pair of upper CFVs of a star of a tree.*

Proof: Let the pair of vertices selected for the device be $\bar{L} = \text{CFV}_{upp}$ and $\bar{R} = \text{CFV}_{upp}$. \bar{R} remains an upper core-forbidden vertex in $G - \bar{L}$, where G is the star of a tree, because the neighbours of \bar{L} become end-vertices and remain core vertices. So, the nullity of $G - \bar{L} - \bar{R}$ is $g_s + 2$. This is Case D1 that gives rise to insulation. Hence, any CFV-CFV pair in a device of a tree gives rise to insulation, not conduction. ■

Theorem 8.1.4 *Case D9 is non-realizable for a pair of CVs of a star of a tree.*

Proof: Whenever a CV is removed, the nullity of the graph decreases by one, and it leaves all other inserted vertices as CVs. This is because by the zero-sum rule, around any original vertex there are two parameters (or degrees of freedom) in the generalised kernel eigenvector. This means that the second inserted vertex removed is also a CV and so the nullity decreases further by one. This is Case D11 and not D9. Hence, any CV-CV pair in a device of a tree gives rise to insulation, not conduction. ■

As mentioned in the proof of Theorem 8.1.2, the nullity of a star of a tree is $n + 1$. Here we give another proof:

Theorem 8.1.5 *The nullity of a star of a tree is $n+1$, where n is the number of vertices of the tree.*

Proof: The degree of an original vertex in a star of a tree is three. This gives rise to a new parameter in the generalised kernel eigenvector when using the zero-sum rule. Now, when a pendant edge of a star is removed, the nullity remains unchanged (Case D5). Repeating the process, leaves g_s isolated vertices that were inserted (core) vertices in the star. Thus, the star of a tree is left with $n+1$ isolated vertices and its nullity is $n+1$. ■

In future work it would be interesting to extend this formal mathematical analysis to wider families of graphs and their stars, for example, general bipartite graphs and regular graphs. It is also possible that other constructions with tendencies to influence conduction behaviour in particular ways will emerge.

8.2 Conduction in distortive and topologically exotic carbon frameworks

So far, unweighted graphs with all β equal have been considered and the predictions for $T(E)$ are independent of the choice of $\tilde{\beta}^2$ parameters. However, weighted graphs can be used to describe important phenomena in chemistry such as Jahn-Teller and Peierls distortion. Also unweighted graphs give physically incorrect results in certain limiting cases, for example, as $n \rightarrow \infty$, the Hückel model for the even path P_n has a HOMO-LUMO gap that tends to zero, but in fact a gap remains in real systems.

Hence, this gives an incorrect picture of the electronic structure and by implication even of the conduction.

We did some work to address this issue and the main results have been published in “Spectra and structural polynomials of graphs of relevance to the theory of molecular conduction” *Ars Math. Comp.* **13**, 379–408, 2017, Fowler, Pickup, Sciriha and Borg [156]. This work is too long for inclusion in this thesis and so the present section just summarises the main points and indicates the future use of this toolkit. The published paper is an archive of exact results on which to base an elaboration of the theory of molecular conduction, where the new formulae will allow us to treat π distortivity and its effect on ballistic conduction through conjugated molecular frameworks of increasing size [63,82], as predicted within the source–sink potential (SSP) approach of Ernzerhof *et al.* [55,81,127,143].

In graph theoretical terms, we can mimic geometric distortion of a molecular framework by studying weighted graphs [157]. The starting point is cycles and paths with alternating edges and/or vertex weights. We obtain all their structural polynomials (s, t, u, v, j) and eigenvectors and use the ‘factorisation’ of larger graphs (finite and practically infinite) as a powerful tool to treat the interpretation of spectra and conduction properties of various families of graphs, such as, ladders and treadmills. We also allow negative edge weights to give access to Möbius graphs [158].

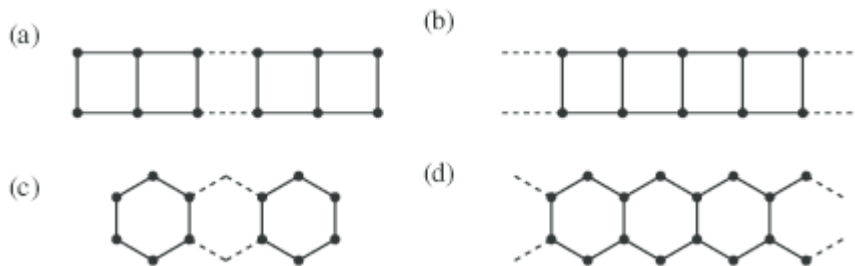


Figure 8.5: Families of graphs treated in [156]: (a) ladders; (b) treadmills; (c) linear polyacenes; (d) cyclic polyacenes.

The graphs shown in Fig. 8.5 possess three common features, which are the following:

1. The graphs are bipartite.
2. They possess an involution that allows the graph to be expressed as a product of simpler graphs with known spectra. This means that the characteristic polynomials can be written neatly in terms of products of the characteristic polynomials of certain ‘half’ graphs, comprising vertex–weighted backbones with some in a slightly more complicated form and hence all relevant structural polynomials can be obtained. Note that in Fig. 8.5 the graphs depicted in (c) and (d) are not formally products of graphs, but are derived by subdivision of a subset of original edges in the Cartesian product of paths.
3. The spectrum changes with edge weights, and this is of prime importance in theories of electronic structure, where molecular structures are modelled by graphs. Alternation of edge weights may stabilise a π system. This feature is termed ‘distortivity’ by physical scientists.

It is well known to physicists and chemists that extended overlapping π -electron systems may achieve greater stability by distorting in such a way that bond lengths alternate, and the sharing of electron density across the π -system is reduced. This is known in the physics literature as Peierls distortion [159], and in the chemical literature as Jahn–Teller distortion [160]. It typically affects π -electron systems in such a way as to reduce their conductivity because it opens up a gap in the middle of the spectrum. In order to assess the importance of distortivity for the specific phenomenon of ballistic molecular conduction, we need explicit characteristic polynomials and spectra for families of weighted graphs representing molecules of chemical interest. For all cases we can then get s , t , u , v and j and so have all the tools for calculation of $T(E)$ as a function of connections and relative weights.

As reported in [161], a simple guess for distortion modes of a π system, when combined with symmetry arguments, gives a powerful tool for the qualitative analysis of distortive tendencies of conjugated molecules. This can be achieved by varying Hückel bond parameters subject to the zero-sum rule around each non-pendant graph vertex. The geometries of many conjugated systems result from a compromise between the tendency of a σ framework to produce symmetrical arrangements with equal and near-equal bond lengths, and the opposing tendency of π electrons to favour bond alternation. For example, pentalene (Fig. 8.6) has its π -localised Kekulé structure lower in total energy than the σ -favourable delocalised transition state [162]. The treatment of π distortivity finds its threshold in the eigenvectors of the bond–bond polarisability matrix, by considering its eigenvalue spectrum, in particular the largest eigenvalue. The authors of [137] obtained a critical value where the maximum eigenvalue is $1.8\beta^{-1}$. They conclude that if the system has eigenvalues of larger magnitude, the distortive tendency of the π system will be strong enough to tip the balance between E_π and E_σ , and loss of symmetry will result. In this way, Hückel theory itself provides an internal prediction for when the potential distortions of the molecular framework will in fact happen. As mentioned above, pentalene is an example. Because we have the above criterion, we can then apply our equations to give conduction as a function of the gap in the distorted molecule and observe trends in $T(E)$. The expectation is that distortivity will increase the HOMO–LUMO gap and reduce transmission at the Fermi level, $T(0)$.

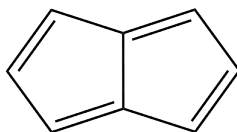


Figure 8.6: Graph representation of pentalene.

8.2.1 Graphs derived from alternating ladders and treadmills

A series of chemically interesting graphs can be derived from our alternating ladders and treadmills by putting one of the two edge (rung) weights to zero, either $a = 0$, or $b = 0$ (see Fig. 8.7).

Some of the graphs that can be derived from ladders are shown in Fig. 8.8. Ladders with backbone chains with odd numbers of vertices lead to polyacenes with arms

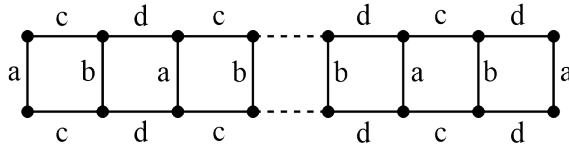


Figure 8.7: Linear ladder showing rung weights a and b and riser weights c and d .

and legs, or to polyacenes themselves (Fig. 8.8(a) and 8.8(b)), by putting the first rung edge parameter or the second to zero. Even-vertex backbones give polyacenes with a single arm and leg, as shown in Fig. 8.8(c), whichever rung weight is set to zero. In the case of treadmills, it does not matter which rung weight is set to zero. In either case one obtains cyclic polyacenes. The appropriate formulae obtained for alternating ladders and alternating treadmills for eigenvalues, eigenvectors and structural polynomials can be used in these cases.

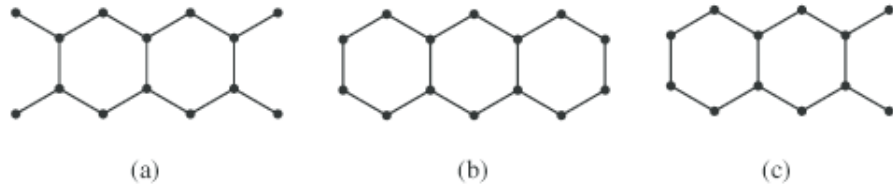


Figure 8.8: Graphs derived from ladders by zeroing rung parameters to zero: (a) $L_{14}(0, 1 | 1, 1)$, with two 7-vertex backbone chains, $a = 0$; (b) $L_{14}(0, 1 | 1, 1)$, with two 7-vertex backbone chains, $b = 0$; (c) $L_{12}(1, 0 | 1, 1)$, with two 6-vertex backbone chains, $b = 0$.

Certain graphs with edge weights having flipped signs, and/or with a pair of crossed backbone edges can be included (see Figs. 8.9 and 8.10). These flipped and crossed graphs are sometime called Möbius graphs [158].

Representation of the various structural polynomials in the ‘factorised’ form has advantages for understanding the structure of the spectrum and has implications for the physics of the transmission as a function of the energy of the incoming electrons. In certain cases, for example, conduction is switched off for the whole range of accessible energies, E [156].

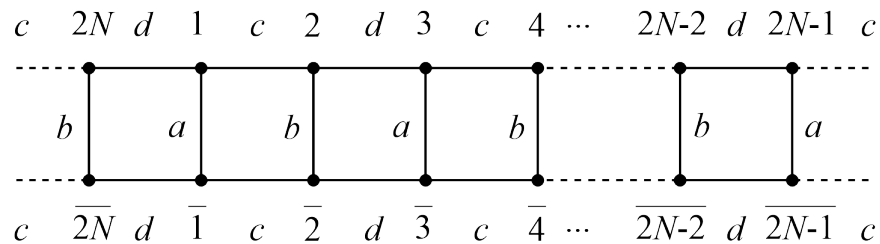


Figure 8.9: A treadmill with $4N$ vertices and alternating rung ($a; b$) and ring edge weights ($c; d$).

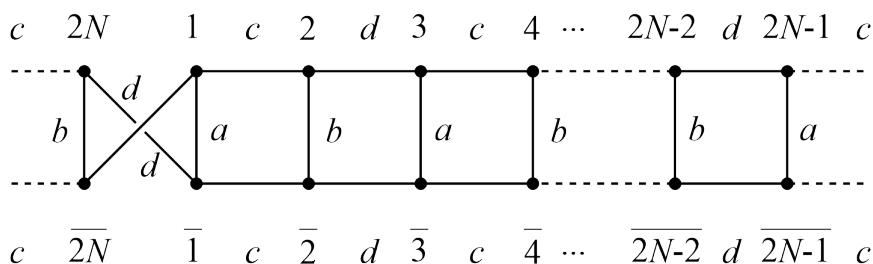


Figure 8.10: A Möbius treadmill with $4N$ vertices and alternating rung (a ; b) and ring edge weights (c ; d).

8.3 Including the Pauli exclusion principle in the SSP model for MEDs

Throughout this thesis, the classification of conduction types is carried out within an ‘empty–molecule’ description. In order to achieve a more realistic, many–electron ground–state picture, theoretical and computational adaptations should be made to the Hückel SSP model of ballistic conduction in single molecules to include the effects of the Pauli exclusion principle. This would imply that an incoming electron cannot occupy an orbital in the molecule that is already occupied by an electron of the same spin. Hence, there can be different transmission functions $T(E)$ for incoming spin–up and spin–down electrons.

Work within the group has started to deal with this effect of spin statistics on conduction. The first application is to systems with a fixed molecular electronic configuration that are then attached to the leads in an MED. This case is relevant to situations in which the system is subjected to a bias potential that traps electrons on the molecular bridge. Here we note the work already carried out, and suggest some possible extensions. This section relies heavily on “A Hückel source–sink–potential theory of Pauli spin blockade in molecular electronic devices” *J. Chem. Phys.* **145**, 204113, 2016, Pickup, Fowler and Sciriha [134], and discusses some results described in “Inclusion of Pauli effects in a simple graph theoretical model of ballistic molecular conduction”, which is a thesis by Seville presented in partial fulfilment of the requirements for the degree of MChem at the University of Sheffield [163].

8.3.1 From the ‘empty–molecule’ to the many–electron picture

The main result of the work on the Pauli–SSP model in [134] is that the SSP formulation for the ‘empty–molecule’ can be carried over to the ‘occupied molecule’ by retaining the four–polynomial formalism, keeping the spectral expansions, but removing terms corresponding to spin–orbitals occupied by electrons of the same spin as the incoming ballistic electron. The restricted structural polynomials obey the interlacing properties of the full polynomials and hence preserve a case/selection rule structure.

These important subcases for Fermi–level conduction are identified in [163]. These are Empty (all E available for transmission), Fermi–Empty ($E \leq 0$ available, all the

bonding orbitals are occupied), and Fermi-Full ($E < 0$ available, all the bonding and non-bonding orbitals are occupied) (see Fig. 8.11). An interesting feature of the new model is that it allows ‘Pauli Blockade’ where conduction of electrons of spin σ is reduced in the region of the eigenvalues for all molecular orbitals that already contain an electron of spin σ .

The authors of [134] comment that the new restricted structural polynomials are no longer the characteristic polynomials of specific vertex-deleted graphs, but their forms as sums over states of the molecular eigenvalues (see for example Eq. (3.2) in Chapter 3 and Eqs (7.34) and (7.41) in Chapter 7) are retained. Fermi-Empty molecules lose half of the terms in the non-nullspace part of the expansion owing to occupation of orbitals with $E > 0$. Consequently, cases that had zero transmission, produced by cancellation of sums over bonding and antibonding shells (predominantly bipartite graphs), will typically now give non-zero conduction. The Fermi-full cases also lose these terms in the non-nullspace part of the expansion, but additionally, all of the nullspace (non-bonding) terms are lost [163].

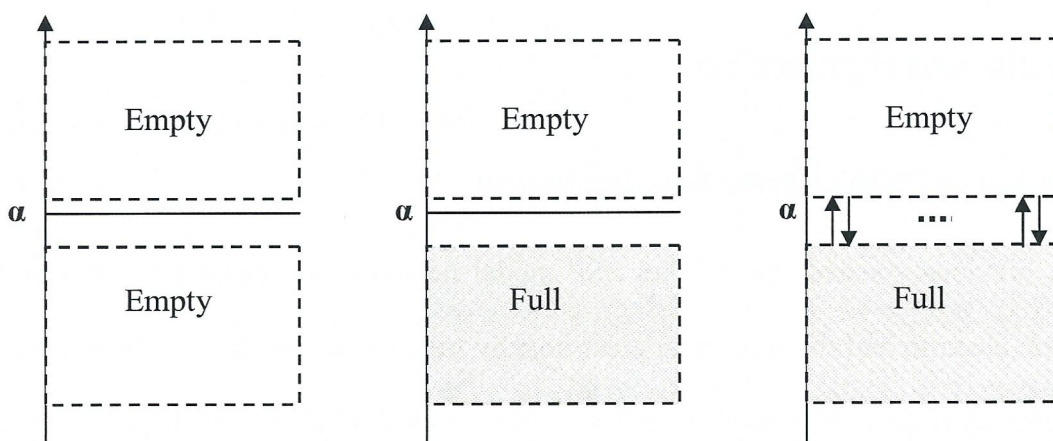


Figure 8.11: ‘Empty’, ‘Fermi-Empty’ and ‘Fermi-Full’ molecules (figure adapted from [163]).

In the Fermi-Empty case, the ballistic electron is free to move through all the non-bonding and antibonding channels, thus effectively giving the same set of nullities for the graph as the ‘empty’ molecule. In the Fermi-Full case, conduction is only possible through antibonding orbitals, changing the effective nullity of the graph to zero, as the NBOs are no longer available.

Within the empty molecule picture, all molecular-orbital channels are left open to the incoming electron, whereas real molecules, have occupied molecular orbitals, and therefore some closed channels. It is clear that modification is required to build up a more realistic, many-electron picture that does not overlook Coulomb [164, 165] and Pauli [166] Blockade effects, i.e., increased resistance caused by either electronic repulsion or occupied spin-orbitals within the device, respectively. The work by Pickup *et al.* [134] was a first step, retaining the advantages of the previously defined formalism whilst including the molecular electrons. As the authors of [134] point out, there is no explicit electron-electron interaction in the Hückel tight-binding model, and so all many-electron effects within the model arise from the Fermi statistics. In this treatment, the many-electron part of the wavefunction is localised on the

molecule, and the N electrons inside the molecule, apart from their statistical effect, are passive spectators to ballistic conduction.

As reported in [134], Pauli Spin Blockade (PSB) has been identified as an experimental effect in [167]. As Perron *et al.* note, PSB has played a role in investigations of the physics of spin-to-charge conversion [168]. PSB has implications for spintronics [169–171]. The PSB effect has also been noted by Ernzerhof *et al.* [128, 132] who applied the SSP method to molecular conduction, introducing electron interactions by means of the Hubbard potential [172]. Pickup *et al.* [134] do not consider electron–electron repulsion directly, but instead focus on the effects of fermion statistics on non-interacting many-electron states: these lead to the closing down of conduction channels associated with energies below the Fermi level. Further effects, in which Pauli Spin Blockade may be lifted, or even reversed, depend on the application of external magnetic fields, were not yet included in their treatment [168, 173–176]. Work on including electron correlations within the molecule and variable electron count on the molecular bridge is ongoing (B.T. Pickup and P.W. Fowler, personal communication).

8.3.2 Some mathematical consequences of the Pauli SSP model

In the context of the present thesis, it is interesting to consider the mathematical differences between Pauli and empty molecule SSP models. In particular, reference [134] includes a discussion of how the selection rules and classification of conduction/insulation cases will be affected.

One major result of the work reported in [134] is that the selection rule approach can still be applied, with necessary changes. Table 8.2 lists the new selection rule cases, and for the most part follows previously published tables such as Tables III and I in [84] and [82], respectively, and the Tables 4.4 and 7.1 in Chapters 4 and 7, respectively. As before the table classifies cases as conducting or insulating, based on multiplicities of the energy E as a root ϵ_A of polynomials s , t , u , v and j , and as in [82], shows active and inert channels (in the table, active channels have $J_{L \rightarrow A}(\epsilon) \neq 0$). For most lines in the table, the only difference from previous versions is that the structural polynomials are restricted spectral expansions; the extra lines PSB and PPR refer to Pauli Spin Blockade (where the shell A has its full complement of electrons of the same spin as the ballistic electron) and Pauli Perfect Reflection (when the restricted j polynomial sum vanishes at all energies, i.e. when at least one terminal vertex is core-forbidden for all included shells). As an aside, we note that the diagram (Fig. 2) given in [134] to illustrate an excited state of pentalene appears to have a typo, in that the occupied anti-bonding molecular orbital should be number 7 not number 6 to achieve PPR.

8.3.3 What survives under the Pauli Effect

The work presented by Seville in [163] shows that many properties presented in earlier work, such as [84] and [104], survive under the inclusion of the Pauli Effect but omni-insulation is not as common as before. The molecules become more conductive

Kind	r_A	Case	g_t	g_u	g_v	g_j	$T(\epsilon_A)$	$J_{p \rightarrow q}^{\text{bond}}(\epsilon_A)$	$J_{L \rightarrow A}(\epsilon)$
Two CFVs	0	D1	$g+1$	$g+1$	$g+2$	$\geq g+1$	0	0	0
	0	D2	$g+1$	$g+1$	g	g	$\neq 0$	$\neq 0$	0
	0	D3	$g+1$	g	$g+1$	$\geq g+1$	0	0	0
	0	D4	$g+1$	g	g	g	$\neq 0$	$\neq 0$	0
	0	D6	g	g	$g+1$	g	$\neq 0$	$\neq 0$	0
	0	D7.1	g	g	g	g	$\neq 0$	$\neq 0$	0
	0	D7.2	g	g	g	$\geq g+1$	0	0	0
CV and CFV	1	D5	$g+1$	$g-1$	g	$\geq g$	0	0	0
	1	D8	g	$g-1$	$g-1$	$\geq g$	0	0	0
Two CVs	1	D9	$g-1$	$g-1$	g	$g-1$	$\neq 0$	$\neq 0$	$\neq 0$
	1	D10	$g-1$	$g-1$	$g-1$	$g-1$	$\neq 0$	$\neq 0$	$\neq 0$
	2	D11.1	$g-1$	$g-1$	$g-2$	$g-1$	0	0	$\neq 0$
	2	D11.2	$g-1$	$g-1$	$g-2$	$\geq g$	0	0	0
CFV	0	I1	$g+1$	–	–	–	0	0	0
		I2	g	–	–	–	$\neq 0$	0	0
CV	1	I3	$g-1$	–	–	–	$\neq 0$	0	$\neq 0$
–	–	PSB	–	–	–	–	0	0	0
≥ 1 CFV	0/1	PPR	–	–	–	–	0	0	0

Table 8.2: Conduction cases for *distinct* and *ipso* molecular devices in the Pauli regime, showing the kind of the vertex pair for the device, the *rank* of the connection matrix r_A for shell A with eigenvalue ϵ_A and degeneracy g , the total transmission $T(\epsilon_A)$, and the bond currents $J_{p \rightarrow q}^{\text{AO}}(\epsilon_A)$. The numbers of repeated roots in structural polynomials, t , u , v , and j are g_t , g_u , g_v , and g_j , respectively. The shell current $J_{L \rightarrow A}(\epsilon)$ applies for *any* energy. CV and CFV stand respectively for core and core-forbidden vertices (defined with respect to the eigenspace A). Case PSB is Pauli Spin Blockade. Case PPR (Pauli Perfect Reflector) occurs when the structural polynomial $j(\epsilon)$ is zero for all values of ϵ [134].

as they progress from Empty to Fermi–Empty to Fermi–Full states. These results are derived from computations based on the decision–trees given in Tables 4.2 and 4.3, rather than on the pure nullity arguments of the selection–rule approach.

An interesting feature arising from the presence of molecular electrons is that there shall be no shell currents that involve spin–orbitals occupied by electrons with a spin opposite to that of the incoming electron. This Pauli Blockade removes the energy levels of occupied spin–orbitals from the structural polynomials and so the transmission peaks at energies below the Fermi level are removed [134] (see Fig. 8.12).

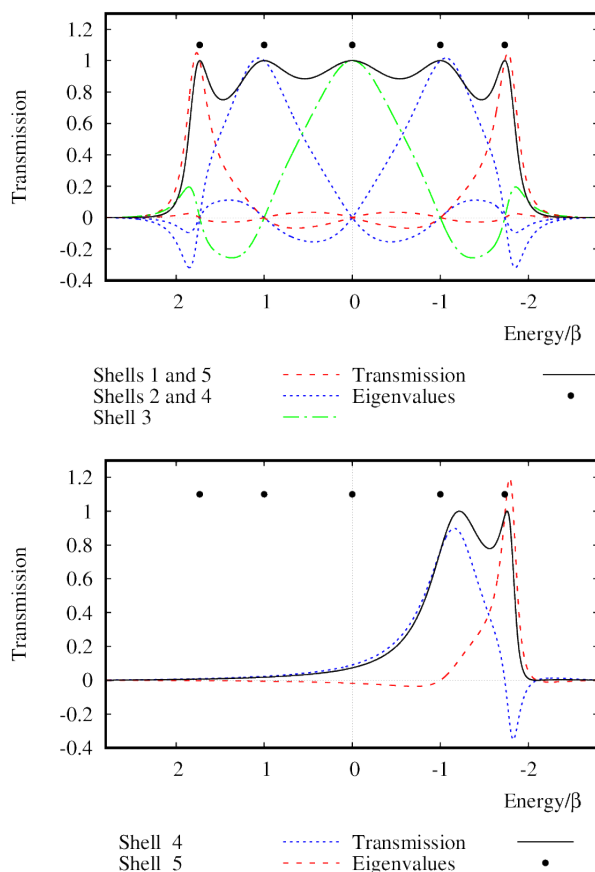


Figure 8.12: A five–membered chain with terminal connections to source and sink. The diagrams show transmission and shell currents for the device with 0 and 3 molecular electrons having the same spin as the incoming electron. Orbital energies are shown for reference as black circles above the curves [134].

The report by Seville [163] gives calculations on large samples of graphs showing how the TLA classifications (Chapter 5) change with inclusion of the Pauli Effect. In other words, a variable TLA profile as we go from Empty to Fermi–Empty to Fermi–Full. Families show specific profiles. For example, Seville found that antiaromatic $(4N)$ -cycles change from ICC to ICC to CCC for Empty to Fermi–Empty to Fermi–Full, whereas aromatic $(4N+2)$ -cycles change from CII to CCC to CCC. Also, bi–cycles with $2p = 4N + 2$, $2q = 4N' + 2$ and prisms with $2p \neq 6N$ are strong omni–conductors for the Fermi–Empty and Fermi–Full states.

For bipartite graphs, examples of 19 distinct profiles were found. For all of these cases, except Case 5, the number of Is and Xs in the TLA never increase and the number of Cs never decreases. All devices become *ipso* omni–conductors for both the

Fermi–Empty and Fermi–Full cases, except Case 5 Fermi–Full which still remains an *ipso* omni–insulator.

The Seville project was also the first place in which the Venn–like diagram of the 2LA appeared, and this was taken up in the work on which Chapter 5 of this thesis is based. Seville gives the smallest example of each of the 2LA cases in order to eliminate the need for formal existence proofs. However, it would be interesting in future work to check the completeness of this observation using more formal methods, analogous to those used in Chapters 5 and 6.

8.4 Conclusion

In conclusion, it has been shown that the techniques available in spectral graph theory continue to open new avenues in the understanding of electron behaviour in π –molecules. Through the exploration of mathematical results, one can predict hitherto unknown electron behaviour in molecules and in turn to establish a sound theoretical base for the yet unknown mechanisms in this area of nanotechnology. As Ratner states in [20], “there are so many possible molecular structures (that) the understanding of molecular transport is still in its infancy ... but molecular electronics is a vibrant and dynamic area of science and technology, and numerous challenges and opportunities lie ahead”. Graph theory has a role as one of the tools for solving these challenges.

Chapter 9

Overview

The point of view taken in this thesis is that the SSP (source-and-sink potential) model developed initially by the Ernzerhof group provides a useful qualitative description of elastic (ballistic) conduction at low bias through a single-molecule empty device. Furthermore, the inspiration for the mathematical treatment described here is that the main conclusions of SSP for conduction in π systems appear to arise from its close correspondence to the purely graph-theoretical treatment of an adjacency problem with scattering boundary conditions.

The starting point is the previously derived expression for transmission of a two-wire device as a function of energy and placement of connections. Transmission of a device $\{G, \bar{L}, \bar{R}\}$ of energy E depends on four polynomials s, t, u, v and in particular on their combination $j^2 = ut - sv$. The polynomials are respectively the characteristic polynomials of $G, G - \bar{L}, G - \bar{R}$ and $G - \bar{L} - \bar{R}$ where G is the molecular graph and \bar{L}, \bar{R} are the connection vertices in G .

Chapter 3 shows how the classification of vertices of a graph based on the Interlacing Theorem leads to predictive selection rules for conduction at the zero of energy (physically, the Fermi level). Conduction depends critically on the number of non-bonding orbitals of the four π systems corresponding to $G, G - \bar{L}, G - \bar{R}$ and $G - \bar{L} - \bar{R}$, with the key feature being the *nullity class* of G (where $g_s(G) = 0, 1$ or > 1).

The idea of omni-conduction and omni-insulation were introduced in Chapter 4, as descriptions of generic conduction behaviour for classes of devices based on a given molecular graph. This led to observations of systematic conduction behaviour within families of chemical graphs. It is proved that all combinations of distinct and *ipso* behaviour are mathematically possible (and physically realised), apart from the ‘strong insulators’ combination of insulation for *all* devices.

Chapter 5 extends this classification to bipartite graphs, using a finer level of detail where inter, intra and *ipso* devices are defined for $\bar{L} \neq \bar{R}$ in different partite sets, $\bar{L} \neq \bar{R}$ in the same partite set, and $\bar{L} = \bar{R}$. It is proved that of the 81 hypothetically possible classes of devices, only 14 are realisable by a connected simple graph, with at least 13 realisable by chemical graphs.

Chapter 6 makes a final extension of this three-letter acronym system to cover all graphs, bipartite and non-bipartite. The key is to redefine the inter and intra classes

of device as those with odd and even (non-zero) graph theoretical distance between connections. Of the 81 hypothetically possible classes of device, 42 are proved to be unrealisable by any graph, 35 are realised by small example graphs (in at least 28 cases chemical), leaving four ‘stubborn’ unresolved cases.

Chapter 7 shows how the SSP model can be reformulated in terms of transmission through eigenchannels based on shells of molecular orbitals (eigenvectors) corresponding to degenerate eigenvalues of the adjacency matrix of the molecular graph. The reformulation has mathematical advantages in that it avoids singularities at extreme values of reflection coefficient, and chemical advantages of interpretability in terms of active and inert channels.

Chapter 8 shows that a construction for omni-insulators described earlier (Chapter 4) can be proved. It is shown that the star of a tree is an omni-insulator for only distinct pair of vertices. To construct a star, each vertex of a parent graph G is replaced by a three-pointed star S_3 , such that pairs of stars corresponding to edges of G are fused by superposition of a terminal vertex of each. The vertices of a star of a tree fall into two classes: the original vertices are all upper core-forbidden vertices, whereas the inserted vertices from the starification construction are all core vertices. This allows partial rationalisation of the observations from extensive calculations. A brief description was also given of mathematical results on factorisation of graph structural polynomials that will allow the treatment in future work of the effects of distortivity of π systems on conduction. The representation of the various structural polynomials in the ‘factorised’ form has advantages for understanding the structure of the spectrum and has implications for the physics of the transmission as a function of the energy of the incoming electrons. This chapter also includes some discussion of recent work from the Sheffield group that deals with improvements of the SSP picture to deal with electron interaction between the electrons on the molecular bridge and the incoming ballistic conduction electron. So far the only interactions included are those described by the Pauli Exclusion Principle. Further refinement to deal with electrostatic repulsion and ultimately electron correlation on the molecular bridge are in progress within the group, though they do not form part of the work carried out by the author of this thesis.

In conclusion, the work in this thesis has shown the power of combining a physical model of conduction with graph-theoretical reasoning. A number of new results have been obtained and will hopefully lead to new and unforeseen technological applications to consolidate molecular electronics as a solid pillar of emerging nanoscience.

Bibliography

- [1] N.L. Biggs, E.K. Lloyd, and R.J. Wilson. *Graph Theory 1736 –1936*. Clarendon Press, Oxford, 1998.
- [2] D.M. Cvetković, M. Doob, and H. Sachs. *Spectra of graphs*. Johann Ambrosius Barth, Leipzig, 1995.
- [3] P.W. Fowler and J. Woolrich. *Chem. Phys. Lett.*, **127**:78–83, 1986.
- [4] T.G. Schmalz, W.A. Seitz, D.J. Klein, and G. E. Hite. *J. Am. Chem. Soc.*, **110**:1113–1127, 1988.
- [5] C.A. Coulson and G.S. Rushbrooke. *Math. Proc. Cambridge Philos. Soc.*, **36**:193–200, 1940.
- [6] H.C. Longuet-Higgins. *J. Chem. Phys.*, **18**:265–274, 1950.
- [7] C. Godsil and G.F. Royle. *Algebraic Graph Theory*. Springer-Verlag, New York, 2001.
- [8] R. Wilson. *Introduction to Graph Theory*. Longman, Harlow, 1996.
- [9] A. Nitzan. *Chemical Dynamics in Condensed Phases Relaxation, Transfer and Reactions in Condensed Molecular Systems*. Oxford University Press, Oxford, 2006.
- [10] A. Nitzan. *Annu. Phys. Rev. Chem*, **52**:681–750, 2001.
- [11] J.C. Cuevas and E. Scheer. *Molecular Electronics an Introduction to Theory and Experiment*. World Scientific, New Jersey, 2010.
- [12] A.R. von Hippel. *Science*, **123**:315–317, 1956.
- [13] A.R. von Hippel. *Molecular Science and Molecular Engineering*. Technology Press of MIT, Cambridge, USA, 1959.
- [14] C. Jia, B. Ma, N. Xin, and X. Guo. *Acc. Chem. Res.*, **48**:2565–2575, 2015.
- [15] J. Munárriz, F. Domínguez-Adame, and A. Malyshev. *Nanotechnology*, **22**:1–7, 2011.
- [16] S. V. Aradhya and L. Venkatraman. *Nat. Nanotechnol.*, **8**:399–410, 2013.
- [17] A. Aviram and M.A. Ratner. *Bulletin of the American Physical Society*, **19**:341, 1974.

- [18] Y. S. Liu and X. Y. Shao, T. Shao, J. Y. Zhang, Y. W. Kuang, D. B. Zhang, Z. G. Shao, H. L. Yu, X. K. Hong, J. F. Feng, X. F. Yang, X. S. Chen, and X. F. Wang. *Carbon*, **109**:411–417, 2016.
- [19] S. Datta. *Quantum Transport: Atom to Transistor*. Cambridge University Press, Cambridge, 2005.
- [20] M.A. Ratner. *Nat. Nanotechnol.*, **8**:378–381, 2013.
- [21] G. Cuniberti, G. Fagas, and K. Richter. *Introducing Molecular Electronics*. Springer, Berlin, 2005.
- [22] J.R. Heath and M.A. Ratner. *Physics Today*, **56**:43–49, 2003.
- [23] G. E. Moore. *Electronics*, **38**:82–85, 1965.
- [24] G. E. Moore. *IEEE Text Speech*, **11**:36–37, 1975.
- [25] G. E. Moore. *IEEE Spectrum: Special Report: 50 Years of Moore’s Law*, **52**:38–57, 2015.
- [26] N. Myhrvold. *The New York Times*, page 3, 7/6/2006.
- [27] D. M. Guldi, H. Nishihara, and L. Venkataraman. *Chem. Soc. Rev.*, **44**:842–844, 2015.
- [28] M. A. Reed. *Proc. IEEE*, **87**:652–658, 1999.
- [29] A. Aviram and M.A. Ratner. *Chem. Phys. Lett.*, **29**:277–283, 1974.
- [30] M. A. Reed. *Nature*, **3**:286–287, 2004.
- [31] R. Wiesendanger. *Scanning probe microscopy and spectroscopy*. Cambridge University Press, UK, 1994.
- [32] J. Ferrer, A. Martin-Rodero, and F. Flores. *Phys. Rev. B*, **38**:10113–10115, 1988.
- [33] A. Martin-Rodero, F. Flores, and N. H. March. *Phys. Rev. B*, **38**:100047–10050, 1988.
- [34] P. Sautet and C. Joachim. *Chem. Phys. Lett.*, **185**:23–30, 1991.
- [35] N. Mingo, L. Jurczyszyn, F. J. Garcia-Vidal, R. Saiz-Pardo, P. L. de Andres, F. Flores, S.Y. Wu, and W. More. *Phys. Rev. B*, **54**:2225–2235, 1996.
- [36] J. Cerdá, M. A. Van Hove, P. Sautet, and M. Salmeron. *Phys. Rev. B*, **56**:15885–15899, 1997.
- [37] G. Rubio, N. Agrait, and S. Vieira. *Phys. Rev. Lett.*, **76**:2302–2305, 1996.
- [38] L. Sun, Y.A. Diaz-Fernandez, T.A. Gschneidner, F. Westerlund, S. Lara-Avila, and K. Moth-Poulsen. *Chem. Soc. Rev.*, **43**:7378–7411, 2014.
- [39] R.M. Metzger. *Chem. Rev.*, **115**:5056–5115, 2015.
- [40] H. Park, J. Park, A. K. L. Lim, E. H. Anderson, A. P. Alivisatos, and P. L. McEuen. *Nature*, **407**:57–60, 2000.

- [41] J. Park, A. N. Pasupathy, J. I. Goldsmith, C. Chang, Y. Yaish, J. R. Petta, M. Rinkoski, J. P. Sethna, H. D. Abrun, P. L. McEuen, and D. C. Ralph. *Nature*, **417**:722–725, 2002.
- [42] H. Grabert and M. H. Devoret. *Single Charge Tunneling: Coulomb Blockade Phenomena in Nanostructures*. Plenum Press, New York, 1992.
- [43] M. A. Reed, C. Zhou, C. J. Muller, T. P. Burgin, and J. M. Tour. *Science*, **278**:252–254, 1997.
- [44] C. Kergueris, J.-P. Bourgoin, S. Palacin, D. Esteve, C. Urbina, M. Magoga, and C. Joachim. *Phys. Rev. B*, **59**:12505–12513, 1999.
- [45] X. D. Cui, Primark A., X. Zarate, J. Tomfohr, O. F. Snakey, A. L. Moore, D. Gust, G. Harris, and S. M. Lindsay. *Science*, **294**:571–574, 2001.
- [46] J. H. Schön, H. Meng, and Z. Bao. *Science*, **294**:2138–2140, 2001.
- [47] A. Bezryadin, C. Dekker, and G. Schmid. *Appl. Phys. Lett.*, **71**:1273–1275, 1997.
- [48] J. Chen, M. A. Reed, A. M. Rawlett, and J. M. Tour. *Science*, **286**:1550–1552, 1999.
- [49] C. P. Collier, E. W. Wong, M. Belohradský, F. M. Raymo, J. F. Stoddart, P. J. Kuekes, R. S. Williams, and J. R. Heath. *Science*, **285**:391–394, 1999.
- [50] C. Dekker. *Physics Today*, **52**:22–28, 1999.
- [51] M.S. Dresselhaus, G. Dresselhaus, and P.C. Eklund. *Science of fullerenes and carbon nanostructures*. Academic Press, San Diego, 1996.
- [52] R. E. Peierls. *Ann. Phys.*, **4**:121–148, 1930.
- [53] N. Xin, J. Guan, C. Zhou, X. Chen, C. Gu, Y. Li, M.A. Ratner, A. Nitzan, J.F. Stoddart, and X. Guo. *Nature Reviews Physics*, **1**:211–230, 2019.
- [54] D. Walter, D. Neuhauser, and R. Baer. *Chem. Phys.*, **299**:139–145, 2004.
- [55] M. Ernzerhof, F. Goyer, M. Zhuang, P. Rocheleau, and H. Bahmann. *J. Chem. Theory Comput.*, **2**:1291–1297, 2006.
- [56] G.C. Solomon, D.Q. Andrews, R.P. Duyne, and M.A. Ratner. *ChemPhysChem*, **10**:257–264, 2009.
- [57] C. Herrmann, G.C. Solomon, J.E. Subotnik, V. Mujica, and M.A. Ratner. *J. Chem. Phys.*, **132**:024103, 2010.
- [58] Y.X. Zhou and M. Ernzerhof. *J. Chem. Phys.*, **132**, 2010.
- [59] A. Baratz and R. Baer. *J. Phys. Chem. Lett.*, **3**:498–502, 2012.
- [60] V. Mujica, M. Kemp, and M.A. Ratner. *J. Chem. Phys.*, **101**:6849–6855, 1994.
- [61] R. Collepardo-Guevara, D. Walter, D. Neuhauser, and R. Baer. *Chem. Phys. Lett.*, **393**:367–371, 2004.

- [62] F. Goyer, M. Ernzerhof, and M. Zhuang. *J. Chem. Phys.*, **126**:144104, 2007.
- [63] B.T. Pickup and P.W. Fowler. *Chem. Phys. Lett.*, **459**:198–202, 2008.
- [64] R. Landauer. *IBM J. Res. Dev.*, **1**:223–231, 1957.
- [65] C. W. J. Beenakker. *Rev. Mod. Phys.*, **69**:731–815, 1997.
- [66] G. Stefanucci and R. van Leeuwen. *Nonequilibrium Many-Body Theory of Quantum Systems*. Cambridge University Press, Cambridge, UK, 2013.
- [67] G.C. Solomon, D.Q. Andrews, R.H. Goldsmith, T. Hansen, M.R. Wasielewski, R.P. Van Duyne, and M.A. Ratner. *J. Am. Chem. Soc.*, **130**:17301–17308, 2008.
- [68] P.W. Fowler, B.T. Pickup, and T.Z. Todorova. *Pure Appl. Chem.*, **83**(8):1515–1528, 2011.
- [69] M. Ernzerhof. *J. Chem. Phys.*, **127**:204709, 2007.
- [70] P.W. Fowler, B.T. Pickup, T.Z. Todorova, and W. Myrvold. *J. Chem. Phys.*, **131**:044104, 2009.
- [71] I. Sciriha and P.W. Fowler. *J. Chem. Inf. Model*, **47**:1763–1775, 2007.
- [72] P. Atkins and J. de Paula. *Physical Chemistry*. Oxford University Press, Oxford, 2010.
- [73] J. N. Murrell, S. F. A. Kettle, and J. M. Tedder. *Valence theory*. John Wiley and Sons, London, 1965.
- [74] S.M. Blinder. Hückel MO Theory. Available at [https://chem.libretexts.org/Bookshelves/Inorganic_Chemistry/Map%3A_Inorganic_Chemistry_\(Housecroft\)/04%3A_Experimental_techniques/4.13%3A_Computational_Methods/4.13C%3A_H%C3%BCckel_MO_Theory](https://chem.libretexts.org/Bookshelves/Inorganic_Chemistry/Map%3A_Inorganic_Chemistry_(Housecroft)/04%3A_Experimental_techniques/4.13%3A_Computational_Methods/4.13C%3A_H%C3%BCckel_MO_Theory).
- [75] A. Streitwieser. *Molecular orbital theory for organic chemists*. John Wiley and Sons, USA, 1962.
- [76] G.B. Arfken and H.J. Weber. *Mathematical methods for physicists*. Academic Press, Orlando, 1985.
- [77] P. Sautet and C. Joachim. *Chem. Phys. Lett.*, **153**:511–516, 1988.
- [78] P. Sautet and C. Joachim. *Phys. Rev. B*, **38**:12238–12247, 1988.
- [79] P. Atkins and R. Friedman. *Molecular Quantum Mechanics*. Oxford University Press, UK, 2007.
- [80] M. Ernzerhof and M. Zhuang. *J. Chem. Phys.*, **119**(8):4134–4140, 2003.
- [81] M. Ernzerhof, M. Zhuang, and P. Rocheleau. *J. Chem. Phys.*, **123**:134704, 2005.
- [82] B.T. Pickup, P.W. Fowler, M. Borg, and I. Sciriha. *J. Chem. Phys.*, **143**:194105, 2015.

- [83] I. Gutman and O. Polansky. *Mathematical Concepts in Organic Chemistry*. Springer–Verlag, Berlin, 1986.
- [84] P.W. Fowler, B.T. Pickup, T.Z. Todorova, M. Borg, and I. Sciriha. *J. Chem. Phys.*, **140**:054115, 2014.
- [85] N. Trinjastić. *Chemical Graph Theory*. CRC Press, Florida, 1992.
- [86] A.L. Cauchy. *Oeuvres complètes d’Augustin Cauchy*. Gauthier–Villars et fils, Paris, 1829.
- [87] P.W. Fowler, B.T. Pickup, T.Z. Todorova, and W. Myrvold. *J. Chem. Phys.*, **131**:244110, 2009.
- [88] I. Sciriha, M. Debono, M. Borg, P.W. Fowler, and B.T. Pickup. *Ars Math. Contemp.*, **6**(2):261–278, 2013.
- [89] R.A. Horn and C.R. Johnson. *Matrix Analysis*. Cambridge University Press, Cambridge, 2010.
- [90] I. Sciriha and I. Gutman. *Util. Math*, **54**:257–272, 1998.
- [91] I. Sciriha. *Discrete Mathematics*, **181**:193–211, 1998.
- [92] C.R. Johnson and B.D. Sutton. *SIAM J. Matrix Anal. Appl.*, **26**:390–399, 2004.
- [93] I. Sciriha. *Linear Algebra Appl.*, **430**:78–85, 2009.
- [94] A.J. Schwenk and R.J. Wilson. *Selected Topics in Graph Theory*, chapter 11, pages 307–336. Academic Press, London, 1978.
- [95] I. Gutman and B. Borovićanin. *Selected Topics on Applications of Graph Spectra*, pages 137–154. Math. Inst., Belgrade, 2011.
- [96] I. Sciriha. *Util. Math.*, **52**:97–111, 1997.
- [97] I. Sciriha. *Ars Math. Contemp.*, **2**(2):217–229, 2009.
- [98] W. Imrich and S. Klavžar. *Handbook of product graphs*. CRC Press, Florida, 2011.
- [99] E. Ghorbani. *Ars Math. Contemp.*, 2016.
- [100] I. Sciriha and A. Farrugia. *Ars Math. Comp.*, **11**:397–402, 2016.
- [101] M. Borg. Master’s thesis, University of Malta, 2010.
- [102] P.W. Fowler, B.T. Pickup, T.Z. Todorova, R. De Los Reyes, and I. Sciriha. *Chem. Phys. Lett.*, **568–569**:33–35, 2013.
- [103] M. Ernzerhof. *J. Chem. Phys.*, **135**:014104, 2011.
- [104] P.W. Fowler, B.T. Pickup, and T.Z. Todorova. *Chem. Phys. Lett.*, **465**:142–146, 2008.
- [105] P.W. Fowler, B.T. Pickup, T.Z. Todorova, and T. Pisanski. *J. Chem. Phys.*, **130**:174708, 2009.

- [106] J.J. Sylvester. *Philos. Mag. Ser. 4*, **1**:295–305, 1851.
- [107] P.W. Fowler, I. Sciriha, M. Borg, V.E. Seville, and B.T. Pickup. *J. Chem. Phys.*, **147**:164115, 2017.
- [108] I. Sciriha. *Electronic Journal of Linear Algebra*, **16**:451–462, 2007.
- [109] P.W. Fowler and D.E. Manolopoulos. *An Atlas of Fullerenes*. Clarendon Press, Oxford, 1995.
- [110] G. Brinkmann and B.D. McKay. *MATCH Commun. Math. Comput. Chem.*, **58**:323–357, 2007.
- [111] G. Brinkmann, O.D. Friedrichs, S. Lisken, A. Peeters, and N.V. Cleemput. *MATCH Commun. Math. Comput. Chem.*, **63**:533–552, 2010.
- [112] G. Brinkmann and A.W.M. Dress. *J. Algorith.*, **23**:345–358, 1997.
- [113] M. Goubko. *MATCH Commun. Math. Comput. Chem.*, **71**:33–46, 2014.
- [114] A. Farrugia, J.B. Gauci, and I. Sciriha. *Spec. Matrices*, **1**:28–41, 2013.
- [115] F. Ruskey and M. Weston. *Electron J. Comb. Dyn. Surv.*, **DS5**, 2005.
- [116] A.K.L. Claus. *Reports of the Proceedings of the Scientific Society of Freiburg in Breisgau*, **4**:116–381, 1867.
- [117] I. Gutman and B. Borovićanin. Nullity of graphs: An updated survey. In D.M. Cvetković and I. Gutman, editors, *Selected Topics on Applications of Graph Spectra*, volume 4 of 5, chapter 8, pages 137–154. Math. Inst. Belgrade, 2011.
- [118] S. Fajtlowicz, P.E. John, and H. Sachs. *Croatica Chemica Acta*, **78**(2):195–201, 2005.
- [119] H. Sachs. *Algebra und Graphentheorie: Beiträge der Jahrestagung “Algebra und Grenzgebiete” in Siebenlehn.*, :65–70, 1985.
- [120] E. Clar and D.G. Stewart. *J. Am. Chem. Soc.*, **75**:2667–2672, 1953.
- [121] G. Allison, R.J. Bushby, J.–L. Paillaud, and M. Thornton-Pett. *J. Chem. Soc. Perkin Trans. 1*, **4**:385–390, 1995.
- [122] Y. Morita, S. Suzuki, K. Sato, and T. Takui. *Nat. Chem.*, **3**:197–204, 2011.
- [123] O.A. Gapurenko, A.G. Starikov, R.M. Minyaev, and V.I. Minkin. *Russ. Chem. Bull.*, **60**:1517–1524, 2011.
- [124] N. Pavliček, A. Mistry, Z. Majzik, N. Moll, G. Meyer, D.J. Fox, and L. Gross. *Nat. Nanotechnol.*, **12**:308–311, 2017.
- [125] A. Narita, X.-Y. Wang, X. Feng, and K. Müllen. *Chem. Soc. Rev.*, **44**:6616–6643, 2015.
- [126] M. Zhuang and M. Ernzerhof. *J. Chem. Phys.*, **120**:4921–4926, 2004.
- [127] M. Ernzerhof. *J. Chem. Phys.*, **125**:124104, 2006.

- [128] A. Goker, F. Goyer, and M. Ernzerhof. *J. Chem. Phys.*, **129**:194901, 2008.
- [129] M. Zhuang and M. Ernzerhof. *J. Chem. Phys.*, **130**:114704, 2009.
- [130] P. Rocheleau and M. Ernzerhof. *J. Chem. Phys.*, **130**:184704, 2009.
- [131] M. Ernzerhof and F. Goyer. *J. Chem. Theory Comput.*, **6**:1818–1824, 2010.
- [132] F. Goyer and M. Ernzerhof. *J. Chem. Phys.*, **134**:174101, 2011.
- [133] P. Rocheleau and M. Ernzerhof. *J. Chem. Phys.*, **137**:174112, 2012.
- [134] B.T. Pickup, P.W. Fowler, and I. Sciriha. *J. Chem. Phys.*, **145**:204113, 2016.
- [135] B.D. McKay and A. Piperno. *J. Symbolic Computation*, **60**:94–112, 2013.
- [136] S. Shaik, A. Shurki, D. Danovich, and P.C. Hiberty. *Chem. Rev.*, **101**:1501–1539, 2001.
- [137] G. Binsch, E. Heilbronner, and J.N. Murrell. *Mol. Phys.*, **11**:305–320, 1966.
- [138] R.S. Dumont. *J. Chem. Phys.*, **134**:044119, 2011.
- [139] W.Y. Kim and K.S. Kim. *Acc. Chem. Res.*, **43**:111–120, 2010.
- [140] K. Yoshizawa, T. Tada, and A. Staykov. *J. Am. Chem. Soc.*, **130**:9406–9413, 2008.
- [141] L.D. Landau and E.M. Lifschitz. *Quantum Mechanics, Non-relativistic theory (Volume 3 of a Course in Theoretical Physics)*. Pergamon Press, Oxford, 1977.
- [142] R.A. Brualdi and H. Schneider. *Linear Algebra Appl.*, **52–53**:769–791, 1983.
- [143] D. Mayou, Y. Zhou, and M. Ernzerhof. *J. Phys. Chem.*, **117**:7870–7884, 2013.
- [144] R. Mallion and D.H. Rouvray. *J. Math. Chem.*, **5**:1–21, 1990.
- [145] C.A. Coulson and H.C. Longuet-Higgins. *Proc. R. Soc. Lond. A*, **191**:39–60, 1947.
- [146] C.A. Coulson and H.C. Longuet-Higgins. *Proc. R. Soc. Lond. A*, **192**:16–32, 1947.
- [147] Y. Tsuji, A. Staykov, and K. Yoshizawa. *J. Am. Chem. Soc.*, **133**:5955–5965, 2011.
- [148] M.B. Monagan, K.O. Geddes, K.M. Heal, G. Labahn, S.M. Vorkoetter, J. McCarron, and P. DeMarco. *Maple 18 Programming Guide*. Maplesoft, Waterloo ON, Canada, 2014.
- [149] H.E. Brouwer and W.E. Haemers. *Spectra of Graphs*. Springer, New York, 2012.
- [150] R. Baer and D. Neuhauser. *J. Am. Chem. Soc.*, **124**:4200–4201, 2002.
- [151] G.C. Solomon, C. Herrmann, T. Hansen, V. Mujica, and M.A. Ratner. *Nat. Chem.*, **2**:223–228, 2010.

- [152] M. Brandbyge, M.R. Sorensen, and K.W. Jacobsen. *Phys. Rev. B*, **56**:14956–14959, 1997.
- [153] D. Jacob and J.J. Palacios. *Phys. Rev. B*, **73**:075429, 2006.
- [154] R. Li, S. Hou, J. Zhang, Z. Qian, Z. Shen, and X. Zhao. *J. Chem. Phys.*, **125**:194113, 2006.
- [155] M. Paulsson and M. Brandbyge. *Phys. Rev. B*, **76**:115117, 2007.
- [156] P.W. Fowler, B.T. Pickup, I. Sciriha, and M. Borg. *Ars Math. Contemp.*, **13**:379–408, 2017.
- [157] E. Heilbronner. *J. Chem. Educ.*, **66**:471–477, 1989.
- [158] P.W. Fowler. *Phys. Chem. Chem. Phys.*, **4**:2878–2883, 2002.
- [159] R.E. Peierls. *Quantum Theory of Solids*. Oxford University Press, Oxford, 1955.
- [160] H.A. Jahn and E. Teller. *Proc. R. Soc. Lond. A*, **161**:220–235, 1937.
- [161] P.W. Fowler and A. Rassat. *Phys. Chem. Chem. Phys.*, **4**:1105–1113, 2002.
- [162] E. Heilbronner and S. Shaik. *Helv. Chim. Acta.*, **75**:539–556, 1992.
- [163] V.E. Seville. MChem thesis, University of Sheffield, 2017.
- [164] C.J. Gorter. *Physica*, **17**:777–780, 1951.
- [165] R.A. Smith and H. Ahmed. *Journal of Applied Physics*, **81**:2699–2703, 1997.
- [166] G. Széchenyi and A. Pályi. *Phys. Rev. B – Condensed Matter and Materials Physics*, **95**:035431, 2017.
- [167] K. Ono, D. Austing, Y. Tokura, and S. Tarucha. *Science*, **297**:1313–1317, 2002.
- [168] J.K. Perron, M.D. Stewart, and N.M. Zimmerman. *Journal of Applied Physics*, **119**:134307, 2016.
- [169] J.R. Petta, A.C. Johnson, J.M. Taylor, E.A. Laird, A. Yacoby, M.D. Lukin, C.M. Marcus, M.P. Hanson, and A.C. Gossard. *Science*, **309**:2180–2184, 2005.
- [170] F.H.L. Koppens, C. Buizert, K.J. Tielrooij, I.T. Vink, K.C. Nowack, T. Meunier, L.P. Kouwenhoven, and L.M.K. Vandersypen. *Nature*, **442**:766–771, 2006.
- [171] K.C. Nowack, F.H.L. Koppens, Y.V. Nazarov, and L.M.K. Vandersypen. *Science*, **318**:1430–1433, 2007.
- [172] J. Hubbard. *Proc. R. Soc. Lond. A*, **276**:238–257, 1963.
- [173] C. Durkan. *Contemporary Physics*, **45**:1–10, 2004.
- [174] N. Lorente and J.P. Gauyacq. *Phys. Rev. Lett.*, **103**:176601, 2009.

- [175] D. Serrate, P. Ferriani, Y. Yoshida, S. Hla, M. Menzel, K. von Bergmann, S. Heinze, A. Kubetzka, and R. Wiesendanger. *Nat. Nanotechnol.*, **5**:350–353, 2010.
- [176] J.E. Subotnik and A. Nitzan. *J. Chem. Phys.*, **129**:14407, 2008.